Programa de Desarrollo de las ciencias básicas (PEDECIBA)

Área Biología

Tesis de Doctorado en Ciencias Biológicas

El inmunorreceptor CD300f microglial contribuye al mantenimiento de la viabilidad neuronal, al remodelamiento sináptico, e influye sobre el comportamiento de ratones.

Lic. Daniela Alí Ruiz

Orientador: Dr. Hugo Peluffo

Co-orientadora: Dra. Nathalia Vitureira

Tribunal

Dra. Silvia Olivera

Dra. Analía Richeri

Dra.Daniella Agrati

AGRADECIMIENTOS

A Hugo por todos estos años de enseñanza, por la libertad, la confianza, paciencia y el apoyo sobre todo en esta etapa de escritura. A Nathalia por todos los cultivos compartidos y la dedicación.

A las Doctoras Silvia Olivera, Analía Richeri y Daniella Agrati por haber accedido a formar parte del tribunal.

A mis compañeros del Laboratorio de Neuroinflamación y Terapia génica del Instituto Pasteur, Bruno, Sabri, Andrés y a las que ya no están Lucha y Frances que de alguna forma siguen en el labo. A Fernanda Kaufmann que me inserto en el mundo del comportamiento.

Al Departamento de Histología y Embriología de la Facultad de Medicina por acogerme todos estos años (desde mi tesis de grado) en especial al Laboratorio de Neurobiología Celular y Molecular por haberme, apoyado y acompañado todo este tiempo, tanto en la Ciencia como en la vida (Ernesto, Vale, Patricia, Laura, Sole).

Finalmente, lo más importante, a mi familia (mi mamá, mi papá, mi hermana, mi hermano, mi suegra y mi cuñado) por el amor incondicional y el apoyo constante que hacen que todo sea más fácil, más lindo y más disfrutable.

A Pablo, el mejor compañero de vida que podría haber elegido, mi compañero de ruta y a los dos que me enseñaron el amor más puro, mis hijos Julia y Mateo.

Índice

ÍNDICE DE FIGURAS

RESUMEN

Los inmunorreceptores poseen un rol clave en la regulación del Sistema Nervioso Central (SNC), participando tanto en las respuestas inmunes como en los procesos inflamatorios. CD300f es un receptor de particular interés de estudio, ya que posee la capacidad de transmitir señales de activación e inhibición de cascadas de señalización lo cual es muy poco común. Esta característica se debe a la presencia de motivos de unión tanto a fosfatasas como a quinasas en su cola citoplasmática.

El Trastorno Depresivo Mayor (TDM) es un trastorno heterogéneo y multifactorial que involucra muchos sistemas fisiológicos. La desregulación del sistema inmunológico se ha asociado con esta patología en modelos animales de depresión y en pacientes con TDM. La regulación del fenotipo microglial por los receptores inmunológicos se ha convertido en un tema central en muchas condiciones neurológicas y psiquiátricas. Los receptores inmunológicos CD300f han ganado atención debido a su importante papel en la regulación del fenotipo microglial y su participación en el TDM en mujeres y en comportamientos similares a la depresión en ratones hembra, así como en la ansiedad en hombres y ratones macho. Nuestro objetivo fue caracterizar la participación del inmunorreceptor CD300f en el mantenimiento de la Homeostasis del SNC y su papel en patologías psiquiátricas. Utilizamos dos cepas de ratones con deficiencia de CD300f, y ratones con deficiencia condicional CD300floxp/loxp x CX3CR1WT/CreERT2. La deficiencia de CD300f indujo comportamientos similares a la depresión, como anhedonia y evitación social en ratones hembra, pero no en ratones macho. Este efecto se potenció en condiciones inflamatorias, un desencadenante bien conocido de estas alteraciones conductuales. Sin embargo, el mecanismo detrás del comportamiento similar a la depresión no se relacionó con el desencadenante de un perfil inflamatorio clásico sistémico o cerebral (por ejemplo, aumento de citoquinas proinflamatorias en sangre o en el cerebro, etc.). De hecho, en condiciones basales, la ausencia de CD300f indujo alteraciones fenotípicas en la microglía y en los macrófagos de barrera del SNC que llevaron al reclutamiento de macrófagos CCR2+. La inhibición farmacológica de su reclutamiento revirtió el comportamiento similar a la depresión. Al generar ratones condicionales CD300floxp/loxp x

CX3CR1WT/CreERT2, pudimos observar que el fenotipo similar a la depresión dependía únicamente de la expresión de CD300f en la microglía/macrófagos de barrera del SNC. Además, este modelo demostró que no había cambios en el desarrollo o en las primeras etapas postnatales detrás de este efecto, ya que la deficiencia de CD300f inducida en ratones adultos pudo reproducir el comportamiento similar a la depresión. Es interesante destacar que la inhibición de la interacción entre CD300f y su ligando en co-cultivos de neuronas y células gliales del hipocampo evidenció el papel de este receptor inmunológico en la promoción de la poda sináptica e incluso la plasticidad sináptica. El mecanismo detrás de este papel probablemente incluye la interacción de CD300f con la fosfatidilserina (PS, por sus siglas en inglés) expuesta en las sinapsis que deben ser eliminadas. En conjunto, nuestro estudio arroja luz sobre las interacciones neuroinmunitarias detrás de la fisiopatología de los trastornos mentales y puede proporcionar nuevos enfoques terapéuticos para estas afecciones.

INTRODUCCIÓN

Durante las últimas décadas hemos experimentado un increíble aumento en el conocimiento acerca de las propiedades y funciones de la glía en la salud y la enfermedad. Gracias al progreso impulsado por el poder de las herramientas modernas, ahora sabemos que las células gliales, incluyendo los astrocitos, microglía y oligodendrocitos, muestran una gran diversidad y son participantes críticos en prácticamente todos los aspectos del desarrollo y funcionamiento normal del cerebro (Augusto-Oliveira et al., 2020; Clayton & Tesar, 2021; Ferro et al., 2021; Stadelmann et al., 2019). Las células gliales, constituyen al menos la mitad del cerebro sano y no solo interactúan estrechamente con las neuronas para respaldar su actividad, sino que también interactúan mutuamente y contribuyen a dar forma a los circuitos neuronales. Estos avances presentan un desafío tremendo a la doctrina neurocéntrica y apuntan hacia una reformulación de nuestra percepción de la actividad cerebral en la salud y la enfermedad, que no solo debe considerar a las neuronas, sino también su asociación con las células gliales (Parpura et al., 2013).

Los astrocitos son el tipo más abundante de células gliales que recubren de manera contigua todo el SNC. La ubicación estratégica de los astrocitos entre los vasos sanguíneos y las sinapsis les permite regular la sinaptogénesis, cumplir funciones metabólicas y de mantenimiento homeostático, y mantener un entorno óptimo para el funcionamiento adecuado de las neuronas (Augusto-Oliveira et al., 2020; Parpura et al., 2013). Los astrocitos expresan el canal de agua aquaporina AQP4, que es importante para mantener el equilibrio hídrico en el SNC (MacAulay, 2021). En la astroglía, AQP4 colocaliza con el canal de potasio Kir4.1, lo que indica que la regulación astrocítica del equilibrio hídrico y del potasio son procesos estrechamente asociados (Binder et al., 2012; Verhoog et al., 2020). De hecho, los astrocitos son los principales controladores del K+ extracelular en el cerebro, que, si no se controla, puede afectar la actividad neuronal regular. Según el modelo de amortiguación espacial, los astrocitos captan principalmente el K+ extracelular a través de los canales Kir4.1 en sitios de alta actividad neuronal, lo redistribuyen a través del sincitio astrocítico y lo liberan en regiones con menor concentración de K+ (Orkand et al., 1966). Este modelo de amortiguación espacial se basa en el hecho de que los astrocitos

están interconectados eléctricamente a través de canales de unión (GJ) y forman un sincitio funcional. Dada la abundancia de astrocitos en el SNC, este sincitio permite controlar el espacio extracelular. Además, los astrocitos son una parte integral de las sinapsis y contribuyen directamente al procesamiento de la información neuronal a través de interacciones recíprocas (Araque et al., 2014). Estas interacciones se basan en la expresión de diversos receptores para los neurotransmisores liberados por las neuronas. Los astrocitos pueden captar y también responder a estos neurotransmisores. Por ejemplo, los transportadores GLAST (EAAT1) y GLT1 (EAAT2) de los astrocitos captan rápidamente el glutamato del espacio extracelular, lo cual es esencial para prevenir la excitotoxicidad en el cerebro (Verkhratsky & Nedergaard, 2018). El glutamato en los astrocitos se convierte rápidamente en glutamina mediante la glutamina sintetasa (GS). La activación de los receptores astrocíticos por neurotransmisores promueve un aumento en el Ca2+ intracelular, lo que induce más adelante la liberación de gliotransmisores de los astrocitos, como el glutamato y el trifosfato de adenosina (ATP), que contribuyen al patrón de actividad neuronal (Shen et al., 2017).

Los oligodendrocitos se generan a partir de células precursoras (glía NG2) y modulan las propiedades estructurales y eléctricas de los axones neuronales mediante el control de su diámetro (Stadelmann et al., 2019). Estas células gliales envuelven las membranas alrededor de los axones neuronales para formar una capa de mielina que evita la fuga de corriente iónica y permite una conducción de señal rápida y eficiente en el SNC. Además, los oligodendrocitos mielinizantes están incrustados en una red de células gliales y neuronales interconectadas y, dentro de esta estructura, brindan soporte metabólico a las neuronas. Investigaciones previas revelaron que las uniones de hendidura (GJs) en oligodendrocitos y astrocitos conectan estos dos tipos de células gliales en el sincitio panglial (Fasciani et al., 2018). Esta conexión ocurre en los paranodos, donde las GJs conectan la capa externa de la mielina con los procesos astrocíticos (Rash, 2010). Los oligodendrocitos, al igual que los astrocitos, expresan el canal Kir4.1 y este canal desempeña un papel importante en la homeostasis extracelular de K+ en la materia blanca (Larson et al., 2018). Además de su papel mielinizante, se ha demostrado que los oligodendrocitos

participan en la transmisión glutamatérgica excitatoria en el SNC y expresan la enzima GS (Xin et al., 2019).

MICROGLÍA

A principios del siglo XIX anatomistas intentaban comprender cómo eran las células que componían el cerebro, de modo de revelar la sorprendente heterogeneidad morfológica de las neuronas. Las células gliales no habían sido descritas aún. Fue en 1856, cuando el famoso patólogo alemán Rudolf Virchow acuñó el término "glía" (del griego "pegamento") para describir el compartimento no neuronal del SNC. Virchow concibió la neuroglía como una especie de tejido conectivo y descubrió que este tejido también contenía elementos celulares. Sin embargo, la microglía aún era desconocida en ese momento y solo se descubrió como un tipo celular separado en 1919 gracias al neurocientífico español Pío del Río Hortega (Figura 1).

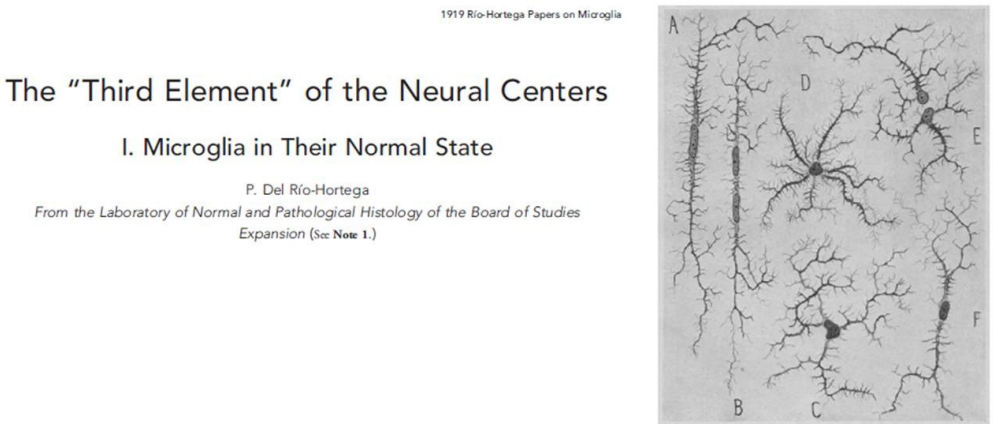

Figura 1: Figura del artículo de Pío del Río Hortega cuando en 1919 definió al "tercer elemento" celular como microglía.

Inicialmente se estableció la concepción de la microglía como células inactivas en la fisiología del SNC. Posteriormente, y de forma más clara con los experimentos pioneros de microscopía *in vivo* de dos fotones en el año 2005 (Davalos et al., 2005; Nimmerjahn, 2005) se llegó a reconocer la continua supervisión del SNC llevada a cabo por ellas.

Microglía-Neuronas

En la actualidad, la microglía se considera como células inmunitarias innatas que residen en el SNC y que ejercen funciones prototípicas similares a los macrófagos durante las infecciones o lesiones, pero que además poseen funciones específicas relacionadas con el SNC (Prinz et al., 2019). Estas células están dotadas de capacidades mnemotécnicas que les permiten generar respuestas adaptadas al contexto. La microglía son células versátiles que establecen interacciones con diversas células en el SNC, tales como neuronas, astrocitos, oligodendrocitos y células endoteliales. Hasta el día de hoy se sigue descubriendo y profundizando en las funciones de la microglía.

Imágenes *in vivo* en la corteza de ratones adultos sanos, muestran procesos microgliales altamente activos que exploran el entorno constantemente (Davalos et al., 2005; Nimmerjahn, 2005). Se ha reportado en muchos estudios que esta movilidad depende de cambios en la actividad neuronal (Cserép et al., 2020; Wake et al., 2009; Yuste et al., 2020). Para llevar a cabo un estado de vigilancia constante se requiere un gasto energético importante, y la microglía posee una gran flexibilidad metabólica (Bernier et al., 2020). Las ramificaciones microgliales en movimiento muestran una respuesta quimiotáctica rápida a la lesión del tejido que depende de receptores de purina y hemicanales de conexina, y parecen recibir señales de los astrocitos circundantes tanto en el cerebro normal como en el lesionado (Davalos et al., 2005; Nimmerjahn, 2005). La motilidad está mediada por señalización purinérgica, es decir, ATP (adenosín trifosfato) y ADP (adenosín difosfato) inducidos por actividad/lesión y el receptor P2RY12 en microglía. En las uniones somáticas entre microglía y neurona, el P2RY12 microglial interactúa directamente con los cúmulos del canal de potasio Kv2.1 en las neuronas (Cserép et al., 2020). La comunicación cruzada entre microglía y neuronas también se lleva a cabo mediante citoquinas, neurotransmisores y neuropéptidos. Por ejemplo, la microglía produce neuropéptidos y factores de crecimiento. Un estudio en ratones adultos demostró que la microglía en la corteza motora contribuye a la formación de espinas dependiente del aprendizaje a través del factor neurotrófico derivado del cerebro (BDNF, por sus siglas en inglés) de origen microglial (Kelsey C. Martin Mhatre V. Ho et al., 2013). En un modelo de lesión de nervio periférico,

la microglía estimulada por ATP libera BDNF e inducen hiperexcitabilidad neuronal al invertir la polaridad de las corrientes GABA neuronales (Coull et al., 2005). Además, el factor de crecimiento similar a la insulina-1 (IGF-1) microglial promueve la supervivencia de progenitores neurales en neuronas corticales de la capa V (Kelsey C. Martin Mhatre V. Ho et al., 2013; Ueno et al., 2013; Ziv et al., 2006).

Otra de las formas por medio de las cuales la microglía se comunica con las neuronas, es expresando receptores para detectar cambios en las concentraciones de neurotransmisores y neuropéptidos, incluyendo receptores metabotrópicos de glutamato (Biber et al., 1999; Taylor et al., 2002, 2003), receptores GABA (Kuhn et al., 2004; M. Lee et al., 2011), receptores adrenérgicos (Färber et al., 2005; Tanaka et al., 2002), y receptores de acetilcolina (Shytle et al., 2004; Susuki et al., 2006) entre muchos otros. Además, la activación de estos receptores modula la liberación de citoquinas por parte de la microglía, incluyendo TNFα e IL-6 en cultivos celulares (M. Lee et al., 2011; Mori et al., 2002; Shytle et al., 2004) y en rodajas cerebrales (Färber et al., 2005). Curiosamente, pueden existir subpoblaciones heterogéneas de microglía que expresan conjuntos distintos de receptores *in vivo*, especialmente en relación con la edad, mostrando así un grado variable de respuesta a un determinado neurotransmisor o neuropéptido (Pannell et al., 2014, 2016; Seifert et al., 2011). En conjunto, cambios en los neurotransmisores en el microentorno podrían estimular a la microglía para liberar citoquinas y quimiocinas inflamatorias, afectando negativamente las redes neuronales cercanas. En resumen, está claro que la microglía participa en múltiples mecanismos de señalización neuronal, destacando su papel como facilitadoras de la función neuronal en el SNC.

Poda sináptica

La microglía desempeña un papel esencial en la identificación y eliminación de conexiones neurales innecesarias. La poda sináptica es el proceso de eliminación de sinapsis que ocurre durante el desarrollo postnatal y a lo largo de la vida adulta (Brioschi et al., 2020; Liu et al., 2021). Este proceso promueve la refinación de circuitos neuronales y aumenta la eficiencia de las redes neuronales (Liu et al., 2021). Aún no se conocen completamente las señales que

la microglía y las neuronas utilizan para regular la poda sináptica. Sin embargo, es importante determinar las señales particulares que reclutan a la microglía a ciertas sinapsis para la poda, de modo que la microglía pueda identificar y eliminar conexiones neurales innecesarias a través de estas vías de señalización específicas.

Los inmunorreceptores microgliales son participantes claves en todos estos procesos. En el cerebro sano, la cascada clásica del complemento funciona como un mecanismo de señalización de "cómeme" para la poda sináptica por medio de la microglía (Sokolova et al., 2021; Scott-Hewitt et al., 2020). Las proteínas del complemento se localizan y se unen específicamente a las sinapsis apoptóticas, inmaduras o débilmente desarrolladas en el SNC (Scott-Hewitt et al., 2020; Schafer et al., 2012). Estas sinapsis son reconocidas por los receptores del complemento y, consecuentemente, son fagocitadas. C1q, la proteína que inicia la cascada, y otra proteína del complemento, C3, son producidas predominantemente por la microglía o los astrocitos y se localizan en las sinapsis para ser eliminadas (Fonseca et al., 2017; Wu et al., 2019). C1q y C3 son reconocidas por el receptor del complemento CR3 (CD11b/CD18), que se expresa exclusivamente en la microglía, mediando la poda de las sinapsis (Anderson et al., 2019; Hong et al., 2016). El marcaje presináptico de C1q se correlaciona con marcadores de apoptosis, como la caspasa-3 clivada o la anexina V (AV). El número de marcadores apoptóticos en la sinapsis está dado por la localización de C1q, lo que estimula la poda sináptica (Györffy et al., 2018). Debido al papel importante del sistema del complemento en la poda sináptica, los ratones knockout (KO) de C1q, C3 o CR3 muestran defectos en la poda y en la conectividad sináptica (Anderson et al., 2019; Hong et al., 2016; Shi et al., 2015; C. Wang et al., 2020).

Otra señal de "Cómeme" que promueve la poda sináptica es la PS. La exposición de PS ocurre típicamente en dendritas apoptóticas o lesionadas (Scott-Hewitt et al., 2020). El receptor activador TREM2 (*triggering receptor expressed on myeloidcells 2),* expresado en la membrana de células mieloides y en la superficie celular de la microglía, es uno de los receptores que promueve la poda sináptica. La PS puede ser reconocida por TREM2 y, consecuentemente, ser marcada para la eliminación (Filipello et al., 2018; Sapar et al., 2018; Shacham-

Silverberg et al., 2018). Hay reportes tanto *in vivo* como *in vitro* que muestran que la interacción entre PS y TREM2 puede regular la poda sináptica en el hipocampo y en el núcleo geniculado lateral dorsal (Scott-Hewitt et al., 2020). Además, los ratones TREM2 KO tienen una disminución en la densidad microglial, un aumento en la densidad de espinas neuronales y una conectividad alterada en el hipocampo (Filipello et al., 2018).

Otro receptor microglial que regula la fagocitosis y la eliminación de sinapsis es el receptor de fractalquina 1 (CX3CR1) de tipo quimiotáctico C-X3-C. Se expresa en gran medida en la microglía y se considera esencial para la comunicación entre microglía y neuronas (Bolós et al., 2018). Su ligando, CX3CL1, es expresado por las neuronas (Zhang et al., 2018). La señalización CX3CR1/CX3CL1 contribuye a la poda sináptica, permitiendo que la microglía identifique qué sinapsis debe ser eliminada. Otro estudio muestra que la fagocitosis de sinapsis se ve disminuida en microglía deficiente de CX3CR1 o en ausencia del ligando CX3CL1. *In vivo,* en ratones CX3CR1 KO sometidos al modelo murino de plasticidad desencadenado por la cauterización y recorte de bigotes, se observó una reducción de la actividad sináptica en la corteza somatosensorial (Gunner et al., 2019). Así como hay señales de "cómeme", hay señales "no me comas", mediadas por otros inmunorreceptores de modo de prevenir la fagocitosis de sinapsis fuertes y activas. Uno de los inmunorreceptores que participa en este tipo de señales es el CD200R1, expresado por la microglía y cuyo ligando CD200 es expresado por las neuronas. En un reporte se demostró que macrófagos y microglía de ratones deficientes de CD200, presentaron un fenotipo activado y eran más numerosos (Hoek et al., 2000). A su vez, en el mismo trabajo mostraron que la falta de CD200 resultó en un inicio más rápido de la encefalomielitis autoinmune experimental (EAE). Fuera del cerebro, la interrupción de la interacción CD200R-CD200 incrementó la susceptibilidad a la artritis inducida por colágeno (CIA de su sigla en inglés) en ratones normalmente resistentes a esta enfermedad. En conjunto, estos trabajos muestran que, en diversos tejidos, CD200R proporciona una señal inhibidora para la línea de los macrófagos/microglía.

El mecanismo de la poda sináptica, que se lleva a cabo por medio de los inmunorreceptores microgliales es altamente regulado. Comienza durante el desarrollo y continúa a lo largo de la edad adulta en diversas regiones cerebrales. Es fundamental que las sinapsis apropiadas sean eliminadas, al mismo tiempo que otras se refuercen y mantengan mediante una poda sináptica estrechamente regulada.

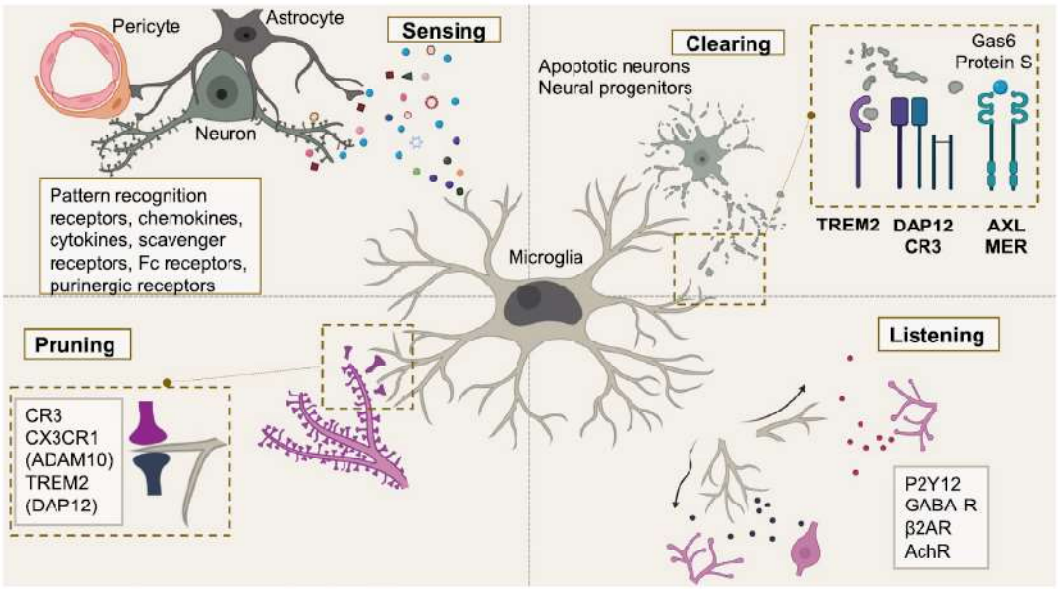

Figura 2: Funciones de la microglía. La figura ilustra la comunicación cruzada entre microglía y neuronas en el SNC. La microglía percibe su entorno a través de proteínas codificadas por genes del sensoma, crucial para mantener la homeostasis del SNC, y responder rápidamente a daños o insultos. Una vez que se detectan excesos de progenitores neurales o residuos, la microglía inicia sus funciones de eliminación a través de TREM2, CR3 (DAP12), AXL, MER (ambos genes codifican para receptores de tirosin quinasa), y otras moléculas aún por definir. Además, la microglía da forma y refina los circuitos neuronales podando sinapsis durante ventanas de desarrollo específicas a través de la vía de señalización del complemento, por medio del receptor de fractalquina y por vías mediadas por TREM2. La microglía también "escucha" activamente la actividad neuronal cercana a través de receptores de neurotransmisores como P2Y12, GABA-R, β2AR, AchR, y otros. (Figura tomada del trabajo de Sebastián De Schepper (De Schepper et al., 2021)).

Regulación del fenotipo microglial

Para poder llevar a cabo todas las funciones en diferentes momentos del desarrollo, la adultez, o el envejecimiento, y a su vez en diferentes condiciones (basales, insultos, neurodegeneración, etc), la microglía presenta diferentes

fenotipos o estados. Durante muchas décadas, la microglía ha sido categorizada y dividida simplemente en función de su densidad celular, morfología, expresión de marcadores superficiales limitados y propiedades electrofisiológicas (De Biase et al., 2017; Lawson et al., 1992). Se consideraba a la microglía como una población de células heterogénea en el SNC (Hanisch, 2013). Dado el hecho de que la microglía cumple funciones pleiotrópicas durante el desarrollo y la homeostasis del SNC, que van desde la formación y refinamiento sináptico, el soporte nutritivo para neuronas y oligodendrocitos, hasta la monitorización de la función del SNC, se pensaba que podrían existir subconjuntos especializados de microglía para cumplir con la amplia gama de respuestas y demandas durante la salud y enfermedad. Además, en condiciones patológicas, la microglía se activa rápidamente, cambia sus perfiles de expresión y, en última instancia, se desplaza a varios estados reactivos dependientes del contexto debido a su extrema plasticidad (Shemer et al., 2015). Las tecnologías de célula única (ARN *singlecell*), la multiómica y los análisis integrativos de la expresión génica y proteica han contribuido a proporcionar nuevas perspectivas sobre los mecanismos moleculares en diferentes condiciones que regulan estados celulares específicos en un contexto dado (por ejemplo, desarrollo, adultez, enfermedad, modelo de lesión, etc.). Se han observado estados microgliales diversos y dependientes del contexto en varias especies y modelos. Algunos ejemplos de estos estados son la microglía asociadas a la enfermedad (DAMs), originalmente asociadas con modelos de patología de la enfermedad de Alzheimer (Keren-Shaul et al., 2017); el fenotipo neurodegenerativo de microglía (MGnD) similar al DAM documentado en varios modelos de enfermedades (Krasemann et al., 2017); microglía con respuesta activada (ARMs) y microglía con respuesta al interferón (IRMs) en un modelo de ratón con patología de la enfermedad de Alzheimer (Sala Frigerio et al., 2019); microglía humana de la enfermedad de Alzheimer (HAMs) (Srinivasan et al., 2020); microglía inflamada en la esclerosis múltiple (MIMS) (Absinta et al., 2021); microglía acumuladora de gotas lipídicas (LDAMs) en ratones y humanos envejecidos (Marschallinger et al., 2020); microglía asociada a tumores cerebrales (microglía asociada a gliomas, GAMs) (De Andrade Costa et al., 2022); firma asociada a la esclerosis lateral amiotrófica (ALS) (Limone et al., 2021) y firma microglial de la enfermedad de Parkinson (PD) (Smajic et al.,

2022). En el cerebro en desarrollo y en el cerebro envejecido, la microglía asociada a la materia blanca (WAMs) (Safaiyan et al., 2021), la microglía asociada al tracto de axones (ATMs) (T. R. Hammond et al., 2019), y la microglía asociada a la región proliferativa (PAMs, relacionada con la fagocitosis de oligodendrocitos en desarrollo)(Q. Li et al., 2020) pueden compartir algunas características con la firma central de DAM. En el SNC en desarrollo en humanos, la microglía también expresa algunos perfiles similares a DAM/MGnD/ARM (Kracht et al., 2020). Hay que tener en cuenta las limitaciones de estas clasificaciones dado que la microglía, a diferencia de las neuronas (las que se considera forman parte de grupos fijos que son terminalmente diferenciados (Yuste et al., 2020)), son células heterogéneas y plásticas y no sabemos cuán dinámicos temporal o espacialmente pueden ser sus estadíos. Por lo tanto, es probable que estas células no estén permanentemente "bloqueadas" en un solo estado funcional. A partir de la evidencia disponible hasta ahora, los estados de la microglía parecen dinámicos y plásticos, posiblemente transitorios y fuertemente dependientes del contexto (Figura 3). Se necesitan nuevas herramientas, incluyendo imageneología para estadíos microgliales, para rastrear las transiciones dentro de células individuales a lo largo del tiempo y a lo largo de la vida, siguiendo diferentes desafíos y perturbaciones, así como en respuesta a tratamientos (Paolicelli et al., 2022).

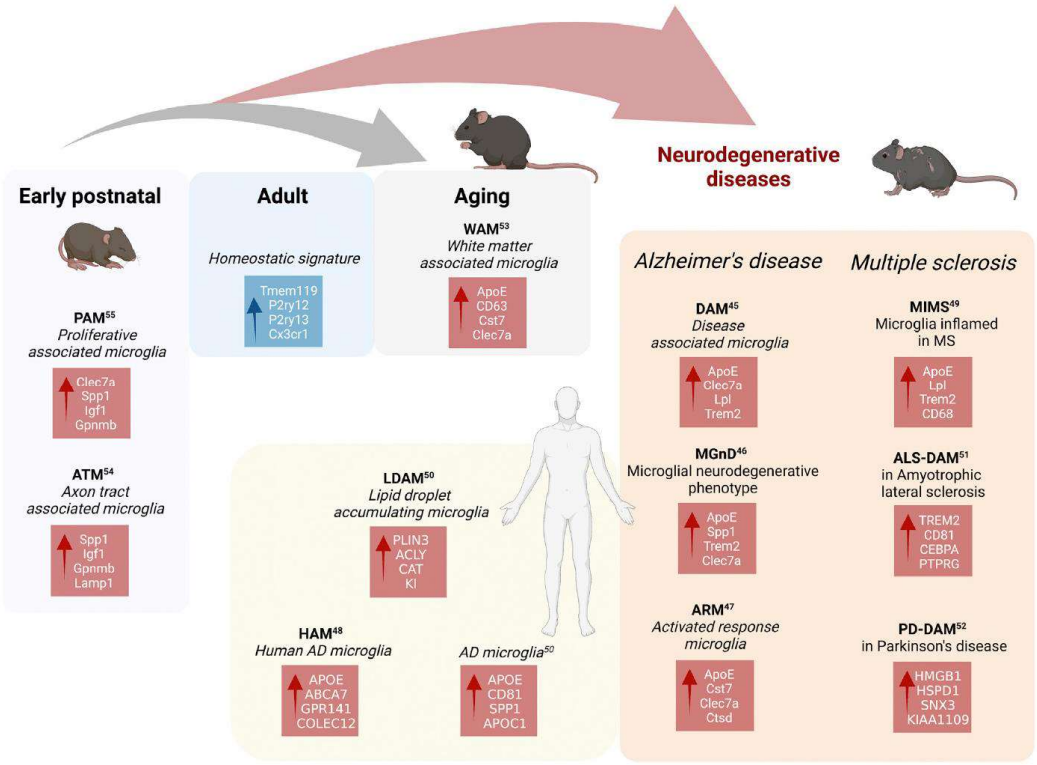

Figura 3: Firmas transcripcionales de diferentes tipos de microglía. El avance de la transcriptómica ha permitido identificar muchas firmas transcripcionales para la microglía, tanto en ratones como humanos, durante el desarrollo y envejecimiento pero que no se limitan exclusivamente a los estadíos o patologías asociadas. (Figura tomada de Paolicelli et al., 2022).

Resulta de vital importancia tener en cuenta que los estados microgliales dependen de determinantes intrínsecos (como especie, ontogenia, sexo o antecedentes genéticos) así como del contexto específico en el que habitan, incluyendo la edad, ubicación espacial y factores ambientales (como nutrición, microbiota, patógenos, medicamentos, etc.). En conjunto, estos factores afectan a la microglía en múltiples niveles (es decir, epigenómico, transcriptómico, proteómico, metabolómico, ultraestructural y fenómico), lo que en última instancia determina las funciones microgliales (Paolicelli et al., 2022).

Inmunorreceptores

Las células de la línea mieloide desempeñan roles fundamentales en las respuestas inmunológicas y en procesos clave como el desarrollo, la homeostasis y la remodelación de todos los tejidos. Estas células identifican mediadores solubles en el entorno tisular y ligandos en la superficie de células vecinas

mediante diversos receptores. Los receptores de reconocimiento de patrones, como los receptores tipo Toll (TLR), receptores tipo NOD y receptores tipo *scavenger*, indican la presencia de patrones moleculares asociados a invasión microbiana o daño tisular. Otros receptores evalúan el estado del organismo y contribuyen a establecer umbrales para las respuestas celulares ante cada patrón molecular, regulando así la intensidad y duración de la respuesta (Colonna, 2023). Al integrar las señales de todos estos receptores, las células mieloides pueden generar respuestas cuidadosamente adaptadas a condiciones específicas (Colonna, 2023).

Inmunorreceptores de la familia CD300

Nuestro grupo ha trabajado durante años con inmunorreceptores, en particular con el par CD200-CD200R y con el inmunorreceptor CD300f. Pertenece a la familia de inmunorreceptores CD300. En humanos, la familia de CD300 está compuesta por seis miembros, entre los que se encuentran receptores con funciones activadoras e inhibidoras de cascadas de señalización (Borrego, 2013). Estos receptores son capaces de formar homodímeros o heterodímeros en la superficie de las células por interacciones a lo largo de sus dominios extracelulares de inmunoglobulina (Borrego, 2013; Martínez-Barriocanal et al., 2010). Su combinación en complejos diferenciales, ya sea en homodímeros o heterodímeros, e interactuando con otros miembros de la familia o con ellos mismos, modula la señalización, sugiriendo cómo los complejos de CD300 pueden regular la activación de las células mieloides por medio de la interacción con sus ligandos naturales (Martinez-Barriocanal et al., 2010) (Figura 4). Se caracterizan por tener dos puentes disulfuro en su dominio IgV, con homología estructural a los receptores TREM, lo que define una superfamilia de inmunoglobulinas de superficie fuertemente conservadas y con un ancestro común (Clark et al., 2009). Dentro de la familia de CD300, se ha caracterizado a CD300b, c, d y e como activadores, por tener residuos transmembrana que interaccionan con proteínas adaptadoras con dominios activadores tipo ITAM (del inglés *immunoreceptor tyrosine-based activation motif*) como DAP-12/DAP10 o FcγR. En cambio, CD300a presenta una larga cola citoplasmática con variedad de motivos ITIM (del inglés *immunoreceptor tyrosine-based inhibitory motif*) que reclutan fosfatasas y median señales inhibitorias (Borrego,

2013). El caso de CD300f es particular, ya que se ha descrito una función dual dada su capacidad de mediar señales tanto activadoras como inhibitorias, ya que presenta motivos ITIM, pero también motivos ITAM que interactúan con PI3K, Grb2 y la cadena gama FcγR, activando cascadas de señalización intracelulares (Borrego, 2013).

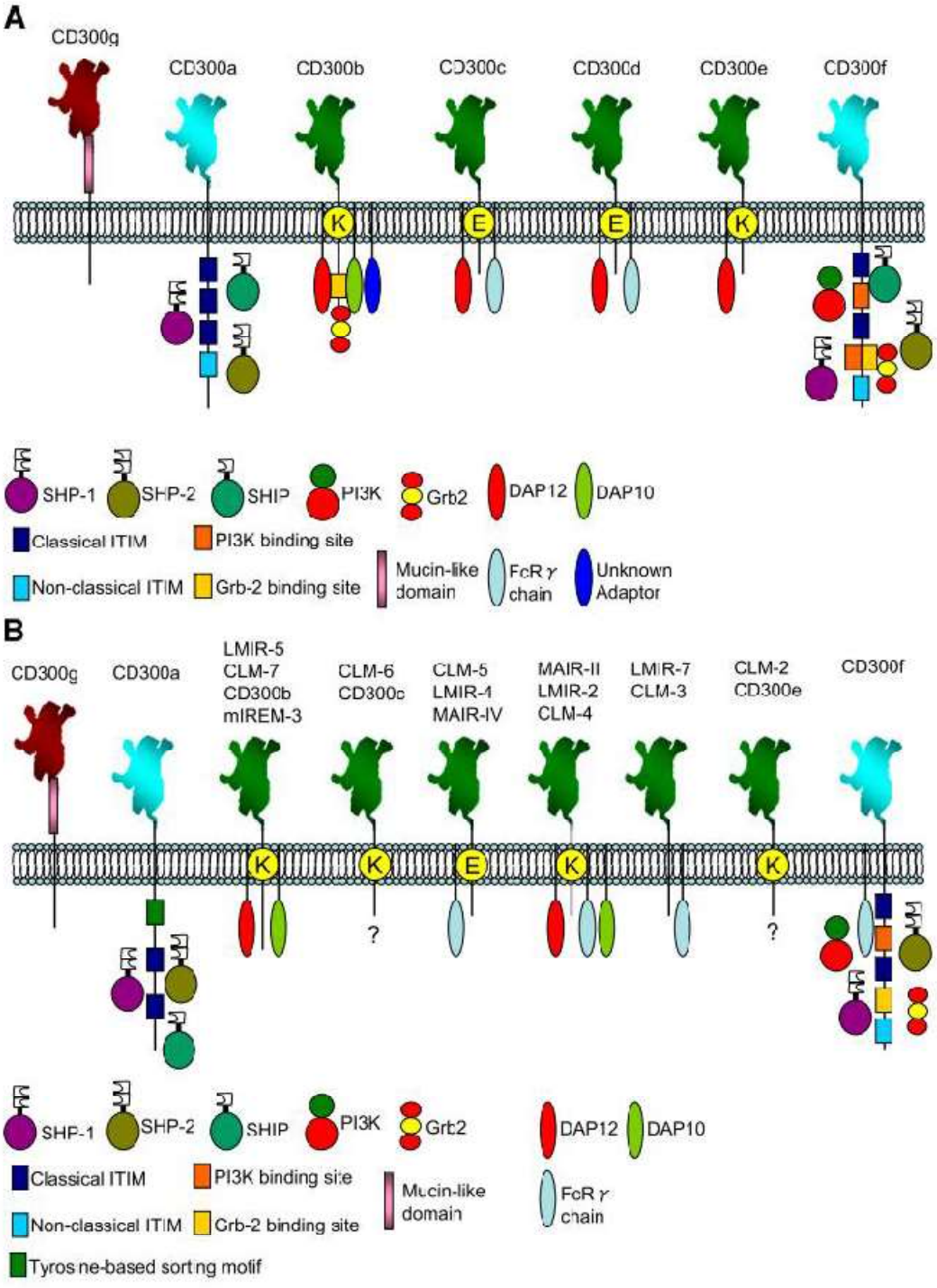

Figura 4: Representación esquemática de los receptores CD300 (A) en humano y (B) ratón. El dominio extracelular de los receptores que contienen ITIM está coloreado en turquesa, y el de los no-ITIM en color verde. El dominio extracelular de CD300g está coloreado en marrón. Se indican los motivos de señalización de cada receptor, y se muestra la interacción con fosfatasas, las moléculas adaptadoras y quinasas. (Figura tomada del trabajo de Francisco Borrego (Borrego, 2013)).

CD300f

Durante mi tesis de grado, nos centramos en identificar qué células del SNC expresaban el ligando de CD300f, qué células expresaban el receptor, y finalmente en estudiar el rol de CD300f en una lesión aguda del SNC, datos que fueron publicados en 2012 (Peluffo, et al., 2012). Dado que el o los ligandos para CD300f eran desconocidos, se utilizó primeramente una proteína de fusión soluble humana (hCD300f-Fc) y microscopía confocal detectándose un marcaje específico principalmente en la sustancia blanca del SNC y en la superficie de oligodendrocitos y ciertos astrocitos *in vitro*. Luego se demostró en un modelo *in vivo* de daño cerebral excitotóxico en rata, que la sobreexpresión del CD300f humano (hCD300f) induce una reducción significativa en el volumen de la lesión. Para validar estos resultados, se clonó el ortólogo de CD300f de rata (rCD300f), y su sobreexpresión después de un daño cerebral agudo también resultó en un efecto neuroprotector comparable al de hCD300f (Peluffo, et al., 2012). Los resultados obtenidos utilizando la proteína de fusión soluble de rata rCD300f-IgG2a, producida en nuestro laboratorio, fueron similares a los patrones de marcaje que se obtuvieron con la proteína de fusión soluble humana hCD300f-Fc, sugiriendo que ambas formas comparten los mismos ligandos. Se demostró *in vitro,* mediante el análisis del patrón de expresión del receptor CD300f en cultivos primarios de células cerebrales de rata por QPCR e inmunocitoquímica, que se encontraba principalmente en microglía, pero también en oligodendrocitos y en menor medida en neuronas (Peluffo, et al., 2012). Sin embargo, en la actualidad se sabe que CD300f es expresado por varias células mieloides del SNC, incluidas la microglía y los macrófagos perivasculares (Borrego, 2013), y que nuestros resultados en cultivo que mostraban expresión en oligodendrocitos y astrocitos eran un artefacto de la QPCR a partir de cultivos no puros de los diferentes tipos celulares (Peluffo, et al., 2012).

También sabemos ahora que los receptores CD300f comparten ligandos fosfolipídicos comunes con TREM2, como la señal de "cómeme" de PS (Choi et al., 2011a; Y. Wang et al., 2015), esfingomielina (Izawa et al., 2014) y lipoproteínas de alta densidad (HDL) y lipoproteínas de baja densidad (LDL) (Izawa et al., 2012). CD300f modula directamente otros receptores, como varios miembros de la familia de receptores CD300, incluido el receptor activador CD300b (Martínez-Barriocanal et al., 2010), FcRγ (Izawa et al., 2009) e IL4Rα (Moshkovits, Karo-atar, et al., 2015) y modula indirectamente DAP12 (Martínez-Barriocanal et al., 2010). De acuerdo con su función inhibitoria, la ausencia de CD300f potencia muchos modelos de enfermedades inflamatorias/autoinmunitarias (Izawa et al., 2012; Matsukawa et al., 2016; Tian, Choi et al., 2014) y se asocia con la susceptibilidad a enfermedades inflamatorias y autoinmunitarias en humanos (Ban et al., 2010; Danik et al., 2009). Es particularmente interesante para las enfermedades desmielinizantes del SNC, ya que se demostró que desempeña un papel clave en la encefalomielitis autoinmunitaria experimental, donde se encuentra una patología neuroinflamatoria exacerbada en los animales CD300f KO (Xi et al., 2010), y también está entre los genes sobreexpresados en la microglía promielinizantes después de un estímulo desmielinizante (Lloyd et al., 2019). También aparece entre los genes más sobreexpresados en la microglía cerebral después de la inyección intraperitoneal (IP) de lipopolisacárido (LPS) (Bennett et al., 2016) y después de una lesión en la médula espinal (Torres-Espín et al., 2013). Muy recientemente, también se asoció con la respuesta neuroprotectora contra la patología de Tau (Ising et al., 2019). En el 2020 nuestro grupo publicó un trabajo en el cual demostramos que el CD300f puede modular el metabolismo de la microglía y la actividad de poda sináptica asociada con comportamientos depresivos (Lago et al., 2020). Identificamos inicialmente un alelo protector de CD300f que curiosamente solo afecta a las mujeres. Ratones hembra CD300f -/- (ratones deficientes para CD300f) y no machos, muestran comportamientos similares a la depresión, pero no desarrollan neuroinflamación clásica. Los perfiles de expresión génica por ARNseq de microglía aislada de hipocampo WT y CD300f−/− fueron ligeramente diferentes, según se observa en el análisis de componentes principales (Figura 5A). De hecho, solo 34 genes mostraron una expresión diferencial significativa

(valor de p ajustado por tasa de descubrimiento [FDR] <0.1) entre microglía de ratones WT y CD300f−/− (Figura 5B). No se encontraron alteraciones significativas asociadas a las vías de KEGG (Enciclopedia de Genes y Genomas de Kyoto) para este conjunto de datos. Al analizar la firma génica microglial homeostática, observamos que la deficiencia de CD300f no alteró la expresión de genes homeostáticos y no experimentó un cambio fenotípico hacia un fenotipo de DAM. Solo un gen marcador de microglía inmadura DAM, el Spp1 (también llamado osteopontina), mostró una disminución significativa en su expresión. Curiosamente, se ha encontrado una disminución en el nivel sérico de Spp1 en pacientes con MDD (Kadriu et al., 2018). Los cerebros de los ratones CD300f−/− también mostraron alteraciones en la expresión de ARN de Siglec1, Sirpβ1 y Apoa1, que, además de Il1rn, se ha demostrado que forman parte de un módulo de coexpresión génica en el MDD (Gandal et al., 2018). En conjunto, estos datos sugieren que los ratones CD300f−/− no desarrollan una neuroinflamación clásica, pero muestran varias características de comunicación neuroinmune alterada, que incluyen un aumento en el número de microglía, posibles alteraciones en el fenotipo de la microglía y los macrófagos perivasculares, y un aumento de mediadores innatos como Il1rn e IL-6, todos previamente asociados con el MDD (Lago et al., 2020).

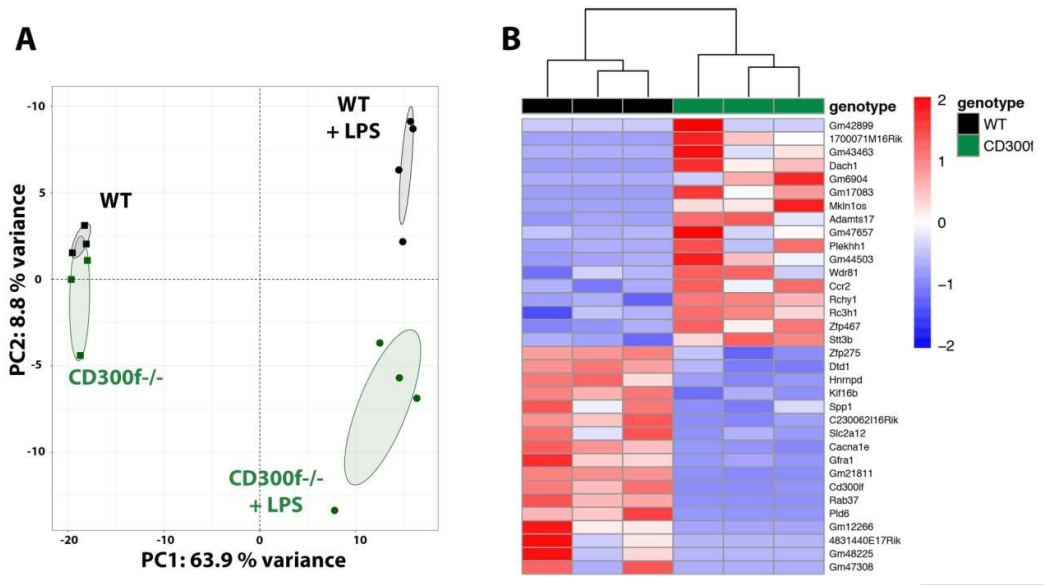

Figura 5: Microglía aisladas de CD300−/− adultas no presentan un fenotipo proinflamatorio. Se aislaron hipocampos de ratones hembra adultas WT y CD300f−/− *naive*

para el aislamiento de células microgliales mediante clasificación celular, CD11b+/CD45low. **(A)** Se realizó ARNseq de los ARNm, y se muestra el agrupamiento general mediante análisis de componentes principales (PCA). El PCA se basó en los niveles de expresión regularizados de los 150 genes más variables, y las elipses de confianza se calcularon en el nivel 0.9. **(B)** Se muestra el mapa de calor de los 34 genes diferencialmente expresados (Padj< 0.1) entre los ratones WT y CD300f−/−.

Evidencias emergentes sugieren que los receptores inmunológicos de la microglía/macrófagos están involucrados en muchos procesos relacionados con el envejecimiento, como el metabolismo energético, la inflamación y el deterioro cognitivo (Moshkovits et al., 2015). Varias líneas de evidencia adicional implican a los receptores inmunológicos en el envejecimiento. Un informe interesante mostró que la ausencia del inmunorreceptor inhibitorio SiglecE acortó la esperanza de vida de los ratones y se asoció con varias condiciones relacionadas con el envejecimiento (Schwarz et al., 2015). La mayoría de estos receptores inmunológicos, incluidos CD300f y TREM2, se sobreexpresan con la edad (Grabert et al., 2016). El envejecimiento induce alteraciones metabólicas en las células microgliales y en macrófagos que contribuyen al deterioro cognitivo (Minhas et al., 2021), y tanto TREM2 como CD300f se ha demostrado que son esenciales para mantener la aptitud metabólica de las células microgliales y de macrófagos en diferentes condiciones neuropatológicas (Lago et al., 2020; Ulland et al., 2017). Además, la mayoría de los genes asociados a la enfermedad de Alzheimer están involucrados en las vías de fagocitosis/lisosomas (Podleśny-drabiniok et al., 2022), donde estos receptores inmunológicos que se unen a lípidos desempeñan un papel central. Finalmente, el análisis de las regiones genómicas no codificantes en la enfermedad de Alzheimer también señala a la microglía, macrófagos de barrera u otros macrófagos residentes en tejidos como actores centrales (Nott et al., 2019; Novikova et al., 2021), vinculando nuevamente estos tipos celulares y su fenotipo con condiciones relacionadas con la edad. En el último trabajo de nuestro grupo recientemente aceptado mostramos, en varias cohortes y en dos cepas diferentes de ratones CD300f-/- y WT de ambos sexos, una importante reducción en la esperanza de vida en los ratones CD300f -/-. Esto se asoció con inflamación sistémica, aumento del deterioro cognitivo, reducción de la captación de glucosa en el cerebro observada mediante escáneres PET y el radio ligando 18FDG, enriquecimiento en fenotipos de

envejecimiento/neurodegeneración, alteraciones en la proteostasis, senescencia, aumento de la fragilidad, y cambios metabólicos sistémicos dependientes del sexo. Además, la ausencia de CD300f alteró el fenotipo inmunometabólico de los macrófagos, también de forma dependiente del sexo. En conjunto, en ese trabajo proporcionamos evidencia sólida que sugiere que el receptor inmunológico CD300f en células mieloides contribuye al envejecimiento saludable (Evans et al., 2023).

HIPÓTESIS

El inmunorreceptor CD300f participa en la modulación de la supervivencia neuronal, en la función sináptica y en el refinamiento sináptico generando alteraciones comportamentales de tipo psiquiátricas en ratones.

OBJETIVO GENERAL

Caracterizar la participación del inmunorreceptor CD300f en el mantenimiento de la Homeostasis del SNC y su papel en patologías psiquiátricas.

OBJETIVOS ESPECÍFICOS

1-Determinar si CD300f modula la supervivencia neuronal a través de las interacciones neurona-microglía *in vitro e in vivo*.

2-Establecer si CD300f modula la sinaptogénesis y la fuerza sináptica *in vitro* mediante un mecanismo mediado por las células gliales.

3-Elucidar si deficiencias en el inmunorreceptor CD300f se asocian con comportamientos tipo trastornos neuropsiquiátricos en ratones.

4-Llevar a cabo una caracterización del fenotipo microglial en ausencia de CD300f, en un modelo de inflamación crónica (envejecimiento).

MATERIALES Y MÉTODOS

**Cultivos celulares*

Todo el trabajo experimental fue aprobado por la Comisión Ética de la UDELAR (Exp. Nº 070153-000528-14) y la Comisión de Ética para el Uso de Animales (CEUA) del Instituto Pasteur de Montevideo (N° 006-20) y se llevó a cabo de acuerdo con las directrices de la Federación de Asociaciones de Ciencia de Animales de Laboratorio (FELASA). Para la realización de los cultivos se utilizaron ratas Wistar neonatas P0-P1 de sexo indistinto. Se realizaron tres tipos de cultivos: co-cultivos de neuronas y células gliales disociadas del hipocampo (de ahora en adelante co-cultivos), cultivos de glía mixta y cultivos enriquecidos de neuronas. En todos los casos los cultivos se realizaron en placas de 20 mm en multiwell de 24 pocillos y las placas de cultivo se trataron con una solución de ácido acético al 5% que contiene 5 µg/ml de poli-D-lisina (Sigma-Aldrich) y 0.4 mg/ml de colágeno de cola de rata.

-Los co-cultivos se realizaron a partir de crías de ratas P0-P1, tal como se describe previamente con modificaciones menores (Branco et al., 2008). Las células disociadas de hipocampo se sembraron a una densidad de 6000 células por pocillo, con medios de cultivo a base de BME (GibCo) que contienen 10% de suero de ternero fetal (GibCo), Glutamax (GibCo), 20 mM de D-glucosa (GibCo), HEPES (1%), piruvato (1%) y penicilina/estreptomicina (GibCo), de ahora en adelante medio de cultivo de glía. Después de 6-7 días *in vitro* (DIV), las células disociadas del hipocampo obtenidas a partir de hipocampo de ratas P0-P1, se sembraron a una densidad de 30-40 mil sobre las células gliales y se mantuvieron en medios de cultivo a base de Neurobasal (GibCo) que contiene B-27 (GibCo), Glutamax, 20 mM de D-glucosa y penicilina/estreptomicina (GibCo), de ahora en adelante medio de cultivo de neuronas. A las 24-48 horas, para minimizar la proliferación se agregó AraC (arabinósido de citosina, 4 µM, Sigma-Aldrich) (Esquema 1).

-Los cultivos de glía mixta se realizaron a partir de crías de ratas P0-P1, como se describió previamente, las células disociadas de hipocampo se sembraron a una densidad de 6000 células por pocillo, con medio de cultivo de glía.

-Los cultivos enriquecidos de neuronas se realizaron a partir de crías de ratas P0-P1, tal como se describió previamente, las células disociadas del hipocampo se sembraron a una densidad de 150 mil neuronas por pocillo y se mantuvieron en medio de cultivo de neuronas. A las 24-48 horas, se agregó AraC (4 μM, Sigma-Aldrich).

Los tratamientos que se realizaron a los diferentes cultivos fueron a los 12 DIV y siempre se realizaron durante 72hs. Dependiendo del experimento los cultivos fueron tratados con rat CD300f-Fc (rCD300f-Fc) o IgG (0.01, 0.1, 1.0 μg/ml, producido para nosotros por Sinobiological sin conservantes), o LPS (1 μg/ml)+IL1β (10 ng/ml). Para bloquear la neurotoxicidad de CD300f-Fc, se usaron anticuerpo anti-CD300f / molécula similar a CMRF-35-1 (CLM1) hecho en ratón (1:20, MAB27881 R&D Systems) y anti-CLM1/CD300f hecho en cabra (1:50, Invitrogen, Catálogo # PA5-47399) o con IgGs controles IgG de ratón (1/200 R&D Systems) e IgG de cabra (1:200, Invitrogen) respectivamente. Para los ensayos de poda sináptica se incubó por 72hs con tetrodotoxina (TTX, 1 μM), AnexinaV (AV 0.5 μl/well), o inhibidor de caspasa III (0.1 μg/ml). Para los ensayos de medios condicionados se incubo por 72hs con GDNF (factor neurotrófico derivado de células gliales; 1.0 ng/ml), CPP (3-(2-Carboxipiperazin-4-il) propil-1-fosfónico, un antagonista selectivo del receptor N-metil-D-aspartato (NMDA); 100 μM, o CBX (carbenoxolona, bloqueador de las uniones intercelulares; 100 μM).

Se generaron dos tipos de medios condicionados: a partir de cultivos de glía mixta tratados a los 12 DIV con rCD300f-Fc o IgGs control (1.0, 0.01 μg/ml) durante 72hs; o a partir de co-cultivos tratados a los 12 DIV con rCD300f-Fc o IgGs control (1.0 μg/ml) durante 72hs. Los medios condicionados se usan a una concentración de 1:2.

Esquema de cultivos

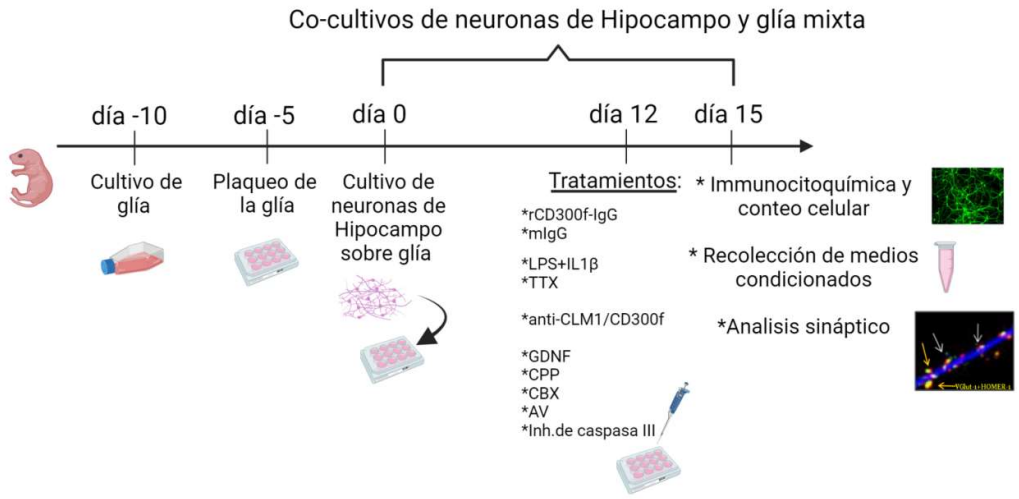

Esquema 1 Esquema de cultivos. Cultivos de hipocampo a partir de ratas neonatas P0-P1, y procesamientos posteriores.

**Ensayo de citoquinas*

Se midió la concentración de citoquinas en medios condicionados a partir de co-cultivos tratados ambos a los 12 DIV con rCD300f-Fc o IgG (1.0 µg/ml) durante 72hs. Se utiliza LEGENDplex™ Mouse Inflammation Panel (13-plex) withFilterPlate (Biolegend) para la medida de IL23, IL1α, IL1β, IFNγ, IFNβ, TNFα, MCP1/CCL2, IL12p70, IL10, IL6, IL17A, IL27 y GM-CSF de acuerdo a las instrucciones del fabricante.

**Ensayo de MTT*

Para el análisis de la supervivencia neuronal en cultivos enriquecidos de neuronas y en cultivos de glía mixta tratados en ambos casos con rCD300f-Fc o IgG (1.0 µg/ml) durante 72hs se realizó un ensayo de MTT. La viabilidad celular se estima indirectamente mediante este ensayo, que se basa en la reducción celular de sales de tetrazolio (Bernas & Dobrucki, 2002). Las células se incuban con MTT (concentración final de 0.5 mg/ml) durante 2 horas en la estufa de cultivo celular para permitir la reducción intracelular del MTT soluble a la forma insoluble del tinte formazán. Después de la incubación, el medio se retiró

cuidadosamente sin perturbar los cristales de formazán formados por las células viables. Luego, se añadió 100 µL de dimetilsulfóxido (DMSO) para solubilizar los cristales de formazán y se midió la absorbancia a 570 nm utilizando un lector de microplacas (Thermo/Labsystem Multiskan MS, Thermo Fisher Scientific, Waltham).

**Inmunocitoquímica*

Para la inmunocitoquímica, en todos los casos las células se fijaron en paraformaldehído al 4% (PFA 4%, Sigma-Aldrich) durante 15 minutos a temperatura ambiente (RT). Una vez fijadas se permeabilizó con PBS conteniendo Triton X-100 al 0.1% (Sigma-Aldrich) (PBST), y se bloqueó en PBS (Sigma-Aldrich) con glicina 0.2M, 10% de suero fetal bovino (FBS, Sigma-Aldrich) y Triton X-100 al 0.1% (Sigma-Aldrich), durante 1 hora a RT. Se añadió el anticuerpo o los anticuerpos primarios en PBS con 5% de FBS y se incubó durante 2hs a RT. Después de tres lavados en PBST, las células se incubaron con anticuerpos secundarios conjugados con fluoróforos 1h (AlexaFluor 488 o 594, Invitrogen; DyLight 649, Jackson). Se realizaron controles negativos, sin incubación con anticuerpos primarios, para descartar la tinción no específica.

Los anticuerpos primarios que se usaron como marcadores celulares fueron: i) como marcador neuronal el anti-βIII tubulina (1:1000, Abcam); ii) como marcador astrocítico utilizamos anticuerpos anti-GFAP (1:1800; Dakopatts-Z0334); iii) como marcador microglial utilizamos el anticuerpo anti-Iba1 (1:200, ab5076, Abcam); iv) y como marcador oligodendrocítico utilizamos el anticuerpo anti-adenomatous polyposis coli (APC) (1:200, OP80 CC-1, EMD4-Bioscience-Calbiochem).

Para los experimentos de plasticidad sináptica se utilizaron los siguientes anticuerpos: marcador neuronal anti MAP-2 (Microtubule Associated Protein 2; 1:1000 Abcam ab5392), y como marcadores sinápticos se utilizó, marcador presináptico VGlut1 (vesicular glutamate transporter; 1:7000 Sysy 135303) y marcador postsináptico Homer-1 (1:500 Sysy 160011).

**Inmunohistoquímica*

Se realizó inmunohistoquímica en cortes cerebrales de ratones hembra de 2.5 años de edad C57BL/6 de tipo salvaje (WT), ratones CD300f-/- (Genentech) (Feng et al., 2000) con el anticuerpo anti- CLEC7A (CLEC7A/Dectin-1 (extracellular) Polyclonal Antibody# ALR-062-200µL). Se inhibió la peroxidasa endógena con metanol 70%, 2% de H_2O_2 en PBS, en agitación y oscuridad a RT, posteriormente se permeabilizó con PBST, y se bloqueó en PBS (Sigma-Aldrich) con glicina 0.2M, 10% de FBS (Sigma-Aldrich) y Triton X-100 al 1.0% (Sigma-Aldrich), durante 1h RT. Se añadió anti-CLEC7A 1/500 en PBS con 5% de FBS y se incubó toda la noche a 4°C. Después de tres lavados en PBST los cortes se incubaron con anticuerpo secundario (anti-rat IgG (HRP) ab 6734 a 1/200) 1.5hs a RT. Después de tres lavados en PBS se reveló con DAB (Sigma-Aldrich) a 0.05 mg/ml en PBS con 3,5% de H_2O_2, se lavó con PBS, se dejó secar a RT. Se enjuagó con agua destilada, se deshidrató en soluciones de etanol con concentraciones crecientes y se aclaró en xileno. Luego, los cortes de tejido se montaron con DPX, se cubrieron con cubreobjetos y se observó bajo un microscopio de luz. Se realizaron controles negativos, sin incubación de anticuerpo primario, para descartar la tinción no específica.

**Análisis de imágenes*

-Supervivencia neuronal

Para la determinación de la supervivencia neuronal en los cultivos, se llevó a cabo la obtención de imágenes de inmunocitoquímica mediante el uso de un microscopio de epifluorescencia (OLYMPUS IX8), a un aumento de 20x. Las fotos se tomaron siempre siguiendo el mismo patrón, generando una cruz con los diámetros vertical y horizontal, en dicha dirección se toma una foto por campo. Se toman en total 16 imágenes por pocillo, comenzando por el centro del pocillo. El número de neuronas se determina sumando todas las células βIII-Tubulina positivas de cada una de las fotos adquiridas y ese número es el que se representa gráficamente por tratamiento y por pocillo. Para el conteo de las células se usó el *software ImageJ-Fiji*. En cada experimento, se normaliza a las condiciones de control (células no tratadas). El número de experimentos independientes realizados se indica en cada figura.

-Poda sináptica

Para el análisis de la poda sináptica se obtienen fotos de la inmunocitoquímica triple con los marcadores MAP-2 (649nm), VGlut1 (488nm) y Homer-1 (568nm). La obtención de las fotos se realizó mediante el uso de microscopio confocal (Zeiss, AxioObserver Z1, LSM 800), a un aumento de 63x y se analizaron utilizando el *software ImageJ-Fiji*. Los parámetros para la obtención de las imágenes se fijaron con el control y se mantuvieron a lo largo de toda la obtención. Las imágenes se obtienen realizando secciones ópticas y luego se realizó una proyección máxima, que es la que se utilizó para cuantificar. Por otro lado cabe destacar que se ajusto la intensidad del láser 488 (VGlut1) a un nivel donde no se detecta saturación de la fluorescencia asociada a VGlut1 (Esquema 2).

Los dos parámetros que se analizaron son: i) la intensidad de fluorescencia de VGlut1 que se midió en cada neurona individual, en la que se determinaron los contactos sinápticos por medio de la colocalización total o parcial de los marcadores sinápticos (VGlut1 y Homer-1), considerando colocalización total cuando hay un solapamiento del 100% entre los dos marcadores y parcial cuando el solapamiento no es 100% (ver esquema 2). En dichos puntos se midió la intensidad de florescencia de VGlut1 con el uso del *software ImageJ-Fiji* y lo que se graficó es el promedio de la intensidad de VGlut1 por neurona por tratamiento, ese dato nos permitió estimar la probabilidad de liberación del neurotransmisor VGlut1 (Herman et al., 2014; Wilson et al., 2005a); ii) la densidad sináptica se midió como la cantidad de contactos sinápticos (determinados como se describió previamente) en las primeras 30μm desde el soma por neurona, mediante el uso del *software ImageJ-Fiji* y se graficó la cantidad de contactos sinápticos el por neurona por tratamiento en 30 μm. En ambos casos se normalizó en función del control sin tratamiento.

Esquema inmunocitoquímica, determinación de co-localización

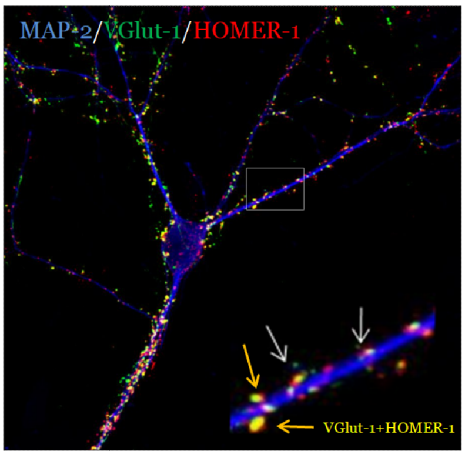

Esquema 2 Determinación de los contactos sinápticos. Las flechas amarillas indican la colocalización total de ambos marcadores, mientras que las blancas indican una colocalización parcial.

-Fenotipo microglial

Para el análisis del fenotipo microglial se analizó la inmunohistoquímica de CLEC7A+ en cortes de cerebro de ratones hembra C57BL/6 de tipo salvaje (WT), ratones CD300f-/- (Genentech) (Feng et al., 2000) de 2.5 años de edad (la cual se describió previamente). Para la obtención de las imágenes de microscopía óptica se utilizó el microscopio OLYMPUS CX41 con cámara Nikon a un aumento de 20x. A partir de las imágenes obtenidas se analizó: i) la densitometría de CLEC7A, evaluando la "Integrated density" por corte por animal (se analizan 3 cortes por ratón), ii) la cantidad de células CLEC7A+ mediante el conteo de todas las células positivas para el marcador por corte por animal (se analizan 3 cortes por ratón).

**Extracción de ARN y qPCR*

Se aisló ARN total de cerebro, utilizando el Reactivo TRIzol (Invitrogen, Cat # A93003) y posteriormente se purificó utilizando el kit Direct-zol RNA MiniPrep Plus (Zymo Research, Cat # R2070) siguiendo el protocolo del fabricante. Todas las muestras fueron tratadas con DNasa I. Las

concentraciones de ARN se cuantificaron utilizando Nanodrop y se realizaron transcripciones inversas utilizando la transcriptasa inversa M-MLV (Invitrogen, Cat # 28025013) y primers aleatorios (Invitrogen, Cat #48190011). Se llevó a cabo la reacción en cadena de la polimerasa cuantitativa (qPCR) utilizando reactivos TaqMan de Applied Biosystems, incluido el Fast Advanced Master Mix (Cat # 4444557) y las sondas siguientes: il1β (Cat # Mm01336189_m1), il6 (Cat # Mm00446190_m1), ccl2 (Cat # Mm00441242_m1), ccl3 (Cat # Mm00441259_g1), trem2 (Cat # Mm04209424_g1), cd11c/itgax (Cat # Mm00498698_m1), gh (Cat # Mm00433590_g1), prl (Cat # Mm00599950_m1) y gapdh (Cat # Mm99999915_g1). La expresión génica relativa de cada muestra se determinó mediante el método de análisis 2-ΔΔCT (Livak). Los genes objetivo se normalizaron al gen de referencia gapdh. La qPCR se realizó utilizando el equipo QuantStudio 3 con las siguientes condiciones de ciclado: 50 °C durante 2 min, 95 °C durante 2 min, 40 ciclos a 95 °C durante 1s y 60 °C durante 20s.

**Análisis de ANRseq y transcriptómica*

Para el experimento de RNAseq, un hemisferio cerebral de cuatro ratones hembras CD300f-/- y cuatro ratones hembras WT de 30 meses de edad se procesaron para extraer ARN total, como se describió anteriormente. La calidad del ARN se determinó en un Bioanalizador 2100 (Agilent). Un Número de Integridad del ARN (RIN) mayor a 8 se consideró aceptable para continuar con la construcción y secuenciación de la biblioteca, que se llevó a cabo en Macrogen (Corea). Se utilizó el kit TruSeq Stranded mRNA LT Sample Prep Kit (Illumina, 15031047 Rev. E) para la construcción de la biblioteca y se obtuvieron lecturas emparejadas (150x2 pares de bases) mediante secuenciación de Illumina. Los datos brutos se depositaron en NCBI (SRA) con el número de acceso SRR21771247-SRR21771254 (PRJNA885873). Se utilizó BBduk (Yu et al., 2012) para recortar las lecturas. La calidad de la secuencia de las lecturas crudas y procesadas se evaluó con FastQC v0.11.9 (Andrews 2010, http://www.bioinformatics.babraham.ac.uk/projects/fastqc/) y MultiQC v1.11. STAR se utilizó para mapear las lecturas al genoma del ratón utilizando GRCm39.primary_assembly y las anotaciones de genes de la versión M25 de

Gencode; el alineamiento se realizó utilizando las opciones estándar de ENCODE. Se obtuvieron recuentos de expresión a nivel de genes utilizando Feature Counts v2.0.1 con las opciones -p -s 2 -M--fraction.

Dada la matriz de recuento de lecturas obtenida, se utilizó el paquete R DESeq2 v1.36.0 para normalizar los datos, corregir la diferente profundidad de secuenciación de las bibliotecas y realizar pruebas de expresión diferencial. Se realizó un prefiltrado mínimo de la matriz de recuento para mantener solo aquellas filas que tienen al menos 10 lecturas. Se llevaron a cabo análisis de componentes principales con los paquetes R FactoMineR v2.4 y factoextra v1.0.7, basados en la transformación de datos estabilizada por varianza (vst, blind=TRUE) después de la selección de los 500 genes principales. Para las pruebas de expresión diferencial y para estimar los logaritmos de los cambios plegados (log2FC) entre los genotipos CD300f-/- y WT, se realizaron pruebas de Wald para ambas hipótesis |log2FC|>0 y |log2FC|>1.

Se realizó la contracción de las estimaciones del tamaño del efecto (log2FC) mediante el método apeglm implementado en DESeq2. Para la corrección de pruebas múltiples, se utilizó un enfoque estratificado de descubrimiento falso, con valores p corregidos por FDR de Benjamini y Hochberg. Definimos como genes diferencialmente expresados aquellos que presentaban un valor p corregido por FDR <0.1 y abs (log2FC corregido por apeglm)>0.35, un umbral que implica un tamaño de efecto mínimo de aproximadamente el 25%. Los mapas de calor de expresión se basaron en datos vst (blind=FALSE) y se produjeron con el paquete R pheatmap v1.0.12 (Kolde 2019 *pheatmap: Pretty Heatmaps*. R package version 1.0.12, https://CRAN.Rproject.org/package=pheatmap>); para cada conjunto de genes de interés, solo se incluyeron en el heatmap aquellos genes con un valor de expresión promedio superior a 10 y |apeglm log2FC|>0.35. Los gráficos de volcán se produjeron con el paquete R/Bioconductor EnhancedVolcano v1.14.0 (Blighe K., Rana S., Lewis M. EnhancedVolcano 2019: publication-ready volcano plots with enhanced coloring and labeling, https://github.com/kevinblighe/EnhancedVolcano). Se realizó un análisis funcional a través del análisis de sobre-representación (ORA) de las vías KEGG y los términos de la ontología génica (dominio de procesos biológicos). También

se llevó a cabo un análisis de enriquecimiento de conjuntos de genes (GSEA) de conjuntos de genes particulares. Se utilizaron los paquetes R/Bioconductor ClusterProfiler (Tianzhi Wu 2021, Yu, G., Wang, 2012) enrichplot (Yu G. 2022. enrichplot: Visualization of Functional Enrichment Result. R package versión 1.16.2, https://yulab-smu.top/) y org.Mm.eg.db (Carlson M. 2019 Genome wide annotation for Mouse. R package version 3.8.2.) para estos análisis funcionales. Los conjuntos de genes de interés se obtuvieron de las siguientes fuentes: el conjunto de genes ATF4 fue proporcionado amablemente por Mauro Costa-Matioli; los conjuntos de genes de microglía asociados a enfermedades (DAM) y de macrófagos inflamatorios de enfermedades (DIM) se obtuvieron de Silvin et al., 2022, Krasemann et al., 2017, broad DAM, conserved DAM, "Keren-Shaul" DAM, broad DIM and conserved DIM; la lista de genes de fragilidad se obtuvo de Cardoso et al., 2018; la firma génica de senescencia SenMayo se obtuvo de Ravichandran et al., 2018. También evaluamos el fenotipo de acumulación de gotas de lípidos en la microglía utilizando listas de genes especificadas en Marschallinger et al., 2020, aunque no se encontró enriquecimiento en el análisis de GSEA. Cabe destacar que todo el procesamiento bioinformático fue llevado a cabo por Natalia Rego integrante del grupo de Bioinformática del Instituto Pasteur de Montevideo.

**Animales*

-Inyección intracerebral

Todo el trabajo experimental fue aprobado por la Comisión Ética de la UDELAR (Exp. Nº 070153-000528-14) y la Comisión de Ética para el Uso de Animales (CEUA) del Instituto Pasteur de Montevideo (N° 006-20) y se llevó a cabo de acuerdo con las directrices de la Federación de Asociaciones de Ciencia de Animales de Laboratorio (FELASA). Para este estudio se utilizaron: ratones machos adultos de 4-5 meses, 6.Cg-Tg (Thy1-YFPH) 2Jrs heterocigotos para la proteína fluorescente amarilla (YFP-H) (Laboratorios Jackson), C57BL/6 de tipo salvaje (WT), ratones CD300f-/- (Genentech) (Feng et al., 2000) y ratas macho Wistar adultas de 4-5 meses. Se indujo el estado de anestesia en los animales, mediante la inhalación de una mezcla gaseosa de isofluorano (Abbott, Abbott Park) y oxígeno (4% isofluorano + 0,8% oxígeno, niveles de

inducción). Luego el animal se fijó en una platina estereotáxica (Kopf), con adaptadores específicos y se mantuvo la anestesia durante todo el procedimiento quirúrgico con 2% isofluorano + 0.4% oxígeno. Seguidamente, mediante material quirúrgico esterilizado, se procedió a la apertura de la piel de la cabeza y a la perforación del cráneo, mediante el uso de un taladro Dremel. Los animales se inyectaron en la neocorteza en las coordenadas: L: -0,15; V: -0,10 cm en ratón y L: -0,35; V: -0,20 cm en rata, con respecto a Bregma utilizando un marco estereotáxico y un nanoinyector (2 µl a 0.4 µl/minuto durante 5 minutos; Quintessential Stereotaxic Nanoinjector, Stoelting CO.) con solución salina (0.9% NaCl), rCD300f-IgG (30 µg/ml) o IgG de control (30 µg/ml). La aguja se dejó en el lugar durante 5 minutos adicionales para permitir la difusión en el parénquima cerebral. Tras suturar la herida, el animal es colocado sobre una manta térmica, hasta que abandona totalmente el estado de anestesia. Los tratamientos se distribuyeron al azar entre los animales en cada caja. Tres días después de que se realizó la inyección, los animales se anestesiaron y perfundieron de forma intracardíaca con PFA al 4% en tampón fosfato 0.1 M (pH 7.4). Los cerebros se fijaron posteriormente con PFA al 4% (4hs), se crioprotegieron en sacarosa al 30% y se congelaron con CO_2. Se realizaron secciones coronales paralelas en criostato (Criostato Leica CM 1850 UV) de 30 µm de espesor, de todo el cerebro. Los cerebros de rata y de ratón WT y CD300f -/- se tiñeron con Nissl, las secciones de tejido cerebral se sumergieron en una solución de azul de toluidina (15 ml de solución A compuesta por 0.5 % de azul de toluidina en agua y 200 ml de solución B compuesta por tres partes de ácido acético 0.2 M y dos partes de acetato de sodio 0.2 M) durante 20 minutos, se enjuagaron con agua destilada, se deshidrataron en soluciones de etanol con concentraciones crecientes y se aclararon en xileno. Luego, las secciones se montaron con medio de montaje DPX (Sigma-Aldrich), se cubrieron con cubreobjetos y se observaron bajo un microscopio de luz. Las neuronas dañadas se identifican por la pérdida de tinción de Nissl, mientras que las neuronas sanas muestran sustancia de Nissl en el citoplasma, una estructura de cromatina más relajada y nucleolos bien definidos. Para el cálculo del porcentaje de hemisferio lesionado, que es lo que se graficó se usó el *software ImageJ-Fiji*, con el que se realizaron dos medidas: la cuantificación del área pálida de Nissl lesionada con observación en paralelo

al microscopio (utilizando aumentos de 10X y 20X) y el área total del hemisferio contralateral (se utilizó el contralateral, para evitar posibles efectos del edema del hemisferio ipsilateral sobre la medida del volumen de lesión). Los datos se expresaron como "% del hemisferio lesionado" (lo que representa el área lesionada en función del área del hemisferio). En el caso de los ratones heterocigotos para la proteína fluorescente amarrilla H (YFP H), dado que el 3% de sus neuronas se ven de color verde, se obtuvieron las imágenes de los cortes seriados en un microscopio de epifluorescencia OLYMPUS, a un aumento de 20x. La neurotoxicidad en los cerebros de ratones YFP se determinó contando el número de neuronas YFP positivas en el hemisferio contralateral menos la cantidad de neuronas YFP del hemisferio lesionado. Los valores se expresaron como "% de muerte neuronal". Para todos los experimentos se utilizó el método ciego, método en el cual el operador no sabe a qué tratamiento fue sometido el animal a la hora de realizar el conteo neuronal o la determinación del área lesionada (Peluffo, et al., 2012).

-Test Comportamentales

Se utilizaron ratones adultos hembras y machos WT y CD300f−/- para el análisis del comportamiento. Todos los experimentos de comportamiento se realizaron durante el día bajo condiciones de luz tenue proporcionada por una lámpara roja y bajo un ambiente de mínimo ruido. El comportamiento fue monitoreado y grabado en video para ser posteriormente evaluado a ciegas. Para los experimentos de depresión inducidos por LPS, se inyectó LPS (2 mg/kg) por vía intraperitonial 24hs antes de las pruebas de comportamiento. En las representaciones gráficas, cada punto corresponde a un animal, el número de experimentos realizado en cada test se encuentra en el pie de figura.

OFT (Prueba de campo abierto): se realizó con el fin de evaluar la actividad locomotora espontánea de los ratones. El test se realizó en una caja blanca de acrílico que mide 40 cm × 60 cm × 50 cm de altura. Los animales se exponen durante 6 minutos en la arena, y la distancia total recorrida se registró y se evaluó utilizando el *software AnyMaze*. La arena se limpió con alcohol al 10% entre animales. El test se realizó en animales hembras y machos de 4 meses con y sin LPS.

MBT (Test de entierro de bolitas): se realizó con el fin de evaluar el comportamiento TOC de los ratones. El test se realizó en una caja con cáscara de arroz (de manera de facilitar el entierro de las bolitas), se colocaron 12 bolitas en 4 filas de 3 bolitas cada una, de manera simétrica, en una caja estándar. Se dejó al ratón 30 minutos. Al finalizar el tiempo se contó la cantidad de bolitas enterradas completamente o 2/3. Las bolitas se limpiaron con alcohol al 10% entre animales. El test se realizó en animales hembras y machos de 6 meses. Este test se ha validado para la evaluación de este tipo de comportamientos (Angoa-pérez et al., 2013).

STC (Prueba social de las Tres Cámaras): la prueba de tres cámaras de Crawley para la sociabilidad y la preferencia por la novedad social se realizó según se describe (Silverman et al., 2010). En resumen, el ratón experimenta primero un período de habituación de 5 minutos en el que se le permite explorar libremente una arena de Plexiglás de 60 x 40 x 23 cm dividida en tres cámaras de igual tamaño e interconectadas (izquierda, centro, derecha). La sociabilidad se mide durante un segundo período de 10 minutos en el que el sujeto puede interactuar con un vaso de rejilla vacío o un vaso que contiene un conespecífico desconocido emparejado por edad y sexo (ratón 1). Se registra el tiempo dedicado a interactuar con el vaso vacío o con el ratón 1 desconocido contenido en el otro vaso, así como el tiempo pasado en cada cámara, utilizando el *software AnyMaze*. La ubicación del vaso vacío en la arena izquierda o derecha durante el período de sociabilidad se equilibró entre los ensayos. Finalmente, la preferencia por la novedad social se evalúa introduciendo un segundo ratón desconocido (ratón 2) en el vaso previamente vacío. Se registró el tiempo pasado en cada arena, así como el tiempo dedicado a interactuar con el ratón 1 o el ratón 2, utilizando el *software* automatizado *AnyMaze*. Se realizó en ratones hembra de 6 meses (Esquema 3).

Esquema arena de comportamiento de las tres cámaras, con los tres períodos

Esquema 3 Arena del comportamiento de las tres cámaras de Crawley. Representa los tres periodos del test, Habituación (5 min), Sociabilidad (10 min), Novedad Social y memoria (10 min).

SST (Prueba de Splash de Sacarosa): en esta prueba, se aplica una solución de sacarosa al 10% sobre el pelaje dorsal de los ratones. Esta solución viscosa ensucia al animal y provoca que inicie el comportamiento de acicalamiento. Este test se ha validado para la evaluación de anhedonia (Pothion et al., 2004). Después de aplicar la solución de sacarosa, los animales se colocan individualmente en recipientes de vidrio y se graban durante 5 minutos. El tiempo que tardan en comenzar el primer acicalamiento y la cantidad total de comportamiento de acicalamiento son los parámetros asociados con el comportamiento motivacional y el comportamiento anhedónico y de autocuidado, respectivamente. El recipiente se limpia con etanol al 10% entre animales para excluir posibles pistas olfativas. Se realizó en animales WT y CD300f -/-hembras y machos de 3 meses y en un grupo de hembras y machos de 7 meses con y sin LPS. También se realizó en un grupo de hembras de 3 meses de una colonia CD300f -/- diferente, generada por nuestro grupo en colaboración con la UBAL del IPMont (denominada $CD300f^{IPMont}$) y en un grupo de hembras CD300f knockout condicionales (KOc) a las 3 y 5 semanas de la administración de Tamoxifeno (TMX).

-Inyección inhibidor CCR2+

Se utilizaron ratones adultos hembras WT y KOc[#] de 4 meses de edad. Se les administró TMX IP a 100 mg/Kg por 4 días consecutivos, a partir del día 5 se inyectó el inhibidor de CCR2 (RS102895) IP a 5 mg/Kg o vehículo (agua) durante 13 días consecutivos siempre a la misma hora. Se realizó el SST tal como se describió previamente a las 3 y a las 5 semanas de la última inyección de TMX de modo de evaluar el efecto del inhibidor de CCR2.

[#]Animales KOc: Se llevó a cabo la generación de ratones con el gen *cd300f* flanqueado por sitios loxP (cd300floxP/loxP) (fue realizado por el compañero Andres Cawen, en el marco de su Maestría). Para el establecimiento de la colonia de ratones KOc se utilizaron los animales generados con el gen cd300f flanqueado (Cd300floxP), que permitan la recombinación y eliminación de la

secuencia intermedia a los sitios loxP insertados, y ratones Cx3cr1tm2.1(cre/ERT2)Litt/WganJ(Parkhurst et al., 2013), adquiridos a The Jackon Laboratory (JAX stock #021160), que expresan tras el promotor del receptor de fractalquina una recombinasa modificada con el receptor de estrógenos humano (CreERT2), permitiendo inducir la recombinación únicamente en presencia de TMX en aquellas células que expresen constitutivamente este gen, ya que el TMX se une al receptor de estrógeno y solo así se da la traslocación al núcleo de la CreERT2 (Esquema 4).

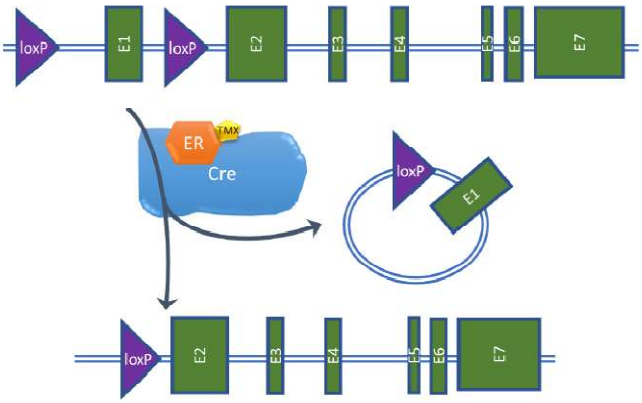

Esquema 4 Sistema de recombinación Cre-lox de los ratones KOc. La recombinasa CreERT2 presenta expresión constitutiva por estar inserto tras el promotor del gen del receptor de fractalquina; se mantiene en el citoplasma en estado basal y solo en presencia de TMX es traslocada al núcleo. CreERT2 reconoce los sitios loxP insertados en el ADN y elimina la secuencia intermedia a estos, en consecuencia, tras la recombinación se pierde el exón 1 y las secuencias reguladoras previas del gen clm1 (ortólogo murino de cd300f) (Se tomó de la tesis de Maestría de Andrés Cawen).

**Análisis estadístico*

Se utilizó el análisis de varianza de una vía (ANOVA) seguido de la prueba de Newman-Keuls o análisis post hoc de Tukey para los datos experimentales con distribución normal. Para la comparación de dos grupos se utilizó el análisis de t de Student, en el caso de ser valores dependientes el de t de Student dependiente. Los análisis estadísticos se realizaron con el *software Prism 8*, y los datos se muestran como media ± error estándar de la media (SEM), considerando $p < 0.05$ como estadísticamente significativo. El número de experimentos independientes realizados se indica en las figuras. No se realizó ninguna prueba de valores atípicos y no se eliminó ningún valor atípico

potencial.

RESULTADOS

CAPITULO 1 CD300f CONTRIBUYE AL MANTENIMIENTO DE LA VIABILIDAD NEURONAL

Caracterización de los co-cultivos

Con el objetivo de analizar el rol de CD300f en la supervivencia celular y en las interacciones neurona-glía *in vitro*, utilizamos el modelo de co-cultivos de hipocampo. Analizamos la composición celular de los co-cultivos por medio de inmunocitoquímica. Se detectó 36% de neuronas βIII-Tubulina positivas, 38% de astrocitos GFAP positivos, 15% de oligodendrocitos APC positivos y 11% de microglía IBA1 positivas (Figura 6).

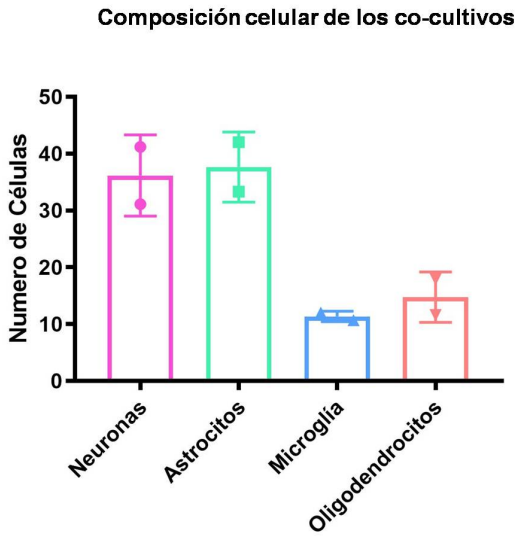

Figura 6: Composición celular de los co-cultivos de neuronas y células gliales disociadas del hipocampo. Inmunomarcado contra βIII-Tubulina para neuronas, GFAP para astrocitos, IBA1 para microglía y APC para oligodendrocitos. Los datos muestran la media ± error estándar de la media (SEM), se realizó un experimento por duplicado.

A continuación, se realizaron co-cultivos y como herramienta para inhibir CD300f se utilizó una proteína de fusión compuesta por el dominio extracelular del receptor CD300f de rata fusionado con una región Fc IgG2a de ratón (rCD300f-IgG2a). La proteína de fusión rCD300f-IgG2a soluble inhibe la activación de CD300f por sus ligandos endógenos, siendo ésta una estrategia

ampliamente utilizada para modular los receptores inmunes (Colonna, 2023; Lloyd et al., 2019; Pannunzio et al., 2022). A los 12 días *in vitro* (DIV), se trataron los co-cultivos con la proteína de fusión a diferentes concentraciones (0.01, 0.1, y 1.0 μg/ml) durante 72hs, así como con los controles de isotipo mIgG2a a las mismas concentraciones.

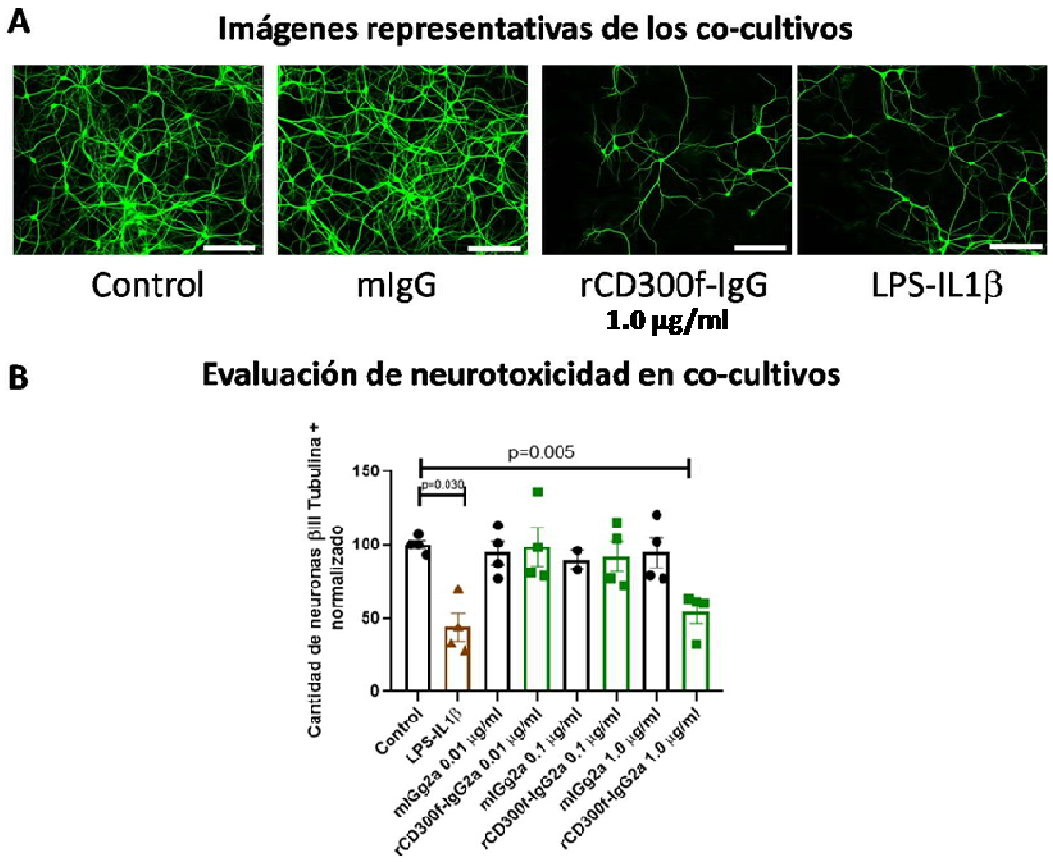

Figura 7: La inhibición de CD300f *in vitro* en co-cultivos induce neurotoxicidad a altas concentraciones. Los co-cultivos fueron tratados con rCD300f-IgG, IgG, LPS+IL1β y control (sin tratamiento) a los 12 DIV, durante 72hs. **(A)** Imágenes representativas de los co-cultivos con células positivas para βIII-Tubulina. Escala de barras 400 μm. **(B)** En los co-cultivos se contaron las células positivas para βIII-Tubulina, y se representan como células βIII-Tubulina+normalizadas. LPS+IL1β se utilizaron como control positivo de muerte neuronal en condiciones inflamatorias. Se realizaron dos experimentos independientes. Los datos se muestran como media ± SEM; p corresponde a un análisis de varianza de una vía seguido de la prueba de Tukey.

Observamos que a altas concentraciones (1.0 μg/ml) se indujo una muerte de células βIII-Tubulina positivas de aproximadamente el 50% en comparación

con el control sin tratamiento y con el control de isotipo (Figura 7A-B). Además, la incubación con compuestos que generan un insulto proinflamatorio bien conocido como el LPS (1.0 μg/ml)+IL1β (10ng/ml), mostró una reducción similar en el número de neuronas βIII-Tubulina positivas (aproximadamente 50%) (Figura7B). Dado que el primer capítulo de esta tesis busca estudiar la neurotoxicidad que ocurre por la interrupción de la interacción endógena del receptor-ligando, seguimos trabajando con el receptor soluble a la concentración de 1.0 μg/ml.

El isotipo IgG2a de ratón puede activar el complemento y la citotoxicidad celular dependiente de anticuerpos (ADCC) (X. Wang et al., 2018). Para evitar estos posibles eventos no específicos de la proteína de fusión rCD300f-IgG2a, generamos una proteína de fusión adicional compuesta por el dominio extracelular de CD300f de rata fusionado con la región Fc de IgG1, que presenta menor capacidad de activación del complemento y menor activación de ADCC (X. Wang et al., 2018).

De modo de validar el uso de la nueva proteína de fusión se reiteró el experimento de supervivencia de neuronas en las mismas condiciones que con rCD300f-IgG2a pero con el uso de rCD300f-IgG1. La incubación de co-cultivos con la proteína de fusión rCD300f-IgG1 a altas concentraciones, reproduce el efecto tóxico de la inhibición de CD300f por medio de rCD300f-IgG2a, mostrando aproximadamente un 60% de muerte neuronal cuando se compara con el control sin tratamiento, o con el control de isotipo IgG (Figura 8). Es por esto que a partir de aquí utilizamos indistintamente las dos versiones de la proteína de fusión rCD300f-IgG2a y rCD300f-IgG1.

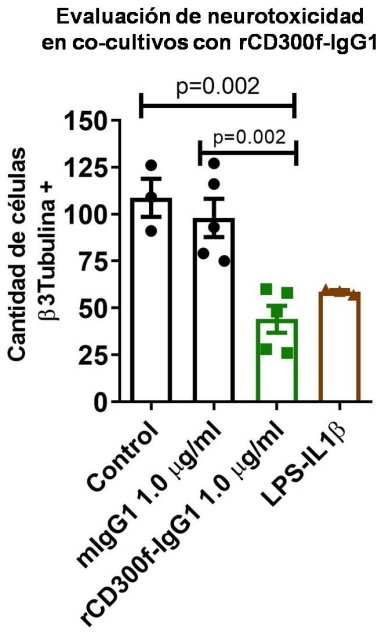

Figura 8: La inhibición de CD300f *in vitro* en co-cultivos induce neurotoxicidad a altas concentraciones. Los co-cultivos fueron tratados con rCD300f-IgG, IgG, LPS+IL1β y control (sin tratamiento) a los 12 DIV, durante 72hs. En los co-cultivos se contaron las células positivas para βIII-Tubulina, y se representan como células βIII-Tubulina+normalizadas. LPS+IL1β se utilizaron como control positivo de muerte neuronal en condiciones inflamatorias. Se realizaron dos experimentos independientes. Los datos se muestran como media ± SEM; p corresponde a un análisis de varianza de una vía seguido de la prueba de Tukey.

Para confirmar la especificidad del efecto, y asegurar de que la muerte ocurre específicamente debido a la inhibición de la interacción endógena receptor-ligandos, y no debido a efectos inespecíficos mediados por el Fc de la proteína de fusión o contaminantes en el proceso de producción y purificación de la proteína de fusión, se realizaron co-cultivos que se trataron con la proteína de fusión preincubada con dos anticuerpos policlonales anti-CD300f diferentes (anti-CD300fhecho en rata R&D Systems o con anti-CD300f hecho en cabra Invitrogen) o sus controles de isotipo. El efecto tóxico se eliminó por completo en ambos casos (Figura 9).

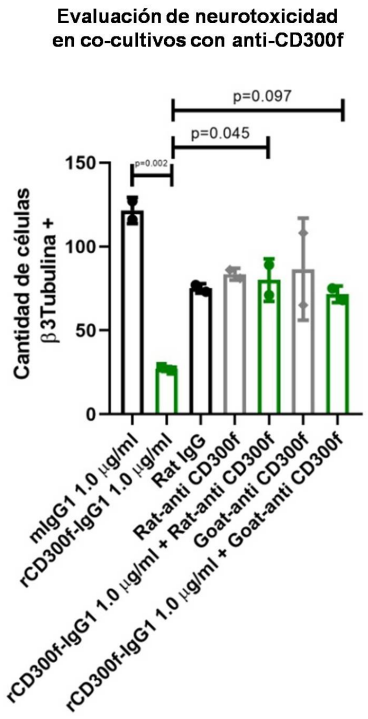

Figura 9: La muerte neuronal inducida por rCD300f-Fc se previene al incubar la proteína de fusión con anticuerpos anti-CD300f. Los co-cultivos fueron tratados con CD300f-IgG, IgG de control o anticuerpos policlonales anti-CD300f, y se contaron las células positivas para βIII-Tubulina 72 horas después, representadas como células βIII-Tubulina+normalizadas. Se realizó un experimento por duplicado. Los datos muestran la media ± SEM; p corresponde a un análisis de varianza de una vía seguido de la prueba de Tukey.

Este resultado valida el uso de la proteína de fusión rCD300f-IgG1 y demuestra que el efecto de toxicidad en los co-cultivos se debe a la inhibición de la interacción endógena entre el receptor y el ligando y que no ocurre por efectos no deseados del Fc, u otros posibles contaminantes provenientes de la producción recombinante de la proteína de fusión.

La inhibición de CD300f endógeno in vivo ¿es capaz de recapitular los efectos neurotóxicos observados in vitro?

Con el objetivo de analizar si la inhibición del CD300f endógeno *in vivo* genera neurotoxicidad al igual que *in vitro*, se utilizó el modelo de inyección intracerebral simulando el tratamiento con la proteína de fusión en los co-cultivos. Una diferencia sin embargo, es que en este caso ocurre una pequeña lesión penetrante al insertar la aguja. Se realizó el análisis de la supervivencia

neuronal *in vivo*, luego de la inyección de solución salina (vehículo), rCD300f-IgG2a (30 µg/ml) o IgG2a de control (30 µg/ml) en la neocorteza de ratas y de ratones y se evaluó el volumen de lesión. En las ratas se determinó la lesión mediante tinción de Nissl, expresada como "% de hemisferio lesionado" (Figura 10A). En los ratones Thy1-YFP-H, con las mismas condiciones de inyección la neurotoxicidad se determinó contando el número de neuronas YFP positivas en el hemisferio contralateral y restando las neuronas YFP positivas en el hemisferio lesionado, y luego se expresó como "% de muerte neuronal" (Figura 10C).

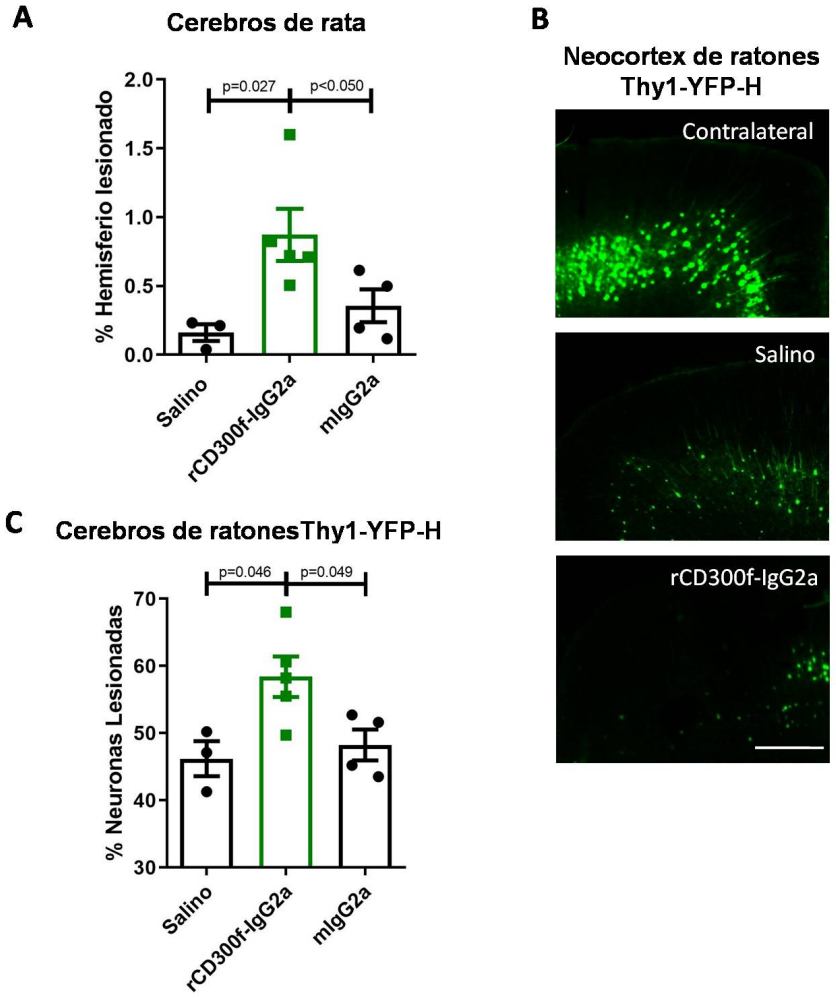

Figura 10: La inhibición de CD300f induce neurotoxicidad *in vivo*. (A) Gráficos de barras que muestran el porcentaje del volumen de lesión medido mediante tinción de Nissl en la corteza de ratas 72 horas después de ser inyectadas con suero fisiológico (n=3), rCD300f-IgG2a (n=5, 30 µg/ml) o IgG2a de control (n=4, 30 µg/ml). **(B)** Imágenes representativas de la corteza de ratones Thy1-YFP-H inyectados con suero fisiológico o rCD300f-IgG2a, y la corteza

contralateral no inyectada (Escala de barras 100 µm). **(C)** Gráfico de barras que muestra el número de neuronas corticales YFP+ en la corteza Thy1-YFP-H después de la inyección intracortical de suero fisiológico (n=4), rCD300f-IgG2a (n=7, 30 µg/ml) o IgG2a de control (n=6, 30 µg/ml). Los datos muestran la media ± SEM; p corresponde a un análisis de varianza de una vía seguido de la prueba de Newman-Keuls.

En concordancia con los resultados obtenidos en los co-cultivos, la inhibición de CD300f después de una lesión cortical penetrante induce una neurotoxicidad incrementada, observándose un aumento significativo del volumen de lesión en comparación con los animales inyectados con solución salina o control mIgG2a, tanto en rata como en ratón (Figura 10A y C).

Para la o es necesario un entorno complejo que incluye neuronas, células gliales y factores solubles

Para determinar si el mecanismo de toxicidad de rCD300f-Fc involucra un tipo celular específico o si rCD300f-Fc es tóxico para las neuronas de manera independiente a las células gliales, se incubaron las neuronas de hipocampo o cultivos de glía mixta por separado con rCD300f-IgG2a o control de isotipo IgG2a, y se midió la viabilidad celular mediante el método de reducción de MTT 72 horas después (Figura 11).

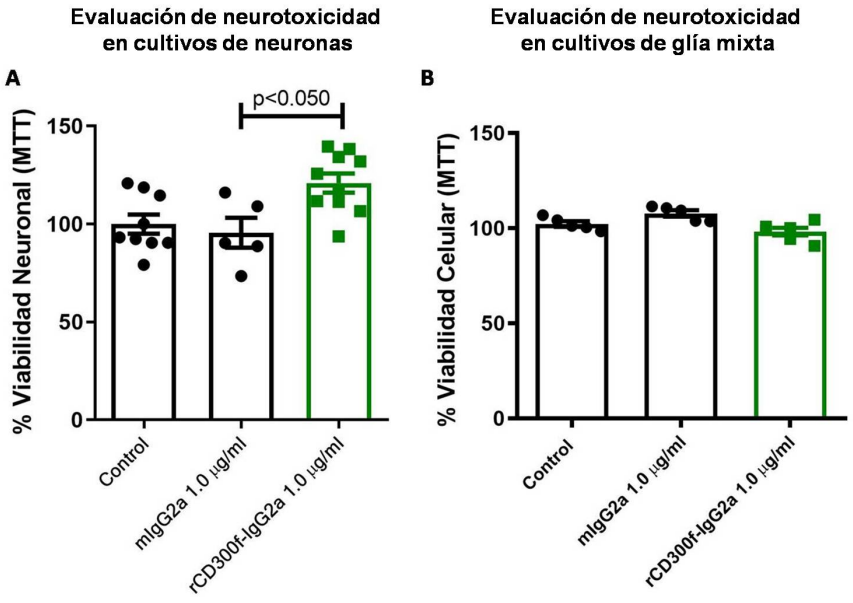

Figura 11: La inhibición de CD300f *in vitro* en cultivos enriquecidos de neuronas o en cultivos de glía mixta no induce neurotoxicidad a altas concentraciones. (A) Se incuban cultivos enriquecidos de neuronas de hipocampo o **(B)** se incuban cultivos de glía

mixta con rCD300f-IgG2a o control de isotipo IgG2a y se determina la viabilidad neuronal mediante el ensayo de MTT. Se realizan dos experimentos independientes. Los datos se muestran como media ± SEM; p corresponde a un análisis de varianza de una vía seguido de la prueba de Tukey.

La proteína de fusión no genero muerte en los cultivos enriquecidos de neuronas en comparación con los controles, sin embargo, indujo un aumento significativo en la reducción de MTT. Se sabe que en ensayos de viabilidad, el MTT es reducido principalmente por la coenzima NAD (P) H y enzimas glicolíticas, por lo tanto, la reducción de MTT celular representa una medida de la tasa de producción de NAD (P) H glicolítico (Stockert et al., 2018). Por lo antes expuesto, nuestros datos sugieren un aumento en la actividad metabólica en las neuronas tratadas con rCD300f-IgG2a. Además, abren la posibilidad de que CD300f soluble pueda estar interactuando con un ligando endógeno expresado en la superficie neuronal (Figura 11A). El tratamiento de cultivos mixtos de células gliales con rCD300f-IgG2a o IgG2a control no mostró una disminución en la viabilidad celular (Figura 11B).

Para comprender mejor el mecanismo por el cual la inhibición del CD300f endógeno en co-cultivos induce la muerte neuronal, se analizó la posibilidad de que sea necesario un factor soluble secretado por las células gliales o por las neuronas, o que sea necesario el contacto celular directo para que ocurra este proceso. Para ello, se trataron cultivos neuronales de hipocampo con medios condicionados derivados de:

-co-cultivos tratados con la proteína de fusión a una concentración de 1.0 μg/ml durante 72hs (MC co-cultivos)

-cultivos de glía mixta tratados con la proteína de fusión a una concentración de 1.0 μg/ml durante 72hs (MC glía mixta)

-diferentes controles: MC control, son medios condicionados de pocillos control (tanto en co-cultivos como en cultivos de glía mixta) que no fueron tratados, y los MC mIgG son medios condicionados de los pocillos tratados (tanto en co-cultivos como en cultivos de glía mixta) con el control de isotipo.

Tratamos cultivos enriquecidos en neuronas de hipocampo con medio condicionado derivado de co-cultivos tratados con rCD300f-IgG1 (1.0 μg/ml) o

IgG1 control (1.0 μg/ml); y cultivos enriquecidos de neuronas de hipocampo con medio condicionado derivado de cultivo de glía mixta tratados con rCD300f-IgG1 (1.0 μg/ml) o IgG1 control (1.0 μg/ml), durante 72 hs. Se determinó la supervivencia neuronal por el conteo de células βIII Tubulina+ (Figura 12A-B).

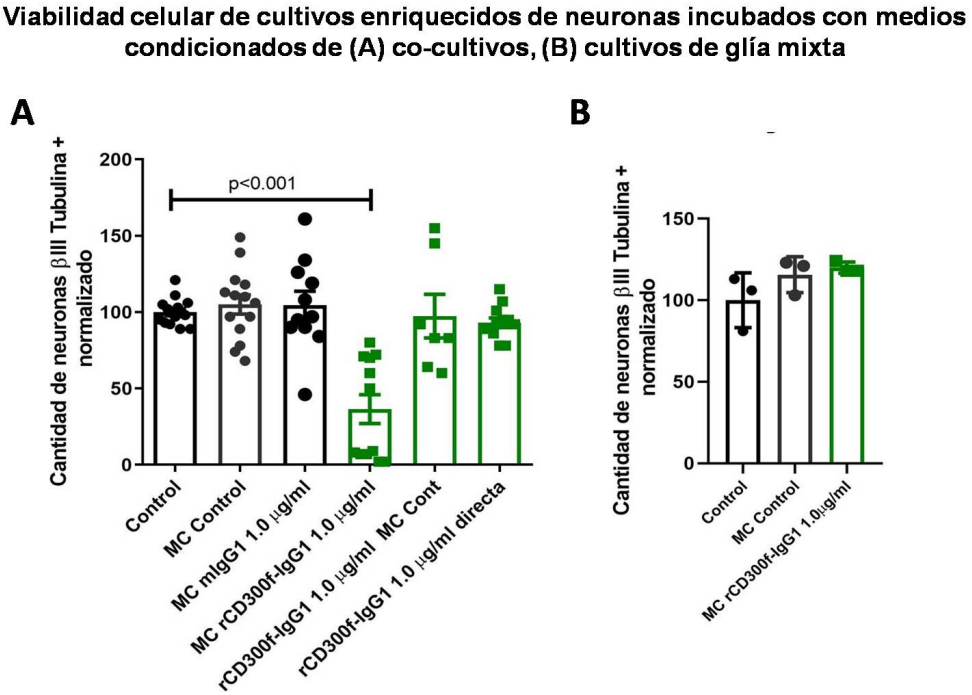

Figura 12: El medio condicionado de co-cultivos tratados con una alta dosis de CD300f-IgG es neurotóxico. **(A)** Se incubaron cultivos enriquecidos de neuronas con medio condicionado de co-cultivos tratados con rCD300f-IgG1 (1,0 μg/ml) o IgG1 de control (1,0 μg/ml). Como controles adicionales, incubamos neuronas con medio condicionado de control y rCD300f-IgG1 fresca (1,0 μg/ml), o rCD300f-IgG1 fresca (1,0 μg/ml directa) (se realizaron tres experimentos independientes). **(B)** Se incubaron cultivos enriquecidos de neuronas con medio condicionado de cultivos de glía mixta (se realizó un solo experimento). Los datos muestran la media ± SEM; p corresponde a un análisis de varianza unidireccional seguido de la prueba de Tukey.

Se observó un fuerte efecto tóxico del medio condicionado proveniente de los co-cultivos tratados con la rCD300f-IgG1, con una muerte neuronal de aproximadamente 60% en comparación con el control sin tratamiento, con el tratado con medio condicionado control, así como con el tratado con medio condicionado con mIgG. Además dicha toxicidad no fue mediada por la combinación de rCD300f-IgG1 con otros componentes del medio condicionado, ya que no se mostró muerte neuronal cuando se incubó el cultivo enriquecido de

neuronas con medio condicionado control más el agregado de rCD300f-IgG1 fresca (1.0 μg/ml, Figura 12A). Sorprendentemente, a diferencia de lo que pasa con los medios condicionados provenientes de los co-cultivos tratados con rCD300f-IgG1, el medio condicionado de los cultivos de glía mixta tratados con rCD300f-IgG1 no resultó tóxico para los cultivos enriquecidos de neuronas, no mostrando diferencias significativas en la supervivencia neuronal cuando se compara con los controles (Figura 12B). Por lo tanto, para la inducción de la neurotoxicidad observada es necesario un entorno complejo, que incluye neuronas, células gliales y factores solubles.

Es conocido que el inmunorreceptor CD300f puede regular negativamente la activación proinflamatoria de las células inmunes innatas, incluso después de la activación de diversos receptores tipo Toll (S.-M. Lee et al., 2011). Para analizar si la neurotoxicidad está dada por un fenotipo proinflamatorio inducido por la inhibición de la señalización de CD300f, se midieron las citoquinas de los medios condicionados de: i) co-cultivos tratados con rCD300f-IgG1 (1.0 μg/ml) durante 72hs; y ii) co-cultivos tratados con mIgG1 (1.0 μg/ml) durante 72hs. Se utilizó el Kit de Biolegend LegendPlex Mouse Inflammation Panel (13-plex) (Figura 13A). No se detectaron alteraciones significativas en la concentración de citoquinas IL23, IL1α, IL1β, IFNγ, IFNβ, TNFα, MCP1/CCL2, IL12p70, IL10, IL6, IL17A, IL27 y GM-CSF en el medio condicionado de los co-cultivos tratados con rCD300f-IgG1 ni en los medios condicionados de los co-cultivos tratados con mIgG sugiriendo que no se genera neurotoxicidad por las vías proinflamatorias clásicas (Figura 13A).

Para caracterizar mejor el mecanismo neurotóxico, se incubaron cultivos enriquecidos de neuronas de hipocampo con medio condicionado de co-cultivos tratados con rCD300f-IgG1 o tratados con IgG1 como control, y además, los cultivos fueron co-tratados con: i) factor neurotrófico derivado de células gliales (GDNF, 1.0 ng/ml); ii) inhibidor del receptor de glutamato NMDA 3-(2-Carboxipiperazin-4-il)propil-1-fosfónico (CPP, 100 μM), o iii) bloqueador de las uniones GAP y de los hemicanales de conexina, carbenoxolona (CBX, 100 μM) (Figura 13B).

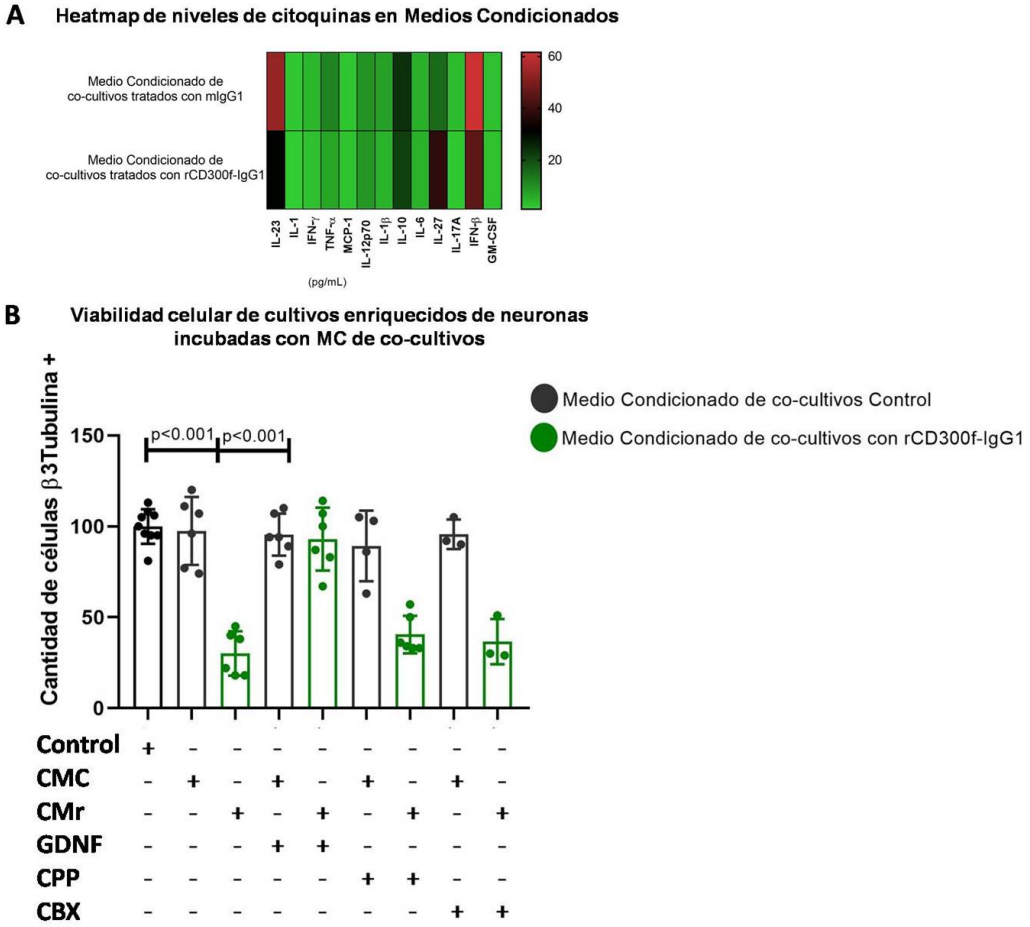

Figura 13: GDNF es capaz de rescatar la neurotoxicidad provocada por el medio condicionado de co-cultivos, en cultivos enriquecidos de neuronas. **(A)** Se midieron los niveles de citoquinas en el medio condicionado de co-cultivos tratados con rCD300f-IgG1 y con IgG1. **(B)** Se incubaron cultivos enriquecidos de neuronas con medio condicionado de cocultivos tratados con rCD300f-IgG1 (1,0 µg/ml) o IgG1 de control (1,0 µg/ml), y se co-trataron con factor trófico GDNF (1,0 ng/ml); inhibidor del receptor de glutamato CPP (100 µM); o inhibidor de uniones gap y hemicanales de conexina CBX (100 µM). Se realizaron dos experimentos independientes. Los datos muestran la media ± SEM; p corresponde a un análisis de varianza unidireccional seguido de la prueba de Tukey.

El tratamiento con medio condicionado de co-cultivos tratados con rCD300f-IgG1 mostró una mortalidad neuronal de aproximadamente 70% en comparación con las condiciones de control sin tratamiento y control con MC control, como ya se había observado previamente. De todos los tratamientos adicionales, solo GDNF fue capaz de revertir la toxicidad, no mostrando diferencias significativas en la supervivencia neuronal en comparación con el control (sin tratamiento), o el control tratado con medio condicionado de mIgG1

(Figura 13B). Esto sugiere que los mediadores tóxicos como el glutamato o el ATP no están involucrados en el mecanismo neurotóxico, y que otros posibles mediadores como lípidos o proteínas tóxicas podrían ser responsables del efecto tóxico.

Muchos de los ligandos que se unen a CD300f, como la fosfatidilserina, la esfingomielina o las lipoproteínas, también son compartidos con otros miembros de la familia de receptores inmunitarios CD300 y con el receptor inmunitario TREM2. Para determinar si los efectos de CD300f-Fc son mediados por la inhibición de otros receptores inmunitarios o si son específicos para CD300f, se realizaron experimentos en ratones CD300f-/-. En estos experimentos se inyectaron cerebros de ratones WT o CD300f-/- con rCD300f-Fc (30 µg/ml) o IgG control (30 µg/ml) directamente en la corteza cerebral como se realizó previamente (Figura 10C), y se evaluó el porcentaje del hemisferio lesionado 72 horas después utilizando tinción de Nissl (Figura 14).

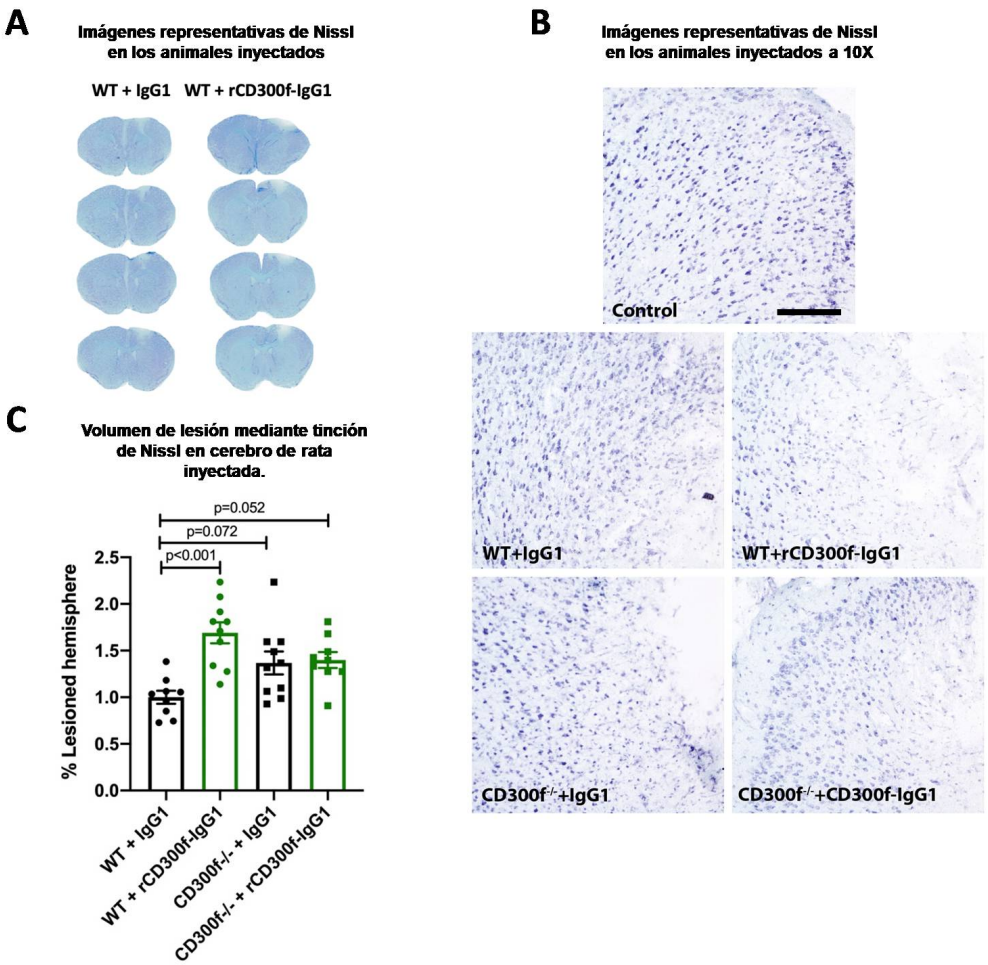

Figura 14: La inhibición de CD300f por rCD300f-Fc es específica. **(A, B)** Imágenes representativas de cortes cerebrales teñidas con Nissl 72 horas después de que animales WT o CD300f-/- fueran inyectados intracorticalmente con IgG1 o rCD300f-IgG1 (Barra de escala 200 μM). **(C)** El análisis del volumen de la lesión se realizó mediante tinción de Nissl 72 horas después de la inyección (WT inyección de IgG1 n=9, rCD300f-IgG1 n=10; KO inyección de IgG1 n=10 y rCD300f-IgG1 n=9). Se realizaron dos experimentos independientes en diferentes días, incluyendo todos los tratamientos en cada día. Los datos muestran la media ± SEM; p corresponde a un análisis de varianza unidireccional seguido de la prueba de Tukey.

La inyección de CD300f-IgG1 en animales WT resultó en neurotoxicidad, con un aumento de aproximadamente el 70% en el hemisferio lesionado en comparación con la inyección de IgG1 de control. Sin embargo, y concordantemente con un efecto específico, no se observó ningún efecto significativo cuando se inyectó CD300f-IgG1 en comparación con la inyección de IgG1 control en ratones CD300f-/-. Estos resultados sugieren que los efectos de la proteína de fusión rCD300f-Fc se encuentran mediados por la inhibición del receptor endógeno CD300f.

Además, se observó que tanto la inyección intracortical de IgG1 de control como de rCD300f-IgG1 en ratones CD300f-/- mostraron una fuerte tendencia hacia el aumento del volumen de la lesión en comparación con los ratones WT inyectados con IgG1 control. El hemisferio lesionado de los animales CD300f-/- mostró un aumento de aproximadamente 40% ($p=0.072$) cuando se inyectó con IgG1 de control y un aumento de aproximadamente 40% ($p=0.052$) cuando se inyectó con rCD300f-IgG1, respectivamente. Estos hallazgos sugieren que la ausencia de CD300f contribuye a la neurotoxicidad después de una lesión cerebral penetrante.

En resumen, estos resultados indican que los efectos de CD300f-Fc se encuentran específicamente relacionados con la inhibición del receptor endógeno CD300f. Además, la ausencia de CD300f en sí misma parece contribuir a la neurotoxicidad después de una lesión cerebral penetrante, por lo que CD300f estaría participando en la neuroprotección y el restablecimiento de la homeostasis del SNC.

CAPITULO 2 CD300f PARTICIPA EN EL PRUNING SINÁPTICO REALIZADO POR LA MICROGLÍA

CD300f modula la sinaptogénesis y la fuerza sináptica in vitro mediante un mecanismo mediado por células gliales.

Además del mantenimiento de la homeostasis en el SNC, se ha demostrado que la microglía participa en la poda sináptica y en la modulación de la neurotransmisión (Stevens et al., 2007).

Para evaluar si CD300f se encuentra involucrado en la modulación de la función sináptica, se analizó el efecto de bloquear CD300f sobre la sinaptogénesis y la abundancia de VGlut1 sináptico en co-cultivos. Como lo describe la bibliografía (Herman et al., 2014; Wilson et al., 2005) una forma de estimar cambios en la fuerza sináptica es utilizando el marcador presináptico VGlut1, ya que cambios en la abundancia de este marcador se correlacionan con la probabilidad de liberación (pr) de contactos sinápticos excitadores. Se realizaron co-cultivos de neuronas y glía mixta y se trataron durante 72hs con rCD300f-IgG2a a diferentes concentraciones, o con sus respectivos controles de isotipo mIgG2a y se dejaron controles sin tratamiento. Se incluyó el tratamiento de LPS-IL1β como control positivo de neuroinflamación y se realizó un tratamiento adicional con TTX (Nakayama et al., 2005). La TTX es una neurotoxina que bloquea los canales de sodio dependientes de voltaje y se utiliza como inductor de la plasticidad sináptica homeostática (Vitureira et al., 2011). Se realizó inmunocitoquímica en los co-cultivos con marcadores presinápticos y postsinápticos VGlut1/Homer, respectivamente y se midió la intensidad de la inmunorreactividad sináptica de VGlut1, para estimar cambios en la fuerza sináptica del circuito (Figura 15).

Sinaptogénesis y estimación de cambios en la fuerza sináptica

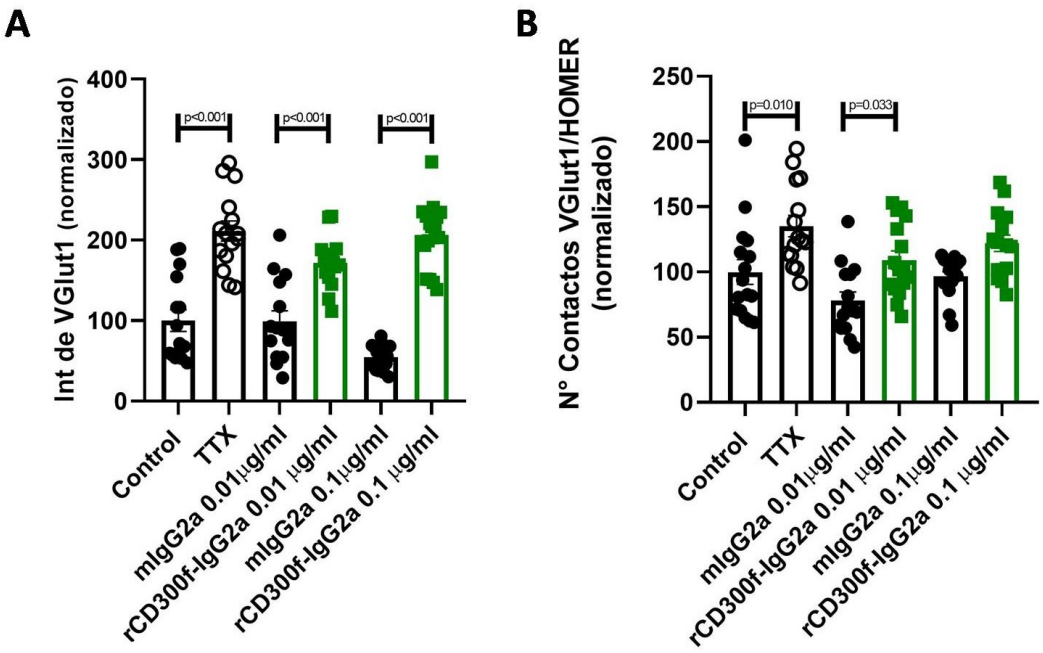

Figura 15: CD300f participa del *pruning* sináptico microglial. Se trataron los co-cultivos durante 72hs con rCD300f-IgG2a a 0,01 y 0,1 µg/ml, los controles de isotipo IgG2a a 0.01 y 0.01 µg/ml, un control sin tratamiento o TTX (1,0 µM). **(A)** Se cuantificó la intensidad de fluorescencia asociada a VGlut1 en cada uno de los contactos sinápticos. Cada contacto sináptico se determinó por la co-localización parcial o completa de los marcadores VGlut1/Homer-1. **(B)** Se cuantifica la cantidad de contactos sinápticos excitadores en un tramo de 30µm desde el soma. Se realizaron dos experimentos con sus respectivos triplicados y se midieron 8 neuronas y 160-190 sinapsis/neurona, por cada tratamiento en cada experimento. Los datos muestran la media ± SEM; p corresponde a un análisis de varianza unidireccional seguido de la prueba de Tukey.

La incubación de los cultivos con TTX indujo la bien descrita sinaptogénesis/plasticidad sináptica (Nakayama et al., 2005), evidenciada por una mayor intensidad de la inmunorreactividad presináptica individual de VGlut1 (Figura 15A), así como por un aumento en el número total de sinapsis positivas para VGlu1/Homer (Figura 15B).

Los co-cultivos tratados con rCD300f-IgG2a, a concentraciones en las que no se genera muerte neuronal (0.01 µg/mL- 0.1µg/mL, Figura 7B) y que además son comparables con la forma soluble de CD300f producida por la microglía en cultivo (0.01 µg/mL) (Ejarque-Ortiz et al., 2015), se comportan de manera similar a lo que ocurre con el tratamiento con TTX. El aumento en la

abundancia de VGlut1 sináptico así como el aumento en número total de sinapsis (Figura 15A-B) sugieren un aumento en la fuerza sináptica del circuito.

¿La modulación de la sinaptogénesis y fuerza sináptica dependiente del CD300f se encuentran mediadas por un factor soluble o es necesario el contacto célula-célula?

Para determinar si existen factores solubles provenientes de la glía que participan en la modulación de la sinaptogénesis y la fuerza sináptica se realizó un cultivo enriquecido de neuronas de hipocampo y se lo trató con rCD300f-Fc, con MC control más la adición de rCD300f-Fc, o con medios condicionados provenientes de cultivos de glía mixta tratados con la proteína de fusión o con control de isotipo IgG1. Se realizó inmunocitoquímica (como se describió previamente) y se midió la intensidad de la inmunorreactividad sináptica de VGlut1 así como el número de contactos sinápticos positivos para VGlut1 /Homer (Figura 16A-B).

Sinaptogénesis y estimación de cambios en la fuerza sináptica en cultivos de neuronas tratados con MC

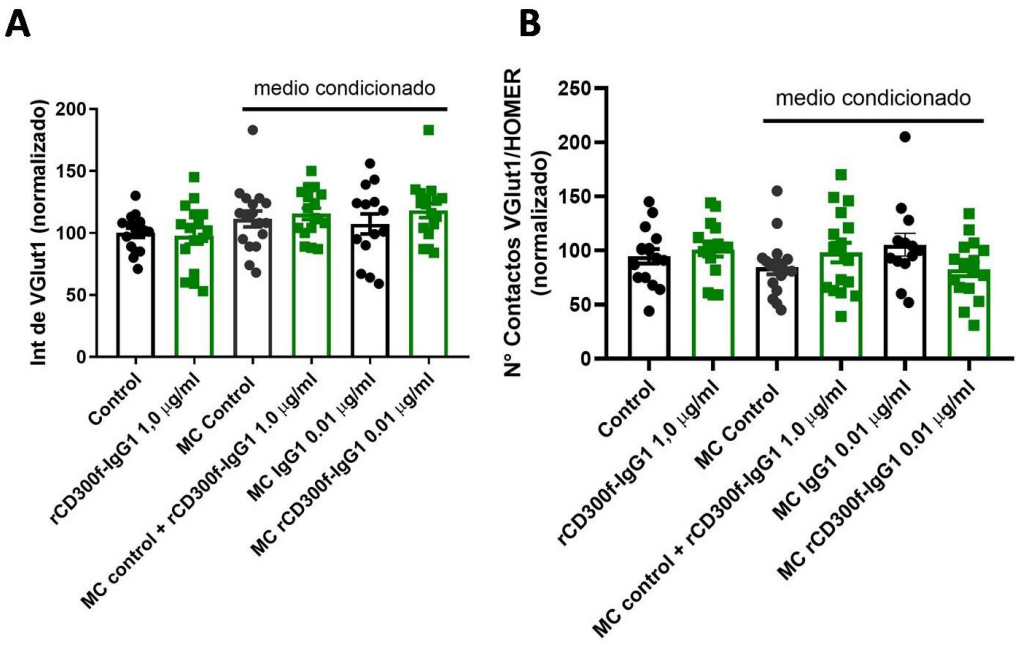

Figura 16: Las alteraciones en la abundancia de VGlut1 sináptico y la sinaptogénesis *in vitro* dependen del contacto neurona-glía. Se trataron los cultivos enriquecidos de neuronas durante 72hs con rCD300f-IgG2a directamente a 1.0 µg/ml, con medios condicionados de cultivos de glía mixta control (MC control), la adición directa de

rCD300f-Fc a 1.0 µg/ml en MC, o con MC de cultivos de glía mixta tratados con CD300f-Fc o IgG. **(A)** Se cuantificó la intensidad de fluorescencia asociada a VGlut1 sináptico. Cada contacto sináptico se determinó como se describió previamente. **(B)** Se cuantificó la cantidad de contactos sinápticos en un tramo de 30µm desde el soma. Los datos muestran la media ± SEM. Se realizaron dos experimentos con sus respectivos triplicados y se midieron 8 neuronas y 160-190 sinapsis/neurona, por cada tratamiento en cada experimento. Test estadístico corresponde a un análisis de varianza unidireccional seguido de la prueba de Tukey.

No se detectaron cambios a nivel de la plasticidad sináptica neuronal cuando se trata los cultivos enriquecidos de neuronas con medios condicionados de glía mixta, sugiriendo que el contacto neurona-glía es necesario en para modular la fuerza sináptica del circuito. Cuando se incubaron los cultivos enriquecidos de neuronas con rCD300f-IgG tampoco se observaron cambios en la plasticidad.

El análisis sináptico con los medios condicionados provenientes de co-cultivos tratados con rCD300f-Fc no se realiza dado el gran porcentaje de muerte que se reportó en los cultivos enriquecidos de neuronas tratados con dichos medios condicionados.

¿Participa el CD300f microglial en la poda sináptica?

Se ha demostrado que la PS representa una señal "cómeme" en las células apoptóticas, y que en las neuronas puede estar involucrada en el *pruning* sináptico por medio de la microglía. Una de las formas de parcialmente prevenir la eliminación sináptica en co-cultivos de neuronas y glía mixta es bloqueando la accesibilidad de la PS expuesta, ya sea por el uso de AV, o por la ausencia de TREM2 microglial (Scott-Hewitt et al., 2020). La AV reconoce selectivamente a la PS, fosfolipido traslocado desde el interior de la célula hacia el exterior de la membrana plasmática durante la apoptosis, por lo que se la utiliza frecuentemente en ensayos de detección de apoptosis (Györffy et al., 2018). Dado que la PS es un ligando conocido de CD300f, nos planteamos la hipótesis de que la inhibición en la poda sináptica esté ocurriendo por medio del bloqueo de la PS expuesta por la proteína CD300f-Fc. Para analizarlo se realizaron co-cultivos que se incubaron durante 72hs con rCD300f-Fc, control IgG1 y AV aislada o en combinación con los otros tratamientos. Para determinarla inmunorreactividad sináptica de VGlut1 y el número de contactos sinápticos

positivos para VGlu1/Homer se realizó la inmunocitoquímica ya descrita (Figura 17A-B).

Sinaptogénesis y estimación de cambios en la fuerza sináptica en co-cultivos con AnexinaV

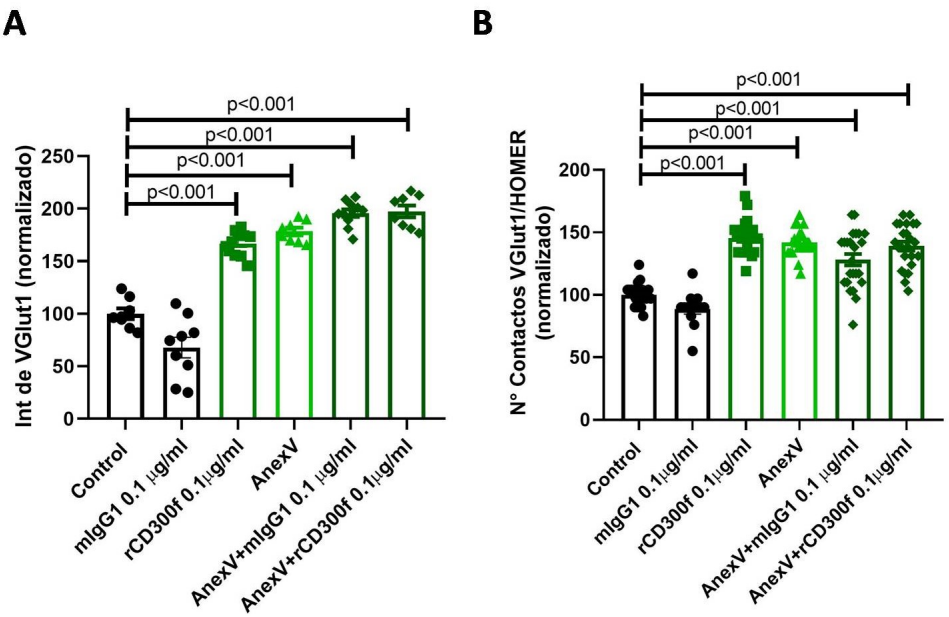

Figura 17: CD300f participa del *pruning* sináptico microglial y sería por la unión a PS. Se trataron los co-cultivos durante 72hs con rCD300f-IgG1 a 0,1 µg/ml, los controles de isotipo IgG1 a 0,1 µg/ml, controles sin tratamiento, con AV a 0,5 µl por pocillo, AV+mIgG1 y AV+rCD300f-IgG1. **(A)** Se cuantificó la intensidad de fluorescencia asociada a VGlut1 en cada uno de los contactos sinápticos. Cada contacto sináptico se determinó como se describió previamente. **(B)** Se cuantifica la cantidad de contactos sinápticos en un tramo de 30µm desde el soma. Se realizaron dos experimentos con sus respectivos triplicados. Los datos muestran la media ± SEM; p corresponde a un análisis de varianza unidireccional seguido de la prueba de Tukey.

Como resultado se observó un aumento en la abundancia de VGlut1 sináptico así como un aumento en número total de sinapsis excitadoras en los co-cultivos tratados con CD300f-Fc y en los tratados con AV como se describió previamente (Scott-Hewitt et al., 2020). Además, en ambos casos los co-cultivos responden a estos tratamientos de forma similar, y el tratamiento con ambos a la vez no genera un efecto sumatorio lo que sugiere que la poda sináptica podría ocurrir mediante el reconocimiento de la PS.

Se ha demostrado que la caspasa-3 una vez clivada se activa y adquiere un rol central en la apoptosis (Györffy et al., 2018), y que estos mecanismos podrían ocurrir también localmente en las sinapsis que deben ser eliminadas (Györffy et al., 2018). Para analizar por qué mecanismo estaría ocurriendo la poda sináptica, incubamos co-cultivos con rCD300f-Fc, control IgG1 e inhibidor de la caspasa-3 durante 72hs. Para determinar la inmunorreactividad sináptica de VGlut1 y el número de contactos sinápticos positivos para VGlu1/Homer se realizó la inmunocitoquímica ya descrita (Figura 18A-B).

Sinaptogénesis y estimación de cambios en la fuerza sináptica en co-cultivos con inhibidor de caspIII

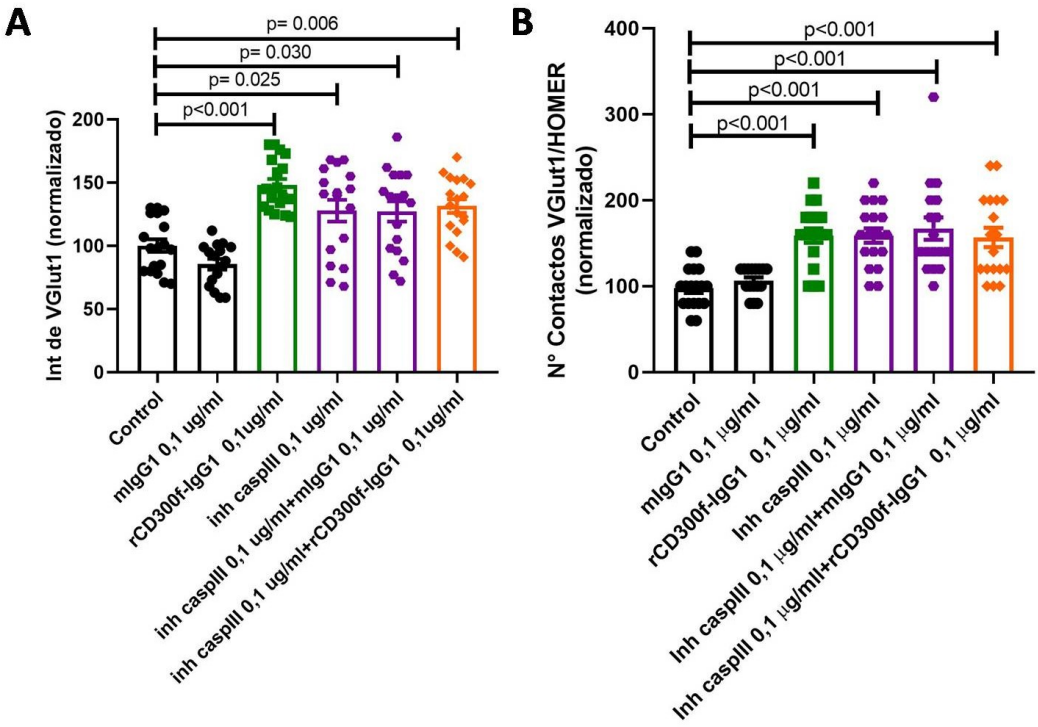

Figura 18: CD300f participa del *pruning* sináptico microglial por apoptosis. Se trataron los co-cultivos durante 72hs con rCD300f-IgG1 a 0,1 µg/ml, los controles de isotipo IgG1 a 0,1 µg/ml, controles sin tratamiento, con inhibidor de caspasa III (Inh caspIII en el grafico) a 0,1 µg/ml, Inh caspIII+mIgG1 e Inh caspIII+rCD300f-IgG1. **(A)** Se cuantificó la intensidad de fluorescencia asociada a VGlut1 en cada uno de los contactos sinápticos. Cada contacto sináptico se determinó como se describió previamente. **(B)** Se cuantificó la cantidad de contactos sinápticos en un tramo de 30µm desde el soma. Se realizaron dos experimentos independientes con sus respectivos triplicados. Los datos muestran la media ± SEM; p corresponde a un análisis de varianza unidireccional seguido de la prueba de Tukey.

Los co-cultivos tratados con el inhibidor de caspasa-3 indujeron un aumento en la abundancia de VGlut1 sináptico (Sokolova et al., 2021), así como un aumento en número total de sinapsis excitadoras lo que sugiere un incremento en la fuerza sináptica del circuito. Esto se debe a que al inhibir la caspasa-3 no permite que la PS se trasloque a la membrana citoplasmática sináptica, por lo que no se da la poda sináptica por medio de mecanismos apoptóticos que debería ocurrir. Cuando se analizan los co-cultivos tratados con rCD300f-Fc + Inhibidor de caspasa-3, no se ven diferencias con los tratados de modo independiente por lo que podría sugerirse en conjunto que CD300f participa de la poda sináptica por un mecanismo apoptótico que involucra a la PS.

CAPITULO 3 DEFICIENCIAS EN CD300f INDUCEN TRASTORNOS COMPORTAMENTALES

Deficiencias en la poda sináptica han sido reportadas en modelos de ratones con trastorno obsesivo compulsivo (TOC) (S.-K. Chen et al., 2010). A su vez, la disfunción microglial crónica está asociada a un fenotipo distrófico y un aumento en su densidad que ha sido asociado a desórdenes psiquiátricos incluyendo modelos de depresión mayor (Yirmiya et al., 2015), desórdenes obsesivos compulsivos (S.-K. Chen et al., 2010), desórdenes de espectro de autista (Tetreault et al., 2012) y esquizofrenia (Garey, 2010).

Aunque los inmunorreceptores microgliales no habían sido asociados al TDM en humanos, una deficiencia en los inmunorreceptores TREM2 y CX3CR1 induce alteraciones en la interacción social y en comportamiento compulsivo de los ratones *naïve* (Filipello et al., 2018; Zhan et al., 2014) o se potencian las conductas de tipo depresivas inducidas por LPS (Corona et al., 2010), resaltando su presunto papel en las condiciones psiquiátricas. Por otro lado nuestro grupo recientemente publicó evidencia clínica a favor del rol del receptor CD300f en la regulación fina del fenotipo microglial y su contribución a TDM (Lago et al., 2020). Encontramos que un polimorfismo prevalente no sinónimo de nucleótido simple (C/T, rs2034310) de la cola citoplasmática del receptor CD300f humano, que inhibe la fosforilación de una treonina por la proteína kinasa C, está asociado con una protección en contra de TDM, principalmente en mujeres. En hombres mostramos que este polimorfismo se

asoció con una protección frente al Trastorno de Ansiedad Generalizado (Kaufmann et al., 2021).

Por lo antes expuesto hipotetizamos que animales deficientes para CD300f presentarían trastornos en el comportamiento de tipo neuropsiquiátricos, por lo que se llevaron a cabo diferentes pruebas comportamentales de modo de describir el fenotipo asociado al inmunorreceptor CD300f en ratones WT y CD300f-/- de ambos sexos y diferentes edades. Realizamos los test separados por sexo y analizamos si se potencian las conductas al ser tratados con LPS como inductor de comportamientos depresivos.

No ocurren cambios a nivel de exploración locomotora espontánea en los animales CD300f -/-

Inicialmente se evaluó el nivel de exploración locomotora espontánea de los animales en el test del campo abierto (Kraeuter et al., 2019) (Figura 19).

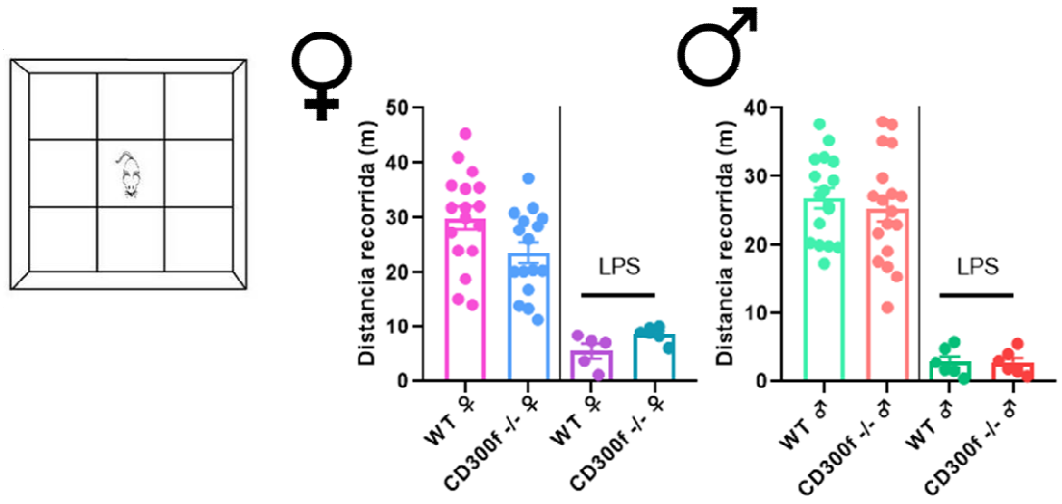

Figura 19: No hay cambios en la exploración locomotora en animales CD300f -/- **(A)** Se evaluó la actividad locomotora espontánea en campo abierto en ratones adultos (4 meses), hembras WT (n=18), CD300f-/- (n=16) y machos WT (n=17), CD300f-/- (n=18) **(B)** Se les administró una inyección IP de LPS 2 mg/kg a ratones adultos (4 meses), hembras WT (n=5), CD300f -/- (n=6) y a machos WT (n=5) y CD300f -/- (n=6) y a las 24 horas se evaluó la actividad locomotora. Cada punto representa un animal diferente y los datos provienen de dos experimentos independientes. Los datos se representan como media ± SEM. Test estadístico

corresponde a un test t de Student (hembras WT vs CD300f-/-, hembras LPS WT vs CD300f -/-; machos WT vs CD300f-/-, machos LPS WT vs CD300f -/-).

Nuestros resultados sugieren que no hay diferencias a nivel de la actividad locomotora espontánea observada en los ratones WT y CD300f -/-, dado que no presentan cambios en la distancia recorrida. Por lo cual, en el caso de presentar diferencias en los siguientes test, no serán debidas a cambios a nivel de locomoción o motores. Cuando se trataron los animales con LPS, como ya ha sido reportado (Corona et al., 2010) las distancias recorridas son menores, no presentando tampoco diferencias significativas entre los genotipos ni entre los sexos.

La deficiencia de CD300f induce un comportamiento de tipo Obsesivo Compulsivo

Para evaluar el TOC se empleó el test de marble burying test (test de enterramiento de bolitas), según protocolo de Angoa-Pérez (Angoa-pérez et al., 2013). Se realizó en un grupo de machos de 4 meses y en un grupo de hembras de 6 meses (Figura 20).

Test de entierro de Bolitas

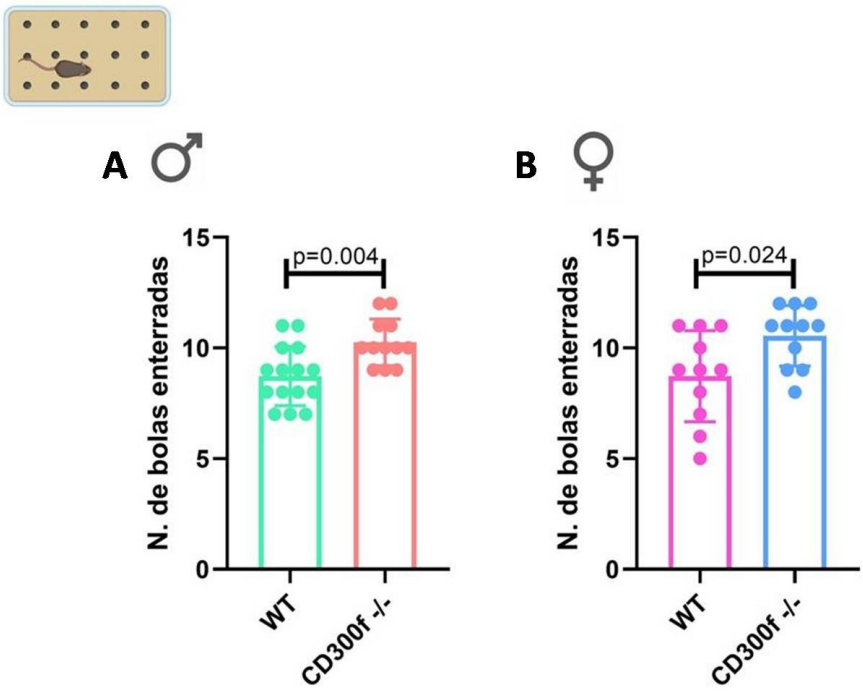

Figura 20: Los animales CD300f -/- presentan comportamiento de tipo TOC. Se evaluó el comportamiento de tipo TOC, dado por la cantidad de bolitas (12 totales) que entierran en 30 minutos, ya sea en su totalidad o 2/3. **(A)** Se realizó en machos adultos (4 meses) WT (n=11) y CD300f -/- (n=11) y en **(B)** hembras adultas (6 meses) WT (n=15) y CD300f -/- (n=12). Cada punto representa un animal diferente y los datos provienen de dos experimentos independientes. Los datos se representan como media ± SEM; p corresponde a un análisis de test t de Student independiente.

Se observó que tanto las hembras como los machos CD300f -/- entierran más bolitas por lo cual los animales CD300f-/- presentarían un comportamiento de tipo TOC (Figura 20). De modo de analizar si las diferencias en el comportamiento se potencian en animales tratados con LPS, se realizó la inyección tal como se describió previamente y a las 24hs se realizó el test. El tratamiento con LPS generó que los animales permanecieran en un rincón de la caja sin enterrar bolitas, por lo cual no se pudo realizar el test, y estos datos no se muestran.

La deficiencia de CD300f induce alteraciones en la interacción social

Para evaluar deficiencias en la interacción social, se realiza es el test de interacción social de las tres cámaras, según el protocolo de Kaidanovich-Beilin (Kaidanovich-Beilin et al., 2011). Se realizó en un grupo de hembras WT y CD300f -/- de 6 meses de edad (Figura 21). Este test evalúa: en una primera instancia la sociabilidad dada por la preferencia de los ratones a estar más tiempo en contacto con un desconocido (ratón 1) frente a un vaso vacío. Y en una segunda instancia la novedad y memoria de estar más tiempo frente a un ratón desconocido nuevo 2 vs. el ratón 1 con que había estado en la fase anterior. En este test hay un control interno del test, dado por el comportamiento de los animales WT, en el que en la primera instancia muestran preferencia por estar en contacto con el ratón 1, antes que con el vaso vacío y en la segunda instancia la preferencia es por el ratón 2 respecto al ratón 1.

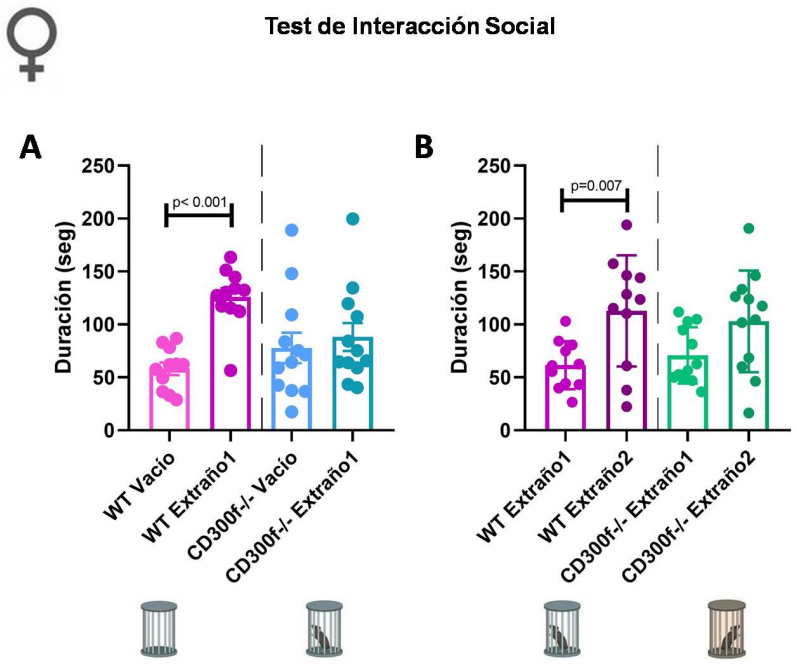

Figura 21: Hembras CD300f -/- de 6 meses de edad presentarían comportamiento de tipo TEA. Se evaluó el comportamiento de interacción social de las tres cámaras. Se realizó en hembras adultas (6 meses) WT (n=11) y CD300f -/- (n=11). **(A)** En la prueba de sociabilidad, los animales CD300f -/- pasan un tiempo similar interactuando con un ratón desconocido que con un vaso vacío. **(B)** En la prueba de novedad social, los animales CD300f -/- a diferencia de los WT, no mostraron una preferencia significativa por interactuar con un ratón nuevo frente a uno familiar. Cada punto representa un animal diferente y los datos provienen de dos experimentos independientes. Los datos muestran la media ± SEM; p corresponde a un análisis de t de Student dependiente.

Como resultado, la validez del test es respaldada mediante el comportamiento de los ratones WT, el cual fue descrito previamente. Se observa que los animales CD300f-/- en la primera instancia no presentan preferencia por explorar el primer ratón extraño o el vaso vacío, y en segunda instancia si bien exploran más al segundo extraño tampoco lo hacen de forma significativa (p= 0.209). Por lo cual, los animales presentan deficiencias en la interacción social que podrían corresponderse con un comportamiento de tipo TEA.

La deficiencia de CD300f induce un comportamiento depresivo y anhedónico en ratones Hembras

Basados en la evidencia clínica en la cual un SNP en la cola citoplasmática de CD300f está asociado con una protección en contra de TDM (principalmente en

mujeres), y en que los ratones CD300f-/- hembras presentan un comportamiento tipo depresivo (Lago et al., 2020) es que se realiza el Sucrose Splash Test (Figura 22). En este test se mide la latencia para comenzar el primer acicalamiento y el tiempo total de acicalamiento que son parámetros asociados con el comportamiento motivacional y anhedónico, y el autocuidado (Isingrini et al., 2010). Se hace en condiciones basales y posteriores a la inyección de LPS (2 mg/Kg) a las 24 hs.

Test Splash de Sacarosa

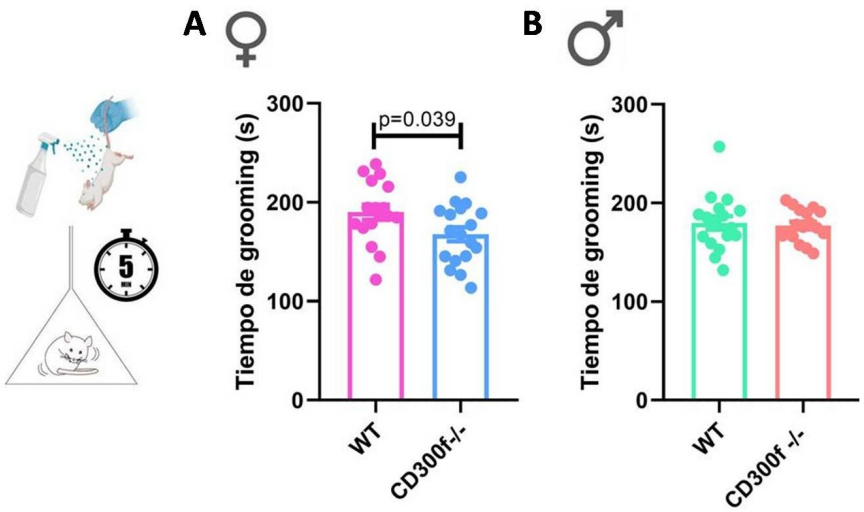

Figura 22: Las hembras CD300f−/− muestran un fenotipo depresivo y anhedónico. Se realizó el Sucrose Splash test en el que se evaluaron ratones adultos (3 meses) machos WT (n=17), CD300f-/- (n=17) y hembras WT (n=17) y CD300f -/- (n=18). **(A)** El tiempo total en el comportamiento de acicalamiento en el SST se registró en hembras para evaluar el comportamiento motivacional/auto-cuidado. Las hembras CD300f -/- se acicalan significativamente por menor tiempo en comparación de las WT, por lo que presentan un fenotipo depresivo. **(B)** En machos se ve como el tiempo de acicalamiento es similar entre ambos genotipos. Cada punto representa un animal diferente y los datos provienen de cuatro experimentos independientes. Los datos muestran la media ± SEM; p corresponde a un análisis de t de Student independiente.

A los tres meses se ve que las hembras CD300f -/- se acicalan por menos tiempo lo que refleja un comportamiento de tipo anhedónico y depresivo, similar al ya descrito por nuestro grupo previamente (Lago et al., 2020). Este comportamiento no se observa en machos (Figura 22).

De modo de analizar si el comportamiento está asociado a la edad, se realizó un nuevo test con animales de 7 meses y se inyectó a un grupo con LPS de modo de ver si el comportamiento depresivo se potencia en esas condiciones.

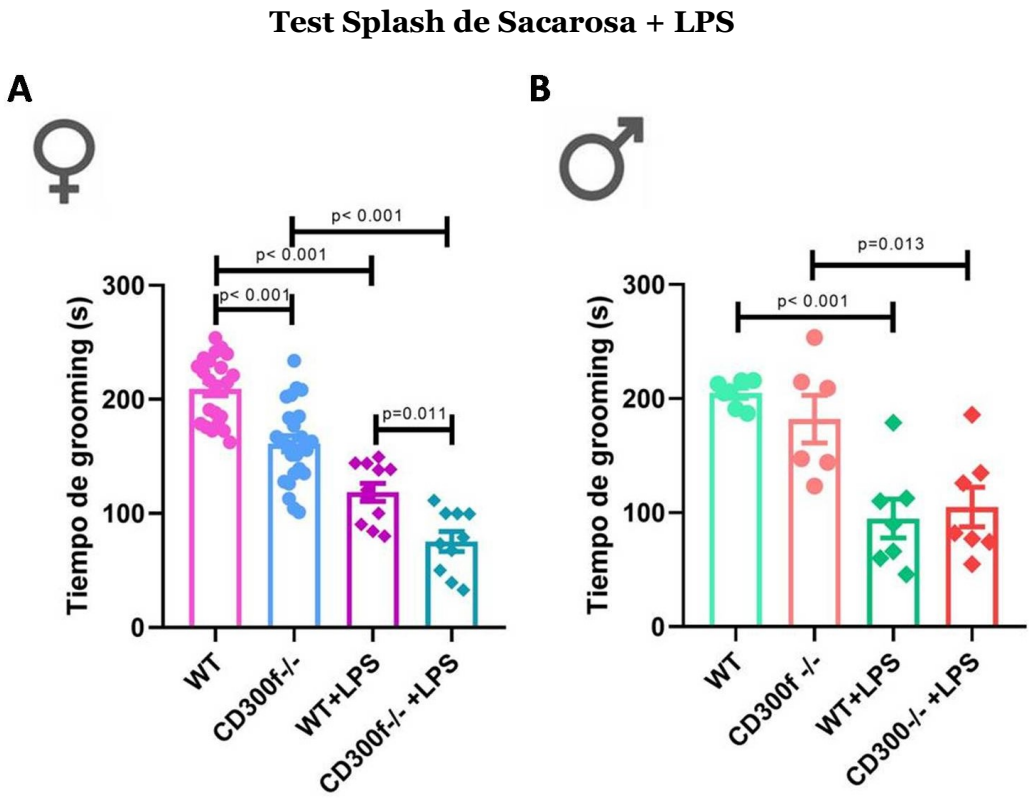

Figura 23: Las hembras CD300f−/− muestran un fenotipo depresivo y anhedónico en condiciones basales y con un estimulo de LPS. Se realizó el Sucrose Splash test en el que se evaluaron ratones adultos (7 meses) machos WT (n=7), y CD300f -/- (n=6) y hembras WT (n=22) y CD300f -/- (n=24). En un grupo de hembras (WT n=11, CD300f -/- n= 10) y machos (WT n=7, CD300f -/- n=7) se administró la inyección IP de LPS (2 mg/kg) y a las 24 hs se realizó el test. **(A)** En hembras de 7 meses se ve potenciado el comportamiento depresivo en comparación a las hembras de 3 meses, dado que las diferencias en el tiempo de acicalamiento son aún mayores comparando hembras WT vs. CD300f-/- en las diferentes edades, el LPS genero tiempos de acicalamiento más cortos. **(B)** En machos de 7 meses tampooco se observó el fenotipo depresivo, y el LPS no genero diferencias en el tiempo de acicalamiento entre animlaes WT y CD300f -/-. Cada punto representa un animal diferente y los datos provienen de cuatro experimentos independientes en **A** y dos en **B**. Los datos muestran la media ± SEM; p corresponde a un análisis de varianza unidireccional seguido de la prueba de Tukey.

Analizando el comportamiento de los animales a los 7 meses sin LPS, en el caso de las hembras se ve que la edad potencia el comportamiento depresivo, comparando las diferencias significativas entre los animales WT y CD300f -/-

de 3 meses y los de 7 meses (Figura 23A). En los machos, al igual que a los 3 meses, a los 7 meses tampoco se observó el comportamiento de tipo depresivo (Figura 23B). En los animales WT tratados con LPS (WT+LPS), el tiempo de acicalamiento, es menor como está descrito (Corona et al., 2010), tanto en hembras como en machos. En las hembras CD300f -/- inyectadas con LPS se observa un comportamiento depresivo mayor. La inyección de LPS en machos no generó diferencias significativas entre los genotipos.

De modo de confirmar el fenotipo observado en las hembras CD300f -/-, generamos en colaboración con la UBAL del Instituto Pasteur de Montevideo (IPMont) una nueva línea de animales CD300f-/- que denominamos CD300f -/- ^{IPMont}, cepa que se genero con la técnica de *CRISPER*, y a dichos animales se le realizó el SST (Figura 24A). Analizando el comportamiento de las hembras de la colonia denominada CD300 -/- ^{IPMont} se observa, (de acuerdo con lo observado en la colonia de animales CD300f-/-), el comportamiento anhedónico, ya que presentan menor tiempo de acicalamiento comparadas con los WT (Figura 24A).

Para evaluar si en el comportamiento de tipo depresivo que se observó, el principal responsable es el CD300f microglial se realizó el comportamiento en una colonia de animales KOc. Se adquirió una colonia de animales KO condicionales (KOc) CX3CR1-CreERT2, que fue utilizada por el compañero Andrés Cawen para generar animales deficientes para CD300f únicamente en microglía y macrófagos de barrera como se describió previamente en materiales y métodos. Esta colonia de animales nos permite por un lado trabajar con animales CD300f -/- solo en los macrófagos residentes del SNC y en la microglía, por lo que nos permite evaluar si es el CD300f expresado en estas células, es el que estaría involucrado en los trastornos comportamentales. Por otro lado nos permite generar el condicional a la edad que consideremos relevante para el análisis (dado que se genera por la inyección IP de TMX), y excluir efectos generados durante el desarrollo. Por lo tanto, para poder determinar si el comportamiento de tipo depresivo observado en las hembras se debe a la falta del inmunorreceptor CD300f microglial, se usaron ratones Cd300floxP/loxP: Cx3cr1+/+ y KOcCd300floxP/loxP: Cx3cr1creERT2/+. Se dividió a los animales en 3 grupos de trabajo: WT (Cd300floxP/loxP:

Cx3cr1+/+); los KOc+TMX (Cd300floxP/loxP: Cx3cr1creERT2/+ +TMX); y los KOc-TMX (Cd300floxP/loxP: Cx3cr1creERT2/+ -TMX). De este modo generamos el genotipo deficiente de CD300f solo en un grupo de animales.

En aquellos animales que recibieron TMX y expresaron la recombinasa CreERT2, la recombinación y la consiguiente eliminación de CD300f ocurre tanto en microglía como en poblaciones de macrófagos (datos no mostrados generados por Andrés Cawen). Sin embargo, después de 3-4 semanas, los monocitos circulantes recuperaron la expresión de CD300f, mientras que la microglía y los macrófagos de barrera continuaron sin de él. Esto se debe a que los monocitos tienen una tasa de renovación alta desde sus progenitores mieloides (Yona et al., 2013), mientras que la microglía presenta autorrenovación a tasas mucho más bajas (Ajami et al., 2007). Se realizó el SST a las 3 o a las 5 semanas después del tratamiento con TMX (Figura 24B-C).

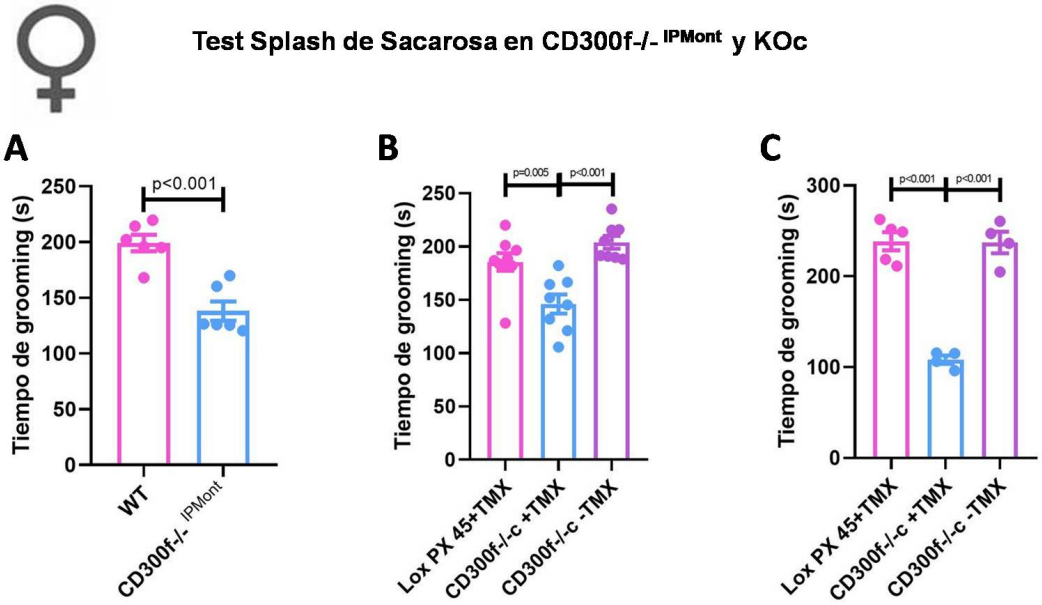

Figura 24: Las hembras CD300f−/− de diferentes colonias y KO condicionales también muestran un fenotipo depresivo y anhedónico. Se realizó el Sucrose Splash test en el que se evaluaron ratones adultos (4 meses) hembras WT y CD300f -/-^{IPMont} y KOc. **(A)** Hembras CD300f -/-^{IPMont} (n=6) se acicalan menos tiempo en comparación a las WT, presentando también en esta colonia un fenotipo depresivo. **(B)** Se realiza el SST a las 3 semanas de la inyeccion de TMX, por lo que se realiza en animales KOc (animales con CD300f -/- en la microglía y en los macrofagos residentes) y se ve la diferencia en el tiempo de acicalamiento, lo que demuestra un comportamiento depresivo, dependiente de CD300f de la microglía (n=8, todos los grupos). **(C)** Se realiza el SST en hembras KOc inyectadas en las

mismas condiciones, pero a las 5 semanas de la inyección de TMX, se observa un comportamiento depresivo potenciado con el paso de las semanas. Cada punto representa un animal diferente y los datos provienen de dos experimentos independientes en **A-B** y uno en **C** (LoxP45+TMX n=5, CD300f -/-c + TMX n=4, CD300f -/-c - TMX n=4). Los datos muestran la media ± SEM; p corresponde a un análisis de t de Student independiente en A y un análisis de varianza unidireccional seguido de la prueba de Tukey en B-C.

En el caso de la colonia KOc, a las 3 semanas luego de la inyección de TMX ya se detecta el comportamiento anhedónico (Figura 24B). Repetimos el experimento en otra cohorte de animales y se realiza el SST a las 5 semanas luego de haber inducido la perdida de CD300f en la microglía y macrófagos de barrera y se observa el mismo fenotipo, en este tiempo más potenciado aún (Figura 24C). Por lo cual, se concluye que el comportamiento de tipo depresivo se encuentra asociado al inmunorreceptor CD300f microglial y/o a los macrófagos de barrera.

CD300f contribuye a la generación del comportamiento de tipo depresivo por medio del reclutamiento de macrófagos CCR2+

Analizando el transcriptoma de microglía de hipocampo de animales WT y CD300f -/- previamente descrito por medio de ARNseq ya publicado por nuestro grupo (Lago et al., 2020), se observaron 34 genes expresados diferencialmente, y detectamos que uno de los genes sobreexpresados en los animales CD300f -/- es el CCR2 (Figura 5). Basados en estos antecedentes y en la bibliografía donde relacionan al eje CCl2-CCR2 con la depresión (Curzytek & Leśkiewicz, 2021), nos planteamos la hipótesis de si en los ratones CD300f -/- el comportamiento tipo depresivo ocurre por esta vía. Para estudiar esta posibilidad, realizamos el SST a animales KOc tratados con un inhibidor específico de CCR2 (Mirzadegan et al., 2000) (Figura 25). El tratamiento se describió previamente en materiales y métodos, resumidamente a un grupo de animales Cd300floxP/loxP: Cx3cr1+/+ y KOc Cd300floxP/loxP: Cx3cr1creERT2/+ se los inyecta con TMX durante 4 días consecutivos y al siguiente día se les administra diariamente a un grupo el inhibidor de CCR2 IP 5 mg/kg durante 13 días mientras que al otro grupo se le administra agua como vehículo (Figura 25A). A las 3 semanas de la última inyección de TMX se le realiza el SST y dos semanas después (a las 5 semanas de la última inyección de

TMX) se les realiza el segundo SST para evaluar el efecto del inhibidor (Figura 25B).

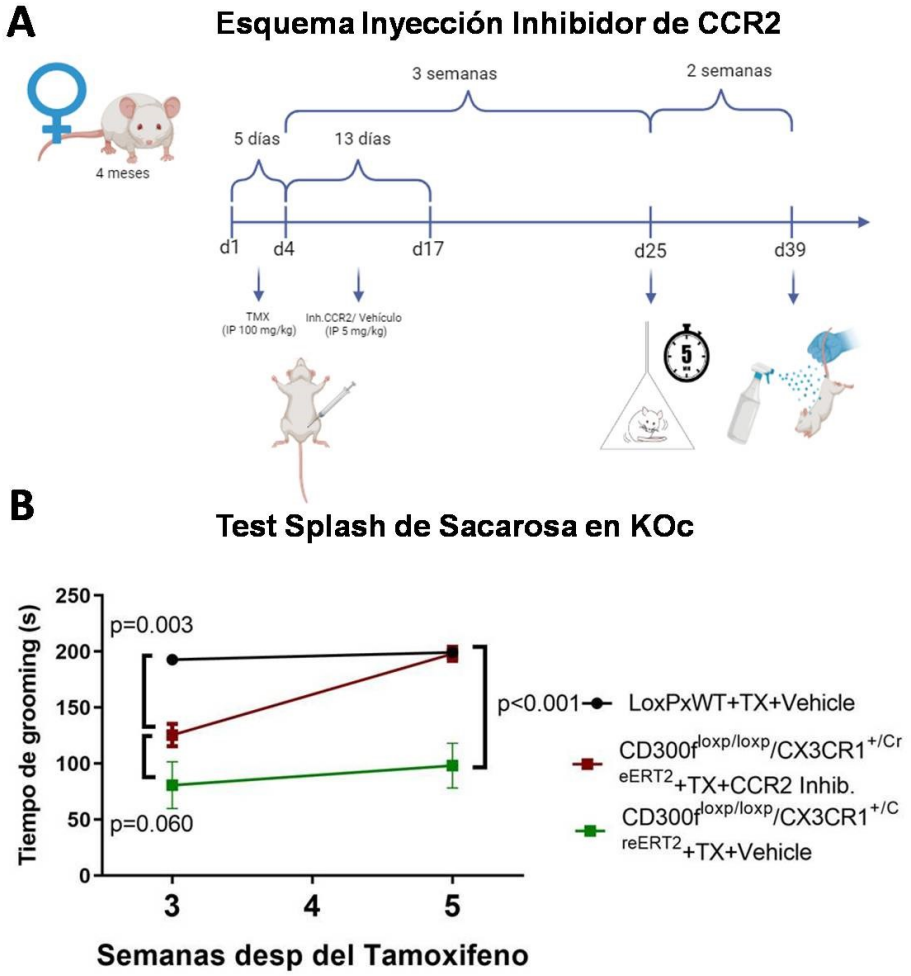

Figura 25: El fenotipo depresivo se elimina inhibiendo el reclutamiento de los macrofagos CCR2+. (A) Línea temporal experimental. **(B)** Se realizó el Sucrose Splash test en el que se evaluaron ratones adultos (4 meses) hembras WT (n=5) y KOc, inyectadas IP con inhibidor de CCR2+ (5mg/kg) (n=4) o vehículo (n=3) a las 3 semanas de la inyección de TMX o a las 5 semanas de la inyección de TMX. A las 3 semanas en los animales KOc se observa el fenotipo depresivo ya establecido, y los animles KOc se acicalan menos en comparación con los WT controles. A las 5 semanas de la inyección de TMX y a las aproximadamente 3 semanas de la inyección del inhibidor de CCR2+, lo que se observa es que el comportamiento depresivo de los animales KOc se pierde en presencia del inhibidor de CCR2+, dado que los animales se acicalan el mismo tiempo que los WT control. Cada punto representa un animal diferente. Los datos muestran la media ± SEM; p corresponde a un análisis de t de Student dependiente.

Se observó que a las 3 semanas de inyectado el TMX los animales KOc presentan un comportamiento anhedónico como se demostró previamente. Analizando los animales inyectados con el inhibidor de CCR2+, se observa que, si bien se acicalan menos que los WT control, presentan una fuerte tendencia (p=0.06) hacia un acicalamiento mayor que los animales inyectados con vehículo. A las 5 semanas de la última inyección de TMX, el inhibidor de CCR2+ muestra un efecto mayor, sorpresivamente se ve como se revierte completamente el comportamiento depresivo y los animales KOc se acicalan tiempos similares a los WT y con una diferencia significativa con los animales KOc inyectados con vehículo (Figura 25B).

De este grupo de resultados se puede concluir que, en condiciones basales, la ausencia de CD300f indujo alteraciones fenotípicas en microglía y macrófagos de la barrera del SNC que llevaron al reclutamiento de macrófagos CCR2+, y la inhibición farmacológica de su reclutamiento revirtió el comportamiento similar a la depresión.

CAPITULO 4 CARACTERIZACIÓN DEL FENOTIPO MICROGLIAL DE CD300f -/- EN ANIMALES ENVEJECIDOS

Como se describió previamente, los estudios transcriptómicos de microglía de hembras adultas evidenciaron solo 34 genes con una expresión diferencial significativa (Figura 5). Además cuando se analizó la firma génica homeostática de la microglía, observamos que la deficiencia de CD300f no alteró la expresión de genes homeostáticos y no experimentó un cambio fenotípico hacia un fenotipo DAM (Keren-Shaul et al., 2017; Krasemann et al., 2017). Una interesante hipótesis emergente postula que, bajo condiciones neurodegenerativas o durante el envejecimiento (Grabert, Michoel, Karavolos, Clohisey, Baillie, Stevens, Freeman, Summers, & McColl, 2016; Hickman et al., 2013) la regulación a la baja de este fenotipo homeostático podría afectar la función del SNC en sí misma (Crotti & Ransohoff, 2016). Por lo tanto, resulta interesante determinar el fenotipo microglial de los animales CD300f-/- en diferentes modelos incluyendo el modelo de inflamación crónica que ocurre durante el envejecimiento.

A su vez como se mencionó previamente, hay evidencias recientes que sugieren que los receptores inmunológicos de microglía/macrófagos están involucrados en muchos procesos relacionados con el envejecimiento, como el metabolismo energético, la inflamación y el deterioro cognitivo (Rozenberg et al., 2017). Se ha demostrado que TREM2 es esencial para la inducción del fenotipo DAM en la microglía (Keren-Shaul et al., 2017), a su vez un estudio reciente sugiere que entre la microglía DAM clásicas (Keren-Shaul et al., 2017), existe una población definida derivada de monocitos denominada macrófagos inflamatorios de enfermedades (DIM) que se acumularían en el cerebro principalmente durante el envejecimiento y la neuroinflamación (Silvin et al., 2022).

En virtud de lo expuesto previamente es que nos planteamos el objetivo de llevar a cabo la caracterización del fenotipo microglial en animales envejecidos CD300f -/-.

Cerebros de ratones hembra CD300f-/- de 30 meses se encuentran enriquecidos en genes característicos de microglía DAM y macrófagos DIM

Con el fin de llevar a cabo el análisis del fenotipo microglial en animales envejecidos WT y CD300f-/-, se realizó ARNseq de microglía aislada de cerebros de ratones hembra de 30 meses. Al realizar el ARNseq, se constató el deterioro de algunas muestras por lo que la cantidad de animales no permitió llevar a cabo un análisis estadístico.

Como enfoque alternativo, se realizó mediante ARNseq el análisis del transcriptoma del cerebro completo de animales hembras de 30 meses de edad WT y CD300f-/- (Figura 26).

Cerebro

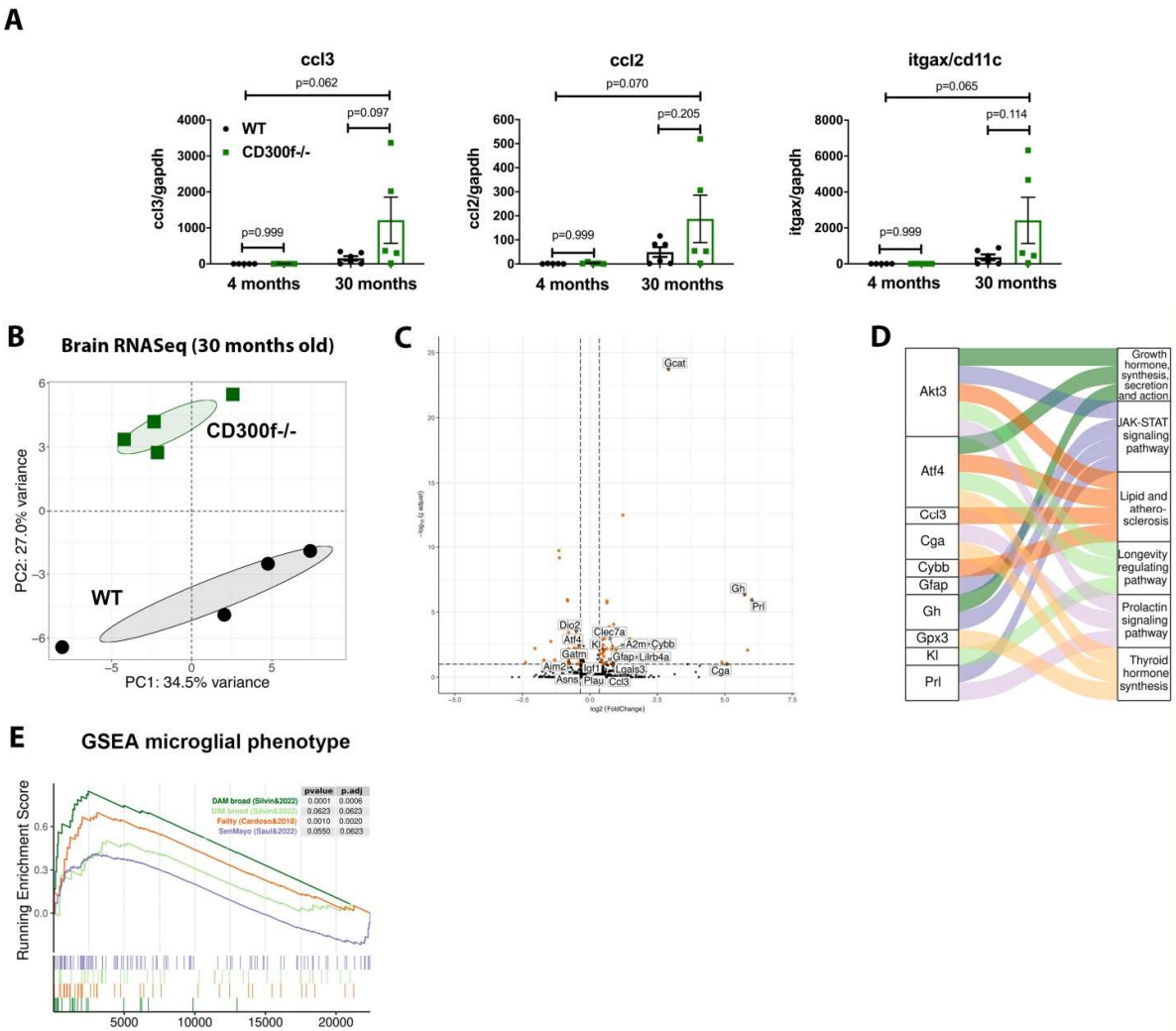

Figura 26: La ausencia de CD300f induce alteraciones cerebrales relacionadas con la edad. En cerebros de hembras adultas y de 30 meses WT y CD300f-/-, **(A)** se analiza la expresión de ARNm mediante qPCR. **(B-E)** El transcriptoma del cerebro de ratones hembra de 30 meses de edad se analizó mediante RNAseq. **(B)** Análisis de componentes principales, **(C)** gráfico de volcán que destaca genes diferencialmente expresados **(D)** y resultados de enriquecimiento de vías KEGG del RNASeq. El gráfico representa las relaciones entre genes diferencialmente expresados y vías KEGG sobreexpresadas (valor de P <0.001, valor de P ajustado por FDR <0.2). **(E)** Los cambios en la expresión génica en el cerebro de ratones CD300f-/- de 30 meses en comparación con ratones de tipo salvaje mostraron firmas de

fragilidad y senescencia, así como un estado DAM microglial y un perfil DIM de macrófagos reclutados. El gráfico de GSEA muestra, para las cinco listas de genes, el puntaje de enriquecimiento en ejecución y la posición de los genes específicos en la clasificación de genes ordenados.

El cerebro es un órgano central afectado por el envejecimiento. En consecuencia, se observaron signos de "inflamaging" en el cerebro de ratones de 30 meses de edad con deficiencia de CD300f mediante qPCR para las quimioquinas ccl2, ccl3 e itgax/cd11c (Figura 26A). Analizando el ARNseq, 67 genes mostraron una expresión diferencial significativa. Se observó una alteración en la expresión de genes conocidos relacionados con la longevidad como gh, igf1, prl, kl y gcat. Además, se mostró que el cerebro de ratones hembras CD300f-/- de 30 meses estaba significativamente enriquecido en genes sobreexpresados por microglía DAM (incluyendo clec7a, ccl3, lilrb4, cybb, lgals3, igf1) observados previamente en envejecimiento, enfermedad de Alzheimer y otras condiciones neurodegenerativas (Keren-Shaul et al., 2017; Krasemann et al., 2017). Interesantemente, el cerebro de ratones CD300f-/- de 30 meses de edad también mostró una firma significativa de macrófagos DIM (Figura 26E). Una exploración adicional de los resultados de RNAseq en el cerebro mostró que el análisis de enriquecimiento KEGG también resaltó la vía de secreción y acción de la hormona de crecimiento. De hecho, el aumento en el ARNm de gh, prl, junto con cga (péptido alfa compartido por varias hormonas pituitarias) confirmó los datos anteriores de qPCR que sugieren que las hembras de ratones CD300f-/- desarrollan neoplasias pituitarias. Otro gen expresado de manera diferencial en el cerebro de ratones CD300f-/- hembras de 30 meses de edad fue atf4, que es un efecto central de la respuesta integrada al estrés (ISR). La alteración de la proteostasis es una característica del envejecimiento, y la regulación al alza de vías como atf4 se ha asociado con condiciones que prolongan la vida (W. Li et al., 2014). Interesantemente, los ratones CD300f-/- de 30 meses de edad mostraron una disminución en el ARNm de atf4 y algunos de sus genes diana (Figura 26C). Finalmente, el estudio de RNAseq también detectó niveles aumentados de ARNm de marcadores inflamatorios relacionados con astrocitos (gfap), microglía (clec7a) y quimioquinas (ccl3)

(Figura 26C). Esto confirmó el análisis de qPCR de todo el cerebro de la expresión de quimioquinas (ccl3) (Figura 26A).

De modo de confirmar los datos obtenidos por ARNseq, nos planteamos el objetivo de llevar a cabo una caracterización inmunohistoquímica para uno de los principales marcadores DAM, el CLEC7A. Se realizó en cortes de cerebro de hembras de 30 meses de edad WT y CD300f -/- (Figura 27).

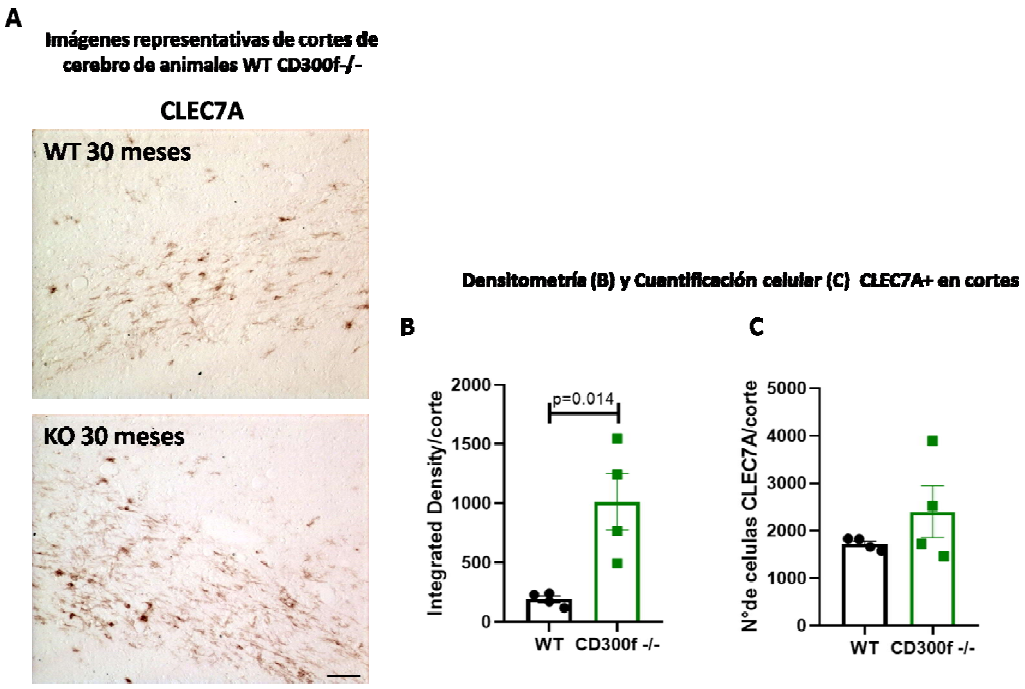

Figura 27: Hembras CD300f envejecidas presentan un aumento en la expresión de CLEC7A. (A) Imágenes de inmunohistoquímica en cortes de 30 µm de cerebros de ratones hembras WT (foto superior) y CD300f -/- (foto infeior) de 30 meses de edad, para el marcador CLEC7A revelado con DAB (barra de calibración = 20 µm). **(B)** Densitometría y **(C)** conteo de células CLEC7A positivas en cortes (3 cortes por ratón) de cerebro de ratones CD300f-/- hembras de 30 meses en comparación con ratones WT, procesados para inmunohistoquímica para CLEC7A. Cada punto representa un animal diferente. Los datos muestran la media ± SEM; p corresponde a un análisis de t de Student independiente.

El análisis mostró un aumento significativo en la intensidad de la inmunorreactividad en todos los animales CD300f-/- analizados (Figura 27B) y un aumento de células CLEC7A+ solo en algunos animales (Figura 27C). Estos datos concuerdan y confirman lo observado en el ARNseq. Estos datos a su vez están acordes a cambios en el deterioro cognitivo de los animales CD300f -/-

con la edad (Evans et al., 2023), los que podrían ser asociados a la microglía DAM.

DISCUSIÓN

CAPITULO 1 CD300f CONTRIBUYE AL MANTENIMIENTO DE LA VIABILIDAD NEURONAL

La microglía posee múltiples y diversas funciones. En el presente trabajo se ha demostrado que el inmunorreceptor microglial CD300f participa directamente en varias de estas funciones. Una de las principales funciones de la microglía es contribuir al mantenimiento de la homeostasis del SNC (Prinz et al., 2019). Inicialmente demostramos que el receptor inmunológico CD300f contribuye a la supervivencia neuronal en co-cultivos de neurona-glía y después de una lesión, mediante un mecanismo que involucra las interacciones glía-neurona. Nuestros datos sugieren que la activación microglial de CD300f es necesaria para mantener interacciones tróficas saludables y, cuando se interrumpe, puede desencadenar respuestas neurotóxicas. De acuerdo con esto, varias líneas de evidencia sugieren que la activación de otros inmunorreceptores como por ejemplo TREM2, otro receptor inmunológico con capacidad de unión a lípidos, también contribuye a la homeostasis del sistema nervioso central (Colonna, 2023; Ulland et al., 2017). La activación de los receptores inmunológicos CD300f y TREM2 con capacidad de unión a lípidos podría ser desencadenada por el reconocimiento de lipoproteínas o estructuras de reciclaje de mielina entre otros estímulos. Aún queda por aclarar cuáles son los ligandos endógenos reales en condiciones fisiológicas para estos receptores así como su grado de especificidad por uno u otro.

Existe un gran paralelismo entre CD300f y TREM2 como se describió previamente. Debido a esto, para comprender la función de CD300f se puede analizar la biología de TREM2, ya que ambos receptores comparten funciones, parte de su expresión específica de tipo celular, se activan presumiblemente por ligandos similares y sus vías de señalización están entrelazadas. De hecho, los

receptores inmunes CD300 son los parientes más cercanos en cuanto a homología de secuencia a los receptores TREM. El espectro de ligandos descritos compartidos por TREM2 y CD300f incluye fosfolípidos y lipoproteínas (Choi et al., 2011b; Izawa et al., 2014; Y. Wang et al., 2015). En particular, reconocen fosfolípidos como PS y esfingomielina que contribuirían a la detección y fagocitosis de células apoptóticas y restos celulares como los restos de mielina respectivamente. Hay reportes que demuestran la existencia de varios *splicing* alternativos de ARNm de los genes ortólogos de CD300f en humano (Alvarez-Errico et al., 2004) en rata (Peluffo, et al., 2012) y en ratón (Moshkovits, Karo-Atar, et al., 2015; Ejarque-ortiz et al., 2015). Una de estas variantes codifica para el receptor CD300f soluble, que carece del dominio transmembrana, y se ha mostrado que la microglía en cultivo produce CD300f soluble (Ejarque-ortiz et al., 2015). Existen reportes recientes en los que se utiliza el receptor CD300f soluble como herramienta para el bloqueo de su interacción endógena con sus ligandos, y se utiliza para analizar qué efecto desencadena a nivel de la sobrevida y fenotipo celular (Pannunzio et al., 2022; Peluffo, et al., 2012). Para el desarrollo de este trabajo se utilizó como principal herramienta la porción extracelular del receptor CD300f unido a una región Fc de anticuerpo que conforma la proteína de fusión rCD300f-Fc dimérica. En un estudio, se demostró que el agregado del receptor soluble TREM-2 en cultivos primarios de microglía (TREM2-Fc) genera un aumento en la supervivencia celular, utilizado a una concentración de 20 nM (Zhong et al., 2017). También se reportó que los niveles del TREM-2 soluble están en el rango de 3-6 $^{ng}/_{ml}$, en el líquido cefalorraquídeo de pacientes con Alzheimer (Zhong et al., 2017). Si bien no existen reportes midiendo niveles *in vivo* de CD300f soluble, nuestro grupo ha mostrado que la microglía de ratón en cultivo produce una versión soluble del CD300f a una concentración de 2 o 5 $^{ng}/_{ml}$ en condiciones basales o luego de una estimulación con LPS respectivamente (Ejarque-Ortiz et al., 2015). Aunque CD300f y TREM2 comparten ligandos de fosfolípidos similares, diversas evidencias sugieren que otras moléculas pueden actuar como co-ligandos otorgando especificidad a diferentes receptores inmunitarios de unión a lípidos. La tinción de células con proteínas de fusión TREM2-Fc o CD300f-Fc muestran que muchas, pero no todas, las células vivas presentan ligandos para estos receptores, a pesar de que hay ligandos de fosfolípidos abundantes, como la

esfingomielina expuesta en la superficie de todas las células. Además, la tinción de células con CD300f-Fc muestra un perfil puntillado que destaca dominios específicos de la superficie celular donde los ligandos están expuestos (Peluffo, et al., 2012). Resultados no publicados de nuestro laboratorio muestran que el tratamiento de células con tripsina disminuye marcadamente la tinción con CD300f-Fc, y lo mismo ocurre con TREM2-Fc (comunicación personal de Marco Colonna). En conjunto, estas observaciones abren la posibilidad de que otras moléculas, aparte de los fosfolípidos, como proteínas, puedan actuar como co-ligandos de fosfolípidos generando un nivel adicional de complejidad y especificidad. Aquí mostramos cómo elevadas concentraciones de rCD300f-Fc (1.0 μg/ml) en co-cultivos generan muerte neuronal. rCD300f-Fc inhibe las interacciones endógenas de CD300f con sus ligandos y de esta manera desencadena mecanismos de toxicidad para las neuronas en los co-cultivos. En concordancia, cuando se analizan los modelos *in vivo*, la inyección de rCD300f-Fc en el cerebro de ratones WT induce un aumento en el volumen de lesión en comparación con IgGs de control. Además, se observó un volumen de lesión similar después de la inyección de rCD300f-Fc o IgGs control en cerebros de ratones CD300f-/-. Esto indica que, aunque la proteína rCD300f-Fc inhibe las interacciones endógenas de CD300f con sus ligandos en cerebros WT, no afecta al cerebro CD300f-/-, y que por lo tanto el efecto es específico de la inhibición de CD300f. Más importante aún, la falta de efectos de rCD300f-Fc en cerebros CD300f-/- evidencia que, aunque CD300f puede compartir ligandos lipídicos con otros receptores de unión a lípidos, posee ligandos adicionales que confieren una activación específica de este receptor. Estos resultados suman evidencias sobre la presencia de co-ligandos probablemente proteicos que contribuyen a determinar la especificidad de los ligandos para CD300f. Finalmente, la inyección de IgGs control o rCD300f-Fc en cerebros CD300f-/-, mostró una tendencia hacia el aumento en el volumen de lesión en comparación con la inyección de IgGs de control en cerebros WT, sugiriendo nuevamente que, de hecho, la deficiencia de señalización de CD300f induce una mayor neurotoxicidad *in vivo*.

Para llevar a cabo la caracterización del posible mecanismo de neurotoxicidad, nos planteamos si la muerte neuronal ocurre por medio de factores solubles que pudieran ser secretados al medio. Para el abordaje de esta hipótesis utilizamos

medios condicionados, tanto de co-cultivos como de cultivos de glía mixta tratados con rCD300f-Fc o IgG control. Únicamente se observó neurotoxicidad en el caso de neuronas tratadas con los medios condicionados de los co-cultivos, lo cual demuestra que la neurotoxicidad es mediada por factores solubles secretados en presencia de la interacción neurona-glía. De hecho, la neurotoxicidad inducida por rCD300f-Fc depende de la presencia tanto de neuronas como de células gliales, ya que no se observó neurotoxicidad del rCD300f-Fc en neuronas aisladas. Además de observar que es mediada por factores solubles, mostramos que pudo revertirse mediante el tratamiento con la neurotrofina GDNF. Una posibilidad es que el inhibir la señalización de CD300f en microglía podría llevar a un estado proinflamatorio tóxico para las neuronas en co-cultivos. Se realizó el análisis de las citoquinas del medio condicionado de los co-cultivos de modo de analizar el perfil inflamatorio, sin embargo, no encontramos diferencias por lo cual concluimos que la neurotoxicidad observada no fue mediada por un aumento en la liberación de citoquinas proinflamatorias. También demostramos que los mecanismos tóxicos subyacentes no implican excitotoxicidad dependiente de NMDA (podría ocurrir liberación de glutamato proveniente tanto de las neuronas como de los astrocitos), ni toxicidad dependiente de ATP extracelular (secretado por la glía o por las neuronas). Por lo tanto, podría haber otros posibles mediadores como lípidos o proteínas tóxicas que serían responsables del efecto tóxico (Dong et al., 2021; Liddelow et al., 2017).

En cuanto al tipo de célula responsable de la neurotoxicidad, dado que CD300f solo se expresa en microglía y macrófagos de barrera en el SNC y principalmente en células mieloides en la periferia, *in vivo* podría ejercerse directamente por microglía que expresa CD300f y/o macrófagos o neutrófilos reclutados después de una lesión cerebral penetrante. Sin embargo, en los co-cultivos, la neurotoxicidad dependiente de CD300f parece estar directa o indirectamente a cargo de las células microgliales, ya que son las únicas células que expresan CD300f en estas condiciones experimentales. Alternativamente, la inhibición de CD300f puede afectar los mecanismos protectores dependientes de microglía, como se ha demostrado *in vitro* y después de lesiones en el SNC, donde ocurre una eliminación de lípidos tóxicos por medio del TREM2 microglial, como la fosfatidilcolina oxidada (Dong et al., 2021). CD300f al igual

que TREM2 podría presumiblemente también unirse y eliminar a la fosfatidilcolina oxidada después de una lesión cerebral penetrante, mientras que la inhibición de este proceso potenciaría la neurotoxicidad. Además, la microglía puede inducir un fenotipo astrocítico neurotóxico dependiente la liberación de citoquinas por parte de la microglía como ser IL-1α, TNFα, y C1q, una toxicidad que se reportó que se mantiene en el medio condicionado de astrocitos (Liddelow et al., 2017) y que por tanto podría estar presente en los medios condicionados de los co-cultivos. Este efecto se encontró que depende de ácidos grasos libres saturados de cadena larga tóxicos asociados a lipoproteínas APOE y APOJ (Guttenplan et al., 2008). Dado que CD300f puede interaccionar con lipoproteínas y presumiblemente endocitarlas, podría potencialmente eliminar estos lípidos tóxicos unidos a lipoproteínas y de esta forma contribuir a la neuroprotección. También se ha demostrado que los astrocitos son capaces de inducir respuestas neurotóxicas produciendo especies reactivas de oxígeno y nitrógeno (Cassina et al., 2002), sin embargo, estas especies no son estables en el medio condicionado y, por lo tanto, no serían responsables directamente del efecto neurotóxico. Serán necesarios estudios adicionales para la identificación de los componentes tóxicos involucrados en este proceso y el tipo de célula que los produciría.

La mayoría de los receptores inmunológicos, como TREM1, CD200R, TREM2 y CD300f, presentan formas solubles. Una de las formas solubles que generalmente se encuentra, es la resultante de la traducción de un transcrito con empalme alternativo que carece del dominio transmembrana, y este es el caso tanto para CD300f humano como para CD300f de ratón (Alvarez-Errico et al., 2007; Ejarque-Ortiz et al., 2015). Sin embargo, el clivaje proteolítico de los receptores inmunológicos expresados en la superficie por metaloproteasas de matriz también puede contribuir a la producción de formas solubles (Colonna, 2023). Las evidencias muestran que el clivaje de los receptores inmunológicos en la superficie celular termina su señalización y refleja su nivel de activación *in vivo*. Además, las formas solubles pueden tener sus propias funciones, como la eliminación de ligandos y la restricción adicional de la activación del receptor inmunológico, o incluso la activación de receptores aún desconocidos. Por ejemplo, CD300b soluble activa TLR4 (Phongsisay et al., 2014). Además, se ha informado de un efecto beneficioso después de la inyección cerebral de TREM2

soluble o su sobreexpresión en un modelo de ratones con patología de Aβ. Estudios longitudinales en pacientes con enfermedad de Alzheimer muestran que niveles más altos de TREM2 soluble en el líquido cefalorraquídeo predicen una disminución cognitiva más lenta y una señal atenuada de amiloide y tau en la tomografía por emisión de positrones. Esto contrasta con los efectos neurotóxicos de la inyección de CD300f soluble en el cerebro normal de ratones y ratas informados aquí, lo que sugiere que, a pesar de todas las similitudes entre estos dos receptores inmunitarios, también pueden tener sus particularidades.

CAPITULO 2 CD300f PARTICIPA EN EL PRUNING SINÁPTICO REALIZADO POR LA MICROGLÍA

Otra de las funciones de la microglía que ha sido ampliamente demostrada es la participación en la poda o *pruning* sináptico, tanto en el cerebro en desarrollo como en el cerebro adulto. En el *pruning* sináptico la microglía tiene la capacidad de eliminar sinapsis específicas de modo de refinar la conectividad neuronal. Además la microglía desempeña un rol en la plasticidad sináptica, con la capacidad de modular la fuerza sináptica ya sea eliminando sinapsis o liberando factores que afecten la eficacia sináptica (Basilico et al., 2019; Filipello et al., 2018; Nimmerjahn, 2005; Paolicelli et al., 2011; Schafer et al., 2012; Tremblay et al., 2010; Weinhard et al., 2018). Aplicando protocolos validados (Herman et al., 2014; Wilson et al., 2005), que relacionan los niveles de VGlut1 con la estimación de la probabilidad de liberación del neurotransmisor de glutamato, evaluamos si estos fenómenos plásticos se observaban en los co-cultivos. En la Figura 10, se observó que en presencia de rCD300f-Fc, a las concentraciones cercanas a las fisiológicas de 0,01 y de 0,1 $^{\mu g}/_{ml}$, hay un aumento significativo de la intensidad de fluorescencia asociada a VGlut1 en comparación con el control sin tratamiento y con los controles de isotipo. A su vez, este aumento es comparable al observado en los cultivos tratados con TTX, utilizado como control positivo de plasticidad sináptica. Cabe destacar que, a las concentraciones de rCD300f-Fc en las que se da este fenómeno, no hay muerte neuronal. Esto sugiere que el receptor CD300f y sus ligandos podrían participar en fenómenos plásticos. Otro componente que participa en determinar la fuerza sináptica es el número total de contactos sinápticos por neurona. Se observó un

aumento significativo en el número de contactos sinápticos en los co-cultivos maduros tratados con rCD300f-Fc de a la concentración de 0,01 $^{\mu g}/_{ml}$ y 0,1 $^{\mu g}/_{ml}$ comparados con sus controles de isotipo y el control sin tratamiento (Figura 10B). Nuevamente, hay un aumento comparable del número de los contactos sinápticos entre rCD300f-Fc a dicha concentración y luego del tratamiento con TTX. Estos datos refuerzan la posible participación del par receptor CD300f-ligando en fenómenos de plasticidad sináptica, asociados posiblemente a una falla en la poda sináptica cuando se interrumpe la interacción del CD300f endógeno y sus ligandos. Lo mismo se ha demostrado para TREM2 en co-cultivos, ya que al inhibir TREM2 aumenta el número de sinapsis (Filipello et al., 2018). En nuestras condiciones hemos observado efectos significativos a nivel de modulación de la fuerza sináptica a una concentración de 10 $^{ng}/_{ml}$, lo cual se encuentra dentro del rango de lo que produce la microglía en cultivo (Ejarque-Ortiz et al., 2015). Además, la evaluación fue realizada hasta una concentración mínima de 10 $^{ng}/_{ml}$ mostrando todavía un efecto máximo, siendo posible que el efecto sea significativo a concentraciones aún menores. Este resultado demuestra que CD300f podría estar participando de fenómenos de plasticidad sináptica, así como participando en el *pruning* sináptico, dado que la inhibición endógena genera aumentos en el número de contactos sinápticos y aumentos en la intensidad de VGlut1. Para confirmar la relevancia fisiológica, en nuestro estudio, deberíamos poder determinar el rango de concentración de CD300f soluble en humanos, así como también utilizar el CD300f soluble de líquido céfalo-raquídeo de humanos, de modo de ver si se obtienen los mismos resultados. Como modo de confirmar lo observado en co-cultivos, podríamos emplear estudios electrofisiológicos. Además, podríamos evaluar si el tratamiento con rCD300f-Fc, al inhibir el *pruning* sináptico, induce una disminución del contenido microglial de componentes sinápticos.

La fagocitosis de sinapsis inmaduras y terminales axonales por parte de la microglía ocurre a través de diversos mecanismos. Está demostrado que este fenómeno se da por medio de varios receptores, entre ellos el receptor de complemento microglial CR3/Mac1 (Schafer et al., 2012) y el receptor fagocítico TREM2 (Filipello et al., 2018). En un estudio reciente, se demostró que la PS expuesta representa una señal neuronal de "cómeme" involucrada en la poda mediada por microglía. En cultivos, demostraron que la eliminación de sinapsis

puede ser parcialmente prevenida bloqueando la accesibilidad de la PS expuesta mediante el uso de AV o mediante la pérdida de TREM2 en la microglía (Scott-Hewitt et al., 2020). Dadas las similitudes biológicas entre CD300f y TREM2, analizamos el efecto de la AV en co-cultivos de modo de analizar si se previene la eliminación de la sinapsis del mismo modo que cuando se inhibe el CD300f endógeno. Observamos que la inhibición de la AV no solo genera un aumento en la cantidad de los contactos sinápticos, sino que también aumenta la intensidad de VGlut1, al igual que rCD300f-Fc. Además, resulta interesante analizar el comportamiento del cultivo frente al tratamiento con rCD300f +AV, dado que esta respuesta no fue aditiva, sino que fue similar a la respuesta dada en los tratados con cada uno de forma individual. Este resultado sugeriría que al igual que TREM2, CD300f estaría participando en la eliminación de las sinapsis locales por medio de la PS expuesta. Se ha descrito que el mecanismo de eliminación de una sinapsis local ocurre por vías celulares apoptóticas bien conocidas, incluyendo exposición local de PS y activación local de caspasa 3 (Scott-Hewitt et al., 2020). Para profundizar aún más en el mecanismo por el cual podría estar ocurriendo esta poda sináptica local que involucra a CD300f en nuestro estudio, bloqueamos la caspasa-3 de modo de bloquear la apoptosis inhibiendo la traslocación de la PS a la membrana externa (Györffy et al., 2018). Al analizar los resultados en presencia del inhibidor de caspasa-3, observamos un aumento en la intensidad de VGlut1, así como en la cantidad de contactos sinápticos. Esto concuerda con nuestra hipótesis dado que, al no exponerse la PS, se genera una disminución en la poda sináptica, lo que se ve reflejado en el aumento de contactos sinápticos. Este resultado también ha sido reportado en otros trabajos (Györffy et al., 2018; Sokolova et al., 2021). Nuevamente, los cultivos tratados simultáneamente con rCD300f-IgG+Inh Casp-3 no generaron una respuesta aditiva, sino que presentaron niveles similares a los tratamientos realizados de manera individual, lo cual nuevamente sugiere que CD300f está involucrado en la poda sináptica y que dicha poda ocurriría por un mecanismo apoptótico local por medio de la exposición de PS. Se ha reportado un mecanismo, hasta ahora desconocido, dependiente de la caspasa-3 que impulsa el fallo sináptico y contribuye a la disfunción cognitiva en la enfermedad de Alzheimer (D'Amelio et al., 2011). Esto indica que la caspasa-3 es un posible objetivo para la terapia farmacológica durante las primeras etapas de la

enfermedad. Resultaría interesante analizar animales con el modelo de Alzheimer y CD300f -/-, de modo de ver si la ausencia de CD300f causa un peor pronóstico en la enfermedad.

Muchos estudios resaltan que el mecanismo apoptótico subyacente a la poda sináptica local se da por medio del complemento, siendo C1q el iniciador de la cascada clásica del complemento, uniéndose a la PS expuesta, de modo de llevar a cabo la apoptosis (Györffy et al., 2018). A futuro resultaría interesante determinar cuáles son las sinapsis vulnerables a la eliminación, y qué vías neuroinmunitarias participan y regulan estos procesos. Esto resultaría clave para desarrollar objetivos terapéuticos efectivos contra patologías que involucran alteraciones sinápticas.

En resumen, en este capítulo se aportan evidencias que muestran que el inmunorreceptor CD300f desempeña un rol crítico en la poda sináptica y en la plasticidad sináptica, permitiendo la adaptabilidad neuronal al entorno y contribuyendo al manteniendo la homeostasis del SNC.

CAPITULO 3 DEFICIENCIAS EN CD300f INDUCEN TRASTORNOS COMPORTAMENTALES

Además del rol de la microglía en procesos cerebrales normales, como la transmisión sináptica y la plasticidad neuronal, la microglía participa en procesos cerebrales patológicos, incluyendo enfermedades neuropsiquiatrías (Salter & Stevens, 2017). Se ha demostrado que los inmunorreceptores juegan un rol clave en el fenotipo microglial que desencadena en estos trastornos (Yirmiya et al., 2015). Aunque no se ha asociado ningún inmunorreceptor microglial con el TDM en humanos, la deficiencia en TREM2 o CX3CR1 induce alteraciones en la interacción social y comportamientos compulsivos en ratones no expuestos previamente a estímulos (Filipello et al., 2018; Zhan et al., 2014) o potencia comportamientos depresivos inducidos por LPS (Corona et al., 2010), resaltando su posible papel en condiciones psiquiátricas. A su vez, alteraciones en la poda sináptica como se mencionó anteriormente han sido asociadas a ratones con comportamientos de tipo TOC (S.-K. Chen et al., 2010), con modelos de depresión mayor (Yirmiya et al., 2015), con desordenes obsesivos compulsivos en ratones (S.-K. Chen et al., 2010), con desordenes de espectro de

autista (Tetreault et al., 2012) y con esquizofrenia (Garey, 2010). Con base a los resultados que se obtuvieron en el presente trabajo, en los que demostramos que la inhibición endógena de CD300f en co-cultivos induce alteraciones en la modulación sináptica aumentando la intensidad del marcador presináptico VGlut1 y el número de contactos sinápticos, es que nos propusimos analizar el fenotipo de los animales CD300f -/- mediante comportamientos asociados a desordenes de "tipo psiquiátricos".

Nos resultó relevante llevar a cabo una evaluación que contemple los mecanismos biológicos subyacentes a las diferencias de sexo, por dos motivos: i) por reportes publicados por nuestro grupo en los que se demostró que CD300f podría influir en la patogénesis de la depresión (Lago et al., 2020) y en el trastorno de la ansiedad (Kaufmann et al., 2021) de manera dependiente del sexo, y ii) es de crucial importancia estudiar las diferencias de prevalencia entre hombres y mujeres en las enfermedades psiquiátricas.

Inicialmente se observó que tanto las hembras como los machos CD300f -/- presentan un fenotipo leve de tipo TOC, dado que en ambos casos los CD300f-/- entierran más bolitas que los WT. Ese tipo de comportamiento, como ya se expuso anteriormente, se encuentra íntimamente relacionado a fallas en la poda sináptica (S.-K. Chen et al., 2010), lo cual podrían desencadenar fallas a nivel de la conectividad neuronal generando dicho comportamiento. Al analizar la interacción social mediante el test de las tres cámaras, unido a los resultados del marble burying test se propone que las hembras CD300f -/- presentarían un comportamiento de tipo TEA. De hecho, se ha reportado que una familia con TEA hereditario poseía alteraciones (genes truncados) en los genes de CD300f y en el gen de RPS24, lo cual podría sugerir que en humanos, alteraciones en CD300f inducirían una patología TEA (Inoue et al., 2015).

El test de interacción social de las tres cámaras se realizó en un grupo de hembras y de machos de 3 meses de edad, y en un grupo de hembras y machos de 1 año de edad, pero el test no logró ser validado, por medio del control interno (comportamiento de los animales WT), por lo cual no fue incluido en el estudio. De modo de poder caracterizar el comportamiento social que presentan los animales CD300f -/-, se deberían emplear otros test comportamentales de interacción social que analicen el comportamiento animal-animal, más del tipo

free dyadic (en el cual se analiza el comportamiento del ratón de interés en una arena, en la cual un animal interactúa con otro animal conespecífico y se evalúan comportamientos tales como olfateo, juego etc).

Se ha publicado que deficiencias en la autofagia microglial, analizadas en ratones conllevan a desregulación en la poda sináptica y a comportamientos de tipo compulsivos y de tipo TEA (Kim et al., 2017). Como mencionamos previamente, la autofagia microglial está involucrada en la regulación de la refinación sináptica y las neuroconductas. La eliminación de atg7 específica de células mieloides por el gen lisozima M-Cre en ratones, que es vital para la autofagia, generó un comportamiento social defectuosos y comportamientos repetitivos, características típicas del TEA, y a su vez presentaron defectos en la refinación sináptica (Kim et al., 2017). Nuestro grupo ha mostrado que la microglía CD300f-/- estimulada *in vivo* con LPS IP posiblemente presente deficiencias a nivel de la autofagia (Lago et al., 2020). Por lo tanto, podría ocurrir que los ratones CD300f -/- presenten fallas en la autofagia microglial, y que esto derive no solo a cambios en la modulación sináptica como observamos, sino que también a cambios a nivel comportamental.

CD300f posee un polimorfismo de nucleótido único (SNP, rs2034310) que es altamente prevalente y determina un intercambio C/T (frecuencias medias ~18 y 29% en las poblaciones europea y americana, respectivamente), produciendo una sustitución no sinónima de Arg por Gln (R218Q) en la cola citoplasmática del receptor y cambios a nivel se señalización celular (Lago et al., 2020). Este polimorfismo en humanos genera protección contra TDM en mujeres, pero no en hombres (Lago et al., 2020), por lo que la protección contra el TDM podría señalar una diferencia de sexo. En este doctorado nos planteamos profundizar en el análisis del comportamiento depresivo en hembras y machos dependiente de CD300f. CD300f aparece entre los genes más sobreexpresados en la microglía después de una inyección IP de LPS (Bennett et al., 2016) y después de una lesión en la médula espinal (Torres-Espín et al., 2013). Muy recientemente, también se asoció CD300f a la respuesta neuroprotectora contra la patología Tau (Ising et al., 2019). Con base a estos reportes es que se analizó el comportamiento en animales con y sin LPS de modo de profundizar en los datos ya publicados. Analizando el comportamiento de los animales adultos (3

meses), observamos, de acuerdo a lo publicado anteriormente, que las hembras CD300f-/- presentaron un comportamiento anhedónico de tipo depresivo, mientras que los machos no. El comportamiento depresivo fue confirmado también en hembras de otra cepa de animales CD300f -/- generado por nuestro grupo en colaboración con la UBAL del Institut Pasteur de Montevideo denominada CD300f^{IPMont}-/-. En los animales machos, la inyección de LPS indujo el comportamiento tipo depresivo, tanto en los WT como en los CD300f -/-, observándose menor tiempo de acicalamiento en los animales inyectados con LPS, comparándolos con los inyectados con salino. Sin embargo, ambos genotipos WT y CD300f-/- mostraron tiempos de acicalamiento similares. En las hembras inyectadas con LPS, comparando los dos genotipos, se observó que las hembras CD300f -/- se acicalan menos tiempo que las WT, al igual que lo que se había observado en las hembras inyectadas con salino. Cuando se analiza el comportamiento en un grupo de hembras de 7 meses de edad en condiciones basales, no solo se ve que presentan el comportamiento de tipo depresivo, sino que también este se ve potenciado. Esta diferencia aún mayor en los tiempos de acicalamiento podría deberse a la edad, dado que en un artículo publicado de nuestro grupo se demostró que la ausencia de CD300f induce un deterioro cognitivo relacionado con la edad (a partir de los 18 meses) (Evans et al., 2023). El desarrollo de la colonia de animales KOc, nos permitió analizar la contribución de CD300f de los macrófagos residentes y de la microglía, y analizar su participación en los trastornos comportamentales. A su vez, nos permite generar la deficiencia de CD3000f a la edad que consideremos relevante para el análisis (dado que se genera por la inyección IP de TMX). Por medio de la inyección de TMX se induce la pérdida específica del gen cd300f en las poblaciones celulares CX3CR1+, el cual se recupera al cabo de 4 semanas en aquellas células que presentan altas tasas de renovación desde progenitores mieloides, pero que se mantiene en las que presentan tasas menores o tienen autorrenovación desde la población local ya establecida (Goldmann et al., 2013). La microglía tiene bajas tasas de recambio en condiciones homeostáticas y presentan autorrenovación dentro del parénquima nervioso (B. P. Hammond et al., 2021). A su vez, sucede lo mismo con los macrófagos de barrera (perivasculares y de meninges) presentes en el SNC, ya que tienen la particularidad de renovarse desde progenitores de la misma población

(Goldmann et al., 2016). A hembras de 4 meses de edad se les administro TMX y a las 3 o 5 semanas de la administración se realizó el SST. Los resultados obtenidos mostraron que a las 3 semanas presentan un comportamiento de tipo depresivo, fenotipo que se ve potenciado a las 5 semanas. Este resultado por un lado muestra el rol de CD300f microglial y de macrófagos de barreras en el comportamiento depresivo y por otro pone en evidencia que este trastorno no es consecuencia de fallas en la poda sináptica durante el desarrollo sino que la ausencia de CD300f microglial o de macrófagos residentes en animales adultos serían los responsables del fenotipo depresivo.

Una de las hipótesis que considerábamos posible era que en ausencia de una señal de restricción (CD300f), la microglía y los macrófagos perivasculares podrían inducir neuroinflamación de bajo grado que podría dar lugar a un comportamiento de tipo depresivo o de tipo TOC. Sin embargo, si bien la ausencia de CD300f condujo a este tipo de comportamientos, estos no estaban asociados a neuroinflamación evidente (estudio de ARNseq, de (Lago et al., 2020)). Además, habíamos observado que los medios condicionados de co-cultivos tratados con rCD300f-Fc, generaban neurotoxicidad en cultivos de neuronas, pero estos medios no presentaban aumentos en ninguna citoquina asociada a la neuroinflamación. A su vez, resultados de nuestro grupo *in vivo* mostraron que el análisis del perfil de expresión génica de ARN mensajero mediante qPCR para la expresión de moléculas proinflamatorias en todo el cerebro o la secuenciación de ARN de células microgliales de animales WT y CD300f-/- en condiciones *naive*, no mostraron cambios significativos entre la mayoría de los genes analizados. Los niveles de ARNm característicos para células infiltrantes como CD4 (subconjunto de linfocitos T), Mpo (neutrófilos) e Il17a (células Th17) permanecieron estables, lo que sugiere la ausencia de infiltración de estas células. Curiosamente, nuestro grupo reportó que aunque no se observaron cambios en el número de macrófagos perivasculares en el SNC de los animales CD300f−/−, dos de sus marcadores más específicos, CD163 y Siglec1 (Keren-Shaul et al., 2017; Zeisel et al., 2015), mostraron un aumento en la expresión de ARNm, lo que sugiere un cambio fenotípico en este tipo celular (Lago et al., 2020). CD163 se encuentra entre los 40 genes comunes que se ven alterados en varias condiciones psiquiátricas importantes, incluyendo el TDM, trastorno bipolar (BP), TEA, esquizofrenia o trastorno por abuso de alcohol

(AAD), y tanto CD163 como Siglec1 están incluidos en una red de coexpresión asociada al TDM (Gandal et al., 2018). Esto sugiere que los macrófagos perivasculares pueden desempeñar un papel en el TDM y que la alteración funcional de estas células en ratones CD300f−/− podría contribuir al fenotipo depresivo. Por otro lado, un reporte demuestra que ratones deficientes para CCR2 (CCR2KO) o ratones deficientes para el receptor de fractalquina (CX3CR1KO) no logran reclutar macrófagos al cerebro y por lo tanto no desarrollan comportamientos similares a la ansiedad después de ser sometidos a la derrota social repetida (RSD de las siglas en inglés) (Wohleb et al., 2013). Otros autores en esta misma línea de pensamiento demuestran que al inhibir la infiltración de monocitos derivados de la médula ósea en el hipocampo con un inhibidor de CCR2, se atenúa el comportamiento de tipo depresivo inducido por el síndrome de privación de cuidado materno (Hu et al., 2022). Sumado a estos reportes y en base a los resultados del análisis del ARNseq de ARNm de microglía de hipocampo de animales WT y CD300f -/-, en el cual uno de los genes sobreexpresados en CD300f -/- es CCR2, nos planteamos la hipótesis de si macrófagos infiltrantes CCR2+ en los ratones CD300f-/- estarían jugando un rol esencial en el comportamiento depresivo. Para abordar dicha hipótesis, se trabajó con dos grupos de hembras KOc, un grupo al que se le administro el inhibidor de CCR2 y otro con vehículo. A las 3 semanas de la última inyección de TMX, se observó como los dos grupos de hembras KOc, con y sin inhibidor presentaban comportamiento de tipo depresivo, tal como lo habíamos observado en los resultados previos en el Doctorado. De todos modos, si se analiza el tiempo de acicalamiento (anhedonia) entre los grupos KOc, las hembras que fueron tratadas con el inhibidor muestran una fuerte tendencia ($p=0.06$) hacia un aumento en el tiempo de acicalamiento comparadas con las hembras tratadas con el vehículo, sugiriendo que el inhibidor habría comenzado a actuar. Al analizar el comportamiento a las 5 semanas de la última inyección de TMX, (aproximadamente a los 20 días de la última inyección del inhibidor) se observó que el comportamiento depresivo fue completamente revertido, los animales KOc+Inhibidor de CCR2 se acicalan tiempos similares a los tiempos de acicalamiento de los animales control. De este grupo de resultados se puede concluir que en condiciones basales la ausencia de CD300f indujo alteraciones fenotípicas en microglía y macrófagos de la barrera del SNC que llevaron al

reclutamiento de macrófagos CCR2+, y que este reclutamiento es esencial para la generación del comportamiento similar a la depresión. No se conoce con exactitud cuál es el mecanismo detrás del reclutamiento de macrófagos CCR2+ que determina el comportamiento depresivo. Lo que sí fue reportado por diferentes grupos y en diferentes modelos es que mediante el eje CCR2-CCl2 se reclutan macrófagos CCR2+, y que esto es esencial para la generación del comportamiento depresivo (Chan et al., 2023; H. J. Chen et al., 2020; Hu et al., 2022; Menard et al., 2017; Mirzadegan et al., 2000; Sawada et al., 2014; Sudre et al., 2023; Wohleb et al., 2013). Por ejemplo, en uno de los reportes mencionados (Wohleb et al., 2013) utilizan el modelo de trasplante de medula ósea y describen que uno de los mecanismos por medio de los cuales los macrófagos CCR2+ podrían inducir el fenotipo depresivo es que al entrar al hipocampo, se diferencian en microglía, lo que genera un aumento no solo en el número de microglía, sino que además generaron una activación de la microglía que puede producir citoquinas inflamatorias, quimioquinas y prostaglandinas. Sin embargo, es importante destacar que este tipo de modelos que involucran trasplante de médula ósea no son fisiológicos. Otro grupo utilizando el modelo de estrés crónico social (con un grupo de ratones susceptibles al estrés, y otro grupo de ratones resilientes) sugiere que el estrés social crónico altera la integridad de la barrera hematoencefálica (BBB) mediante la disminución de la proteína de unión estrecha Cldn5 en el núcleo accumbens (NAc) (Menard et al., 2017). Esto, combinado con el reclutamiento inducido por el estrés de señales inmunológicas periféricas, resulta en el paso de proteínas circulantes en la sangre como la IL-6, y el desarrollo de comportamientos similares a la depresión de ratones susceptibles al estrés, pero no en los resilientes. En el mismo trabajo evaluaron si los monocitos periféricos que expresan el receptor de quimiocinas C-C 2 (Ccr2+) pueden infiltrar el parénquima cerebral en regiones relacionadas con el estrés. Luego de 10 días del estrés Crónico de Derrota Social (CSDS de sus siglas en inglés) demostraron un aumento significativo de células CCR2+ en el compartimento perivascular y en la expresión de ARNm de Ccr2 en los ratones, lo cual se correlacionó con la evitación social (Menard et al., 2017). Otro reporte utiliza el modelo de estrés prenatal (PNS, por sus siglas en inglés) que está asociado con trastornos neuropsiquiátricos en la descendencia, como ansiedad, depresión y trastornos

del espectro autista. En los ratones WT, el PNS conduce a inflamación en la placenta y el cerebro fetal, incluyendo un aumento en la quimioquina CCL2. Además, el PNS en ausencia de CCL2 (CCL2−/−) no logró aumentar la citoquina proinflamatoria IL-6 en el cerebro fetal. La descendencia del PNS también presentó déficits en sociabilidad y comportamiento similar a la ansiedad que estaban ausentes en la descendencia del PNS con eliminación de CCL2. El triptófano y la serotonina (5-HT) estaban elevados en la placenta del PNS WT, pero no en los animales CCL2−/− por lo que sugieren que hay una interacción compleja entre la inflamación y el metabolismo de la serotonina regulando la aparición de anormalidades conductuales después del PNS (H. J. Chen et al., 2020).

CAPITULO 4 CARACTERIZACIÓN DEL FENOTIPO MICROGLIAL DE CD300f-/- EN ANIMALES ENVEJECIDOS

La mayoría de los estudios sobre la función de CD300f han demostrado que tiene un perfil protector y antiinflamatorio en modelos de ratones con esclerosis múltiple (Xi et al., 2010), lupus (Tian et al., 2016; Tian, Choi, Murakami, Allen, Morse, et al., 2014), alergias (Izawa et al., 2012) o daño cerebral agudo (Peluffo, et al., 2012). Sin embargo, la activación *in vitro* de CD300f potenció el perfil proinflamatorio de la microglía cuando estas fueron estimuladas con LPS (Ejarque-ortiz et al., 2015). Por otro lado, no se observaron cambios en las principales moléculas de señalización proinflamatoria en la microglía de ratones deficientes en CD300f *in vivo* después de un desafío intraperitoneal con LPS (Lago et al., 2020), lo que sugiere roles complejos de este receptor inmunitario en la regulación de la inflamación. Se ha demostrado que las variantes genéticas de CD300f también están involucradas en la susceptibilidad a enfermedades inflamatorias y autoinmunitarias en humanos (Ban et al., 2010b; Danik et al., 2009; Lago et al., 2020). Interesantemente, CD300f también se ha asociado a funciones inflamatorias no clásicas de la microglía y potencialmente a los macrófagos asociados a barreras del SNC (BAM), lo que lleva a la modulación de condiciones neuropsiquiátricas como el trastorno depresivo mayor y la ansiedad (Kaufmann et al., 2021; Lago et al., 2020).

En nuestro trabajo recientemente aceptado, mostramos diversas evidencias que apuntan hacia la idea de que los ratones CD300f-/- muestran varios rasgos

distintivos del envejecimiento y patologías asociadas al envejecimiento que se relacionan con una disminución de la salud a lo largo de la vida (Evans et al., 2023). Estos incluyen la aparición temprana de diversas neoplasias, inflamación crónica de bajo grado o "*inflamaging*" (inflamación asociada al envejecimiento), fragilidad, alteraciones en las vías de proteostasis cerebral, aumento de la senescencia cerebral y del deterioro cognitivo, y en el caso de las hembras, también alteraciones metabólicas sistémicas. Un proceso importante que dificulta entender la posible causa de la muerte durante el envejecimiento es el hecho de que la edad biológica difiere de la edad cronológica y varía entre sujetos (Horvath & Raj, 2018).

Aunque no hemos descartado todas las posibles causas de la muerte, hemos analizado muchos parámetros biológicos relevantes. No se observaron alteraciones generales ni en los marcadores clínicos de patologías renales y hepáticas, ni en la mayoría de los recuentos de células sanguíneas hasta los 18 meses de edad. Algunos ratones CD300f-/- mostraron alteraciones patológicas en diferentes sistemas, como una disminución marcada en el recuento de plaquetas (trombocitopenia), aumento del peso del bazo (posiblemente indicativo de enfermedades autoinmunes), hipoglucemia o anemia. Por lo tanto, nuestros datos apuntan a la ausencia de una patología subyacente importante única en los ratones CD300f-/-, si no a las causas generales esperadas de la muerte relacionadas con el envejecimiento. En consecuencia, se observó un aumento en la GGT plasmática en ratones hembra CD300f-/- que tuvieron que ser sacrificadas debido a consideraciones éticas de punto final, y niveles elevados circulantes de esta enzima se han asociado con la mortalidad por todas las causas (Ndrepepa et al., 2018).

Es por esto que como objetivo final, nos propusimos llevar a cabo una caracterización fenotípica microglial en envejecimiento como modelo de inflamación crónica por medio del análisis del transcriptoma del cerebro completo de hembras WT y CD300f-/- de 30 meses de edad mediante RNAseq. Dicho estudio demostró que CD300f regula el fenotipo de la microglía y de los macrófagos durante el envejecimiento. Esto podría ampliar el efecto de la deficiencia de CD300f a todo el organismo, afectando a los macrófagos residentes en tejidos de todo el cuerpo y en diferentes órganos. Como posible

receptor de tipo DAMP (patrón molecular asociado a daño, por sus siglas en inglés), el CD300f podría cooperar con otros receptores, como TREM2, para detectar DAMPs y otros lípidos tóxicos derivados del daño crónico de bajo grado en los tejidos durante el envejecimiento (Dong et al., 2021). Esto permitiría eliminarlos del espacio extracelular al mismo tiempo que atenúa la reacción inflamatoria, contribuyendo a restablecer la homeostasis. De hecho, el CD300f también puede inhibir la señalización proinflamatoria de receptores PAMP, como los receptores tipo Toll (S.-M. Lee et al., 2011). Esto es especialmente importante para el SNC, ya que tolera mal la inflamación y es un tejido con una importante cantidad de lípidos y restos lipídicos generados por el recambio normal de la mielina, después de una lesión o bajo condiciones neurodegenerativas crónicas. Según un estudio reciente (Silvin et al., 2022), la microglía DAM es de origen embrionario y aparecerían solo en el contexto de la neurodegeneración y no durante el envejecimiento normal. Por el contrario, el mismo estudio sugiere que las DIM (macrófagos derivados de monocitos) se acumularían principalmente con la edad, la neuroinflamación y al menos en la neurodegeneración relacionada con la enfermedad de Alzheimer (Silvin et al., 2022). Nuestro análisis del fenotipo de la microglía y los macrófagos mediante secuenciación de ARN mostró un aumento en los estados DAM y DIM en ratones hembra de 30 meses de edad con deficiencia de CD300f. Por lo tanto, estos datos apuntarían hacia un envejecimiento aumentado, pero también procesos neurodegenerativos en el cerebro de los ratones con deficiencia de CD300f. Además, a diferencia de TREM2, el CD300f contribuiría al mantenimiento del fenotipo homeostático de la microglía durante el envejecimiento, ya que la ausencia de CD300f estimula la aparición de fenotipos DAM en detrimento de los fenotipos denominados homeostáticos. Si el mantenimiento del fenotipo homeostático de la microglía es necesario para un envejecimiento cerebral saludable, o si, por el contrario, el fenotipo DAM es una reacción importante de las células microgliales para hacer frente a los cambios cerebrales asociados al envejecimiento, necesita establecerse en futuros estudios.

Para relacionar el fenotipo comportamental con el fenotipo microglial, deben realizarse análisis fenotípicos microgliales más profundos de animales CD300f -/- adultos. Por ejemplo, sería interesante llevar a cabo estudios transcriptómicos

de *single-cell RNAseq*, o incluso de transcriptómica espacial para comprender tanto el fenotipo de la microglía como el de los macrófagos CCR2+ que son reclutados.

CONCLUSIONES

El presente trabajo aporta evidencias que apoyan la hipótesis de que CD300f participa en la modulación de la supervivencia neuronal *in vitro* y después de una lesión cerebral penetrante *in vivo*, y que la inhibición de CD300f altera el fenotipo microglial generando un microentorno neurotóxico. A su vez, CD300f participaría en fenómenos de plasticidad sináptica contribuyendo a llevar a cabo o regular la poda sináptica por medio de un mecanismo apoptótico que involucraría a la PS (Figura 28).

Reportamos una asociación clara que vincula la función CD300f con el comportamiento de tipo TOC tanto en machos como en hembras y con alteraciones en el comportamiento de interacción social que podrían corresponder con un comportamiento de tipo TEA en hembras. Las alteraciones comportamentales de tipo depresivo, solo se observaron en hembras, por lo que CD300f estaría involucrado en la modulación de comportamientos patológicos de manera dependiente del sexo (Figura 28).

Analizando el fenotipo microglial, observamos que los animales adultos presentan cambios sutiles en el fenotipo que llevan al reclutamiento de macrófagos CCR2+. Además, cuando ocurre una inflamación crónica de bajo grado como durante el envejecimiento, se evidencia el rol anti-inflamatorio del CD300f microglial reportado para otras patologías sistémicas (Figura 28).

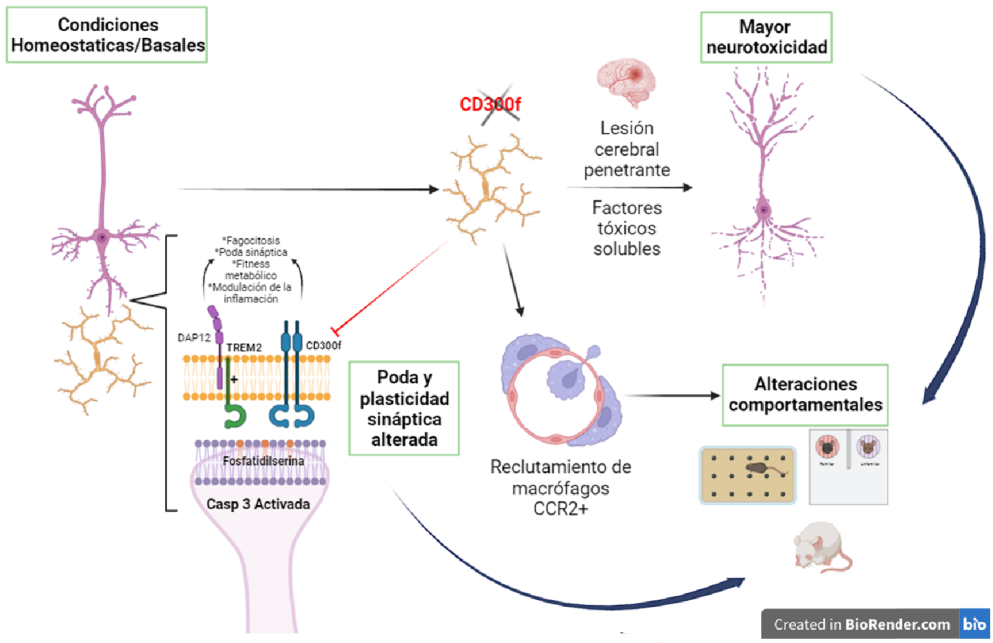

Figura 28: Caracterizacion del rol del inmunorreceptor CD300f en el SNC. Esquema de las conclusiones finales.

En su conjunto, el presente trabajo aporta evidencias de la importancia del inmunorreceptor CD300f microglial en la función del SNC. Demostramos que CD300f es clave para el mantenimiento de la homeostasis del SNC, y que participa en la poda sináptica y en los procesos de plasticidad sináptica regulando el fenotipo microglial. A su vez se evidenció que la ausencia de este imnunorreceptor desencadena cambios comportamentales que al menos en el caso de los comportamientos de tipo depresivos involucra procesos más complejos que incluyen el reclutamiento de células de la inmunidad innata y que dependen del sexo.

REFERENCIAS

Absinta, M., Maric, D., Gharagozloo, M., Garton, T., Smith, M. D., Jin, J., Fitzgerald, K. C., Song, A., Liu, P., Lin, J. P., Wu, T., Johnson, K. R., McGavern, D. B., Schafer, D. P., Calabresi, P. A., & Reich, D. S. (2021). A lymphocyte–microglia–astrocyte axis in chronic active multiple sclerosis. *Nature*, *597*(7878), 709–714. https://doi.org/10.1038/s41586-021-03892-7

Ajami, B., Bennett, J. L., Krieger, C., Tetzlaff, W., & Rossi, F. M. V. (2007). Local self-renewal can sustain CNS microglia maintenance and function throughout adult life. *Nature Neuroscience*, *10*(12), 1538–1543. https://doi.org/10.1038/nn2014

Alvarez-Errico, D., Aguilar, H., Kitzig, F., Brckalo, T., Sayós, J., & López-Botet, M. (2004). IREM-1 is a novel inhibitory receptor expressed by myeloid cells. *European Journal of Immunology*, *34*(12), 3690–3701. https://doi.org/10.1002/eji.200425433

Alvarez-Errico, D., Sayós, J., & López-Botet, M. (2007). The IREM-1 (CD300f) inhibitory receptor associates with the p85alpha subunit of phosphoinositide 3-kinase. *Journal of Immunology (Baltimore, Md.: 1950)*, *178*(2), 808–816. http://www.ncbi.nlm.nih.gov/pubmed/17202342

Anderson, S. R., Zhang, J., Steele, M. R., Romero, C. O., Kautzman, A. G., Schafer, D. P., & Vetter, M. L. (2019). Complement targets newborn retinal ganglion cells for phagocytic elimination by microglia. *Journal of Neuroscience*, *39*(11), 2025–2040. https://doi.org/10.1523/JNEUROSCI.1854-18.2018

Angoa-pérez, M., Kane, M. J., Briggs, D. I., Francescutti, D. M., & Kuhn, D. M. (2013). *Marble Burying and Nestlet Shredding as Tests of Repetitive , Compulsive-like Behaviors in Mice*. *December*, 1–7. https://doi.org/10.3791/50978

Araque et al., 2013 Sheean. (2014). Araque et al. *Bone*, *23*(1), 1–7. https://doi.org/10.1016/j.neuron.2014.02.007.Gliotransmitters

Augusto-Oliveira, M., Arrifano, G. P., Takeda, P. Y., Lopes-Araújo, A., Santos-Sacramento, L., Anthony, D. C., Verkhratsky, A., & Crespo-Lopez, M. E. (2020). Astroglia-specific contributions to the regulation of synapses, cognition and behaviour. *Neuroscience and Biobehavioral Reviews*, *118*(July), 331–357. https://doi.org/10.1016/j.neubiorev.2020.07.039

Ban, M., McCauley, J. L., Zuvich, R., Baker, A., Bergamaschi, L., Cox, M., Kemppinen,

A., D'Alfonso, S., Guerini, F. R., Lechner-Scott, J., Dudbridge, F., Wason, J., Robertson, N. P., De Jager, P. L., Hafler, D. A., Barcellos, L. F., Ivinson, A. J., Sexton, D., Oksenberg, J. R., … Sawcer, S. (2010a). A non-synonymous SNP within membrane metalloendopeptidase-like 1 (MMEL1) is associated with multiple sclerosis. *Genes and Immunity*, *11*(8), 660–664. https://doi.org/10.1038/gene.2010.36

Ban, M., McCauley, J. L., Zuvich, R., Baker, A., Bergamaschi, L., Cox, M., Kemppinen, A., D'Alfonso, S., Guerini, F. R., Lechner-Scott, J., Dudbridge, F., Wason, J., Robertson, N. P., De Jager, P. L., Hafler, D. A., Barcellos, L. F., Ivinson, A. J., Sexton, D., Oksenberg, J. R., … Sawcer, S. (2010b). A non-synonymous SNP within membrane metalloendopeptidase-like 1 (MMEL1) is associated with multiple sclerosis. *Genes and Immunity*, *11*(8), 660–664. https://doi.org/10.1038/gene.2010.36

Basilico, B., Pagani, F., Grimaldi, A., Cortese, B., Di Angelantonio, S., Weinhard, L., Gross, C., Limatola, C., Maggi, L., & Ragozzino, D. (2019). Microglia shape presynaptic properties at developing glutamatergic synapses. *Glia*, *67*(1), 53–67. https://doi.org/10.1002/glia.23508

Bennett, M. L., Bennett, F. C., Liddelow, S. A., Ajami, B., Zamanian, J. L., Fernhoff, N. B., Mulinyawe, S. B., Bohlen, C. J., Adil, A., Tucker, A., Weissman, I. L., Chang, E. F., Li, G., Grant, G. A., Hayden Gephart, M. G., & Barres, B. A. (2016). New tools for studying microglia in the mouse and human CNS. *Proceedings of the National Academy of Sciences of the United States of America*, *113*(12), E1738-46. https://doi.org/10.1073/pnas.1525528113

Bernas, T., & Dobrucki, J. (2002). Mitochondrial and nonmitochondrial reduction of MTT: interaction of MTT with TMRE, JC-1, and NAO mitochondrial fluorescent probes. *Cytometry*, *47*(4), 236–242. http://www.ncbi.nlm.nih.gov/pubmed/11933013

Bernier, L. P., York, E. M., Kamyabi, A., Choi, H. B., Weilinger, N. L., & MacVicar, B. A. (2020). Microglial metabolic flexibility supports immune surveillance of the brain parenchyma. *Nature Communications*, *11*(1). https://doi.org/10.1038/s41467-020-15267-z

Biber, K., Laurie, D. J., Berthele, A., Sommer, B., Tölle, T. R., Gebicke-Härter, P. J., Van Calker, D., & Boddeke, H. W. G. M. (1999). Expression and signaling of group I metabotropic glutamate receptors in astrocytes and microglia. *Journal of*

Neurochemistry, *72*(4), 1671–1680. https://doi.org/10.1046/j.1471-4159.1999.721671.x

Binder, D. K., Nagelhus, E. A., & Ottersen, O. P. (2012). Aquaporin-4 and epilepsy. *Glia*, *60*(8), 1203–1214. https://doi.org/10.1002/glia.22317

Bolós, M., Perea, J. R., Terreros-Roncal, J., Pallas-Bazarra, N., Jurado-Arjona, J., Ávila, J., & Llorens-Martín, M. (2018). Absence of microglial CX3CR1 impairs the synaptic integration of adult-born hippocampal granule neurons. *Brain, Behavior, and Immunity*, *68*, 76–89. https://doi.org/10.1016/j.bbi.2017.10.002

Borrego, F. (2013a). The CD300 molecules: an emerging family of regulators of the immune system. *Blood*, *121*(11), 1951–1960. https://doi.org/10.1182/blood-2012-09-435057

Borrego, F. (2013b). The CD300 molecules: an emerging family of regulators of the immune system. *Blood*, *121*(11), 1951–1960. https://doi.org/10.1182/blood-2012-09-435057

Branco, T., Staras, K., Darcy, K. J., & Goda, Y. (2008). Local Dendritic Activity Sets Release Probability at Hippocampal Synapses. *Neuron*, *59*(3), 475–485. https://doi.org/10.1016/j.neuron.2008.07.006

Brioschi, S., d'Errico, P., Amann, L. S., Janova, H., Wojcik, S. M., Meyer-Luehmann, M., Rajendran, L., Wieghofer, P., Paolicelli, R. C., & Biber, K. (2020). Detection of Synaptic Proteins in Microglia by Flow Cytometry. *Frontiers in Molecular Neuroscience*, *13*(September), 1–12. https://doi.org/10.3389/fnmol.2020.00149

Cardoso, A. L., Fernandes, A., Aguilar-Pimentel, J. A., de Angelis, M. H., Guedes, J. R., Brito, M. A., Ortolano, S., Pani, G., Athanasopoulou, S., Gonos, E. S., Schosserer, M., Grillari, J., Peterson, P., Tuna, B. G., Dogan, S., Meyer, A., van Os, R., & Trendelenburg, A. U. (2018). Towards frailty biomarkers: Candidates from genes and pathways regulated in aging and age-related diseases. *Ageing Research Reviews*, *47*(July), 214–277. https://doi.org/10.1016/j.arr.2018.07.004

Cassina, P., Peluffo, H., Pehar, M., Martinez-Palma, L., Ressia, A., Beckman, J. S., Estévez, A. G., & Barbeito, L. (2002). Peroxynitrite triggers a phenotypic transformation in spinal cord astrocytes that induces motor neuron apoptosis. *Journal of Neuroscience Research*, *67*(1), 21–29. https://doi.org/10.1002/jnr.10107

Chan, K. L., Poller, W. C., Swirski, F. K., & Russo, S. J. (2023). Central regulation of stress-evoked peripheral immune responses. *Nature Reviews Neuroscience*, *24*(10), 591–604. https://doi.org/10.1038/s41583-023-00729-2

Chen, H. J., Antonson, A. M., Rajasekera, T. A., Patterson, J. M., Bailey, M. T., & Gur, T. L. (2020). Prenatal stress causes intrauterine inflammation and serotonergic dysfunction, and long-term behavioral deficits through microbe- and CCL2-dependent mechanisms. *Translational Psychiatry*, *10*(1). https://doi.org/10.1038/s41398-020-00876-5

Chen, S.-K., Tvrdik, P., Peden, E., Cho, S., Wu, S., Spangrude, G., & Capecchi, M. R. (2010). Hematopoietic origin of pathological grooming in Hoxb8 mutant mice. *Cell*, *141*(5), 775–785. https://doi.org/10.1016/j.cell.2010.03.055

Choi, S.-C., Simhadri, V. R., Tian, L., Gil-Krzewska, A., Krzewski, K., Borrego, F., & Coligan, J. E. (2011a). Cutting edge: mouse CD300f (CMRF-35-like molecule-1) recognizes outer membrane-exposed phosphatidylserine and can promote phagocytosis. *Journal of Immunology (Baltimore, Md.□: 1950)*, *187*(7), 3483–3487. https://doi.org/10.4049/jimmunol.1101549

Choi, S.-C., Simhadri, V. R., Tian, L., Gil-Krzewska, A., Krzewski, K., Borrego, F., & Coligan, J. E. (2011b). Cutting Edge: Mouse CD300f (CMRF-35-Like Molecule-1) Recognizes Outer Membrane-Exposed Phosphatidylserine and Can Promote Phagocytosis. *The Journal of Immunology*, *187*(7), 3483–3487. https://doi.org/10.4049/jimmunol.1101549

Clark, G. J., Ju, X., Azlan, M., Tate, C., Ding, Y., & Hart, D. N. J. (2009). The CD300 molecules regulate monocyte and dendritic cell functions. *Immunobiology*, *214*(9–10), 730–736. https://doi.org/10.1016/j.imbio.2009.06.004

Clayton, B. L. L., & Tesar, P. J. (2021). Oligodendrocyte progenitor cell fate and function in development and disease. *Current Opinion in Cell Biology*, *73*, 35–40. https://doi.org/10.1016/j.ceb.2021.05.003

Colonna, M. (2023). The biology of TREM receptors. *Nature Reviews Immunology*, *23*(9), 580–594. https://doi.org/10.1038/s41577-023-00837-1

Corona, A. W., Huang, Y., O'Connor, J. C., Dantzer, R., Kelley, K. W., Popovich, P. G., & Godbout, J. P. (2010). Fractalkine receptor (CX3CR1) deficiency sensitizes mice to the behavioral changes induced by lipopolysaccharide. *Journal of Neuroinflammation*, *7*(1), 93. https://doi.org/10.1186/1742-2094-7-93

Coull, J. A. M., Beggs, S., Boudreau, D., Boivin, D., Tsuda, M., Inoue, K., Gravel, C., Salter, M. W., & De Koninck, Y. (2005). BDNF from microglia causes the shift in neuronal anion gradient underlying neuropathic pain. *Nature*, *438*(7070), 1017–1021. https://doi.org/10.1038/nature04223

Crotti, A., & Ransohoff, R. M. (2016). Microglial Physiology and Pathophysiology: Insights from Genome-wide Transcriptional Profiling. *Immunity*, *44*(3), 505–515. https://doi.org/10.1016/j.immuni.2016.02.013

Cserép, C., Pósfai, B., Lénárt, N., Fekete, R., László, Z. I., Lele, Z., Orsolits, B., Molnár, G., Heindl, S., Schwarcz, A. D., Ujvári, K., Környei, Z., Tóth, K., Szabadits, E., Sperlágh, B., Baranyi, M., Csiba, L., Hortobágyi, T., Maglóczky, Z., … Dénes, Á. (2020). Microglia monitor and protect neuronal function through specialized somatic purinergic junctions. *Science*, *367*(6477), 528–537. https://doi.org/10.1126/science.aax6752

Curzytek, K., & Leśkiewicz, M. (2021). Targeting the CCL2-CCR2 axis in depressive disorders. *Pharmacological Reports*, *73*(4), 1052–1062. https://doi.org/10.1007/s43440-021-00280-w

D'Amelio, M., Cavallucci, V., Middei, S., Marchetti, C., Pacioni, S., Ferri, A., Diamantini, A., De Zio, D., Carrara, P., Battistini, L., Moreno, S., Bacci, A., Ammassari-Teule, M., Marie, H., & Cecconi, F. (2011). Caspase-3 triggers early synaptic dysfunction in a mouse model of Alzheimer's disease. *Nature Neuroscience*, *14*(1), 69–79. https://doi.org/10.1038/nn.2709

Danik, J. S., Paré, G., Chasman, D. I., Zee, R. Y. L., Kwiatkowski, D. J., Parker, A., Miletich, J. P., & Ridker, P. M. (2009a). Novel loci, including those related to Crohn disease, psoriasis, and inflammation, identified in a genome-wide association study of fibrinogen in 17 686 women: the Women's Genome Health Study. *Circulation. Cardiovascular Genetics*, *2*(2), 134–141. https://doi.org/10.1161/CIRCGENETICS.108.825273

Danik, J. S., Paré, G., Chasman, D. I., Zee, R. Y. L., Kwiatkowski, D. J., Parker, A., Miletich, J. P., & Ridker, P. M. (2009b). Novel loci, including those related to Crohn disease, psoriasis, and inflammation, identified in a genome-wide association study of fibrinogen in 17 686 women: the Women's Genome Health Study. *Circulation. Cardiovascular Genetics*, *2*(2), 134–141. https://doi.org/10.1161/CIRCGENETICS.108.825273

Davalos, D., Grutzendler, J., Yang, G., Kim, J. V, Zuo, Y., Jung, S., Littman, D. R., Dustin, M. L., & Gan, W.-B. (2005). ATP mediates rapid microglial response to local brain injury in vivo. *Nature Neuroscience*, *8*(6), 752–758. https://doi.org/10.1038/nn1472

De Andrade Costa, A., Chatterjee, J., Cobb, O., Sanapala, S., Scheaffer, S., Guo, X., Dahiya, S., & Gutmann, D. H. (2022). RNA sequence analysis reveals ITGAL/CD11A as a stromal regulator of murine low-grade glioma growth. *Neuro-Oncology*, *24*(1), 14–26. https://doi.org/10.1093/neuonc/noab130

De Biase, L. M., Schuebel, K. E., Fusfeld, Z. H., Jair, K., Hawes, I. A., Cimbro, R., Zhang, H. Y., Liu, Q. R., Shen, H., Xi, Z. X., Goldman, D., & Bonci, A. (2017). Local Cues Establish and Maintain Region-Specific Phenotypes of Basal Ganglia Microglia. *Neuron*, *95*(2), 341-356.e6. https://doi.org/10.1016/j.neuron.2017.06.020

De Schepper, S., Crowley, G., & Hong, S. (2021). Understanding microglial diversity and implications for neuronal function in health and disease. *Developmental Neurobiology*, *81*(5), 507–523. https://doi.org/10.1002/dneu.22777

Dong, Y., D'Mello, C., Pinsky, W., Lozinski, B. M., Kaushik, D. K., Ghorbani, S., Moezzi, D., Brown, D., Melo, F. C., Zandee, S., Vo, T., Prat, A., Whitehead, S. N., & Yong, V. W. (2021). Oxidized phosphatidylcholines found in multiple sclerosis lesions mediate neurodegeneration and are neutralized by microglia. *Nature Neuroscience*, *24*(4), 489–503. https://doi.org/10.1038/s41593-021-00801-z

Ejarque-ortiz, A., Sol, C., Martínez-barriocanal, Á., & Schwartz, S. (2015). *The Receptor CMRF35-Like Molecule-1 (CLM-1) Enhances the Production of LPS- Induced Pro-Inflammatory Mediators during Microglial Activation*. *1*, 1–17. https://doi.org/10.1371/journal.pone.0123928

Ejarque-Ortiz, A., Solà, C., Martínez-Barriocanal, Á., Schwartz, S., Martín, M., Peluffo, H., & Sayós, J. (2015). The Receptor CMRF35-Like Molecule-1 (CLM-1) Enhances the Production of LPS-Induced Pro-Inflammatory Mediators during Microglial Activation. *PloS One*, *10*(4), e0123928. https://doi.org/10.1371/journal.pone.0123928

Evans, F., Alı, D., Rego, N., Malagelada, C., Escande, C., & Peluffo, H. (2023). *Article CD300f immune receptor contributes to healthy aging by regulating inflammaging , metabolism , and cognitive decline ll CD300f immune receptor*

contributes to healthy aging by regulating inflammaging , metabolism , and cognitive decline. https://doi.org/10.1016/j.celrep.2023.113269

Färber, K., Pannasch, U., & Kettenmann, H. (2005). Dopamine and noradrenaline control distinct functions in rodent microglial cells. *Molecular and Cellular Neuroscience*, *29*(1), 128–138. https://doi.org/10.1016/j.mcn.2005.01.003

Fasciani, I., Pluta, P., González-Nieto, D., Martínez-Montero, P., Molano, J., Paíno, C. L., Millet, O., & Barrio, L. C. (2018). Directional coupling of oligodendrocyte connexin-47 and astrocyte connexin-43 gap junctions. *Glia*, *66*(11), 2340–2352. https://doi.org/10.1002/glia.23471

Feng, G., Mellor, R. H., Bernstein, M., Keller-Peck, C., Nguyen, Q. T., Wallace, M., Nerbonne, J. M., Lichtman, J. W., & Sanes, J. R. (2000). Imaging neuronal subsets in transgenic mice expressing multiple spectral variants of GFP. *Neuron*, *28*(1), 41–51. http://www.ncbi.nlm.nih.gov/pubmed/11086982

Ferro, A., Auguste, Y. S. S., & Cheadle, L. (2021). Microglia, Cytokines, and Neural Activity: Unexpected Interactions in Brain Development and Function. *Frontiers in Immunology*, *12*(July), 1–14. https://doi.org/10.3389/fimmu.2021.703527

Filipello, F., Morini, R., Corradini, I., Zerbi, V., Canzi, A., Michalski, B., Erreni, M., Markicevic, M., Starvaggi-Cucuzza, C., Otero, K., Piccio, L., Cignarella, F., Perrucci, F., Tamborini, M., Genua, M., Rajendran, L., Menna, E., Vetrano, S., Fahnestock, M., … Matteoli, M. (2018). The Microglial Innate Immune Receptor TREM2 Is Required for Synapse Elimination and Normal Brain Connectivity. *Immunity*, *48*(5), 979-991.e8. https://doi.org/10.1016/j.immuni.2018.04.016

Fonseca, M. I., Chu, S. H., Hernandez, M. X., Fang, M. J., Modarresi, L., Selvan, P., MacGregor, G. R., & Tenner, A. J. (2017). Cell-specific deletion of C1qa identifies microglia as the dominant source of C1q in mouse brain. *Journal of Neuroinflammation*, *14*(1), 1–15. https://doi.org/10.1186/s12974-017-0814-9

Gandal, M. J., Haney, J. R., Parikshak, N. N., Leppa, V., Ramaswami, G., Hartl, C., Schork, A. J., Appadurai, V., Buil, A., Werge, T. M., Liu, C., White, K. P., CommonMind Consortium, S., PsychENCODE Consortium, D. H., iPSYCH-BROAD Working Group, Horvath, S., & Geschwind, D. H. (2018). Shared molecular neuropathology across major psychiatric disorders parallels polygenic overlap. *Science (New York, N.Y.)*, *359*(6376), 693–697. https://doi.org/10.1126/science.aad6469

Garey, L. (2010). When cortical development goes wrong: schizophrenia as a neurodevelopmental disease of microcircuits. *Journal of Anatomy*, *217*(4), 324–333. https://doi.org/10.1111/j.1469-7580.2010.01231.x

Goldmann, T., Wieghofer, P., Müller, P. F., Wolf, Y., Varol, D., Yona, S., Brendecke, S. M., Kierdorf, K., Staszewski, O., Datta, M., Luedde, T., Heikenwalder, M., Jung, S., & Prinz, M. (2013). A new type of microglia gene targeting shows TAK1 to be pivotal in CNS autoimmune inflammation. *Nature Neuroscience*, *16*(11), 1618–1626. https://doi.org/10.1038/nn.3531

Goldmann, T., Wieghofer, P., Prutek, F., Hagemeyer, N., Frenzel, K., Staszewski, O., Kierdorf, K., Amann, L., Krueger, M., Locatelli, G., Hochgarner, H., Zeiser, R., Geissmann, F., Priller, J., Rossi, F., Bechmann, I., Linnarsson, S., Jung, S., Prinz, M., … Columbia, B. (2016). *Origin, fate and dynamics of macrophages at CNS interfaces Tobias*. *17*(7), 797–805. https://doi.org/10.1038/ni.3423.Origin

Grabert, K., Michoel, T., Karavolos, M. H., Clohisey, S., Baillie, J. K., Stevens, M. P., Freeman, T. C., Summers, K. M., & Mccoll, B. W. (2016). *Microglial brain region – dependent diversity and selective regional sensitivities to aging*. *19*(3). https://doi.org/10.1038/nn.4222

Grabert, K., Michoel, T., Karavolos, M. H., Clohisey, S., Baillie, J. K., Stevens, M. P., Freeman, T. C., Summers, K. M., & McColl, B. W. (2016). Microglial brain region-dependent diversity and selective regional sensitivities to aging. *Nature Neuroscience*, *19*(3), 504–516. https://doi.org/10.1038/nn.4222

Gunner, G., Cheadle, L., Johnson, K. M., Ayata, P., Badimon, A., Mondo, E., Nagy, M. A., Liu, L., Bemiller, S. M., Kim, K. W., Lira, S. A., Lamb, B. T., Tapper, A. R., Ransohoff, R. M., Greenberg, M. E., Schaefer, A., & Schafer, D. P. (2019). Sensory lesioning induces microglial synapse elimination via ADAM10 and fractalkine signaling. *Nature Neuroscience*, *22*(7), 1075–1088. https://doi.org/10.1038/s41593-019-0419-y

Györffy, B. A., Kun, J., Török, G., Bulyáki, É., Borhegyi, Z., Gulyássy, P., Kis, V., Szocsics, P., Micsonai, A., Matkó, J., Drahos, L., Juhász, G., Kékesi, K. A., & Kardos, J. (2018). Local apoptotic-like mechanisms underlie complementmediated synaptic pruning. *Proceedings of the National Academy of Sciences of the United States of America*, *115*(24), 6303–6308. https://doi.org/10.1073/pnas.1722613115

Hammond, B. P., Manek, R., Kerr, B. J., Macauley, M. S., & Plemel, J. R. (2021). Regulation of microglia population dynamics throughout development, health, and disease. *Glia*, *69*(12), 2771–2797. https://doi.org/10.1002/glia.24047

Hammond, T. R., Dufort, C., Dissing-Olesen, L., Giera, S., Young, A., Wysoker, A., Walker, A. J., Gergits, F., Segel, M., Nemesh, J., Marsh, S. E., Saunders, A., Macosko, E., Ginhoux, F., Chen, J., Franklin, R. J. M., Piao, X., McCarroll, S. A., & Stevens, B. (2019). Single-Cell RNA Sequencing of Microglia throughout the Mouse Lifespan and in the Injured Brain Reveals Complex Cell-State Changes. In *Immunity* (Vol. 50, Issue 1). https://doi.org/10.1016/j.immuni.2018.11.004

Hanisch, U. K. (2013). Functional diversity of microglia - How heterogeneous are they to begin with? *Frontiers in Cellular Neuroscience*, *7*(MAY), 1–18. https://doi.org/10.3389/fncel.2013.00065

Herman, M. A., Ackermann, F., Trimbuch, T., & Rosenmund, C. (2014). Vesicular glutamate transporter expression level affects synaptic vesicle release probability at hippocampal synapses in culture. *The Journal of Neuroscience : The Official Journal of the Society for Neuroscience*, *34*(35), 11781–11791. https://doi.org/10.1523/JNEUROSCI.1444-14.2014

Hickman, S. E., Kingery, N. D., Ohsumi, T. K., Borowsky, M. L., Wang, L., Means, T. K., & El Khoury, J. (2013). The microglial sensome revealed by direct RNA sequencing. *Nature Neuroscience*, *16*(12), 1896–1905. https://doi.org/10.1038/nn.3554

Hoek, R. H., Ruuls, S. R., Murphy, C. A., Wright, G. J., Goddard, R., Zurawski, S. M., Blom, B., Homola, M. E., Streit, W. J., Brown, M. H., Barclay, A. N., & Sedgwick, J. D. (2000). Down-regulation of the macrophage lineage through interaction with OX2 (CD200). *Science*, *290*(5497), 1768–1771. https://doi.org/10.1126/science.290.5497.1768

Hong, S., Beja-glasser, V. F., Nfonoyim, B. M., Frouin, A., Ramakrishnan, S., Merry, K. M., Shi, Q., Rosenthal, A., Barres, A., Lemere, C. A., Selkoe, D. J., & Stevens, B. (2016). ADF/Cofilin-Actin Rods in Neurodegenerative Diseases. *Curr Alzheimer Res.*, *352*(6286), 712–716. https://doi.org/10.1126/science.aad8373.Complement

Horvath, S., & Raj, K. (2018). DNA methylation-based biomarkers and the epigenetic clock theory of ageing. *Nature Reviews Genetics*. https://doi.org/10.1038/s41576-018-0004-3

Hu, H., Yang, X., He, Y., Duan, C., & Sun, N. (2022). Psychological stress induces depressive-like behavior associated with bone marrow-derived monocyte infiltration into the hippocampus independent of blood–brain barrier disruption. *Journal of Neuroinflammation*, *19*(1), 1–14. https://doi.org/10.1186/s12974-022-02569-w

Inoue, E., Watanabe, Y., Egawa, J., Sugimoto, A., Nunokawa, A., Shibuya, M., Igeta, H., & Someya, T. (2015). Rare heterozygous truncating variations and risk of autism spectrum disorder: Whole-exome sequencing of a multiplex family and follow-up study in a Japanese population. *Psychiatry and Clinical Neurosciences*, *69*(8), 472–476. https://doi.org/10.1111/pcn.12274

Ising, C., Venegas, C., Zhang, S., Scheiblich, H., Schmidt, S. V., Vieira-Saecker, A., Schwartz, S., Albasset, S., McManus, R. M., Tejera, D., Griep, A., Santarelli, F., Brosseron, F., Opitz, S., Stunden, J., Merten, M., Kayed, R., Golenbock, D. T., Blum, D., … Heneka, M. T. (2019). NLRP3 inflammasome activation drives tau pathology. *Nature*, *575*(7784), 669–673. https://doi.org/10.1038/s41586-019-1769-z

Isingrini, E., Camus, V., Le Guisquet, A. M., Pingaud, M., Devers, S., & Belzung, C. (2010). Association between repeated unpredictable chronic mild stress (UCMS) procedures with a high fat diet: A model of fluoxetine resistance in mice. *PLoS ONE*, *5*(4). https://doi.org/10.1371/journal.pone.0010404

Izawa, K., Isobe, M., Matsukawa, T., Ito, S., Maehara, A., Takahashi, M., Yamanishi, Y., Kaitani, A., Oki, T., Okumura, K., Kitamura, T., & Kitaura, J. (2014). Sphingomyelin and ceramide are physiological ligands for human LMIR3/CD300f, inhibiting FcεRI-mediated mast cell activation. *Journal of Allergy and Clinical Immunology*, *133*(1), 270-273.e7. https://doi.org/10.1016/j.jaci.2013.08.008

Izawa, K., Kitaura, J., Yamanishi, Y., Matsuoka, T., Kaitani, A., Sugiuchi, M., Takahashi, M., Maehara, A., Enomoto, Y., Oki, T., Takai, T., & Kitamura, T. (2009). An Activating and Inhibitory Signal from an Inhibitory Receptor LMIR3/CLM-1: LMIR3 Augments Lipopolysaccharide Response through Association with FcR in Mast Cells. *The Journal of Immunology*, *183*(2), 925–936. https://doi.org/10.4049/jimmunol.0900552

Izawa, K., Yamanishi, Y., Maehara, A., Takahashi, M., Isobe, M., Ito, S., Kaitani, A., Matsukawa, T., Matsuoka, T., Nakahara, F., Oki, T., Kiyonari, H., Abe, T.,

Okumura, K., Kitamura, T., & Kitaura, J. (2012a). The Receptor LMIR3 Negatively Regulates Mast Cell Activation and Allergic Responses by Binding to Extracellular Ceramide. *Immunity*, *37*(5), 827–839. https://doi.org/10.1016/j.immuni.2012.08.018

Izawa, K., Yamanishi, Y., Maehara, A., Takahashi, M., Isobe, M., Ito, S., Kaitani, A., Matsukawa, T., Matsuoka, T., Nakahara, F., Oki, T., Kiyonari, H., Abe, T., Okumura, K., Kitamura, T., & Kitaura, J. (2012b). The receptor LMIR3 negatively regulates mast cell activation and allergic responses by binding to extracellular ceramide. *Immunity*, *37*(5), 827–839. https://doi.org/10.1016/j.immuni.2012.08.018

Kadriu, B., Gold, P. W., Luckenbaugh, D. A., Lener, M. S., Ballard, E. D., Niciu, M. J., Henter, I. D., Park, L. T., De Sousa, R. T., Yuan, P., Machado-Vieira, R., & Zarate, C. A. (2018). Acute ketamine administration corrects abnormal inflammatory bone markers in major depressive disorder. *Molecular Psychiatry*, *23*(7), 1626–1631. https://doi.org/10.1038/mp.2017.109

Kaidanovich-Beilin, O., Lipina, T., Vukobradovic, I., Roder, J., & Woodgett, J. R. (2011). Assessment of social interaction behaviors. *Journal of Visualized Experiments : JoVE*, *48*. https://doi.org/10.3791/2473

Kaufmann, F. N., Lago, N., Alí-Ruiz, D., Jansen, K., Souza, L. D. M., Silva, R. A., Lara, D. R., Ghisleni, G., Peluffo, H., & Kaster, M. P. (2021). Sex-dependent role of CD300f immune receptor in generalized anxiety disorder. *Brain, Behavior, & Immunity - Health*, *11*(September 2020), 100191. https://doi.org/10.1016/j.bbih.2020.100191

Kelsey C. Martin Mhatre V. Ho, J.-A. L., Ruben Martin and Stephen L. Buchwald, Mhatre V. Ho and Kelsey C. Martin, J.-A. L., Craik, C., Manuscript, A., & Kantrowitz. (2013). Microglia promote learning-dependent synapse formation through BDNF. *Cell*, *155*(7), 1596–1609. https://doi.org/10.1016/j.cell.2013.11.030.Microglia

Keren-Shaul, H., Spinrad, A., Weiner, A., Matcovitch-Natan, O., Dvir-Szternfeld, R., Ulland, T. K., David, E., Baruch, K., Lara-Astaiso, D., Toth, B., Itzkovitz, S., Colonna, M., Schwartz, M., & Amit, I. (2017). A Unique Microglia Type Associated with Restricting Development of Alzheimer's Disease. *Cell*, *169*(7), 1276-1290.e17. https://doi.org/10.1016/j.cell.2017.05.018

Kim, H. J., Cho, M. H., Shim, W. H., Kim, J. K., Jeon, E. Y., Kim, D. H., & Yoon, S. Y. (2017). Deficient autophagy in microglia impairs synaptic pruning and causes social behavioral defects. *Molecular Psychiatry*, *22*(11), 1576–1584. https://doi.org/10.1038/mp.2016.103

Kracht, L., Borggrewe, M., Eskandar, S., Brouwer, N., Chuva de Sousa Lopes, S. M., Laman, J. D., Scherjon, S. A., Prins, J. R., Kooistra, S. M., & Eggen, B. J. L. (2020). Human fetal microglia acquire homeostatic immune-sensing properties early in development. *Science*, *369*(6503), 530–537. https://doi.org/10.1126/science.aba5906

Kraeuter, A. K., Guest, P. C., & Sarnyai, Z. (2019). The Open Field Test for Measuring Locomotor Activity and Anxiety-Like Behavior. *Methods in Molecular Biology*, *1916*, 99–103. https://doi.org/10.1007/978-1-4939-8994-2_9

Krasemann, S., Madore, C., Cialic, R., Baufeld, C., Calcagno, N., El Fatimy, R., Beckers, L., O'Loughlin, E., Xu, Y., Fanek, Z., Greco, D. J., Smith, S. T., Tweet, G., Humulock, Z., Zrzavy, T., Conde-Sanroman, P., Gacias, M., Weng, Z., Chen, H., … Butovsky, O. (2017). The TREM2-APOE Pathway Drives the Transcriptional Phenotype of Dysfunctional Microglia in Neurodegenerative Diseases. *Immunity*, *47*(3), 566-581.e9. https://doi.org/10.1016/j.immuni.2017.08.008

Kuhn, S. A., Van Landeghem, F. K. H., Zacharias, R., Färber, K., Rappert, A., Pavlovic, S., Hoffmann, A., Nolte, C., & Kettenmann, H. (2004). Microglia express GABAB receptors to modulate interleukin release. *Molecular and Cellular Neuroscience*, *25*(2), 312–322. https://doi.org/10.1016/j.mcn.2003.10.023

Lago, N., Kaufmann, F. N., Negro-Demontel, M. L., Alí-Ruiz, D., Ghisleni, G., Rego, N., Arcas-García, A., Vitureira, N., Jansen, K., Souza, L. M., Silva, R. A., Lara, D. R., Pannunzio, B., Abin-Carriquiry, J. A., Amo-Aparicio, J., Martin-Otal, C., Naya, H., McGavern, D. B., Sayós, J., … Peluffo, H. (2020). CD300f immunoreceptor is associated with major depressive disorder and decreased microglial metabolic fitness. *Proceedings of the National Academy of Sciences of the United States of America*, *117*(12), 6651–6662. https://doi.org/10.1073/pnas.1911816117

Larson, V. A., Mironova, Y., Vanderpool, K. G., Waisman, A., Rash, J. E., Agarwal, A., & Bergles, D. E. (2018). Oligodendrocytes control potassium accumulation in white matter and seizure susceptibility. *ELife*, *7*, 1–33. https://doi.org/10.7554/eLife.34829

Lawson, L. J., Perry, V. H., & Gordon, S. (1992). Turnover of resident microglia in the normal adult mouse brain. *Neuroscience*, *48*(2), 405–415. https://doi.org/10.1016/0306-4522(92)90500-2

Lee, M., Schwab, C., & Mcgeer, P. L. (2011). Astrocytes are GABAergic cells that modulate microglial activity. *Glia*, *59*(1), 152–165. https://doi.org/10.1002/glia.21087

Lee, S.-M., Kim, E.-J., Suk, K., & Lee, W.-H. (2011). CD300F Blocks Both MyD88 and TRIF-Mediated TLR Signaling through Activation of Src Homology Region 2 Domain-Containing Phosphatase 1. *The Journal of Immunology*, *186*(11), 6296–6303. https://doi.org/10.4049/jimmunol.1002184

Li, Q., Cheng, Z., Zhou, L., Darmanis, S., Neff, N. F., Gulati, G., Bennett, M. L., Sun, L. O., Clarke, L. E., Yu, G., Quake, S. R., Wyss-coray, T., & Ben, A. (2020). *Developmental heterogeneity of microglia and brain myeloid*. *101*(2), 207–223. https://doi.org/10.1016/j.neuron.2018.12.006.Developmental

Li, W., Li, X., & Miller, R. A. (2014). ATF4 activity: A common feature shared by many kinds of slow-aging mice. *Aging Cell*, *13*(6), 1012–1018. https://doi.org/10.1111/acel.12264

Liddelow, S. A., Guttenplan, K. A., Clarke, L. E., Bennett, F. C., Bohlen, C. J., Schirmer, L., Bennett, M. L., Münch, A. E., Chung, W. S., Peterson, T. C., Wilton, D. K., Frouin, A., Napier, B. A., Panicker, N., Kumar, M., Buckwalter, M. S., Rowitch, D. H., Dawson, V. L., Dawson, T. M., … Barres, B. A. (2017). Neurotoxic reactive astrocytes are induced by activated microglia. *Nature*, *541*(7638), 481–487. https://doi.org/10.1038/nature21029

Limone, F., Mordes, D., Couto, A., Pietiläinen, O., Joseph, B. J., Burberry, A., Ghosh, S. D., Meyer, D., Goldman, M., Bortolin, L., Cobos, I., Therrien, M., Stevens, B., Kadiu, I., McCarroll, S. A., & Eggan, K. (2021). Single-nucleus sequencing reveals enriched expression of genetic risk factors sensitises Motor Neurons to degeneration in ALS. *BioRxiv*, 2021.07.12.452054. https://www.biorxiv.org/content/10.1101/2021.07.12.452054v1%0Ahttps://www.biorxiv.org/content/10.1101/2021.07.12.452054v1.abstract

Liu, Y. J., Spangenberg, E. E., Tang, B., Holmes, T. C., Green, K. N., & Xu, X. (2021). Microglia elimination increases neural circuit connectivity and activity in adult mouse cortex. *Journal of Neuroscience*, *41*(6), 1274–1287.

https://doi.org/10.1523/JNEUROSCI.2140-20.2020

Lloyd, A. F., Davies, C. L., Holloway, R. K., Labrak, Y., Ireland, G., Carradori, D., Dillenburg, A., Borger, E., Soong, D., Richardson, J. C., Kuhlmann, T., Williams, A., Pollard, J. W., des Rieux, A., Priller, J., & Miron, V. E. (2019). Central nervous system regeneration is driven by microglia necroptosis and repopulation. *Nature Neuroscience*, *22*(7), 1046–1052. https://doi.org/10.1038/s41593-019-0418-z

MacAulay, N. (2021). Molecular mechanisms of brain water transport. *Nature Reviews Neuroscience*, *22*(6), 326–344. https://doi.org/10.1038/s41583-021-00454-8

Marschallinger, J., Iram, T., Zardeneta, M., Lee, S. E., Lehallier, B., Haney, M. S., Pluvinage, J. V., Mathur, V., Hahn, O., Morgens, D. W., Kim, J., Tevini, J., Felder, T. K., Wolinski, H., Bertozzi, C. R., Bassik, M. C., Aigner, L., & Wyss-Coray, T. (2020). Lipid-droplet-accumulating microglia represent a dysfunctional and proinflammatory state in the aging brain. In *Nature Neuroscience* (Vol. 23, Issue 2). https://doi.org/10.1038/s41593-019-0566-1

Martinez-Barriocanal, A., Comas-Casellas, E., Schwartz, S., Martin, M., & Sayos, J. (2010). CD300 Heterocomplexes, a New and Family-restricted Mechanism for Myeloid Cell Signaling Regulation. *Journal of Biological Chemistry*, *285*(53), 41781–41794. https://doi.org/10.1074/jbc.M110.140889

Martínez-Barriocanal, A., Comas-Casellas, E., Schwartz, S., Martín, M., & Sayós, J. (2010). CD300 heterocomplexes, a new and family-restricted mechanism for myeloid cell signaling regulation. *The Journal of Biological Chemistry*, *285*(53), 41781–41794. https://doi.org/10.1074/jbc.M110.140889

Matsukawa, T., Izawa, K., Isobe, M., Takahashi, M., Maehara, A., Yamanishi, Y., Kaitani, A., Okumura, K., Teshima, T., Kitamura, T., & Kitaura, J. (2016). Ceramide-CD300f binding suppresses experimental colitis by inhibiting ATP-mediated mast cell activation. *Gut*, *65*(5), 777–787. https://doi.org/10.1136/gutjnl-2014-308900

Menard, C., Pfau, M. L., Hodes, G. E., Kana, V., Wang, V. X., Bouchard, S., Takahashi, A., Flanigan, M. E., Aleyasin, H., Leclair, K. B., Janssen, W. G., Labonté, B., Parise, E. M., Lorsch, Z. S., Golden, S. A., Heshmati, M., Tamminga, C., Turecki, G., Campbell, M., … Russo, S. J. (2017). Promoting Depression. *Nature Neuroscience*, *20*(November), 1752–1760.

Minhas, P. S., Latif-Hernandez, A., McReynolds, M. R., Durairaj, A. S., Wang, Q.,

Rubin, A., Joshi, A. U., He, J. Q., Gauba, E., Liu, L., Wang, C., Linde, M., Sugiura, Y., Moon, P. K., Majeti, R., Suematsu, M., Mochly-Rosen, D., Weissman, I. L., Longo, F. M., … Andreasson, K. I. (2021). Restoring metabolism of myeloid cells reverses cognitive decline in ageing. *Nature*, *590*(7844), 122–128. https://doi.org/10.1038/s41586-020-03160-0

Mirzadegan, T., Diehl, F., Ebi, B., Bhakta, S., Polsky, I., McCarley, D., Mulkins, M., Weatherhead, G. S., Lapierre, J. M., Dankwardt, J., Morgans D., J., Wilhelm, R., & Jarnagin, K. (2000). Identification of the binding site for a novel class of CCR2b chemokine receptor antagonists. Binding to a common chemokine receptor motif within the helical bundle. *Journal of Biological Chemistry*, *275*(33), 25562–25571. https://doi.org/10.1074/jbc.M000692200

Mori, K., Ozaki, E., Zhang, B., Yang, L., Yokoyama, A., Takeda, I., Maeda, N., Sakanaka, M., & Tanaka, J. (2002). Effects of norepinephrine on rat cultured microglial cells that express α1, α2, β1 and β2 adrenergic receptors. *Neuropharmacology*, *43*(6), 1026–1034. https://doi.org/10.1016/S0028-3908(02)00211-3

Moshkovits, I., Karo-atar, D., Itan, M., Reichman, H., & Rozenberg, P. (2015). *CD300f associates with IL-4 receptor α and amplifies IL-4 – induced immune cell responses*. *112*(28). https://doi.org/10.1073/pnas.1507625112

Moshkovits, I., Karo-Atar, D., Itan, M., Reichman, H., Rozenberg, P., Morgenstern-Ben-Baruch, N., Shik, D., Ejarque-Ortiz, A., Hershko, A. Y., Tian, L., Coligan, J. E., Sayós, J., & Munitz, A. (2015). CD300f associates with IL-4 receptor α and amplifies IL-4-induced immune cell responses. *Proceedings of the National Academy of Sciences of the United States of America*, *112*(28), 8708–8713. https://doi.org/10.1073/pnas.1507625112

Nakayama, K., Kiyosue, K., & Taguchi, T. (2005). Diminished neuronal activity increases neuron-neuron connectivity underlying silent synapse formation and the rapid conversion of silent to functional synapses. *The Journal of Neuroscience : The Official Journal of the Society for Neuroscience*, *25*(16), 4040–4051. https://doi.org/10.1523/JNEUROSCI.4115-04.2005

Ndrepepa, G., Colleran, R., & Kastrati, A. (2018). Clinica Chimica Acta Gamma-glutamyl transferase and the risk of atherosclerosis and coronary heart disease. *Clinica Chimica Acta*, *476*(November 2017), 130–138. https://doi.org/10.1016/j.cca.2017.11.026

Nimmerjahn, A. (2005). Resting Microglial Cells Are Highly Dynamic Surveillants of Brain Parenchyma in Vivo. *Science*, *308*(5726), 1314–1318. https://doi.org/10.1126/science.1110647

Nott, A., Holtman, I. R., Coufal, N. G., Schlachetzki, J. C. M., Yu, M., Hu, R., Han, C. Z., Pena, M., Xiao, J., Wu, Y., Keulen, Z., Pasillas, M. P., O'Connor, C., Nickl, C. K., Schafer, S. T., Shen, Z., Rissman, R. A., Brewer, J. B., Gosselin, D., … Glass, C. K. (2019). Brain cell type–specific enhancer–promoter interactome maps and disease-risk association. *Science*, *366*(6469), 1134–1139. https://doi.org/10.1126/science.aay0793

Novikova, G., Kapoor, M., Tcw, J., Abud, E. M., Efthymiou, A. G., Chen, S. X., Cheng, H., Fullard, J. F., Bendl, J., Liu, Y., Roussos, P., Björkegren, J. L., Liu, Y., Poon, W. W., Hao, K., Marcora, E., & Goate, A. M. (2021). Integration of Alzheimer's disease genetics and myeloid genomics identifies disease risk regulatory elements and genes. *Nature Communications*, *12*(1). https://doi.org/10.1038/s41467-021-21823-y

Orkand, R. K., Nicholls, J. G., & Kuffler, S. W. (1966). Effect of nerve impulses on the membrane potential of glial cells in the central nervous system of amphibia. *Journal of Neurophysiology*, *29*(4), 788–806. https://doi.org/10.1152/jn.1966.29.4.788

Pannell, M., Meier, M. A., Szulzewsky, F., Matyash, V., Endres, M., Kronenberg, G., Prinz, V., Waiczies, S., Wolf, S. A., & Kettenmann, H. (2016). The subpopulation of microglia expressing functional muscarinic acetylcholine receptors expands in stroke and Alzheimer's disease. *Brain Structure and Function*, *221*(2), 1157–1172. https://doi.org/10.1007/s00429-014-0962-y

Pannell, M., Szulzewsky, F., Matyash, V., Wolf, S. A., & Kettenmann, H. (2014). The subpopulation of microglia sensitive to neurotransmitters/neurohormones is modulated by stimulation with LPS, interferon-γ, and IL-4. *Glia*, *62*(5), 667–679. https://doi.org/10.1002/glia.22633

Pannunzio, B., Amo-Aparicio, J., Julián, C., López-Vales, R., Peluffo, H., & Lago, N. (2022). CD200R1 Contributes to Successful Functional Reinnervation after a Sciatic Nerve Injury. *Cells*, *11*(11), 1–16. https://doi.org/10.3390/cells11111786

Paolicelli, R. C., Bolasco, G., Pagani, F., Maggi, L., Scianni, M., Panzanelli, P., Giustetto, M., Ferreira, T. A., Guiducci, E., Dumas, L., Ragozzino, D., & Gross, C. T. (2011).

Synaptic Pruning by Microglia Is Necessary for Normal Brain Development. *Science*, *333*(6048), 1456–1458. https://doi.org/10.1126/science.1202529

Parkhurst, C. N., Yang, G., Ninan, I., Savas, J. N., Yates, J. R., Lafaille, J. J., Hempstead, B. L., Littman, D. R., & Gan, W. B. (2013). Microglia promote learning-dependent synapse formation through brain-derived neurotrophic factor. *Cell*, *155*(7), 1596–1609. https://doi.org/10.1016/j.cell.2013.11.030

Parpura, V., Heneka, M. T., Montana, V., Oliet, S. H. R., Haydon, P. G., Jr, R. F. S., & Spray, D. C. (2013). *NIH Public Access*. *121*(1), 4–27. https://doi.org/10.1111/j.1471-4159.2012.07664.x.Glial

Peluffo, H., Alí-Ruiz, D., Ejarque-Ortíz, A., Heras-Alvarez, V., Comas-Casellas, E., Martínez-Barriocanal, A., Kamaid, A., Alvarez-Errico, D., Negro, M. L., Lago, N., Schwartz Jr, S., Villaverde, A., & Sayós, J. (2012). Overexpression of the Immunoreceptor CD300f Has a Neuroprotective Role in a Model of Acute Brain Injury. *Brain Pathology*, *22*(3), 318–328. https://doi.org/10.1111/j.1750-3639.2011.00537.x

Peluffo, H., Alí-Ruiz, D., Ejarque-Ortíz, A., Heras-Alvarez, V., Comas-Casellas, E., Martínez-Barriocanal, A., Kamaid, A., Alvarez-Errico, D., Negro, M. L., Lago, N., Schwartz, S., Villaverde, A., & Sayós, J. (2012). Overexpression of the immunoreceptor CD300f has a neuroprotective role in a model of acute brain injury. *Brain Pathology (Zurich, Switzerland)*, *22*(3), 318–328. https://doi.org/10.1111/j.1750-3639.2011.00537.x

Phongsisay, V., Iizasa, E., Hara, H., & Yamasaki, S. (2014). LMIR5 extracellular domain activates myeloid cells through Toll-like receptor 4. *Molecular Immunology*, *62*(1), 169–177. https://doi.org/10.1016/j.molimm.2014.06.012

Podleśny-drabiniok, A., Marcora, E., & Goate, A. M. (2022). *Emerging from Alzheimer ' s Disease Genetics*. *43*(12), 965–979. https://doi.org/10.1016/j.tins.2020.10.002.Microglial

Pothion, S., Bizot, J. C., Trovero, F., & Belzung, C. (2004). Strain differences in sucrose preference and in the consequences of unpredictable chronic mild stress. *Behavioural Brain Research*, *155*(1), 135–146. https://doi.org/10.1016/j.bbr.2004.04.008

Prinz, M., Jung, S., & Priller, J. (2019). Microglia Biology: One Century of Evolving Concepts. *Cell*, *179*(2), 292–311. https://doi.org/10.1016/j.cell.2019.08.053

Rash, J. E. (2010). Molecular disruptions of the panglial syncytium block potassium siphoning and axonal saltatory conduction: pertinence to neuromyelitis optica and other demyelinating diseases of the central nervous system. *Neuroscience*, *168*(4), 982–1008. https://doi.org/10.1016/j.neuroscience.2009.10.028

Ravichandran, M., Priebe, S., Grigolon, G., Rozanov, L., Groth, M., Laube, B., Guthke, R., Platzer, M., Zarse, K., & Ristow, M. (2018). Impairing L-Threonine Catabolism Promotes Healthspan through Methylglyoxal-Mediated Proteohormesis. *Cell Metabolism*, *27*(4), 914-925.e5. https://doi.org/10.1016/j.cmet.2018.02.004

Rozenberg, P., Reichman, H., Zab-Bar, I., Itan, M., Pasmanik-Chor, M., Bouffi, C., Qimron, U., Bachelet, I., Fulkerson, P. C., Rothenberg, M. E., & Munitz, A. (2017). CD300f:IL-5 cross-talk inhibits adipose tissue eosinophil homing and subsequent IL-4 production. *Scientific Reports*, *7*(1), 1–15. https://doi.org/10.1038/s41598-017-06397-4

Safaiyan, S., Besson-Girard, S., Kaya, T., Cantuti-Castelvetri, L., Liu, L., Ji, H., Schifferer, M., Gouna, G., Usifo, F., Kannaiyan, N., Fitzner, D., Xiang, X., Rossner, M. J., Brendel, M., Gokce, O., & Simons, M. (2021). White matter aging drives microglial diversity. *Neuron*, *109*(7), 1100-1117.e10. https://doi.org/10.1016/j.neuron.2021.01.027

Sala Frigerio, C., Wolfs, L., Fattorelli, N., Thrupp, N., Voytyuk, I., Schmidt, I., Mancuso, R., Chen, W. T., Woodbury, M. E., Srivastava, G., Möller, T., Hudry, E., Das, S., Saido, T., Karran, E., Hyman, B., Perry, V. H., Fiers, M., & De Strooper, B. (2019). The Major Risk Factors for Alzheimer's Disease: Age, Sex, and Genes Modulate the Microglia Response to Aβ Plaques. *Cell Reports*, *27*(4), 1293-1306.e6. https://doi.org/10.1016/j.celrep.2019.03.099

Salter, M. W., & Stevens, B. (2017). Microglia emerge as central players in brain disease. *Nature Medicine*, *23*(9), 1018–1027. https://doi.org/10.1038/nm.4397

Sapar, M. L., Ji, H., Wang, B., Poe, A. R., Dubey, K., Ren, X., Ni, J. Q., & Han, C. (2018). Phosphatidylserine Externalization Results from and Causes Neurite Degeneration in Drosophila. *Cell Reports*, *24*(9), 2273–2286. https://doi.org/10.1016/j.celrep.2018.07.095

Sawada, A., Niiyama, Y., Ataka, K., Nagaishi, K., Yamakage, M., & Fujimiya, M. (2014). Suppression of bone marrow-derived microglia in the amygdale improves anxiety-like behavior induced by chronic partial sciatic nerve ligation in mice. *Pain*, *155*(9),

1762–1772. https://doi.org/10.1016/j.pain.2014.05.031

Schafer, D. P., Lehrman, E. K., Kautzman, A. G., Koyama, R., Mardinly, A. R., Yamasaki, R., Ransohoff, R. M., Greenberg, M. E., Barres, B. A., & Stevens, B. (2012). Microglia Sculpt Postnatal Neural Circuits in an Activity and Complement-Dependent Manner. *Neuron*, *74*(4), 691–705. https://doi.org/10.1016/j.neuron.2012.03.026

Schwarz, F., Pearce, O. M. T., Wang, X., Samraj, A. N., Läubli, H., Garcia, J. O., Lin, H., Fu, X., Garcia-Bingman, A., Secrest, P., Romanoski, C. E., Heyser, C., Glass, C. K., Hazen, S. L., Varki, N., Varki, A., & Gagneux, P. (2015). Siglec receptors impact mammalian lifespan by modulating oxidative stress. *ELife*, *4*. https://doi.org/10.7554/eLife.06184

Scott-Hewitt, N., Perrucci, F., Morini, R., Erreni, M., Mahoney, M., Witkowska, A., Carey, A., Faggiani, E., Schuetz, L. T., Mason, S., Tamborini, M., Bizzotto, M., Passoni, L., Filipello, F., Jahn, R., Stevens, B., & Matteoli, M. (2020). Local externalization of phosphatidylserine mediates developmental synaptic pruning by microglia. *The EMBO Journal*, *39*(16), 1–20. https://doi.org/10.15252/embj.2020105380

Seifert, S., Pannell, M., Uckert, W., Färber, K., & Kettenmann, H. (2011). Transmitter- and hormone-activated Ca2+ responses in adult microglia/brain macrophages in situ recorded after viral transduction of a recombinant Ca2+ sensor. *Cell Calcium*, *49*(6), 365–375. https://doi.org/10.1016/j.ceca.2011.03.005

Shacham-Silverberg, V., Sar Shalom, H., Goldner, R., Golan-Vaishenker, Y., Gurwicz, N., Gokhman, I., & Yaron, A. (2018). Phosphatidylserine is a marker for axonal debris engulfment but its exposure can be decoupled from degeneration. *Cell Death and Disease*, *9*(11). https://doi.org/10.1038/s41419-018-1155-z

Shemer, A., Erny, D., Jung, S., & Prinz, M. (2015). Microglia Plasticity During Health and Disease: An Immunological Perspective. *Trends in Immunology*, *36*(10), 614–624. https://doi.org/10.1016/j.it.2015.08.003

Shen, W., Nikolic, L., Meunier, C., Pfrieger, F., & Audinat, E. (2017). An autocrine purinergic signaling controls astrocyte-induced neuronal excitation. *Scientific Reports*, *7*(1), 1–13. https://doi.org/10.1038/s41598-017-11793-x

Shi, Q., Colodner, K. J., Matousek, S. B., Merry, K., Hong, S., Kenison, J. E., Frost, J. L., Le, K. X., Li, S., Dodart, J. C., Caldarone, B. J., Stevens, B., & Lemere, C. A. (2015).

Complement C3-deficient mice fail to display age-related hippocampal decline. *Journal of Neuroscience*, *35*(38), 13029–13042. https://doi.org/10.1523/JNEUROSCI.1698-15.2015

Shytle, R. D., Mori, T., Townsend, K., Vendrame, M., Sun, N., Zeng, J., Ehrhart, J., Silver, A. A., Sanberg, P. R., & Tan, J. (2004). Cholinergic modulation of microglial activation by α7 nicotinic receptors. *Journal of Neurochemistry*, *89*(2), 337–343. https://doi.org/10.1046/j.1471-4159.2004.02347.x

Silverman, J. L., Yang, M., Lord, C., & Crawley, J. N. (2010). Behavioural phenotyping assays for mouse models of autism. *Nature Reviews Neuroscience*, *11*(7), 490–502. https://doi.org/10.1038/nrn2851

Silvin, A., Uderhardt, S., Piot, C., Amit, I., Kipnis, J., Ginhoux, F., Silvin, A., Uderhardt, S., Piot, C., Mesquita, S. Da, Yang, K., & Geirsdottir, L. (2022). Article Dual ontogeny of disease-associated microglia and disease inflammatory macrophages in aging and neurodegeneration Dual ontogeny of disease-associated microglia and disease inflammatory macrophages in aging and neurodegeneration. *Immunity*, 1–18. https://doi.org/10.1016/j.immuni.2022.07.004

Smajic, S., Prada-Medina, C. A., Landoulsi, Z., Ghelfi, J., Delcambre, S., Dietrich, C., Jarazo, J., Henck, J., Balachandran, S., Pachchek, S., Morris, C. M., Antony, P., Timmermann, B., Sauer, S., Pereira, S. L., Schwamborn, J. C., May, P., Grunewald, A., & Spielmann, M. (2022). Single-cell sequencing of human midbrain reveals glial activation and a Parkinson-specific neuronal state. *Brain*, *145*(3), 964–978. https://doi.org/10.1093/brain/awab446

Sokolova, D., Childs, T., & Hong, S. (2021). Insight into the role of phosphatidylserine in complement-mediated synapse loss in Alzheimer's disease. *Faculty Reviews*, *10*(19). https://doi.org/10.12703/r/10-19

Srinivasan, K., Friedman, B. A., Etxeberria, A., Huntley, M. A., van der Brug, M. P., Foreman, O., Paw, J. S., Modrusan, Z., Beach, T. G., Serrano, G. E., & Hansen, D. V. (2020). Alzheimer's Patient Microglia Exhibit Enhanced Aging and Unique Transcriptional Activation. *Cell Reports*, *31*(13), 1–35. https://doi.org/10.1016/j.celrep.2020.107843

Stadelmann, C., Timmler, S., Barrantes-Freer, A., & Simons, M. (2019). Myelin in the central nervous system: Structure, function, and pathology. *Physiological Reviews*, *99*(3), 1381–1431. https://doi.org/10.1152/physrev.00031.2018

Stevens, B., Allen, N. J., Vazquez, L. E., Howell, G. R., Christopherson, K. S., Nouri, N., Micheva, K. D., Mehalow, A. K., Huberman, A. D., Stafford, B., Sher, A., Litke, A. M., Lambris, J. D., Smith, S. J., John, S. W. M., & Barres, B. A. (2007). The Classical Complement Cascade Mediates CNS Synapse Elimination. *Cell*, *131*(6), 1164–1178. https://doi.org/10.1016/j.cell.2007.10.036

Stockert, J. C., Horobin, R. W., Colombo, L. L., & Blázquez-Castro, A. (2018). Tetrazolium salts and formazan products in Cell Biology: Viability assessment, fluorescence imaging, and labeling perspectives. *Acta Histochemica*, *120*(3), 159–167. https://doi.org/10.1016/j.acthis.2018.02.005

Sudre, G., Gildea, D. E., Shastri, G. G., Sharp, W., Jung, B., Xu, Q., Auluck, P. K., Elnitski, L., Baxevanis, A. D., Marenco, S., & Shaw, P. (2023). Mapping the cortico-striatal transcriptome in attention deficit hyperactivity disorder. *Molecular Psychiatry*, *28*(2), 792–800. https://doi.org/10.1038/s41380-022-01844-9

Tanaka, K. F., Kashima, H., Suzuki, H., Ono, K., & Sawada, M. (2002). Existence of functional β1- and β2-adrenergic receptors on microglia. *Journal of Neuroscience Research*, *70*(2), 232–237. https://doi.org/10.1002/jnr.10399

Taylor, D. L., Diemel, L. T., Cuzner, M. L., & Pocock, J. M. (2002). Activation of group II metabotropic glutamate receptors underlies microglial reactivity and neurotoxicity following stimulation with chromogranin A, a peptide up-regulated in Alzheimer's disease. *Journal of Neurochemistry*, *82*(5), 1179–1191. https://doi.org/10.1046/j.1471-4159.2002.01062.x

Taylor, D. L., Diemel, L. T., & Pocock, J. M. (2003). Activation of microglial group III metabotropic glutamate receptors protects neurons against microglial neurotoxicity. *Journal of Neuroscience*, *23*(6), 2150–2160. https://doi.org/10.1523/jneurosci.23-06-02150.2003

Tetreault, N. A., Hakeem, A. Y., Jiang, S., Williams, B. A., Allman, E., Wold, B. J., & Allman, J. M. (2012). Microglia in the Cerebral Cortex in Autism. *Journal of Autism and Developmental Disorders*, *42*(12), 2569–2584. https://doi.org/10.1007/s10803-012-1513-0

Tian, L., Choi, S.-C., Lee, H.-N., Murakami, Y., Qi, C.-F., Sengottuvelu, M., Voss, O., Krzewski, K., & Coligan, J. E. (2016). Enhanced efferocytosis by dendritic cells underlies memory T-cell expansion and susceptibility to autoimmune disease in

CD300f-deficient mice. *Cell Death and Differentiation*, *23*(6), 1086–1096. https://doi.org/10.1038/cdd.2015.161

Tian, L., Choi, S.-C., Murakami, Y., Allen, J., Morse, H. C., Qi, C.-F., Krzewski, K., & Coligan, J. E. (2014). p85α recruitment by the CD300f phosphatidylserine receptor mediates apoptotic cell clearance required for autoimmunity suppression. *Nature Communications*, *5*(1), 3146. https://doi.org/10.1038/ncomms4146

Tian, L., Choi, S.-C., Murakami, Y., Allen, J., Morse III, H. C., Qi, C.-F., Krzewski, K., & Coligan, J. E. (2014). p85α recruitment by the CD300f phosphatidylserine receptor mediates apoptotic cell clearance required for autoimmunity suppression. *Nature Communications*, *5*. https://doi.org/10.1038/ncomms4146

Torres-Espín, A., Hernández, J., & Navarro, X. (2013). Gene Expression Changes in the Injured Spinal Cord Following Transplantation of Mesenchymal Stem Cells or Olfactory Ensheathing Cells. *PLoS ONE*, *8*(10). https://doi.org/10.1371/journal.pone.0076141

Tremblay, M. Ě., Lowery, R. L., & Majewska, A. K. (2010). Microglial interactions with synapses are modulated by visual experience. *PLoS Biology*, *8*(11). https://doi.org/10.1371/journal.pbio.1000527

Ueno, M., Fujita, Y., Tanaka, T., Nakamura, Y., Kikuta, J., Ishii, M., & Yamashita, T. (2013). Layer v cortical neurons require microglial support for survival during postnatal development. *Nature Neuroscience*, *16*(5), 543–551. https://doi.org/10.1038/nn.3358

Ulland, T. K., Wang, Y., & Colonna, M. (2017). *diseases*. *27*(6), 410–415. https://doi.org/10.1016/j.smim.2016.03.011.Regulation

Verhoog, Q. P., Holtman, L., Aronica, E., & van Vliet, E. A. (2020). Astrocytes as Guardians of Neuronal Excitability: Mechanisms Underlying Epileptogenesis. *Frontiers in Neurology*, *11*(November). https://doi.org/10.3389/fneur.2020.591690

Verkhratsky, A., & Nedergaard, M. (2018). Physiology of astroglia. *Physiological Reviews*, *98*(1), 239–389. https://doi.org/10.1152/physrev.00042.2016

Vitureira, N., Letellier, M., White, I. J., & Goda, Y. (2011). Differential control of presynaptic efficacy by postsynaptic N-cadherin and β-catenin. *Nature Neuroscience*, *15*(1), 81–89. https://doi.org/10.1038/nn.2995

Wake, H., Moorhouse, A. J., Jinno, S., Kohsaka, S., & Nabekura, J. (2009). *Resting Microglia Directly Monitor the Functional State of Synapses In Vivo and Determine the Fate of Ischemic Terminals*. *29*(13), 3974–3980. https://doi.org/10.1523/JNEUROSCI.4363-08.2009

Wang, C., Yue, H., Hu, Z., Shen, Y., Li, J., Wang, X., Wang, L., Sun, B., Shi, P., Wang, L., & Gu, Y. (2020). *<10.1126@Science.Aaz2288.Pdf>*. *694*(February), 688–694.

Wang, X., Mathieu, M., & Brezski, R. J. (2018). IgG Fc engineering to modulate antibody effector functions. *Protein and Cell*, *9*(1), 63–73. https://doi.org/10.1007/s13238-017-0473-8

Wang, Y., Cella, M., Mallinson, K., Ulrich, J. D., Young, K. L., Robinette, M. L., Gilfillan, S., Krishnan, G. M., Sudhakar, S., Zinselmeyer, B. H., Holtzman, D. M., Cirrito, J. R., & Colonna, M. (2015). TREM2 lipid sensing sustains the microglial response in an Alzheimer's disease model. *Cell*, *160*(6), 1061–1071. https://doi.org/10.1016/j.cell.2015.01.049

Weinhard, L., Di Bartolomei, G., Bolasco, G., Machado, P., Schieber, N. L., Neniskyte, U., Exiga, M., Vadisiute, A., Raggioli, A., Schertel, A., Schwab, Y., & Gross, C. T. (2018). Microglia remodel synapses by presynaptic trogocytosis and spine head filopodia induction. *Nature Communications*, *9*(1). https://doi.org/10.1038/s41467-018-03566-5

Wilson, N. R., Kang, J., Hueske, E. V, Leung, T., Varoqui, H., Murnick, J. G., Erickson, J. D., & Liu, G. (2005a). *Presynaptic Regulation of Quantal Size by the Vesicular Glutamate Transporter VGLUT1*. *25*(26), 6221–6234. https://doi.org/10.1523/JNEUROSCI.3003-04.2005

Wilson, N. R., Kang, J., Hueske, E. V, Leung, T., Varoqui, H., Murnick, J. G., Erickson, J. D., & Liu, G. (2005b). Presynaptic Regulation of Quantal Size by the Vesicular Glutamate Transporter VGLUT1. *Journal of Neuroscience*, *25*(26), 6221–6234. https://doi.org/10.1523/JNEUROSCI.3003-04.2005

Wohleb, E. S., Powell, N. D., Godbout, J. P., & Sheridan, J. F. (2013). Stress-induced recruitment of bone marrow-derived monocytes to the brain promotes anxiety-like behavior. *Journal of Neuroscience*, *33*(34), 13820–13833. https://doi.org/10.1523/JNEUROSCI.1671-13.2013

Wu, T., Dejanovic, B., Gandham, V. D., Gogineni, A., Edmonds, R., Schauer, S., Srinivasan, K., Huntley, M. A., Wang, Y., Wang, T. M., Hedehus, M., Barck, K. H.,

Stark, M., Ngu, H., Foreman, O., Meilandt, W. J., Elstrott, J., Chang, M. C., Hansen, D. V., … Hanson, J. E. (2019). Complement C3 Is Activated in Human AD Brain and Is Required for Neurodegeneration in Mouse Models of Amyloidosis and Tauopathy. *Cell Reports*, *28*(8), 2111-2123.e6. https://doi.org/10.1016/j.celrep.2019.07.060

Xi, H., Katschke, K. J., Helmy, K. Y., Wark, P. A., Kljavin, N., Clark, H., Eastham-Anderson, J., Shek, T., Roose-Girma, M., Ghilardi, N., & van Lookeren Campagne, M. (2010). Negative regulation of autoimmune demyelination by the inhibitory receptor CLM-1. *The Journal of Experimental Medicine*, *207*(1), 7–16. https://doi.org/10.1084/jem.20091508

Xin, W., Mironova, Y. A., Shen, H., Marino, R. A. M., Waisman, A., Lamers, W. H., Bergles, D. E., & Bonci, A. (2019). Oligodendrocytes Support Neuronal Glutamatergic Transmission via Expression of Glutamine Synthetase. *Cell Reports*, *27*(8), 2262-2271.e5. https://doi.org/10.1016/j.celrep.2019.04.094

Yirmiya, R., Rimmerman, N., & Reshef, R. (2015). Depression as a Microglial Disease. *Trends in Neurosciences*, *38*(10), 637–658. https://doi.org/10.1016/j.tins.2015.08.001

Yona, S., Viukov, S., Guilliams, M., & Misharin, A. (2013). Tissue Macrophages Under Homeostasis. *Immunity*, *38*(1), 79–91. https://doi.org/10.1016/j.immuni.2012.12.001.Fate

Yu, G., Wang, L. G., Han, Y., & He, Q. Y. (2012). ClusterProfiler: An R package for comparing biological themes among gene clusters. *OMICS A Journal of Integrative Biology*, *16*(5), 284–287. https://doi.org/10.1089/omi.2011.0118

Yuste, R., Hawrylycz, M., Aalling, N., Aguilar-Valles, A., Arendt, D., Arnedillo, R. A., Ascoli, G. A., Bielza, C., Bokharaie, V., Bergmann, T. B., Bystron, I., Capogna, M., Chang, Y., Clemens, A., de Kock, C. P. J., DeFelipe, J., Dos Santos, S. E., Dunville, K., Feldmeyer, D., … Lein, E. (2020). A community-based transcriptomics classification and nomenclature of neocortical cell types. *Nature Neuroscience*, *23*(12), 1456–1468. https://doi.org/10.1038/s41593-020-0685-8

Zeisel, A., Munoz-Manchado, A. B., Codeluppi, S., Lonnerberg, P., La Manno, G., Jureus, A., Marques, S., Munguba, H., He, L., Betsholtz, C., Rolny, C., Castelo-Branco, G., Hjerling-Leffler, J., & Linnarsson, S. (2015). Cell types in the mouse cortex and hippocampus revealed by single-cell RNA-seq. *Science*, *347*(6226),

1138–1142. https://doi.org/10.1126/science.aaa1934

Zhan, Y., Paolicelli, R. C., Sforazzini, F., Weinhard, L., Bolasco, G., Pagani, F., Vyssotski, A. L., Bifone, A., Gozzi, A., Ragozzino, D., & Gross, C. T. (2014). Deficient neuron-microglia signaling results in impaired functional brain connectivity and social behavior. *Nature Neuroscience*, *17*(3), 400–406. https://doi.org/10.1038/nn.3641

Zhang, J., Liu, Y., Liu, X., Li, S., Cheng, C., Chen, S., & Le, W. (2018). Dynamic changes of CX3CL1/CX3CR1 axis during microglial activation and motor neuron loss in the spinal cord of ALS mouse model. *Translational Neurodegeneration*, *7*(1), 1–14. https://doi.org/10.1186/s40035-018-0138-4

Zhong, L., Chen, X.-F., Wang, T., Wang, Z., Liao, C., Wang, Z., Huang, R., Wang, D., Li, X., Wu, L., Jia, L., Zheng, H., Painter, M., Atagi, Y., Liu, C.-C., Zhang, Y.-W., Fryer, J. D., Xu, H., & Bu, G. (2017). Soluble TREM2 induces inflammatory responses and enhances microglial survival. *The Journal of Experimental Medicine*, jem.20160844. https://doi.org/10.1084/jem.20160844

Ziv, Y., Ron, N., Butovsky, O., Landa, G., Sudai, E., Greenberg, N., Cohen, H., Kipnis, J., & Schwartz, M. (2006). Immune cells contribute to the maintenance of neurogenesis and spatial learning abilities in adulthood. *Nature Neuroscience*, *9*(2), 268–275. https://doi.org/10.1038/nn1629

ANEXOS

CD300f immunoreceptor is associated with major depressive disorder and decreased microglial metabolic fitness

Natalia Lago[a,1], Fernanda N. Kaufmann[b,1], María Luciana Negro-Demontel[a,c], Daniela Alí-Ruiz[a], Gabriele Ghisleni[d], Natalia Rego[e], Andrea Arcas-García[f], Nathalia Vitureira[a,g], Karen Jansen[d], Luciano M. Souza[d], Ricardo A. Silva[d], Diogo R. Lara[h], Bruno Pannunzio[a,c], Juan Andrés Abin-Carriquiry[i], Jesús Amo-Aparicio[j], Celia Martin-Otal[f], Hugo Naya[f], Dorian B. McGavern[k], Joan Sayós[f], Rubèn López-Vales[j], Manuella P. Kaster[b], and Hugo Peluffo[a,c,2]

[a]Neuroinflammation and Gene Therapy Laboratory, Institut Pasteur de Montevideo, 11400 Montevideo, Uruguay; [b]Department of Biochemistry, Federal University of Santa Catarina, Florianópolis, 88040-900 Santa Catarina, Brazil; [c]Departamento de Histología y Embriología, Facultad de Medicina, Universidad de la República, 11200 Montevideo, Uruguay; [d]Department of Life and Health Sciences, Catholic University of Pelotas, 96015-560 Rio Grande do Sul, Brazil; [e]Bioinformatics Unit, Institut Pasteur de Montevideo, 11400 Montevideo, Uruguay; [f]Immune Regulation and Immunotherapy Group, CIBBIM-Nanomedicine, Vall d'Hebrón Institut de Recerca, Universitat Autònoma de Barcelona, 08193 Barcelona, Spain; [g]Department of Physiology, Facultad de Medicina, Universidad de la República, 11200 Montevideo, Uruguay; [h]Department of Cellular and Molecular Biology, Pontifical Catholic University of Rio Grande do Sul, 90619-900 Porto Alegre, Brazil; [i]Instituto de Investigaciones Biológicas Clemente Estable, 11600 Montevideo, Uruguay; [j]Departament de Biologia Cel·lular, Fisiologia i Immunologia, Institut de Neurociències, Centro de Investigación Biomédica en Red sobre Enfermedades Neurodegenerativas, Universitat Autònoma de Barcelona, 08193 Bellaterra, Spain; and [k]Viral Immunology and Intravital Imaging Section, National Institute for Neurological Disorders and Stroke, National Institutes of Health, Bethesda, MD 20892

Edited by Shizuo Akira, Osaka University, Osaka, Japan, and approved February 4, 2020 (received for review July 11, 2019)

A role for microglia in neuropsychiatric diseases, including major depressive disorder (MDD), has been postulated. Regulation of microglial phenotype by immune receptors has become a central topic in many neurological conditions. We explored preclinical and clinical evidence for the role of the CD300f immune receptor in the fine regulation of microglial phenotype and its contribution to MDD. We found that a prevalent nonsynonymous single-nucleotide polymorphism (C/T, rs2034310) of the human CD300f receptor cytoplasmic tail inhibits the protein kinase C phosphorylation of a threonine and is associated with protection against MDD, mainly in women. Interestingly, CD300f$^{-/-}$ mice displayed several characteristic MDD traits such as augmented microglial numbers, increased interleukin 6 and interleukin 1 receptor antagonist messenger RNA, alterations in synaptic strength, and noradrenaline-dependent and persistent depressive-like and anhedonic behaviors in females. This behavioral phenotype could be potentiated inducing the lipopolysaccharide depression model. RNA sequencing and biochemical studies revealed an association with impaired microglial metabolic fitness. In conclusion, we report a clear association that links the function of the CD300f immune receptor with MDD in humans, depressive-like and anhedonic behaviors in female mice, and altered microglial metabolic reprogramming.

microglia | RNA-seq | depression | immunereceptor | CD300

Under physiological conditions, microglial cells continuously sense the neural environment and rapidly respond to neuronal activity, capillary leakage, cellular debris, and pathogens. Altered microglial function was postulated to contribute to psychiatric diseases including major depressive disorder (MDD) (1, 2). A significant association was observed between microglial and perivascular macrophage activation or increased cell number and untreated long-term MDD, as evidenced by brain translocator protein 18 kDa (TSPO) PET ligand [18F]FEPPA staining (2). Interestingly, antidepressant treatment prevented the progressive TSPO staining and MDD symptoms (2). The chronic microglial dysfunction associated with a dystrophic phenotype and increased cell numbers observed in MDD is accompanied by a well-documented increase in serum levels of inflammatory cytokines including interleukin 1 receptor antagonist (Il1rn) and interleukin 6 (IL-6) (3, 4). Despite the rapid advance in massive sequencing capacities, no microglial-specific transcriptomic profile has been published for the major psychiatric disorders. Very recently, transcriptomic methods have contributed to the precise description of a microglial phenotype termed disease- or damage-associated microglia (DAM) (5, 6). An interesting emerging hypothesis postulates that under neurodegenerative conditions or aging (6–8), the down-regulation of this homeostatic phenotype may impact central nervous system (CNS) dysfunction per se (9). It is therefore interesting to determine if this microglial phenotype is associated with psychiatric diseases.

Activating and inhibitory immunoreceptors, signaling mainly through DAP12 (also known as TYROBP) (8), were shown to

Significance

A role for innate immune receptors expressed by microglia and barrier macrophages has been postulated in neuropsychiatric diseases, including major depressive disorder (MDD). We discovered that a prevalent single-nucleotide polymorphism of the human CD300f immune receptor alters its signaling and is associated with protection against MDD in women but not in men. Interestingly, CD300f-deficient female, but not male, mice displayed depressive-like behaviors. In these mice, the absence of CD300f induced phenotypical changes of microglial cells that altered their metabolic fitness. Despite the high incidence of MDD, no effective treatments are available in many cases, and these discoveries could lead to the development of new pipelines for drugs targeting microglial cells, perivascular macrophages, and in particular the CD300f immune receptor.

Author contributions: N.L., F.N.K., G.G., N.R., N.V., J.A.-A., H.N., D.B.M., J.S., R.L.-V., M.P.K., and H.P. designed research; N.L., F.N.K., M.L.N.-D., D.A.-R., G.G., N.R., A.A.-G., N.V., K.J., L.M.S., R.A.S., D.R.L., B.P., J.A.A.-C., J.A.-A., C.M.-O., J.S., M.P.K., and H.P. performed research; N.L., M.L.N.-D., N.R., N.V., H.N., D.B.M., J.S., and R.L.-V. contributed new reagents/analytic tools; N.L., F.N.K., M.L.N.-D., D.A.-R., G.G., N.R., A.A.-G., N.V., J.A.-A., H.N., J.S., R.L.-V., M.P.K., and H.P. analyzed data; and N.L., F.N.K., N.R., M.P.K., and H.P. wrote the paper.

The authors declare no competing interest.

This article is a PNAS Direct Submission.

Data deposition: Raw data from the RNA sequencing experiment have been deposited in the NCBI Sequence Read Archive, https://www.ncbi.nlm.nih.gov/sra (accession no. PRJNA496060).

[1]N.L and F.N.K. contributed equally to this work.

[2]To whom correspondence may be addressed. Email: hugo.peluffo@pasteur.edu.uy.

This article contains supporting information online at https://www.pnas.org/lookup/suppl/doi:10.1073/pnas.1911816117/-/DCSupplemental.

First published March 9, 2020.

play a central role in microglial function both in the healthy and lesioned nervous system (5, 8, 10, 11). In particular, inhibitory immune receptors act as microglial restraining signals or checkpoints, ensuring mechanisms that actively limit microglial reactivity under both physiological and pathological conditions (12, 13). Activating and inhibitory immune receptors in microglial cells, such as TREM2, participate in synaptic pruning and clearance of cellular debris and apoptotic cells in the CNS (14). Although no microglial immune receptors have been associated to human MDD, a deficiency in the microglial immune receptors TREM2 or CX3CR1 induce alterations in social interaction and compulsive behaviors in naïve mice (14, 15) or potentiate depressive-like behaviors induced by lipopolysaccharide (LPS) (16), highlighting their putative role in psychiatric conditions.

Despite the importance of immune receptors on microglial function, many of them have not been studied in detail. In particular, CD300f immune receptors, which are expressed by several CNS myeloid cells including microglia and perivascular macrophages (5), share common phospholipid ligands with TREM2 such as the eat-me signal phosphatidylserine (17, 18), sphingomyelin (19), and high-density lipoprotein (HDL) and low-density lipoprotein (LDL) (20) and indirectly modulate DAP12 (21). CD300f is a very unique receptor, as it displays a dual activating/inhibitory capacity, recruiting phosphatases like SHP1/SHP2 via its ITIM motifs as well as activating PI3K and Grb2 adaptors, among others (22, 23). Moreover, it directly modulates other receptors, such as several members of the CD300 receptor family including CD300b activating receptor (21), FcRγ (24), and IL4Rα (25). In accordance with its inhibitory function, the absence of CD300f potentiates many inflammatory/autoimmune disease models (20, 26, 27) and is associated with human inflammatory and autoimmune disease susceptibility (28, 29).

Regardless of the strong evidence suggesting the importance of this receptor for the regulation of inflammatory conditions, very few studies have evaluated its role in the nervous system. CD300f is particularly interesting for the CNS demyelinating diseases, as it was shown to play a key role in experimental autoimmune encephalomyelitis, where exacerbated neuroinflammatory pathology is found in the knockout animals (30), and also being among the genes up-regulated in promyelinating microglia after a demyelinating stimuli (31). It appears among the top up-regulated genes in brain microglia after intraperitoneal (i.p.) LPS injection (32) and after spinal cord injury (33). Very recently, it was also associated to the neuroprotective response against Tau pathology (34). Despite all of this evidence implicating CD300f in CNS physiology and pathophysiology, no one has revealed any behavioral phenotypes in CD300f$^{-/-}$ mice under naïve conditions (20, 30, 35), and no studies have been performed in the CNS of these animals.

Here, we explored the participation of the CD300f immune receptor in regulating neuroinflammation as well as its involvement in behavioral alterations in mice and humans relevant for MDD.

Results

Association of a CD300f SNP with MDD. A single-nucleotide polymorphism (SNP, rs2034310) in the CD300f immune receptor has been associated with multiple sclerosis (29). This genetic variation is highly prevalent and determines a C/T exchange (mean frequencies ∼18 and 29% of European and American populations, respectively), producing a nonsynonymous substitution from Arg to Gln (R218Q) in the intracellular tail of CD300f. We took advantage of this natural highly prevalent polymorphism to evaluate its possible association with MDD in a cross-sectional population-based study. The study comprised a total of 1,110 individuals, 625 controls without MDD and 485 with MDD diagnosis. The sociodemographic information according to diagnosis is depicted in *SI Appendix*, Table S1. A high prevalence of MDD was observed in women ($P < 0.001$) and between smokers ($P < 0.001$). When analyzing the sociodemographic variables according to genotype distribution, we did not find differences according to sex ($P = 0.860$), socioeconomic class ($P = 0.964$), body mass index ($P = 0.524$), or presence of inflammatory or metabolic diseases ($P = 0.697$). However, ethnicity was significantly associated to genotype and the presence of the T allele was significantly higher in non-Caucasian individuals ($P < 0.001$). Additionally, the genotype frequencies were in agreement with those predicted by Hardy–Weinberg equilibrium for the rs2034310 SNP ($\chi^2 = 0.043$, $P = 0.836$). When evaluating the genotype frequencies according to diagnosis (*SI Appendix*, Table S2), it was observed that the CT genotype was associated with a protection against MDD when compared to the CC genotype (odds ratio [OR] = 0.693 95% CI 0.538 to 0.891; $P = 0.004$). This association remained significant after adjusting for age, sex, and ethnicity (OR = 0.698 95% CI 0.539 to 0.903; $P = 0.006$). Due to the small number of individuals with the TT genotype, we further used the dominant model grouping CT and TT subjects. The presence of the T allele (CT/TT) also conferred protection against MDD when compared to the CC genotype (OR = 0.736 95% CI 0.578 to 0.937; $P = 0.013$). These effects remained independently associated with protection against MDD after adjustment for the same variables described above (OR = 0.740 95%CI 0.578 to 0.948; $P = 0.017$), suggesting that genetic alterations in CD300f receptor function may impact susceptibility to MDD. Additionally, no significant allelic distribution differences were observed between C and T carriers according to MDD diagnosis ($P = 0.110$). An important point that has been neglected in psychiatric research is the evaluation of biological mechanisms underlying sex differences. In fact, MDD is twofold more prevalent in women and the lack of sex-specific biological evaluations can partially explain the treatment resistance and relapse for this disorder. To unravel possible sex-specific associations between the CD300f SNP and MDD, we stratified our sample (Table 1) and found that the association of the T allele with protection against MDD was only observed in women (OR = 0.625 95%CI 0.454 to 0.861; $P = 0.004$), even after adjusting for possible confounders (OR = 0.632 95% CI 0.457 to 0.874; $P = 0.006$). Despite the lower power of analysis obtained in the stratified sample of men (52.24%) when compared to the women's sample (99.59%), these results might suggest that sex differences might account for the influence of CD300f receptors on MDD.

Peripheral NLRP3/Caspase 1/IL-1β–mediated inflammation has been linked to a group of MDD patients (36); however, the CT genotype was not associated with increased serum IL-1β levels (CC: 9.66 ± 1.34 pg/mL, CT: 10.65 ± 1.47 pg/mL, and TT: 10.52 ± 4.98 pg/mL; $F(2.165) = 0.15$, $P = 0.559$). Thus, alterations in CD300f signaling may be associated with MDD in the absence of peripheral IL-1β–dependent inflammation.

The SNP Affects CD300f Immune Receptor Signaling. The arginine R218 to glutamine amino acid (R218Q) substitution in the intracellular tail of CD300f that confers protection against female depression is in the context of a putative protein kinase A (PKA)/protein kinase C (PKC) phosphorylation motif. To test this hypothesis COS7 cells transfected with human CD300f receptor (hCD300f) were submitted to different treatments: pervanadate (inhibiting phosphatases), forskolin (activating PKA), and phorbol-*myristate*-acetate (PMA) (activating PKC). Western blots using antibodies against specific phosphoSer/Thr recognizing the motif [R/K][R/K]X[pS/pT] demonstrated a PKC-dependent pS/pT phosphorylation of CD300f (Fig. 1*A*). This Ser/Thr phosphorylation was dependent on the R218 arginine residue, as the substitution of this amino acid by a glutamine blunted the phosphorylation (Fig. 1*B*). Therefore, we concluded that R218 is necessary for the PKC phosphorylation of CD300f cytoplasmic tail. Moreover, mutants of the serine S216, threonine T221, or both, demonstrated that the threonine T221 is the

Table 1. Genotype and allele distribution according to sex and diagnosis for MDD

Characteristics	MDD				
	No	Yes	*P*	Unadjusted OR (95%)/*P**	Adjusted OR (95%)/*P*†
Women					
rs2034310 SNP genotype					
CC	154 (51.2)	201 (62.6)	0.006	1	1
CT	131 (43.5)	100 (31.2)		0.585 (0.419–0.817)/0.002	0.592 (0.422–0.831)/**0.002**
TT	16 (5.3)	20 (6.2)		0.958 (0.480–1.910)/0.902	0.964 (0.481–1.935)/0.919
Dominant model					
CC	154 (51.2)	201 (62.6)	0.005	1	1
CT/TT	147 (48.8)	120 (37.4)		0.625 (0.454–0.861)/0.004	0.632 (0.457–0.874)/**0.006**
Men					
rs2034310 SNP genotype					
CC	182 (56.2)	95 (58.3)	0.626	1	1
CT	127 (39.2)	58 (35.6)		0.875 (0.588–1.302)/0.510	0.886 (0.594–1.321)/0.551
TT	15 (4.6)	10 (6.1)		1.277 (0.553–2.952)/0.567	1.307 (0.564–3.029)/0.533
Dominant model					
CC	182 (56.2)	95 (58.3)	0.657	1	1
CT/TT	142 (43.8)	68 (41.7)		0.917 (0.627–1.343)/0.657	0.929 (0.634–1.364)/0.708

Data are presented as number (percent) or proportion.
**P* values were computed by χ^2 tests comparing MDD patients and controls.
†Adjusted OR (95% CI/*P*) values were obtained from logistic regression analysis adjusting for age and ethnicity. Significance of adjusted OR is highlighted in bold.

only residue phosphorylated by PKC in the cytoplasmic tail of hCD300f (Fig. 1*C*). We also observed that the phosphorylation of T221 is an event downstream of the phosphorylation of the five tyrosine residues within the cytoplasmic tail of CD300f (*SI Appendix*, Fig. S1*A*), and also that the two tyrosine residues that conform the putative PLCγ binding motifs, Y205 and Y236, could

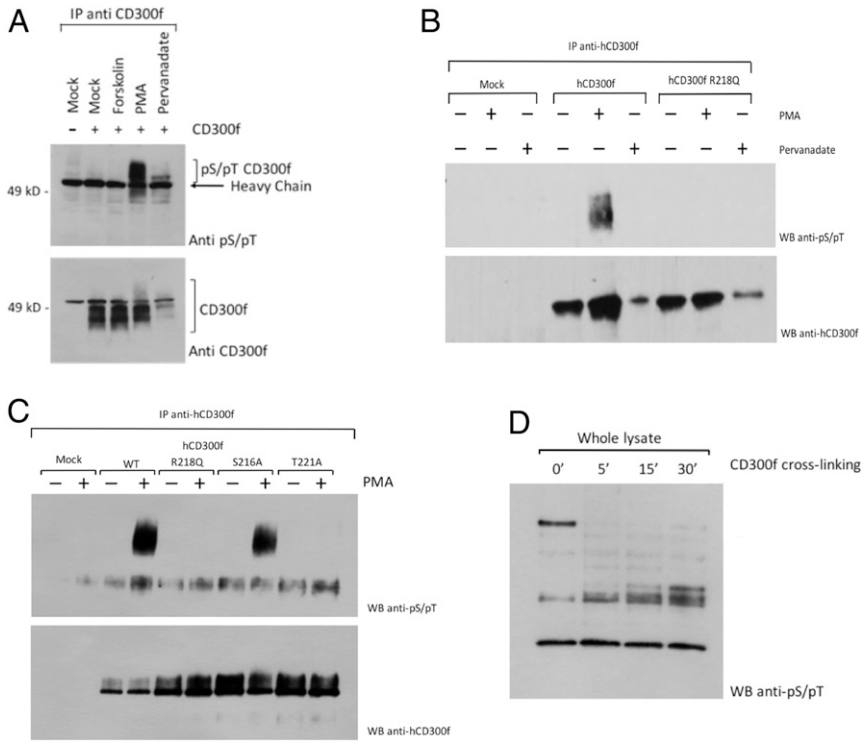

Fig. 1. The R218Q substitution of CD300f SNP modifies its normal signaling. COS-7–transfected cells with an empty vector or the hCD300f construct were exposed to different stimuli. Immunoprecipitation (IP) with anti-CD300f monoclonal antibody (mAb) was performed and Western blot with a Phospho-(Ser/Thr) PKA Substrate Antibody, which detects phospho-serine/threonine residue with arginine at the −3 position (K/R)(K/R)X(pS/pT). Blotting with anti-CD300f Ab was done as loading control (*A*). COS-7 cells were transfected with an empty vector or the indicated hCD300f constructs and cells were treated with PMA or pervanadate. IP with anti-CD300f mAb was performed and blots were performed with Phospho-(Ser/Thr) PKA Substrate Antibody. Blotting with anti-CD300f Ab was performed as loading control (*B*). COS-7 cells were transfected with an empty vector or the indicated hCD300f constructs. When indicated, transfected cells were exposed to PMA, IP with anti-CD300f mAb was performed, and blots were processed with Phospho-(Ser/Thr) PKA Substrate Antibody. Blotting with anti-CD300f Ab was performed as loading control (*C*). U937 cells were stimulated with 10 μg/mL UPD2 mAb for different periods. An IP with anti-CD300f mAb was performed and proteins were blotted with Phospho-(Ser/Thr) PKA Substrate Antibody (*D*).

be essential for the activation of PLCγ, which in turn promotes the activation of PKC (*SI Appendix*, Fig. S1 *B* and *C*). Moreover, we discovered that PKC activation is part of the normal CD300f signaling pathway using the U937 monocytic cell line (Fig. 1*D*). Collectively, these data (Fig. 1 and *SI Appendix*, Fig. S1) show that PKCδ isoenzyme is involved in the CD300f activating signaling and that the R218Q substitution of SNP modifies its normal signaling.

CD300f Deficiency Induces Depressive-Like Behavior and Anhedonia in Female Mice. The association of the rs2034310 CD300f SNP with MDD prompted us to analyze possible changes in the general behavioral phenotype of the CD300f$^{-/-}$ mice, especially behavioral alterations considered relevant for MDD. Three different strains of CD300f$^{-/-}$ mice have been generated to date, including the one used in the present study. None of these knockouts have reported alterations in development or other basic physiological variables, including immune system function or systemic inflammation in naïve conditions (20, 30, 35). However, no behavioral studies have been performed on these animals. When 4- to 5-mo-old wild-type (WT) and CD300f$^{-/-}$ mice of both sexes were exposed to an open field arena [in the parallel rod floor test arena (37)], the CD300f$^{-/-}$ animals displayed decreased spontaneous locomotor activity (Fig. 2*A*). However, these animals did not show alterations in motor coordination or ataxia when analyzed both by the parallel rod floor test (37) (Fig. 2*B*) or when exposed to a forced locomotor task such as the rotarod (Fig. 2*C*). These results suggest that CD300f$^{-/-}$ mice do not have a defect in motor function that explains the reduced spontaneous activity. The adult CD300f$^{-/-}$ female and male animals did not show other general alterations in CNS physiology such as the thermal sensitivity of the hind paws measured by the Hargreaves test (*SI Appendix*, Fig. S2*A*) or in the mechanical sensitivity of the hind paws tested with the Von Frey filaments (*SI Appendix*, Fig. S2*B*). Additionally, adult male and female mice were exposed to behavioral despair models such as the tail suspension test (TST) and the forced swim test (FST) and to the sucrose splash test (SST) to evaluate motivational and hedonic behaviors. These tests assess the two cardinal symptoms of MDD: depressive-like behavior and anhedonia (loss of pleasure seeking). Female CD300f$^{-/-}$ mice did not show significant alterations in spontaneous locomotor activity in a regular open field test (OFT) (Fig. 2*D*); however, they displayed a significant increase in immobility time when compared to WT animals in both the TST (Fig. 2*E*) and the FST (Fig. 2*F*) that reflects a depressive-like behavior. Moreover, the female CD300f$^{-/-}$ animals showed a significant decrease in the total time spent grooming after the sucrose splash when compared to WT animals (Fig. 2*G*) and an increase in the latency to start grooming, indicative of reduced motivational behavior (Fig. 2*H*). Together, these results suggest that female CD300f$^{-/-}$ mice displayed anhedonic behaviors. CD300f deficiency also potentiated the anhedonic behavior observed in the LPS-induced depression model in female mice (Fig. 2*I*), showing that the absence of this receptor may contribute to multifactorial mechanisms of depressive behaviors. Interestingly, the depressive-like and anhedonic symptoms were not observed in adult 4- to 5-mo-old males (*SI Appendix*, Fig. S3). Finally, to test whether CD300f$^{-/-}$ female mice have long-lasting and progressive MDD-like behavioral alterations, we exposed a different cohort of aged females (18 mo old) to the previous behavioral test batteries. Aged CD300f$^{-/-}$ female mice (aCD300f$^{-/-}$) had an altered

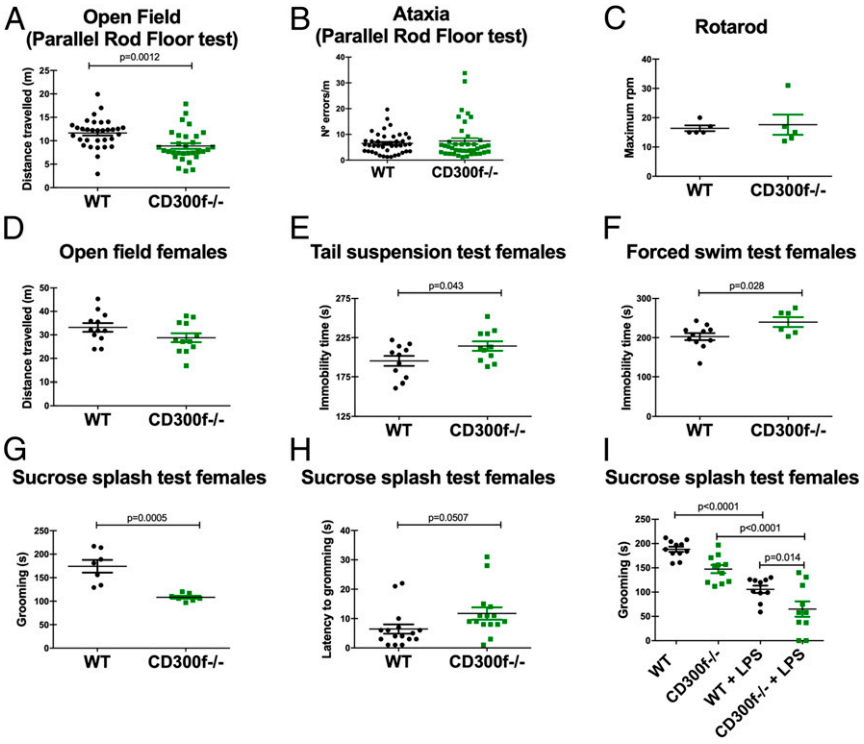

Fig. 2. CD300f$^{-/-}$ female mice display depressive-like and anhedonic phenotype. Adult (4 to 5 mo) male and female mice were evaluated for spontaneous locomotor activity in an open field arena (in the parallel rod floor test in *A*, or only females in a regular open field arena in *D*) and for motor impairment in the parallel rod floor test (for ataxia in *B*) or the rotarod (test with increased revolutions per minute is shown in *C*). The total immobility time in the TST in *E* and the FST in *F* was measured in females to evaluate depressive-like behavior. The total time in grooming behavior (*G*) and the latency to start grooming behavior (*H*) in the SST were recorded in females to evaluate motivational/self-care behavior and hedonic-like behavior, respectively. i.p. injection of LPS (2 mg/kg) induced 24 h after a potentiated anhedonic response in CD300f$^{-/-}$ female mice (*I*, two-way ANOVA followed by Bonferroni's post hoc test). Each dot represents a different animal and data are from at least two independent experiments. Data are represented as mean ± SEM.

behavioral phenotype consistent with depressive-like and anhedonic behaviors similar to that observed in adult CD300f$^{-/-}$ female mice (*SI Appendix*, Fig. S3). Taken together, these results show that the CD300f$^{-/-}$ female, but not male, mice display long-lasting behavioral alterations consistent with key behavioral symptoms associated with MDD in patients.

CD300f Deficiency and Neuroinflammation. The CD300f immune receptor is expressed in vitro in postnatal microglial cultures (38, 39). We isolated CD11b^{+}/CD45^{low} microglial cells from naïve spinal cord by fluorescence-activated cell sorting (FACS) (*SI Appendix*, Fig. S4 *A* and *B*), and qPCR for CD300f messenger RNA (mRNA) showed ~40-fold enrichment in the microglial fraction (*SI Appendix*, Fig. S4 *C* and *D*) when compared to total spinal cord extracts. These data are in accordance with mouse and human RNA sequencing (RNA-seq) experiments showing that CD300f mRNA is expressed only in microglia in the naïve CNS parenchyma and by CNS barrier macrophages (32, 40).

To understand the biological role of CD300f in the CNS, we first explored the hypothesis that it might participate in the regulation of microglial phenotype and restrain neuroinflammatory signals. We sorted CD11b^{+}/CD45^{low} microglial cells from the hippocampus of saline- or LPS-injected WT and CD300f$^{-/-}$ female mice and performed RNA-seq studies to compare their phenotype with the reported homeostatic microglial signature (8, 10, 32). Highly enriched microglial samples were obtained (*SI Appendix*, Fig. S5). The RNA-seq gene expression profiles of naïve WT and CD300f$^{-/-}$ microglia were slightly different, as observed by principal component analysis (Fig. 3*A*). In fact, only 34 genes were significantly differentially expressed (false discovery rate [FDR]-adjusted *P* value <0.1) between microglia from naïve WT and CD300f$^{-/-}$ mice (Fig. 3*B*). No significant alterations associated to KEGG (Kyoto Encyclopedia of Genes and Genomes) pathways were found for this dataset. When the homeostatic microglial gene signature was analyzed, we observed that CD300f deficiency did not alter expression of homeostatic genes (*SI Appendix*, Fig. S6*A*) and did not undergo a phenotypic shift toward a DAM phenotype (5, 6) (*SI Appendix*, Fig. S6*B*). Only one DAM and immature microglial marker gene, Spp1 (also termed osteopontin), showed a

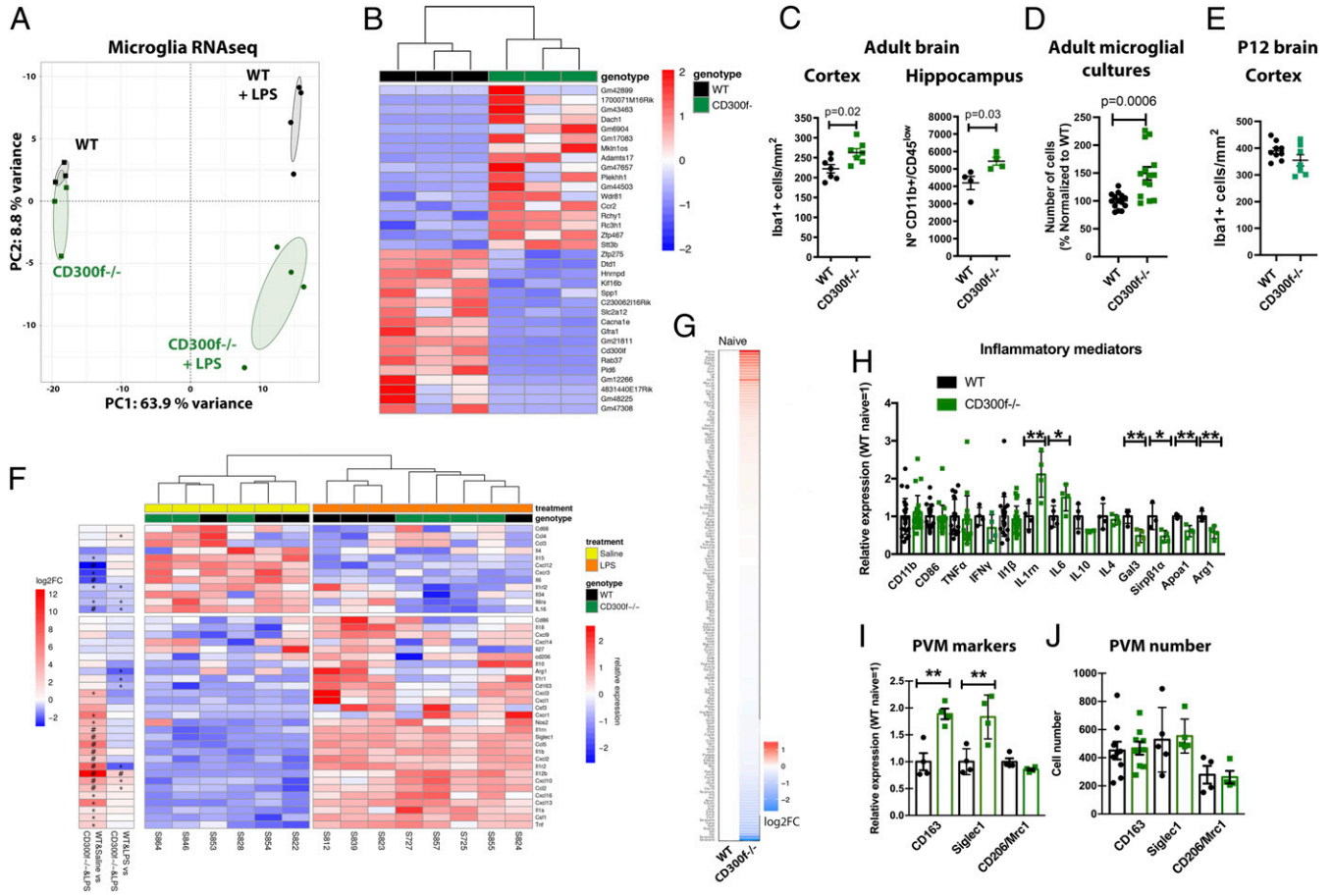

Fig. 3. Acutely isolated CD300$^{-/-}$ microglia show mild alterations in their transcriptome and increased numbers in the naïve hippocampus. The hippocampi of female WT and CD300f$^{-/-}$ mice injected with saline or LPS (2 mg/kg) were collected for the isolation of CD11b^{+}/CD45^{low} microglial cells by cell sorting. RNA-seq of mRNAs was undertaken, and the overall grouping by principal component analysis (PCA) is shown (*A*). PCA was based on the regularized expression levels of the 150 most variable genes, and the confidence ellipses were computed at the 0.9 level. The heat map of the 34 differentially expressed genes (P_{adj} < 0.1) among saline-injected WT and CD300f$^{-/-}$ is shown (*B*). Expression levels are shown scaled by row after regularized transformation of estimated values. CD300$^{-/-}$ adult mice cortex or hippocampus, but not P12 brain cortex (*E*), showed increased microglial cell density (IBA1+ cells by immunohistochemistry or CD11b^{+}/CD45^{low} cell by FACS, respectively (*C*). Adult CD300f$^{-/-}$ microglial cultures showed increased cell density (each dot represents a well of three independent cultures, *D*). Most inflammatory genes were not altered in CD300f$^{-/-}$ microglia in naïve conditions or after LPS injection (see selected genes in *F*), or in total brain and spinal cord extracts of naïve animals (*G* and *H*). Alterations in the mRNA of some perivascular macrophage markers were observed (*I*), while no changes in their cell number by FACS could be detected (*J*). Each dot represents a different animal in *C*, *E*, and *H*–*J*. Data are represented as mean ± SEM. Heat map in *F* as in *B* and additional log2 raw fold changes for specific combinations of genotypes and conditions are shown. In *F*, each * represents P_{adj} < 0.1; each # represents P_{adj} < 0.1 and abs(log2FC) ≥ 1 with P_{adj} < 0.1. In *H* and *I*, * and ** represent P < 0.05 and *P* < 0.01 respectively.

significant down-regulation. Interestingly, decreased serum Spp1 has been found in MDD patients (41).

While RNA-seq results showed no change in the main CD300f$^{-/-}$ microglial signature genes in naïve animals, we observed increased microglia numbers. Indeed, the direct cell counts of IBA1 immunoreactive cells in adult mice motor cortex showed an 18.3 ± 4.6% increase in CD300f$^{-/-}$ mice (Fig. 3*C*). These data were replicated in a different colony housed at the Universitat Autònoma de Barcelona, where FACS staining of CD11b^{+}/CD45^{low} hippocampal microglial cells showed a 29.8 ± 5.4% cell density increase in adult CD300f$^{-/-}$ mice (Fig. 3*C*). This increased CD300f$^{-/-}$ microglial cell division rate could be replicated in adult microglial purified cell cultures (Fig. 3*D*). In addition, in vivo, no differences could be detected by FACS staining for active Caspase 3 in WT and CD300f$^{-/-}$ mice (naïve WT: 1.50 ± 0.24 and CD300f$^{-/-}$: 1.48 ± 0.21; or i.p. LPS-treated WT: 1.19 ± 0.24 and CD300f$^{-/-}$: 1.03 ± 0.40, mean ± SEM). Thus, decreased levels of apoptosis in CD300f$^{-/-}$ microglia or increased apoptosis in WT microglia do not account for the in vivo increased microglial numbers. Interestingly, an increase in microglial density and a chronic microglial dysfunction has been associated with a dystrophic phenotype linked to psychiatric disorders, including MDD (1). The increase in microglial density in adult CD300f$^{-/-}$ brain occurs gradually, as no changes in microglial density was observed in postpartum day 12 (P12) mice when microglia has already stopped proliferating (32) (Fig. 3*E*). Taken together, these data suggest that CD300f$^{-/-}$ microglia maintain their homeostatic phenotype despite subtle changes in gene expression and cell number under naïve conditions. Moreover, the absence of CD300f immune receptor per se did not predispose microglial cells toward a proinflammatory phenotype.

While the absence of CD300f in microglial cells did not trigger a neuroinflammatory milieu, it could potentiate an externally induced neuroinflammatory process. To explore this hypothesis we used two well-described models of neuroinflammation that do not involve major blood–brain barrier disruption, tissue damage, or myeloid cell recruitment, i.p. LPS injection and peripheral nerve injury (42). When WT and CD300f$^{-/-}$ female mice were intraperitoneally injected with LPS, a differential expression of 1,304 microglial genes was observed (FDR-adjusted *P* value <0.1; Dataset S1). Interestingly, while LPS induced a well-known differential gene expression in WT microglia (see selected genes in Fig. 3*F*), most of the altered gene expression observed in the CD300$^{-/-}$ LPS-treated mice was not related to classical inflammatory mediators such as tumor necrosis factor α, IL-1β, nitric oxide synthase 2, or chemokines (see selected genes in Fig. 3*F*). In other words, among the 5,865 microglial differentially expressed genes after LPS treatment in WT animals (Wald test, FDR-adjusted *P* value <0.1), only 197 genes were altered by CD300f deficiency, and with a few exceptions (such as Arg1, IL-12β, or CCL12) were not classical neuroinflammatory mediators (Dataset S1 and *SI Appendix*, Fig. S7). Thus, the transcriptomic effect induced by LPS in WT animals was not potentiated or inhibited by the absence of CD300f, which instead showed a different profile. In accordance with the absence of widespread changes in inflammatory mediators after LPS injection, a peripheral sciatic nerve injury-induced neuroinflammation did not show enhanced spinal cord inflammation at different time points (from 2 to 28 d postlesion) in CD300f$^{-/-}$ mice compared to WT. This includes no changes in IBA1 microglial staining, Luminex cytokine measurements, or qPCR (*SI Appendix*, Fig. S8).

To further test the hypothesis that CD300f immune receptor could modulate neuroinflammation, we analyzed the expression levels of 179 inflammatory/phagocytic genes in the total spinal cord and brain extracts from naïve WT or CD300f$^{-/-}$ naïve animals of both sexes. No significant alterations in most of the analyzed genes were observed (Fig. 3 *G* and *H*). This finding is consistent with the modest alterations in global gene expression observed by RNA-seq in microglial cells. Interestingly, among the very few gene expression alterations observed in the naïve brains of the CD300f$^{-/-}$ animals were the increased mRNA for Il1rn and IL-6 (Fig. 3*H*), two well-documented MDD-associated cytokines (3, 4). Moreover, the CD300f$^{-/-}$ brains also showed alterations in the mRNA expression of Siglec1, Sirpβ1, and Apoa1, which in addition to Il1rn have been shown to be part of a gene coexpression module in MDD (43). Besides microglial cells, perivascular macrophages also express CD300f (5). The mRNA for two specific markers of these cells, CD163 and Siglec1 (5, 44), were increased in brain extracts of CD300f$^{-/-}$ animals (Fig. 3*I*), and interestingly CD163 has been described as a common marker of several psychiatric conditions including MDD (43). However, no changes were observed in the mRNA for CD206, another perivascular macrophage marker (Fig. 3*I*) (5, 44), or in the number of CD163+, Siglec1+, or CD206+ cells (Fig. 3*J*).

Altogether, these data suggest that CD300f$^{-/-}$ mice do not develop classical neuroinflammation but display several features of altered neuroimmune communications including increased microglial number, possible alterations in microglial and perivascular macrophage phenotype, and increased innate mediators such as Il1rn and IL-6, all previously associated to MDD.

Analysis of Microglial Phenotype Associated to the Depressive Phenotype. When WT and CD300f$^{-/-}$ female mice were intraperitoneally injected with LPS, CD300f deficiency worsened the depressive phenotype (Fig. 2*I*). Moreover, the transcriptomic effect induced by LPS in WT microglia was mainly maintained in CD300f$^{-/-}$ LPS-treated animals but they also showed additional transcriptomic changes (Fig. 3*A*), highlighting a different nonclassical proinflammatory mechanism for the induction or potentiation of the depressive-like phenotype. Interestingly, significant enrichment in KEGG pathways and Gene Ontology analysis of biological processes were found for this RNA-seq dataset mainly associated to autophagy and several metabolic pathways (Fig. 4*A* and *SI Appendix*, Fig. S9). Much recent evidence shows that receptor systems that mediate macrophage activation are linked to metabolic pathways, and that metabolic reprogramming is an integral part of the activation process (45). The adoption of the Warburg, or glycolytic metabolism, by macrophages is critical for their activation in response to LPS and other activators (46). Interestingly, we observed that key metabolic components were down-regulated in CD300f$^{-/-}$ microglia from LPS-treated animals when compared to WT LPS-treated mice (Fig. 4 *B* and *C*). This down-regulation impacted several pathways such as glycolysis (e.g., glucose transporters SLC2a1 and SLC2a3, also termed Glut1 and Glut 3 or hexokinase 1, Hk1; Fig. 4 *B* and *C*), gluconeogenesis (e.g., phosphoenolpyruvate carboxykinase 2, Pck2/Pepck2; Fig. 4 *B* and *C*), mitochondrial fatty acid β-oxidation (e.g., carnitine palmitoyltransferase 1a, Cpt1a; *SI Appendix*, Fig. S10), lipid synthesis (e.g., Acyl-CoA Synthetase Short Chain Family Member 2, Acss2), or Krebs cycle (e.g., Isocitrate dehydrogenase, Idh1, or mitochondrial pyruvate carrier 2, Mpc2; *SI Appendix*, Fig. S11). In many cases, the down-regulation of key enzymes in the CD300f$^{-/-}$ microglia of LPS-treated animals was even significant when compared with WT microglia, as observed for Hk1, Pck2, Idh1, or Acadm, among others (Fig. 4*B* and asterisks in Fig. 4*C*). In accordance, CD300f$^{-/-}$ microglia acutely isolated from LPS-treated mice showed reduced basal mitochondrial (Fig. 4*D*) and glycolytic activity (Fig. 4*E*). Moreover, the glycolytic shift normally observed in WT cells after the addition of mitochondrial stressors could not be induced in CD300f$^{-/-}$ microglia from LPS-treated mice (Fig. 4*E*). The total mitochondrial mass, however, did not differ between these two groups (Fig. 4 *F* and *G*), suggesting that mitochondrial dysfunction rather than lower mitochondrial content occurs in CD300f$^{-/-}$ microglia after peripheral LPS-induced activation. In accordance with our RNA-seq data and previous reports suggesting

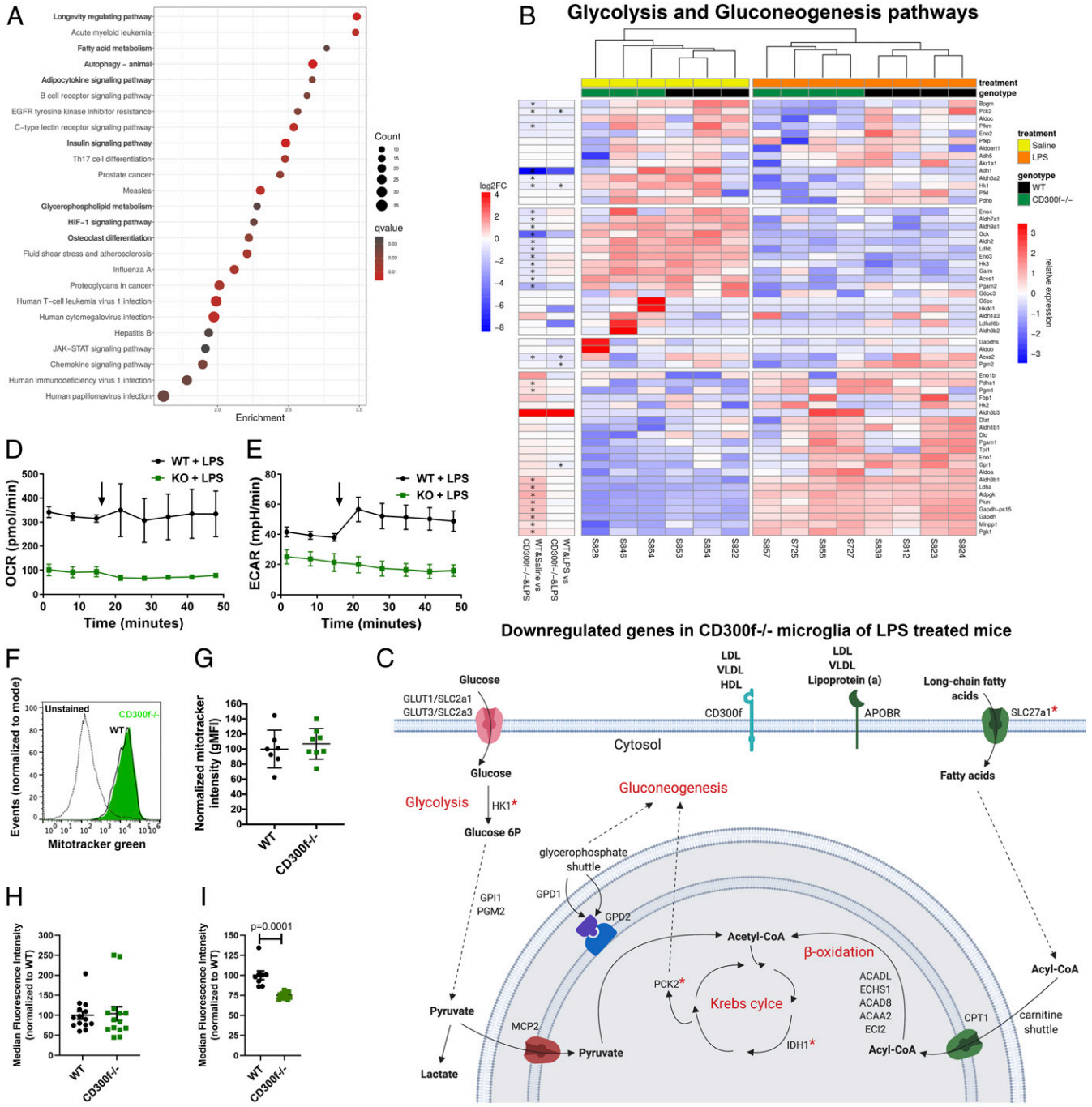

Fig. 4. Loss of CD300f$^{-/-}$ induces altered metabolic reprogramming of microglial cells. The hippocampi of female WT and CD300f$^{-/-}$ mice injected with saline or LPS (2 mg/kg) were collected for the isolation of CD11b^{+}/CD45^{low} microglial cells by cell sorting. RNA-seq of mRNAs was undertaken, and KEGG pathways enrichment analysis was performed on the list of differentially expressed genes for WT+LPS vs. CD300f$^{-/-}$+LPS (1,304 genes; FDR-adjusted P value <0.1, *A*). Expression profiles for the genes associated to the glycolysis and gluconeogenesis pathways were selected and the heat map show the expression levels scaled by row after regularized transformation of estimated values. Log2 raw fold changes for some specific combination of genotypes and conditions are shown. Each * represents $P_{adj} < 0.1$; each # represents $P_{adj} < 0.1$ and abs(log2FC) ≥ 1 with $P_{adj} < 0.1$ (*B*). A schematic representation of key metabolic pathway genes down-regulated in LPS-injected CD3000$^{-/-}$ versus LPS-injected WT mice (*C*, red asterisks represent genes also down-regulated when compared to saline-injected WT mice). Seahorse experiments using acutely isolated CD11b^{+} hippocampal microglial cells by magnetic beads were performed, and the oxygen consumption rate (*D*) and extracellular acidification rate (*E*) were measured. FACS analysis of CD11b^{+}/CD45^{low} microglial cells with MitoTracker Green for estimating the mitochondrial mass was undertaken (*F* and *G*). Phagocytosis of fluorobeads (*H*) and endocytosis of pHrodo-LDL (*I*) was analyzed in WT and CD300f$^{-/-}$ adult microglial purified cultures. VLDL, very-low-density lipoprotein.

that CD300f may act as a lipoprotein receptor, CD300f$^{-/-}$ microglia showed a decreased receptor-mediated LDL endocytosis, while no alteration on nonreceptor-mediated phagocytosis was detected (Fig. 4 *H* and *I*). Moreover, key microglial transcription factors such as Mafb, Egr1, Maf1, and Cebpg were down-regulated and differential expression of 23 genes of the autophagy pathway were observed in the CD300f$^{-/-}$ microglia from LPS-injected animals (*SI Appendix*, Fig. S12). Collectively, these data suggest that the

metabolic reprogramming needed for microglial activation is compromised in CD300f$^{-/-}$ mice, and that this also alters autophagy processes, in a similar fashion as TREM2$^{-/-}$ microglia in an Alzheimer's disease model (11).

CD300f Modulates Synaptogenesis and Synaptic Strength In Vitro by a Glial-Mediated Mechanism. Microglia have been associated with synaptic pruning and modulation of neurotransmission (47). To evaluate how microglial CD300f might be involved in neurotransmission alterations, we analyzed the effect of blocking CD300f on the modulation of synaptogenesis and excitatory synaptic strength in mixed neuron–glia hippocampal cultures. The cultures were stained for the presynaptic and postsynaptic markers vGlut1/Homer, respectively (Fig. 5 *A* and *B*). Moreover, we measured the intensity of synaptic vGlut1 immunoreactivity, which was shown to accurately estimate the probability of neurotransmitter release (48) and thus of synaptic strength. Incubation of cultures with tetrodotoxin (TTX) induced the well-described synaptogenesis/synaptic plasticity (49) evidenced by an increased number of total vGlu1/Homer-positive synapses (Fig. 5*C*), as well as an increased intensity of individual presynaptic vGlut1 immunoreactivity (Fig. 5*D*). Similarly, the addition of the soluble competitive inhibitor CD300f-Fc fusion protein to these cultures at concentrations comparable (0.01 μg/mL) to the soluble CD300f form produced by microglia in culture (39) also induced an increase in the total number of synapses and in the probability of neurotransmitter release (Fig. 5 *C* and *D*). Under these conditions, no neuronal cell death was detected (*SI Appendix*, Fig. S13*A*). To determine if this effect was mediated by glial cells, hippocampal neuron-enriched cultures were incubated directly with rCD300f-Fc, or alternatively with conditioned medium from mixed glial cultures treated with rCD300f-Fc. Interestingly, no changes in the number of synapses (*SI Appendix*, Fig. S13*B*) or in the probability of release (*SI Appendix*, Fig. S13*C*) could be observed in hippocampal neuron cultures treated directly with rCD300f-Fc or with the different mixed glial conditioned media. Taken together, these results suggest that CD300f may be involved in the turnover of synapses and regulation neurotransmission by a glial and contact-dependent mechanism.

Hippocampal Noradrenaline Level-Dependent Depressive Phenotype of CD300f-Deficient Animals. MDD has been classically associated with decreased levels of serotonin, dopamine, and noradrenaline in brain regions involved in mood regulation such as the hippocampus (50). Alteration of microglial-mediated synaptic plasticity could alter neurotransmitter levels. To evaluate if the behavioral changes observed in female CD300f$^{-/-}$ mice are associated with changes in monoaminergic neurotransmission, the levels of serotonin, dopamine, and noradrenaline were analyzed in the hippocampus. Interestingly, hippocampal noradrenaline was significantly decreased, whereas no other significant changes were observed in the levels of serotonin or dopamine (Fig. 5 *E*–*G*). This decrease has been associated with some forms of MDD (50). The reduction in noradrenaline was due to neurotransmitter content, as no alteration was observed in noradrenergic projections in the hippocampus (*SI Appendix*, Fig. S13 *D*–*F*). Importantly, the administration of bupropion, a selective noradrenaline and dopamine uptake inhibitor used as antidepressant in the clinic, reversed the anhedonic behavior in CD300f$^{-/-}$ female animals but did not affect the WT (Fig. 5*H*). Taken together, these data suggest that CD300f may participate in microglial-mediated neuroplasticity and, when altered, induce a noradrenaline-dependent depressive-like phenotype.

Discussion

The main finding of this work indicates that the functional status of the CD300f immune receptor influences the development of MDD in both female mice and female humans. In mice, this persistent effect occurs in the absence of overt neuroinflammation and is associated to increased microglial cell number, alterations in several MDD-related cytokines (IL-6, IL1rn, and Spp1) and cell

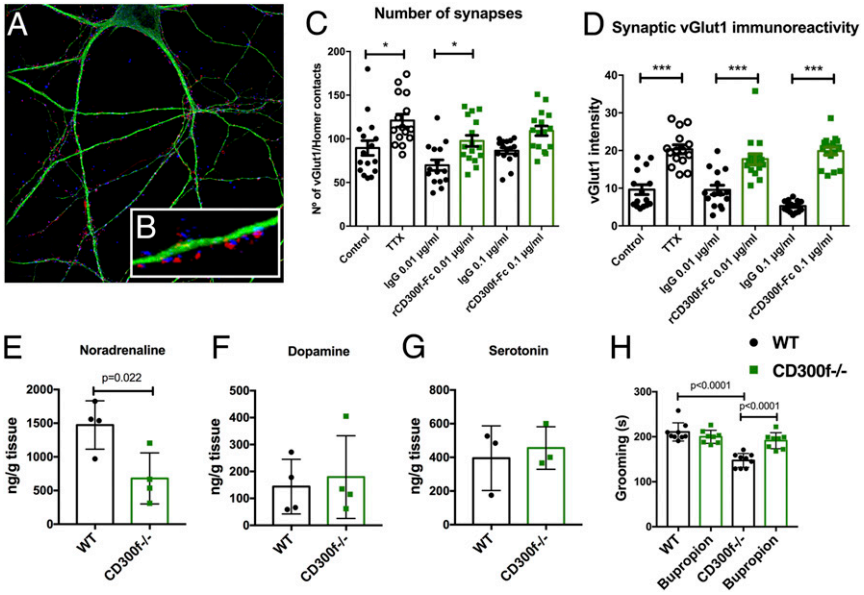

Fig. 5. Loss of CD300f$^{-/-}$ alters synaptic strength and reduces noradrenaline levels in the hippocampus. Mixed hippocampal–glial cocultures (36.2 ± 5.1% neurons, 11.4 ± 0.7% microglia, 37.7 ± 4.4% astrocytes and 14.8 ± 3.2% oligodendrocytes) were treated with recombinant CD300f-Fc fusion protein, immunoglobulin G (IgG) isotype control, or TTX. The number of synaptic contacts (partial colocalization of vGlut1 and Homer, *A*–*C*) and the synaptic strength (vGlut1 staining intensity in each of these synaptic contacts, *D*) were quantified. Data are from two independent experiments run in duplicate, and $n = 8$ neurons per well were analyzed in *C* and *D*. Data are represented as mean ± SEM. Female mice were perfused with saline and the hippocampus extracted for the analysis of different neurotransmitter levels by HPLC (*E*–*G*). Administration of bupropion (10 mg/kg i.p.) reversed the anhedonic behavior in the SST (*H*, two-way ANOVA followed by Bonferroni's post hoc test). Each dot represents a different animal and data in *H* are from two independent experiments.

markers (CD163), and modulation of synaptic strength and is dependent on hippocampal noradrenergic neurotransmission. Moreover, the CD300f immune receptor emerges as a central regulator of microglial immunometabolic reprogramming and, in conjunction with perivascular macrophage phenotype alterations, may contribute to the depressive-like phenotype.

CD300f Immune Receptor Is Involved in MDD. Association of inflammation and depression has been well documented both in animal models and clinical studies (36, 51). MDD frequently accompanies patients suffering from sustained systemic inflammation (52, 53). It was also recently proposed that TREM2, which shares most of its ligands with CD300f (17–19), may act as a CNS damage-associated molecular pattern (DAMP) receptor or neurodegeneration-associated molecular pattern receptor (54). Several DAMPs and their receptors have been associated to MDD (55). Thus, CD300f could also function as a DAMP receptor modulating microglial and perivascular macrophage phenotype. We hypothesized that in the absence of a restraining signal (CD300f), microglial and perivascular macrophages would induce low-grade neuroinflammation that could lead to a depressive-like behavior. Interestingly, the absence of CD300f led to depressive-like and anhedonic behaviors, but this was not associated with overt neuroinflammation. In fact, qPCR mRNA profiling for proinflammatory gene expression in the whole brain or RNA-seq of sorted microglial cells showed no significant changes in most of the genes analyzed. In addition, microglia demonstrated no evident morphological alterations, and the signature mRNA levels for infiltrating cells such as CD4 (subset of T lymphocytes), Mpo (neutrophils), and Il17a (Th17 cells) remained stable, suggesting no infiltration of these cells. Interestingly, while no changes in the number of perivascular macrophages were observed in the CNS of CD300f$^{-/-}$ animals, two of their most specific markers, CD163 and Siglec1 (5, 44), showed increased mRNA expression, arguing in favor of a phenotypic change in this cell type. Interestingly, transcriptomic profiling showed that increased expression of CD163 is found among the top 40 common genes altered in several major psychiatric conditions, including MDD, bipolar disorder (BP), autism spectrum disorder (ASD), schizophrenia (SCZ), or alcohol abuse disorder (AAD), and both CD163 and Siglec1 are included in a MDD coexpression network (43). Moreover, individuals that committed suicide displayed increased density of perivascular macrophages (56, 57). This suggests that perivascular macrophages may have a role in MDD and that functional alteration of these cells in CD300f$^{-/-}$ mice might contribute to the depressive phenotype. This warrants further studies to explore the hypothesis that alterations in CNS tissue resident macrophages contribute to MDD and other psychiatric conditions.

The three different CD300f$^{-/-}$ mice models generated to date did not show any alterations in the immune system or inflammatory markers in the systemic circulation (20, 30, 35), even at 15 mo of age (35). In agreement with the lack of inflammation observed in the CD300f$^{-/-}$ mice, patients carrying the T allele of the rs2034310 SNP and showing protection against MDD did not show alterations in IL-1β protein levels in serum when compared to the other genotypes, suggesting that the mechanism by which CD300f acts during MDD may not be related to classical inflammatory processes. Interestingly, several reports have shown important noninflammatory intricate neuroimmune communications during development, homeostasis, and neurological diseases (58). In fact, among the very few genes found to be upregulated in the brains of naïve CD300f$^{-/-}$ mice were Il1ra (IL1rn), the soluble inhibitor of IL-1α and IL-1β signaling, and also IL-6, the two most common cytokines previously shown to be selectively increased in serum of MDD patients (3, 4). In this sense, CD300f may contribute to neuroimmune communication in several ways aside from the regulation of the classical neuroinflammatory pathways.

Previously published epidemiological data showed that women are more susceptible to MDD than men (59), and the data we obtained in the population-based study reported here are in accordance. Strikingly, absence of CD300f only induced a depressive-like phenotype in female mice and not in males. Moreover, the protection against MDD conferred by the T allele of CD300f rs2034310 SNP in humans showed significant differences in women but not men. This difference may be due to a limited power of analysis in the male cohort or instead point to a true gender difference. This intriguing effect needs to be studied further in a larger patient cohort. The observation that the T allele of CD300f rs2034310 SNP confers protection against MDD in humans has several important implications. The mechanism by which this protection occurs implies a dominant effect, as only one T allele is needed in heterozygosis. The C/T exchange produces a nonsynonymous substitution of arginine to glutamine in the cytoplasmic tail of the receptor and we show here that this alters the physiological signaling of CD300f mediated by PKCδ phosphorylation. Additional studies are needed to further understand the functional implications of this substitution.

CD300f and the Modulation of Neurotransmission. The most widely accepted hypothesis for the etiology of MDD at the neurochemical level is dysfunctional monoaminergic neurotransmission, mainly of serotonin, in several brain regions of MDD patients. However, clinical and experimental observations show that this constitutes a reductionist view, and that a more complex view includes alterations in other neurotransmitters (e.g., noradrenaline and dopamine), in neurotrophic factors (e.g., brain-derived neurotrophic factor), neurogenesis, and the hypothalamic–pituitary–adrenal axis (60). Our results show that the CD300f$^{-/-}$ female mice have reduced hippocampal noradrenaline content, but not of dopamine or serotonin. When the neurons of the locus coeruleus, the main source of noradrenergic neurons in the brain, are activated by an arousal or a novelty, noradrenaline is released in the hippocampus, and in accordance with the data observed here its activity is down-regulated in MDD (61). Interestingly, the administration of the antidepressant bupropion, which selectively inhibits the uptake of noradrenaline and dopamine, raising its extracellular levels at the synapses, reversed the anhedonic behavior of the CD300f$^{-/-}$ female mice. In humans, chronic treatment with antidepressants was shown to reduce binding of the TSPO PET ligand [18F]FEPPA in the brains of MDD patients, likely reflecting decreased microglial and perivascular macrophage reactivity or cell number (2) and associating microglial phenotype with antidepressant action.

Deficiency in microglial receptors such as CX3CR1 (15) and TREM2 (62) cause alterations in synaptic transmission and social behavior. Interestingly, the inhibition of the endogenous CD300f in mixed hippocampal cultures modulated synaptic strength and synaptogenesis. One of the main functions of CD300f as an activating receptor is to enhance macrophage efferocytosis by phosphatidylserine ligation in apoptotic cells, contributing to tissue clearance and resolution of inflammatory processes (26). This mechanism of phagocytosis could potentially also be used for the engulfment of dendritic spines or axonal terminals (63), which would result in the observed increased number of synapses following inhibition of CD300f. In addition, microglial CD300f could also bind the phospholipids of the ApoE lipoprotein (64) and prune synapses by this mechanism. In favor of this hypothesis, we show that the mechanism of the modulation of synaptic strength and number is both contact- and glial-dependent. Alternatively, CD300f may modulate microglial immunometabolic reprogramming and indirectly modulate phagocytosis and synaptic pruning. In line with this hypothesis, it has been shown that alterations in cerebral metabolism in MDD patients is more frequent in women

than in men (65), and creatine, a metabolic stimulator, has antidepressive effects in female (but not male) rats (66) and in women (67). Interestingly, a recent report shows that the knockout of TREM2 or PGRN, two mainly microglial genes, can modulate whole-brain metabolism (68), suggesting that the CD300f knockout may lead to widespread brain metabolic alterations.

CD300f and the Regulation of the Microglial Phenotype. A recent report includes CD300f in the list of genes putatively constituting the microglial reactome, a group of microglial genes coregulated in response to several classical neuroinflammatory triggers such as LPS, kainic acid-induced status epilepticus, and the presymptomatic superoxide dismutase amyotrophic lateral sclerosis model (69). As described before (32), after an i.p. LPS injection in WT mice CD300f was up-regulated and among the most significant differentially expressed genes (37th of 5,866). We observed that the CD300f deficiency induces an increase in microglial number in the absence of major changes in microglial signature genes or dysregulation of DAM genes. This suggests that the mild changes in microglial phenotype observed here under naïve conditions, and associated with a psychiatric condition, may differ from the more stereotyped phenotype associated to neurodegenerative conditions. Although several studies analyzing the transcriptome of psychiatric conditions have been published (43), a microglial-specific transcriptome for MDD or other psychiatric conditions is still missing. Interestingly, the fact that only mild changes occur in the set of genes analyzed between WT and CD300f$^{-/-}$ animals is in line with the subtle changes in gene expression patterns observed in MDD patients when compared to ASD, SCZ, BP, or AAD (43). Accordingly, although very mild microglial transcriptomic changes were observed in TREM2$^{-/-}$ (30 to 40 genes) (18) or Hoxb8$^{-/-}$ animals (21 genes) (70), they display alterations in microglial synapse elimination and social interaction or in obsessive–compulsive behavior, respectively. A relevant question is when the cellular changes occur. The mild microglial transcriptomic changes observed in CD300f$^{-/-}$, TREM2$^{-/-}$, or Hoxb8$^{-/-}$ mice could be masking more dramatic changes occurring during development, as reported previously in other models of psychiatric disorder involving microglia (71).

In conclusion, we demonstrate a clear association between the CD300f immune receptor with MDD in women as well as depressive-like and anhedonic behaviors in female mice only. Our findings reinforce the notion that a significant amount of the genetic load, which influences the development of depression, may exert its function through microglia. Importantly, CD300f emerges as a central player in the metabolic reprogramming needed for microglial activation. Despite the high incidence in MDD, no effective treatments are available in many cases, and these discoveries could lead to the development of new pipelines for drugs targeting microglial cells, perivascular macrophages, and in particular CD300f immune receptor.

Methods

Animals. Adult (4 to 5 mo old) female or male C57BL/6 (Charles River) WT mice and CD300f$^{-/-}$ [Genentech (30)] mice were obtained from the SPF animal facility of Institut Pasteur de Montevideo-Uruguay. Animals were maintained under controlled environment (20 ± 1 °C, 12-h light/dark cycle, free access to food and water).

Cell Sorting of Microglia. Mice were deeply anesthetized with sodium pentobarbitone (100 mg/kg, i.p.) and perfused with ice-cold PBS to eliminate blood. Spinal cord or hippocampus was harvested and cut in small pieces and enzymatic digestion was performed for 30 min at 37 °C. The digested tissue was passed through a cell strainer (40 μm, Falcon; BD Bioscience Discovery Labware), and the cell suspension was centrifuged at 500 × *g* for 10 min at 4 °C. The supernatant was discarded and cells resuspended in 2 mM EDTA and 0.5% fetal bovine serum (FBS) in phosphate-buffered saline (PBS). Cells were incubated with anti-CD11b MicroBeads (1:10, 130-049-601; Miltenyi Biotec) for 15 min at 4 °C and then applied to a magnetic LS column (Miltenyi Biotec). Cells retained on the column were flushed and resuspended in appropriate buffer and incubated with CD11b-PECy7 (1:200; eBioscience) and CD45-PerCP (1:200; eBioscience) for 1 h at 4 °C. The final pellet was resuspended in PBS and 2% FBS and subjected to flow cytometry. The sorting was performed using a FACSARIA III (BD Bioscience) cell sorter. We obtained about 30,000 purified cells from hippocampus samples and about 230,000 purified cells from whole brain. Microglial cells were assessed on a flow cytometer (FACS Calibur; BD Biosciences) and only populations presenting >90% purity were used for gene expression analysis. Sorted cells were directly collected in RLT buffer (QIAGEN) and RNA extraction was performed immediately after cell sorting to avoid RNA degradation. For LPS-induced neuroinflammation, LPS (2 mg/kg) was injected intraperitoneally 16 h before the RNA harvesting.

Metabolic Rate and Mitochondrial Mass Measurements. Four-month-old CD300f$^{-/-}$ and WT female mice were intraperitoneally injected with a single injection of LPS at 2 mg/kg. Twenty-four hours after injection, mice were deeply anesthetized with sodium pentobarbital (Dolethal) and transcardially perfused with 60 mL of 0.9% NaCl in distilled water. Whole brains were obtained and maintained in DMEM (Thermo Fisher Scientific) at 4 °C. Cell suspensions from brains were obtained as described above for FACS. Cells were then magnetically labeled with CD11b microbeads (MACS Miltenyi) and loaded onto LS MACS columns (Miltenyi Biotec) following the recommended protocol. CD11b+ cells were plated in an XFp cell culture miniplate (Agilent) following the protocol for cells suspensions. Seahorse XF Base Medium (Agilent) supplemented with 1 mM pyruvate (Sigma-Aldrich), 2 mM glutamine (Sigma-Aldrich), and 25 mM glucose (Sigma-Aldrich) was used. A mixture of oligomycin (1 μM) and FCCP (1.5 μM) was loaded into the proper cartridge (Agilent). Measurements of extracellular acidification rate and oxygen consumption rate from live cells were performed using the Seahorse XFp Cell Energy Phenotype protocol in a XFp Analyzer (Agilent). Three measures were taken under basal conditions and five measures after addition of oligomycin and FCCP. Final values were normalized by the amount of DNA loaded in every well. Three mice per group were used.

RNA-Seq and Data Analysis. Library preparation and RNA-seq were performed by the Centro Nacional de Análisis Genómico Centre for Genomic Regulation following the SMARTseq2 protocol (72) with some modifications. Briefly, RNA was quantified using the Qubit RNA HS Assay Kit (Thermo Fisher Scientific) and the input material used for the initial complementary DNA (cDNA) synthesis varied in function of the available sample concentration (0.2 to 10 ng). Reverse transcription was performed using SuperScrpit II (Invitrogen) in the presence of oligo-dT30VN (1 μM; 5′-AAGCAGTGGTATCAACGCAGAGTACT30VN-3′), template-switching oligonucleotides (1 μM), and betaine (1 M). The cDNA was amplified using the KAPA Hifi Hotstart ReadyMix (Kappa Biosystems), 100 nM ISPCR primer (5′-AAGCAGTGGTATCAACGCAGAGT-3′), and 15 cycles of amplification. Following purification with Agencourt Ampure XP beads (1:1 ratio; Beckmann Coulter), product size distribution and quantity were assessed on a Bioanalyzer High Sensitivity DNA Kit (Agilent). The amplified cDNA (200 ng) was fragmented for 10 min at 55 °C using Nextera XT (Illumina) and amplified for 12 cycles with indexed Nextera PCR primers. The Nextera library was purified twice with Agencourt Ampure XP beads (0.8:1 ratio) and quantified again on a Bioanalyzer using a High Sensitivity DNA Kit.

The libraries were sequenced on HiSeq2500 (Illumina, Inc.) in paired-end mode with a read length of 2 × 76 bp using TruSeq SBS Kit v4 and Nextera XT Index Kit of 8 bp + 8 bp. We generated on average 45 million paired-end reads for each sample in a fraction of a sequencing v4 flow cell lane, following the manufacturer's protocol. Image analysis, base calling, and quality scoring of the run were processed using the manufacturer's software Real Time Analysis (RTA 1.18.66.3) and followed by generation of FASTQ sequence files by CASAVA. See *SI Appendix* for data analysis procedures. Gene expression data for the different performed comparison are shown in Dataset S1. Raw data from the RNA-seq experiment have been deposited in the NCBI Sequence Read Archive under accession no. PRJNA496060.

Behavioral Analysis. Adult female and male WT and CD300f$^{-/-}$ mice (4 to 5 mo old, 35 to 40 g) were used for behavior analysis. All behavior experiments were performed during the illuminated part of the cycle under conditions of dimly lit by a red lamp and low noise. Behavior was monitored and videotaped to be scored later by a blind trained observer. For LPS induced depression experiments, LPS (2 mg/kg) was injected intraperitoneally 24 h before the behavioral tests.

OFT. The OFT was performed in order to assess the locomotor activity of mice. The apparatus consisted of an acrylic white box measuring 40 cm × 60 cm × 50 cm high. The animals were exposed during 6 min to the arena and the total distance traveled was recorded and evaluated using the AnyMaze software. The arena was cleaned with 10% alcohol between animals in order to exclude possible clues.

TST. Mice were submitted to the TST, which is a moderately stressful inescapable situation and despair model, where they are suspended by the tail and the depressive-like behavior can be evaluated. The lack of attempts to escape the aversive situation is considered immobility. In order to perform the TST, mice were suspended by the tail above the floor by adhesive tape ∼1 cm by the tip of the tail and the immobility time (in seconds) was recorded and evaluated during 6 min.

FST. The FST is a model of behavioral despair generally used in the evaluation of antidepressant or depressant effects of compounds or manipulations. In this test each mouse was individually forced to swim in an open cylindrical container (10 cm diameter × 25 cm high) containing ∼19 cm deep of water at 25 ± 1 °C and the immobility time was recorded during 6 min. In this test, mobility is defined when mice executed vigorous movements in order to get out of the acute stressful situation. Small movements executed by the animals just to keep balance or to keep the head above the water were not considered mobility.

SST. In this test, a 10% sucrose solution was spread on the dorsal coat of the mice. This viscose solution dirties the animal and they initiate grooming behavior. After applying the sucrose solution, the animals were individually placed in glass recipients and taped during 5 min. The latency to start the first grooming and the total amount of grooming behavior were the parameters associated with motivational behavior and anhedonic and self-care behavior, respectively. The recipients were cleaned with 10% ethanol between animals to exclude possible olfactive clues. The treatment with bupropion (10 mg/kg intraperitoneal, generously donated by Gramón Bagó Laboratories) or vehicle (PBS) was performed 30 min prior to the sucrose splash test.

Clinical study. This included a cross-sectional population-based study comprising 1,110 subjects aged 18 to 35 y and enrolled in a study carried out in the city of Pelotas, Southern Brazil, between June 2011 and May 2013. Sample selection was performed by multistage clusters, considering a population of 97,000 individuals in the 495 census-based sectors in the city. To ensure the necessary sample inclusion, 82 census-based sectors were systematically drawn. After identification, participants received morning visits by trained researchers in order to collect sociodemographic and clinical information. Several variables such as ethnicity and the use of psychiatry medication were self-reported. Subjects were diagnosed with the MDD (current or past episode) using the structured diagnosis interview, the Mini International Neuropsychiatric Interview according to DSM-IV criteria (M.I.N.I. 5.0., Brazilian version/DSM-IV; Medical Outcome Systems, Inc.).

Study approval. Studies including animals were performed according to the guidelines of the Institut Pasteur de Montevideo Animal Care Committee (protocols 004-16 and 014-16) and following the guidelines of the European Commission on Animal Care and Uruguayan national law and ethical guidelines on animal care. The study including human patients was approved by the Ethics Committee of the Catholic University of Pelotas (2010/15) and all patients provided written informed consent to participate.

Statistics. Allelic frequencies were determined by gene counting, and departures from the Hardy–Weinberg equilibrium were verified using χ^2 tests. Comparisons of allelic and genotype frequencies between MDD patients and control subjects were evaluated using χ^2 tests. Sociodemographic characteristics according to diagnosis and genotype were analyzing by χ^2 tests. Continuous variables were evaluated using Student's *t* test, one-way ANOVA, or two-way ANOVA for repeated measures followed by Bonferroni's post hoc test, as appropriate. The magnitude of the association of different genotypes with MDD was estimated using OR tests with 95% CI, adjusting for age and ethnicity in logistic regression analysis. Bonferroni's correction was used to account for multiple comparisons. Statistical analyses were performed with the Statistical Program for Social Sciences (SPSS) statistical software version 20.0 and data were presented as mean ± SEM or percentage, considering $P < 0.05$ as statistically significant.

Data Availability. The raw data from RNA-seq are available in the NCBI Sequence Read Archive under accession no. SRA PRJNA496060 and in Dataset S1.

ACKNOWLEDGMENTS. This work was supported by grants from Fundació Marató TV3 (110533-110532), Catalunya, Spain; Comisión Sectorial de Investigación Científica, Uruguay; Programa de Desarrollo de las Ciencias Básicas, Uruguay; Fondo de Convergencia Estructural del MERCOSUR (COF 03/1111); Banco de Seguros del Estado, Uruguay; Spanish Ministry of Economy and Competitiveness (SAF2010-17851and SAF2013-48431-R); Red Española de Terapia Celular; Conselho Nacional de Desenvolvimento Científico e Tecnológico (CNPq); Coordenação de Aperfeiçoamento de Pessoal de Ensino Superior (CAPES); and Programa de Apoio a Núcleos de Excelência-Fundação de Amparo à Pesquisa do Estado do Rio Grande do Sul (08/2009 - Pronex 10/0055-0). Gramón Bagó Laboratories (Uruguay) donated the bupropion. R.A.S., D.R.L., K.J., L.M.S., and M.P.K. are CNPq Research Fellows. F.N.K. received a fellowship from CAPES and support from International Brain Research Organization and International Society for Neurochemistry. We thank all members of the transgenic animal unit (UATE) and of the Cell Biology Unit (especially Paula Céspedes) of the Institut Pasteur de Montevideo for assistance and Iris Castillo, Bruno Borrelli, and Camila Julian.

1. R. Yirmiya, N. Rimmerman, R. Reshef, Depression as a microglial disease. *Trends Neurosci.* **38**, 637–658 (2015).
2. E. Setiawan *et al.*, Association of translocator protein total distribution volume with duration of untreated major depressive disorder: A cross-sectional study. *Lancet Psychiatry* **5**, 339–347 (2018).
3. M. Maes *et al.*, Increased serum IL-6 and IL-1 receptor antagonist concentrations in major depression and treatment resistant depression. *Cytokine* **9**, 853–858 (1997).
4. C. A. Köhler *et al.*, Peripheral cytokine and chemokine alterations in depression: A meta-analysis of 82 studies. *Acta Psychiatr. Scand.* **135**, 373–387 (2017).
5. H. Keren-Shaul *et al.*, A unique microglia type associated with restricting development of Alzheimer's disease. *Cell* **169**, 1276–1290.e17 (2017).
6. S. Krasemann *et al.*, The TREM2-APOE pathway drives the transcriptional phenotype of dysfunctional microglia in neurodegenerative diseases. *Immunity* **47**, 566–581.e9 (2017).
7. K. Grabert *et al.*, Microglial brain region-dependent diversity and selective regional sensitivities to aging. *Nat. Neurosci.* **19**, 504–516 (2016).
8. S. E. Hickman *et al.*, The microglial sensome revealed by direct RNA sequencing. *Nat. Neurosci.* **16**, 1896–1905 (2013).
9. A. Crotti, R. M. Ransohoff, Microglial physiology and pathophysiology: Insights from genome-wide transcriptional profiling. *Immunity* **44**, 505–515 (2016).
10. O. Butovsky *et al.*, Identification of a unique TGF-β-dependent molecular and functional signature in microglia. *Nat. Neurosci.* **17**, 131–143 (2014).
11. T. K. Ulland *et al.*, TREM2 maintains microglial metabolic fitness in Alzheimer's disease. *Cell* **170**, 649–663.e13 (2017).
12. R. M. Ransohoff, A. E. Cardona, The myeloid cells of the central nervous system parenchyma. *Nature* **468**, 253–262 (2010).
13. A. Deczkowska, I. Amit, M. Schwartz, Microglial immune checkpoint mechanisms. *Nat. Neurosci.* **21**, 779–786 (2018).
14. F. Filipello *et al.*, The microglial innate immune receptor TREM2 is required for synapse elimination and normal brain connectivity. *Immunity* **48**, 979–991.e8 (2018).
15. Y. Zhan *et al.*, Deficient neuron-microglia signaling results in impaired functional brain connectivity and social behavior. *Nat. Neurosci.* **17**, 400–406 (2014).
16. A. W. Corona *et al.*, Fractalkine receptor (CX3CR1) deficiency sensitizes mice to the behavioral changes induced by lipopolysaccharide. *J. Neuroinflammation* **7**, 93 (2010).
17. S. C. Choi *et al.*, Cutting edge: Mouse CD300f (CMRF-35-like molecule-1) recognizes outer membrane-exposed phosphatidylserine and can promote phagocytosis. *J. Immunol.* **187**, 3483–3487 (2011).
18. Y. Wang *et al.*, TREM2 lipid sensing sustains the microglial response in an Alzheimer's disease model. *Cell* **160**, 1061–1071 (2015).
19. K. Izawa *et al.*, Sphingomyelin and ceramide are physiological ligands for human LMIR3/CD300f, inhibiting FcεRI-mediated mast cell activation. *J. Allergy Clin. Immunol.* **133**, 270–3.e1-7 (2014).
20. K. Izawa *et al.*, The receptor LMIR3 negatively regulates mast cell activation and allergic responses by binding to extracellular ceramide. *Immunity* **37**, 827–839 (2012).
21. A. Martínez-Barriocanal, E. Comas-Casellas, S. Schwartz, Jr, M. Martín, J. Sayós, CD300 heterocomplexes, a new and family-restricted mechanism for myeloid cell signaling regulation. *J. Biol. Chem.* **285**, 41781–41794 (2010).
22. D. Alvarez-Errico *et al.*, IREM-1 is a novel inhibitory receptor expressed by myeloid cells. *Eur. J. Immunol.* **34**, 3690–3701 (2004).
23. D. Alvarez-Errico, J. Sayós, M. López-Botet, The IREM-1 (CD300f) inhibitory receptor associates with the p85alpha subunit of phosphoinositide 3-kinase. *J. Immunol.* **178**, 808–816 (2007).
24. K. Izawa *et al.*, An activating and inhibitory signal from an inhibitory receptor LMIR3/CLM-1: LMIR3 augments lipopolysaccharide response through association with FcRgamma in mast cells. *J. Immunol.* **183**, 925–936 (2009).
25. I. Moshkovits *et al.*, CD300f associates with IL-4 receptor and amplifies IL-4-induced immune cell responses. *Proc. Natl. Acad. Sci. U.S.A.* **112**, 8708–8713 (2015).
26. L. Tian *et al.*, p85α recruitment by the CD300f phosphatidylserine receptor mediates apoptotic cell clearance required for autoimmunity suppression. *Nat. Commun.* **5**, 3146 (2014).
27. T. Matsukawa *et al.*, Ceramide-CD300f binding suppresses experimental colitis by inhibiting ATP-mediated mast cell activation. *Gut* **65**, 777–787 (2016).

28. J. S. Danik *et al*., Novel loci, including those related to crohn disease, psoriasis, and inflammation, identified in a genome-wide association study of fibrinogen in 17 686 women: The women's genome health study. *Circ. Cardiovasc. Genet.* **2**, 134–141 (2009).
29. M. Ban *et al*., A non-synonymous SNP within membrane metalloendopeptidase-like 1 (MMEL1) is associated with multiple sclerosis. *Genes Immun.* **11**, 660–664 (2010).
30. H. Xi *et al*., Negative regulation of autoimmune demyelination by the inhibitory receptor CLM-1. *J. Exp. Med.* **207**, 7–16 (2010).
31. A. F. Lloyd *et al*., Central nervous system regeneration is driven by microglia necroptosis and repopulation. *Nat. Neurosci.* **22**, 1046–1052 (2019).
32. M. L. Bennett *et al*., New tools for studying microglia in the mouse and human CNS. *Proc. Natl. Acad. Sci. U.S.A.* **113**, E1738–E1746 (2016).
33. A. Torres-Espín, J. Hernández, X. Navarro, Gene expression changes in the injured spinal cord following transplantation of mesenchymal stem cells or olfactory ensheathing cells. *PLoS One* **8**, e76141 (2013).
34. C. Ising *et al*., NLRP3 inflammasome activation drives tau pathology. *Nature* **575**, 669–673 (2019).
35. L. Tian *et al*., Enhanced efferocytosis by dendritic cells underlies memory T-cell expansion and susceptibility to autoimmune disease in CD300f-deficient mice. *Cell Death Differ.* **23**, 1086–1096 (2016).
36. F. N. Kaufmann *et al*., NLRP3 inflammasome-driven pathways in depression: Clinical and preclinical findings. *Brain Behav. Immun.* **64**, 367–383 (2017).
37. H. M. Kamens, T. J. Phillips, S. E. Holstein, J. C. Crabbe, Characterization of the parallel rod floor apparatus to test motor incoordination in mice. *Genes Brain Behav.* **4**, 253–266 (2005).
38. H. Peluffo *et al*., Overexpression of the immunoreceptor CD300f has a neuroprotective role in a model of acute brain injury. *Brain Pathol.* **22**, 318–328 (2012).
39. A. Ejarque-Ortiz *et al*., The receptor CMRF35-like molecule-1 (CLM-1) enhances the production of LPS-induced pro-inflammatory mediators during microglial activation. *PLoS One* **10**, e0123928 (2015).
40. Y. Zhang *et al*., An RNA-sequencing transcriptome and splicing database of glia, neurons, and vascular cells of the cerebral cortex. *J. Neurosci.* **34**, 11929–11947 (2014).
41. B. Kadriu *et al*., Acute ketamine administration corrects abnormal inflammatory bone markers in major depressive disorder. *Mol. Psychiatry* **23**, 1626–1631 (2018).
42. R. M. Hoek *et al*., Down-regulation of the macrophage lineage through interaction with OX2 (CD200). *Science* **290**, 1768–1771 (2000).
43. M. J. Gandal *et al*., Shared molecular neuropathology across major psychiatric disorders parallels polygenic overlap. **697**, 693–697 (2018).
44. A. Zeisel *et al*., Brain structure. Cell types in the mouse cortex and hippocampus revealed by single-cell RNA-seq. *Science* **347**, 1138–1142 (2015).
45. L. A. J. O'Neill, E. J. Pearce, Immunometabolism governs dendritic cell and macrophage function. *J. Exp. Med.* **213**, 15–23 (2016).
46. M. Liu *et al*., Metabolic rewiring of macrophages by CpG potentiates clearance of cancer cells and overcomes tumor-expressed CD47-mediated 'don't-eat-me' signal. *Nat. Immunol.* **20**, 265–275 (2019).
47. B. Stevens *et al*., The classical complement cascade mediates CNS synapse elimination. *Cell* **131**, 1164–1178 (2007).
48. N. R. Wilson *et al*., Presynaptic regulation of quantal size by the vesicular glutamate transporter VGLUT1. *J. Neurosci.* **25**, 6221–6234 (2005).
49. K. Nakayama, K. Kiyosue, T. Taguchi, Diminished neuronal activity increases neuron-neuron connectivity underlying silent synapse formation and the rapid conversion of silent to functional synapses. *J. Neurosci.* **25**, 4040–4051 (2005).
50. P. Willner, J. Scheel-Krüger, C. Belzung, The neurobiology of depression and antidepressant action. *Neurosci. Biobehav. Rev.* **37**, 2331–2371 (2013).
51. R. Dantzer, J. C. O'Connor, G. G. Freund, R. W. Johnson, K. W. Kelley, From inflammation to sickness and depression: When the immune system subjugates the brain. *Nat. Rev. Neurosci.* **9**, 46–56 (2008).
52. P. P. Katz, E. H. Yelin, Prevalence and correlates of depressive symptoms among persons with rheumatoid arthritis. *J. Rheumatol.* **20**, 790–796 (1993).
53. L. Capuron, A. Ravaud, R. Dantzer, Early depressive symptoms in cancer patients receiving interleukin 2 and/or interferon alfa-2b therapy. *J. Clin. Oncol.* **18**, 2143–2151 (2000).
54. A. Deczkowska *et al*., Disease-associated microglia: A universal immune sensor of neurodegeneration. *Cell* **173**, 1073–1081 (2018).
55. T. Franklin *et al*., Depression and sterile inflammation: Essential role of danger associated molecular patterns. *Brain Behav. Immun.* **72**, 2–13 (2018).
56. T. P. Schnieder *et al*., Microglia of prefrontal white matter in suicide. *J. Neuropathol. Exp. Neurol.* **73**, 880–890 (2014).
57. S. G. Torres-Platas, C. Cruceanu, G. G. Chen, G. Turecki, N. Mechawar, Evidence for increased microglial priming and macrophage recruitment in the dorsal anterior cingulate white matter of depressed suicides. *Brain Behav. Immun.* **42**, 50–59 (2014).
58. M. L. Estes, A. K. Mcallister, Alterations in immune cells and mediators in the brain: It's not always neuroinflammation! *Brain Pathol.* **24**, 623–630 (2014).
59. World Health Organization, "Depression and other common mental disorders: Global health estimates" (World Health Organization,Geneva, 2017).
60. I. Mahar, F. R. Bambico, N. Mechawar, J. N. Nobrega, Stress, serotonin, and hippocampal neurogenesis in relation to depression and antidepressant effects. *Neurosci. Biobehav. Rev.* **38**, 173–192 (2014).
61. C. Moret, M. Briley, The importance of norepinephrine in depression. *Neuropsychiatr. Dis. Treat.* **7** (suppl. 1), 9–13 (2011).
62. F. Filipello *et al*., The microglial innate immune receptor TREM2 is required for synapse elimination and normal brain connectivity. *Immunity* **48**, 979–991.e8 (2018).
63. B. A. Györffy *et al*., Local apoptotic-like mechanisms underlie complement- mediated synaptic pruning. *Proc. Natl. Acad. Sci. U.S.A.* **115**, 6303–6308 (2018).
64. W. Chung *et al*., Novel allele-dependent role for APOE in controlling the rate of synapse pruning by astrocytes. *Proc. Natl. Acad. Sci. U.S.A.* **113**, 10186–10191 (2016).
65. P. F. Renshaw *et al*., Multinuclear magnetic resonance spectroscopy studies of brain purines in major depression. *Am. J. Psychiatry* **158**, 2048–2055 (2001).
66. P. J. Allen, K. E. D. Anci, R. B. Kanarek, P. F. Renshaw, Chronic creatine supplementation alters depression-like behavior in rodents in a sex-dependent manner. *Neuropsychopharmacology* **35**, 534–546 (2010).
67. I. K. Lyoo *et al*., A randomized, double-blind placebo-controlled trial of oral creatine monohydrate augmentation for enhanced response to a selective serotonin reuptake inhibitor in women with major depressive disorder. *Am. J. Psychiatry* **169**, 937–945 (2012).
68. J. K. Götzl *et al*., Opposite microglial activation stages upon loss of PGRN or TREM 2 result in reduced cerebral glucose metabolism. *EMBO Mol. Med.* **11**, e9711 (2019).
69. H. Hirbec *et al*., The microglial reaction signature revealed by RNAseq from individual mice. *Glia* **66**, 971–986 (2018).
70. S. De, *et al*., Two distinct ontogenies confer heterogeneity to mouse brain microglia. *Development* **145**, dev152306 (2018).
71. O. Matcovitch-Natan *et al*., Microglia development follows a stepwise program to regulate brain homeostasis. *Science* **353**, aad8670 (2016).
72. S. Picelli *et al*., Smart-seq2 for sensitive full-length transcriptome profiling in single cells. *Nat. Methods* **10**, 1096–1098 (2013).

Brain, Behavior, & Immunity - Health 11 (2021) 100191

Contents lists available at ScienceDirect

Brain, Behavior, & Immunity - Health

journal homepage: www.editorialmanager.com/bbih/default.aspx

Full Length Article

Sex-dependent role of CD300f immune receptor in generalized anxiety disorder

Fernanda N. Kaufmann [a], Natalia Lago [b], Daniela Alí-Ruiz [b], Karen Jansen [c], Luciano D.M. Souza [c], Ricardo A. Silva [c], Diogo R. Lara [d], Gabriele Ghisleni [c], Hugo Peluffo [b,e], Manuella P. Kaster [f,*]

[a] Department of Psychiatry and Neuroscience, Faculty of Medicine and CERVO Brain Research Center, Université Laval, Quebec City, Canada
[b] Neuroinflammation and Gene Therapy Laboratory, Institut Pasteur de Montevideo, Montevideo, Uruguay
[c] Department of Life and Health Sciences, Catholic University of Pelotas, Rio Grande do Sul, Brazil
[d] Department of Cellular and Molecular Biology, Pontifical Catholic University of Rio Grande do Sul, Porto Alegre, Brazil
[e] Departamento de Histología y Embriología, Facultad de Medicina, Universidad de la República, Montevideo, Uruguay
[f] Department of Biochemistry, Federal University of Santa Catarina, Florianópolis, Santa Catarina, Brazil

ARTICLE INFO

Keywords:
Generalized anxiety disorder
Immune system
CD300f receptors
Polymorphism

ABSTRACT

Generalized Anxiety Disorder (GAD) presents a high prevalence in the population, leading to distress and disability. Immune system alterations have been associated with anxiety-related behaviors in rodents and GAD patients. CD300f immune receptors are highly expressed in microglia and participate not only in the modulation of immune responses but also in pruning and reshaping synapses. It was recently demonstrated that CD300f might be influential in the pathogenesis of depression in a sex-dependent manner. Here, we evaluated the role of CD300f immune receptor in anxiety, using CD300f knockout mice (CD300f−/−) and patients with GAD. We observed that male CD300f−/− mice had numerous behavioral changes associated with a low-anxiety phenotype, including increased open field central locomotion and rearing behaviors, more exploration in the open arms of the elevated plus-maze test, and decreased latency to eat in the novelty suppressed feeding test. In a cross-sectional population-based study, including 1111 subjects, we evaluated a common single-nucleotide polymorphism rs2034310 (C/T) in the cytoplasmatic tail of CD300f gene in individuals with GAD. Notably, we observed that the T allele of the rs2034310 polymorphism conferred protection against GAD in men, even after adjusting for confounding variables. Overall, our data demonstrate that CD300f immune receptors are involved in the modulation of pathological anxiety behaviors in a sex-dependent manner. The biological basis of these sex differences is still poorly understood, but it may provide significant clues regarding the neuropathophysiological mechanisms of GAD and can pave the way for future specific pharmacological interventions.

1. Introduction

Anxiety disorders comprise a heterogeneous spectrum of conditions in which Generalized Anxiety Disorder (GAD) is the most widespread mental health condition (American Psychiatric Association, 2013; DSM-5). The12-month prevalence of GAD is 3.9% (2.1-6.6%), and the lifetime prevalence is estimated to be 12% (8-13.7%) (Murray et al., 2012; Haller et al., 2014). The features of GAD are persistent and excessive worrying, anxiety and tension, allied to somatic symptoms and hypervigilance, for six months or more, that leads to significant distress and disability (Wittchen, 2002).

Anxiety disorders aggregate in families and heritability ranges from 30 to 60% complemented by a combination of environmental factors that shape risk and resilience (Polderman et al., 2015; Craske et al., 2017). Moreover, GAD is twice as prevalent in women, with more disability and worse outcomes (Rubio and López-Ibor, 2007; Vesga-López et al., 2008). On the other hand, men are more likely to have GAD with a comorbid substance use disorder (Rubio and López-Ibor, 2007; Vesga-López et al., 2008). The biological basis of these differences is still poorly understood, but they might be the result of different neuropathophysiological mechanisms and specific etiological factors across sex, including genetic variability, physiological and hormonal differences, and changes in stress responses (Vesga-López et al., 2008).

Immune alterations are frequently observed in GAD patients (Vieira

* Corresponding author.
E-mail addresses: manuella.kaster@ufsc.br, manu.kaster@gmail.com (M.P. Kaster).

https://doi.org/10.1016/j.bbih.2020.100191
Received 5 September 2020; Received in revised form 1 December 2020; Accepted 3 December 2020
Available online 14 December 2020

et al., 2010; Copeland et al., 2012; Costello et al., 2019). Notably, genome-wide expression profiles of a community sample identified 631 differentially expressed genes in blood cells of men with GAD, but not women, compared to control individuals. Of these, 123 genes with altered expression were involved in immune responses (Wingo and Gibson, 2015). In mice submitted to psychosocial stress, anxiety occurs in parallel with microglial activation and endothelial dysfunction, leading to monocyte recruitment to the brain (McKim et al., 2018). The immune dysregulation can impact essential brain functions, including neurotransmitter metabolism, cell communication, and synaptic plasticity, as well as the neural circuitry controlling anxiety and emotional regulation (Capuron and Miller, 2011).

The CD300f immunoreceptors (or CLM-1, in rodents) are expressed in peripheral immune cells and in the central nervous system (CNS), especially in microglia and perivascular macrophages (Clark et al., 2009). Activation of CD300f receptors leads to the inhibition of inflammatory process (Keswani et al., 2020; Shiba et al., 2017; Matsukawa et al., 2015) and has neuroprotective properties in diseases related to neurodegeneration and inflammation such as autoimmune encephalomyelitis and excitotoxic brain injury (Martínez-Barriocanal et al., 2017; Zaqueu Lima et al., 2017., Peluffo et al., 2015). Recently, it was reported that CD300f might be influential in the pathogenesis of depression in humans in a sex-dependent manner (Lago-Kaufmann et al., 2020). Here, we explored the involvement of the CD300f immunoreceptor in behavioral paradigms used to evaluate anxiety in rodents. Furthermore, we took advantage of specific single nucleotide polymorphism in the CD300f gene that modifies the receptor phosphorylation and intracellular signaling (Lago-Kaufmann., 2020) to understand the role of these receptors in emotional modulation in humans.

2. Methods

2.1. Behavioral analysis in rodents

Male and female C57/BL6 (originally from The Jackson Laboratory) and global CD300f knockout (CD300f−/− in C57/BL6 background, Xi et al., 2010) mice (4-5-months-old) were obtained from the SPF animal facility of the Institute Pasteur de Montevideo-Uruguay. Animals were housed under a controlled environment (20 ± 1 °C, 12 h-light/dark cycle, free access to food and water). All behavioral analyses were videotaped and scored using the Any Maze software. Mice were handled according to the guidelines of the Institut Pasteur de Montevideo Animal Care Committee (protocols #004-16 and #014-16) and following the guidelines of the European Commission on Animal Care and Uruguayan national law and ethical guidelines on animal care.

2.1.1. Open field test

The apparatus consisted of an acrylic box (40 cm × 60 cm x 50 cm). For the evaluation of exploratory behavior and locomotion, the animals were exposed during 6 min to the arena, and the total distance traveled, time spent in the periphery and in the center of the arena, as well as the number of supported and unsupported rears, and the amount of grooming was recorded (Lago-Kaufmann et al., 2020).

2.1.2. Elevated Plus Maze test

The Elevated Plus Maze (EPM) test was used to assess anxiety status (Lister, 1987). The apparatus consisted of a central square platform (6 × 6 cm) and two open arms (30 × 6 cm) aligned perpendicularly to two closed arms (30 × 6 × 16 cm) and elevated 50 cm above the floor. Mice were individually placed in the central platform and recorded for 5 min. The relative time spent in closed versus opened arms is a measure of anxiety. The number of closed arm entries was used as a measure of spontaneous locomotion.

2.1.3. Novelty suppressed feeding test

The Novelty Suppressed Feeding Test (NSF) measures the latency of mice in approaching and eating food in a new environment following an extended period (18 h) of food deprivation and longer latencies in each parameter considered indicative of anxiety-like behavior. After 18 h of food deprivation, mice were placed in an acrylic box (40 cm × 60 cm x 50 cm) for 10 min with a small piece of mouse chow placed in the center. Immediately after the mouse began to eat the chow, the test ended, and those mice that did not eat within 10 min were considered as zero (Samuels and Hen, 2011).

2.2. Clinical study

2.2.1. Study design and participants

Our sample was derived from a cross-sectional population-based study, including 1111 subjects aged 18–35 years old carried out in the city of Pelotas, Southern Brazil, between June 2011 and May 2013 (Lago-Kaufmann et al., 2020). Sociodemographic and clinical variables were self-reported. Body mass index (BMI) was calculated by the equation: weight (kg)/height (m^2). GAD diagnosis was performed using the structured diagnosis interview, the Brazilian version of the Mini International Neuropsychiatric Interview (MINI 5.0), according to DSM-5 criteria (Medical Outcome Systems Inc., Jacksonville, FL, USA). The study was approved by the University's Ethics Committee (2010/15), and all patients provided written informed consent.

2.2.2. Blood sample collection and genotyping

Ten milliliters of blood were withdrawn (8:00-11:00 a.m.) by venipuncture after the interview. Blood samples were centrifuged (3500 g, at room temperature) for the separation of the leukocytes enriched fraction, and the DNA extraction was performed using a standardized salting-out procedure (Lahiri and Nurnberger, 1991). CD300f rs2034310 (C/T) single nucleotide polymorphism (SNP) has a minor allele frequency of 0.1725 in the European population (http://www.ncbi.nlm.nih.gov/projects/SNP/). Genotyping was performed using forward and reverse primers and probes contained in the 40× Human Custom TaqMan Genotyping Assay (Life Technologies, Foster City, CA, USA). The reactions were carried out using 2 ng of genomic DNA from each subject, TaqMan Genotyping Master Mix 1× (Applied Biosystems), and Custom TaqMan Genotyping Assay 1× in a real-time PCR thermal cycler (7500 Fast Real PCR System; Applied Biosystems), as previously described (Lago-Kaufmann et al., 2020). Fluorescence data files were analyzed using automated allele-calling software (SDS 2.0.1; Applied Biosystems).

2.3. Statistical analysis

Differences between wild-type (WT) and CD300f−/− mice were determined by unpaired Students' t-test using Graph Pad Prism 6.0 (GraphPad Software Inc., San Diego, USA). The Kolmogorov-Smirnov test assessed data normality, and outlier values were identified using Grubbs' test. Data are presented as mean ± SEM. Human data were analyzed by SPSS 22.0 (IBM Corporation, Armonk, NY). Variables are presented as number and percentage (%), or mean and standard deviation (SD). The sociodemographic characteristics, according to the genotypes, were compared using Chi-squared or One-Way ANOVA followed by Bonferroni's *post-hoc* test. The allele and genotype frequencies were evaluated by direct counting, and the Hardy-Weinberg equilibrium was calculated using the Chi-squared test. The magnitude of the association between different genotypes and GAD was estimated using odds ratio (OR) with 95% confidence intervals (CI), adjusted for age, sex, and ethnicity in the logistic regression analysis. Bonferroni's correction was used to account for multiple comparisons. $p < 0.05$ was considered significant.

3. Results

3.1. Anxiety-related behaviors in CD300f−/− male mice

We performed the open field test (OFT) to evaluate locomotion and

anxious-like behavior in male WT and CD300−/− mice. No differences in the spontaneous locomotor activity were observed in WT and CD300f−/− mice [t(31) = 1.45, p = 0.157], Fig. 1A. However, as observed in Fig. 1B, CD300f−/− mice spent more time in the center of the OFT [t(30) = 3.22, p = 0.003], which indicates a reduction in anxiety-like behavior. To confirm this hypothesis, we further evaluated other parameters that could indicate less anxiety in a new environment. CD300f−/− male mice presented a higher number of rearing episodes in the OFT compared to WT mice [t(11) = 3.25, p = 0.007, Fig. 1C]. Moreover, rearing behavior can be distinguished between supported rearing, which is related to locomotion and activity and unsupported rearing, related to emotional states (Sturman et al., 2018). In our study, we have noticed that CD300f−/− do not show any changes in supported rearing [t(11) = 0.32, p = 0.758, Supplementary Fig. 1A], but presented a tendency to increased unsupported rearing compared to WT mice [t(11) = 2.01, p = 0.069, Fig. 1D]. Studies have demonstrated that grooming behavior is increased when the animal is habituated to the new environment (Rojas-Carvajal et al., 2018). Here, no differences were observed between CD300f−/− and WT mice in the latency to start grooming [t(10) = 0.44, p = 0.672, Supplementary Fig 1B] or in total time of grooming behavior [t(11) = 0.00, p > 0.999, Fig. 1E]. Defecation in the OFT is another important sign of anxiety. We observed that 66,7% of WT mice defecated in the OFT against 20.0% of CD300f−/− (Supplementary Fig 1C). Additionally, 27.3% of CD300f−/− jumped attempting to escape from the OFT while no WT presented such behavior (Supplementary Fig 1D).

To further confirm the reduction in anxiety-related behaviors in male CD300f−/− mice, we used the EPM, which is the gold standard test to assess avoidance and anxiety (Biedermann et al., 2017). The analysis showed that CD300f−/− male mice had increased entries [t(15) = 2.55, p = 0.022, Supplementary Fig 1E] and spent more time in the open arms [t(15) = 2.18, p = 0.045, Fig. 1F, and heatmaps in 1.G] and decreased

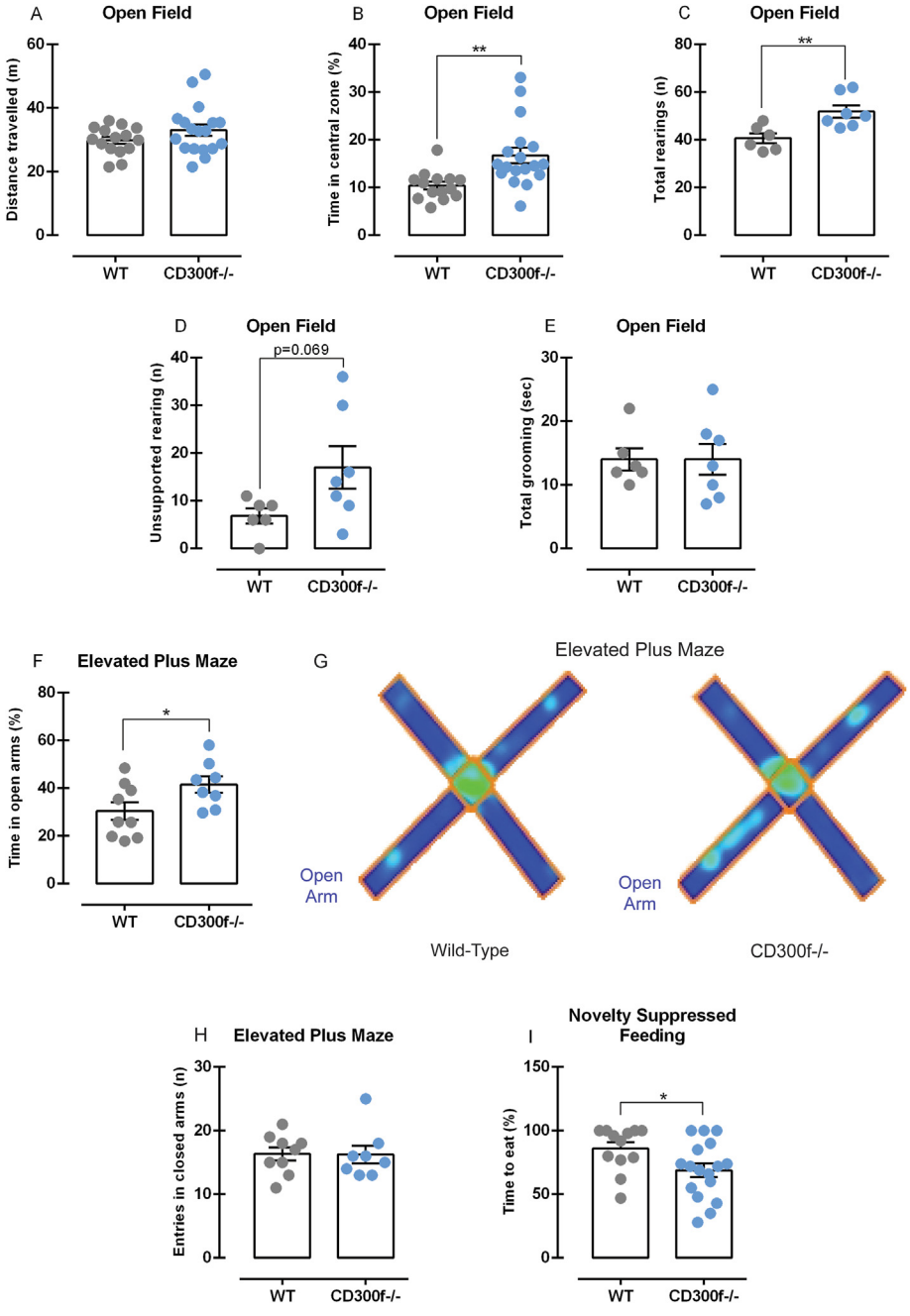

Fig. 1. Anxiety-related behaviors of CD300f−/− male mice in different behavioral contexts. The total distance traveled in the OF was measured (meters) to evaluate mice spontaneous ambulatory activity (n = 15 WT and 18 CD300f−/−, 1.A), and the % of time spent in the center of the OF was used to evaluate anxious-like behavior (n = 14 WT and 18 CD300f−/−, 1.B). The total rearing (n = 6 WT and 7 CD300f−/−, 1.C) and the number of unsupported (n = 6 WT and 7 CD300f−/−, 1.D) rearing were counted to evaluate explorative behavior and emotionality. Grooming behavior was recorded (seconds) to evaluate mice habituation to a new environment (n = 6 WT and 7 CD300f−/−, 1.E). The % of time spent in the open arms of the EPM (calculated using the total time in the open arms + the total time in the closed arms as 100%) was indicative of anxiety-like behavior (n = 9 WT and 8 CD300f−/−, 1.F). Heatmaps illustrating WT and CD300f−/− mice behavior in the EPM, respectively (1.G). The number of entries in the closed arms of the EPM was indicative of spontaneous locomotion (n = 9 WT and 8 CD300f−/−, 1.H). The latency to start eating in the NSF test was used as an indicative of anxious-like behavior in a new environment (n = 12 WT and 17 CD300f−/−, 1.I). Data are represented as mean ± S.E.M. * represents $p < 0.05$, and ** represents $p < 0.01$ compared to WT. *Abbreviations: OF: Open Field; EPM: Elevated Plus Maze; NSF: Novelty Suppressed Feeding; WT: Wild-type mouse; CD300f−/−: CD300f knockout mouse.*

time in the closed arms [t(15) = 2.18, p = 0.045, Supplementary Fig. 1F] when compared to WT, while no differences were observed in the number of entries in the closed arms [t(15) = 0.04, p = 0.962, Fig. 1H]. Next, we assessed behavior in a new environment in a fasting-state using the NSF test. CD300f−/− mice had a decreased latency to eat compared to WT mice [t(27) = 2.22, p = 0.035, Fig. 1I], but no differences were observed in the time to approach the food pellet [t(26) = 0.37, p = 0.714, Supplementary Fig 1G]. Altogether, these results demonstrate that, when placed in a new environment, CD300f−/− mice present lower anxiety-like behaviors, better habituation, and better emotional state in different behavioral paradigms compared to WT mice.

3.2. Anxiety-related behaviors in CD300f−/− female mice

As CD300f has been previously related to major depressive disorder and depression-like behaviors only in females, we explored whether the anxiolytic-like effect observed in CD300f−/− male mice was sex-dependent. Fig. 2 depicts the results of female mice in the OFT and EPM. Statistical analysis demonstrated no differences in the distance traveled [t(22) = 1.660, p = 0.111, Fig. 2A], time spent in the central zone [t(22) = 1.18, p = 0.252, Fig. 2B] and number of entries in the central zone [t(22) = 0.09, p = 0.931, Fig. 2C] of the OFT when comparing WT and CD300−/− female mice. Moreover, we analyzed a separated cohort of female mice in the EPM test. No differences were observed in the number of entries in the open arms [t(12) = 1.16, p = 0.268, Fig. 2D) or in the time spent in the open arms [t(12) = 0.60, p = 0.557, Fig. 2E] or closed arms [t(12) = 0.60, p = 0.557, Fig. 2F] of the EPM when comparing CD300f−/− and WT female mice. These data reveal that female CD300f−/− mice do not display behavior alterations related to anxiety, only depressive-like behavior as previously described (Lago et al., 2020).

3.3. Association of CD300f SNP with GAD subjects in a sex-dependent manner

The non-synonymous rs2034310 (C/T) SNP in the cytoplasmic tail of CD300f has been shown to alter receptor signaling (Lago-Kaufmann et al., 2020). We evaluated the association of the SNP with GAD in a population-based study that comprised 1111 individuals, 938 (84.4%) control subjects, and 173 (15.6%) diagnosed with GAD. We found an increased prevalence of GAD in women (73.4%) when compared to men (26.6%), ($\chi2$ = 25.11, df = 1, p < 0.001), in individuals from the intermediate socioeconomic class ($\chi2$ = 18.71, df = 1, p < 0.001), making use of tobacco ($\chi2$ = 43.17, df = 1, p < 0.001) and making use of psychiatric medication ($\chi2$ = 35.00, df = 1, p < 0.001). In addition, an increased prevalence of clinical comorbidities (autoimmune, cardiovascular, metabolic, and infectious diseases) was observed in GAD patients ($\chi2$ = 19.69, df = 1, p < 0.001). No differences in the age [t(1107) = -1.94, p = 0.053], ethnicity ($\chi2$ = 0.61, df = 1, p = 0.433), and BMI [t(1065) = -0.72, p = 0.472] between controls and GAD patients were observed (Table 1).

When we analyzed the sociodemographic characteristics according to the rs2034310 (C/T) SNP genotypes, no differences were observed for age [F(2,1109) = 1.33, p = 0.265], gender ($\chi2$ = 0.29, df = 2, p = 0.861), socioeconomic class ($\chi2$ = 0.59, df = 4, p = 0.964), tobacco use ($\chi2$ = 1.60, df = 2, p = 0.448), BMI [F(2,1067) = 0.65, p = 0.524], psychiatric medication use ($\chi2$ = 1.21, df = 2, p = 0.547), or presence of clinical conditions (autoimmune, cardiovascular, metabolic and infectious diseases, $\chi2$ = 0.96, df = 2, p = 0.619) (Supplementary Table 1). Ethnicity was significantly associated with genotype ($\chi2$ = 16.86, df = 2, p < 0.001) and a higher frequency of the T allele was observed in non-Caucasian individuals. Additionally, the genotype frequencies agreed with those predicted by Hardy-Weinberg equilibrium for the rs2034310 (C/T) SNP ($\chi2$ = 0.03775, p = 0.846).

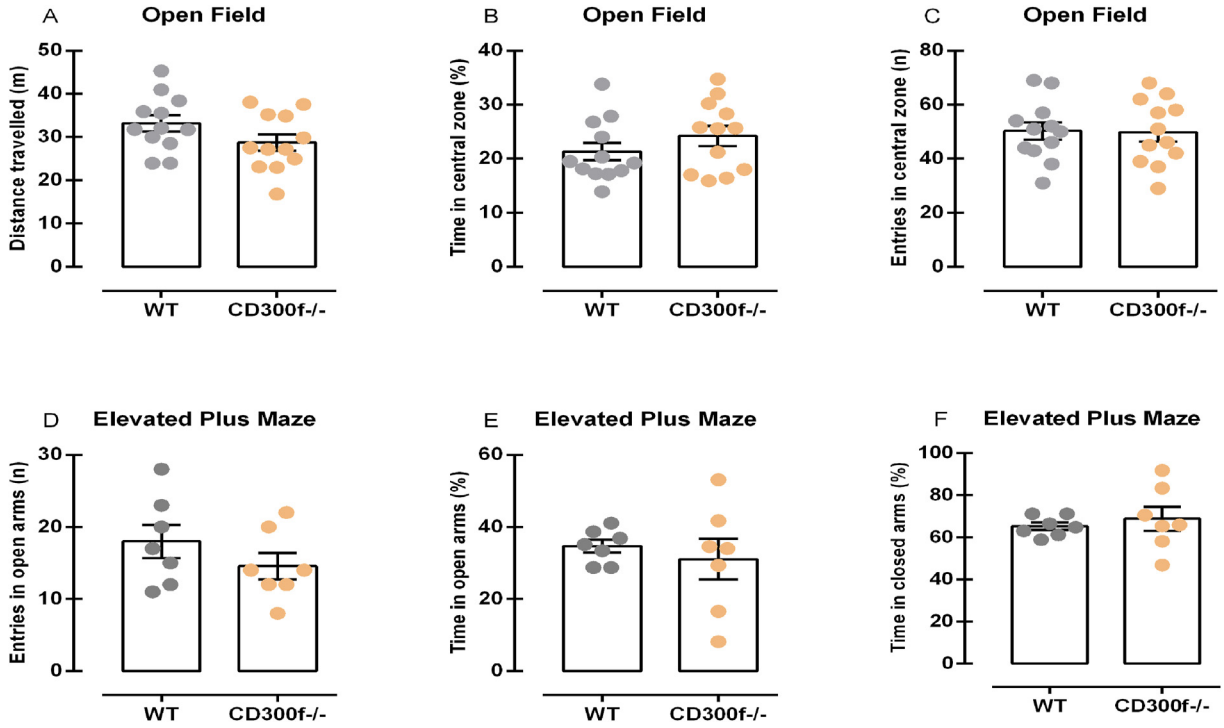

Fig. 2. Anxiety-related behaviors of CD300f−/− female mice in different behavioral contexts. The total distance traveled in the OF was measured (meters) to evaluate female mice spontaneous ambulatory activity (n = 12 WT and 12 CD300f−/−, 2.A) and the % of time spent in the center (n = 12 WT and 12 CD300f−/−, 2.B), as well as the number of entries in the central zone (n = 12 WT and 12 CD300f−/−, 2.C) of the OF, was used to evaluate anxious-like behavior. The number of entries in the open arms of the EPM (n = 7 WT and 7 CD300f−/−, 2.D), the time spent in the open arms (n = 7 WT and 7 CD300f−/−, 2.E) and closed arms (n = 7 WT and 7 CD300f−/−, 2.F) of the EPM (calculated using the total time in the open arms or closed arms + the total time in the closed arms as 100%) was used as indicative of anxiety. Data are represented as mean ± S.E.M. *Abbreviations: OF: Open Field; EPM: Elevated Plus Maze; WT: Wild-type mouse; CD300f−/−: CD300f knockout mouse.*

Table 1
Sociodemographic and clinical characteristics of the population-based sample according to the GAD diagnosis.

Characteristics	Generalized Anxiety Disorder (GAD)		
	No	Yes	p-value
Age in years (mean ± S.E.M.)	25.80 ± 0.17	26.66 ± 0.39	0.053
Sex (% male)	442 (47.2)	46 (26.	<0.001
Ethnicity (% Caucasian)	717 (76.5)	127 (73.4)	0.433
Socioeconomic Class			
Low	169 (18.0)	52 (30.2)	<0.001
Intermediate	469 (50.1)	87 (50.6)	
High	299 (31.9)	33 (19.2)	
Tobacco use (% yes)	181 (19.4)	73 (42.4)	<0.001
Body mass index (kg/m^2)	26.01 ± 0.17	26.34 ± 0.49	0.472
Psychiatric medication	54 (5.7)	33 (19.1)	<0.001
Clinical diseases (% yes)	206 (22.0)	66 (38.2)	<0.001
Total	938 (84.4)	173 (15.6)	

Data are presented as mean ± standard error of the mean (S.E.M.) or n (%). p-values were computed using χ^2 tests or Student's t-test, as appropriated. $p < 0.05$ was considered as statistically significant. GAD: Generalized Anxiety Disorder.

We further evaluated the rs2034310 (C/T) SNP genotypes according to the GAD diagnosis. Considering that sex differences can underlie the biological alterations for several diseases, including psychiatric disorders (Hodes and Epperson, 2019), that only male CD300f−/− mice show an anxiolytic-like phenotype, we further stratified our population by sex to analyze the impact of this polymorphism in GAD diagnosis. As depicted in Table 2, in the male population, the CT genotype confers protection against GAD ($p = 0.012$) even after the adjusted analysis considering sex, age, and ethnicity as confounding variables ($p = 0.015$). The frequency of the TT genotype in our study, and in the general population, was lower when compared to the other genotypes (Lago-Kaufmann et al., 2020). Then, to evaluate the T allele effect in the GAD diagnosis, we performed a dominant model, where we joined T allele carriers in a unique group (CT/TT). In the dominant model, we observed that men individuals carrying the T allele presented a decreased prevalence of GAD ($p = 0.009$). Indeed, the T allele was significantly associated with protection against GAD ($p = 0.007$) in the dominant model, even after adjusted multinomial regression analysis ($p = 0.010$). Interestingly, when we analyzed the SNP association with GAD diagnosis in women, we did not find any significant association of CT genotype ($p = 0.159$) or TT genotype ($p = 0.997$) even after adjusting for the same variables described above ($p = 1.107$) and ($p = 0.820$), respectively. We also performed the analysis in the dominant model joining the T allele carriers, however, no association where observed in the unadjusted ($p = 0.205$) or adjusted ($p = 0.129$) analysis. Overall, our human data demonstrate that the rs2034310 (C/T) polymorphism is associated with GAD diagnosis and confers protection against GAD in a sex-specific manner.

Table 2
Sex differences in the genotype and allele distribution according to GAD diagnosis.

Genotypes	Generalized Anxiety Disorder (GAD)			Unadjusted OR (95%)/p*	Adjusted OR (95%)/p#
	No	Yes	p		
Total population					
rs2034310 SNP Genotype					
CC	520 (55.4)	114 (65.9)	**0.033**	1	1
CT	366 (39.0)	50 (28.9)		0.623 (0.435-0.892)/**0.010**	0.609 (0.422-0.877)/**0.008**
TT	52 (5.5)	9 (5.2)		0.789 (0.378-1.648)/0.529	0.738 (0.348-1.565)/0.428
Dominant model					
CC	520 (55.4)	114 (65.9)	**0.011**	1	1
CT/TT	418 (44.6)	59 (34.1)		0.644 (0.458-0.904)/**0.011**	0.625 (0.442-0.885)/**0.008**
Allele-					
C	1406 (74.9%)	278 (80.0)	0.397	–	–
T	470 (25.0)	68 (19.6)			
Women					
rs2034310 SNP Genotype					
CC	277 (56.0)	79 (62.2)	0.357	1	1
CT	190 (38.4)	40 (31.5)		0.738 (0.484-1.127)/0.159	0.702 (0.457-1.127)/1.107
TT	28 (5.7)	8 (6.3)		1.002 (0.439-2.285)/0.997	0.907 (0.393-2.096)/0.820
Dominant model					
CC	277 (56.0)	79 (62.2)	0.243	1	1
CT/TT	218 (44.0)	48 (37.8)		0.772 (0.517-1.152)/0.205	0.729 (0.484-1.097)/0.129
Men					
rs2034310 SNP Genotype					
CC	242 (54.8)	35 (76.1)	**0.020**	1	1
CT	176 (39.8)	10 (21.7)		0.393 (0.189-0.814)/**0.012**	0.404 (0.194-0.841)/**0.015**
TT	24 (5.4)	1 (2.2)		0.288 (0.038-2.197)/0.230	0.308 (0.040-2.363)/0.257
Dominant model					
CC	242 (54.8)	35 (76.1)	**0.009**	1	1
CT/TT	200 (45.2)	11 (23.9)		0.380 (0.188-0.768)/**0.007**	0.393 (0.194-0.797)/**0.010**

Data are presented as number or proportion (%) and computed by $\chi 2$ tests comparing patients with GAD and controls. * Unadjusted or # adjusted OR (95% CI/p) values were obtained from logistic regression analysis, and in the total population was adjusted for age, sex, and ethnicity and in women and men subpopulation was adjusted for age and ethnicity. $p < 0.05$ was considered as statistically significant. GAD: Generalized Anxiety Disorder.

4. Discussion

Dysfunctional microglia are associated with many neurological and psychiatric disorders, yet our knowledge about the pathological mechanisms involved is incomplete (Stein et al., 2017; Ramirez et al., 2017; Li et al., 2014; Wang et al., 2018; McKim et al., 2018). In the CNS, CD300f immunoreceptors are expressed in microglial and perivascular macrophages and regulate not only neuroinflammatory responses, but also important aspects of microglia phenotype, and synaptic connectivity and plasticity through mechanisms not directly related to classical neuroinflammatory cascades (Lago-Kaufmann et al., 2020). It was recently demonstrated that these receptors contribute to mood regulation in female major depressive disorder (Lago-Kaufmann et al., 2020). Here, we set out to address the possibility that CD300f receptors might also be involved in anxiety-related outcomes. Our results demonstrate that the CD300f immunoreceptors modulate behavioral responses associated with anxiety in male mice and humans. While CD300f−/− male mice displayed reduced anxiety-related behaviors in different paradigms, a polymorphism in the CD300f gene was protective against GAD in a population-based study. These responses were observed only in males and expand our previous findings showing sex-specific effects of CD300f in the modulation of psychiatric symptoms.

CD300f−/− mice displayed a decrease in negative valence behaviors associated with anxiety, characterized by an increase in OFT central locomotion, an increase in rearing behaviors, more exploration in the open arms of the EPM test, decreased latency to eat in the NSF test and decrease defecation in the OFT. These tasks explore the neophobic anxiety and the natural aversion of rodents to exposed areas. Thus, the reduction in this natural aversion can indicate a decrease in anxiety-related behaviors (Bailey and Crawley, 2009). Animal models of anxiety do not claim to faithfully reproduce the complexity and heterogeneity of the human conditions. However, they are essential tools to better understand basic differences in anxiety responses and perhaps discover

potential new targets for more specific pharmacological intervention (Bourin, 2020).

From the epidemiological point of view, our study shows that the T allele of CD300f rs2034310 SNP independently confers protection against GAD in humans. This effect is probably mediated by a dominant effect, as only one T allele is needed in heterozygosis. The C/T exchange produces a non-synonymous substitution of Arg to Gln in the cytoplasmic tail of the receptor that abrogates the protein kinase C delta (PKC-δ) phosphorylation of a threonine in its cytoplasmic tail. The CD300f immune receptor contains in its complex cytoplasmic tail several signaling motifs, including immunoreceptor tyrosine-based inhibition motifs (ITIM), and another tyrosine motif that can be involved in the internalization of this receptor from the cell surface. In fact, internalization indicates that this receptor is involved in processes such as phagocytosis, exposure of antigens, regulation of effector mechanisms, and even viral infection (Choi et al., 2011). In addition, activating antibodies against the CD300f receptor led to the inhibition of the transcription factor NFκB-mediated TLR-2, 3, 4, and 9 signaling and expression of interleukin-8 and metalloproteinase-9 (Lee et al., 2011). Indeed, these pathways were already observed to be altered in anxiety models (Décarie-Spain et al., 2018; Zimmerman et al., 2012), and its inhibition could be associated with low anxiety in the CD300f−/− male mice. However, additional studies are needed to understand the functional implications of this substitution in those pathways.

According to the data we obtained in our population-based study, the T allele of CD300f rs2034310 SNP was protective against GAD in men but not women. Previously published epidemiological studies show that women are more susceptible to GAD than men. However, these conditions have singular clinical manifestations and treatment responses in man and woman, suggesting distinctive biological mechanisms (Craske et al., 2017; Kaczkurkin et al., 2016). We still have a limited understanding of the role of sex differences in most of the anxiety disorders, including GAD and a range of candidate mechanisms have been proposed, including sex chromosome-dependent gene expression and brain development (Donner and Lowry, 2013).

The role of CD300f in behavioral modulation is still largely unexplored. Recently we demonstrated the involvement of CD300f immunoreceptors in major depressive disorder and the T allele presence as a protective mechanism only in women (Lago-Kaufmann et al., 2020). However, CD300f immunoreceptors have also been putatively linked to a familial case of Autism Spectrum Disorder (Inoue et al., 2015). Interestingly, this condition shows a sex ratio heavily skewed towards males and is associated with anxiety-related symptoms and difficulties with behavioral avoidance. Thus, the potential role of CD300f in this and other psychiatric conditions still needs to be explored.

The mechanisms underlying the sex-specific effects of CD300f are largely unknown. Our previous work only showed mild changes in proinflammatory molecules of naïve CD300−/− female and male mice brain, including increased mRNA for il6, il1rn, CD163, and siglec1, and no changes in microglial homeostatic or disease-associated microglial (DAM) genes besides spp1 (Lago-Kaufmann). Moreover, no important changes in the inflammatory response were observed in the spinal cord after a sciatic nerve crush injury in CD300f−/− mice (Lago-Kaufmann). On the other hand, the absence of CD300f affected synaptic plasticity, noradrenaline levels in the hippocampus, and microglial immunometabolic phenotype (Lago-Kaufmann et al., 2020). Thus, these mechanisms should be compared between male and female mice in future experiments to unravel the intriguing question of how is it possible that a unique modification in a single immunoreceptor contributes to the generation of two different psychiatric manifestations in males and females.

The impact of immunoreceptors in brain-related disorders is a huge field of interest, and this is the first study to examine the role of CD300f receptors in anxiety. Collectively, our results from CD300f−/− mice and individuals with GAD suggest a sex-specific role for CD300f receptors in anxiety-related behaviors in men. Understanding the link between CD300f signaling and behavioral impact in a sex-dependent manner is of great importance to establish the complete contribution of this new target to psychiatric disorders.

Declaration of competing interest

None.

Acknowledgements

This work has been supported by grants from Conselho Nacional de Desenvolvimento Científico e Tecnológico (CNPq), Coordenação de Aperfeiçoamento de Pessoal de Ensino Superior (CAPES) and PRONEX-FAPERGS (08/2009 - Pronex 10/0055-0), International Brain Research Organization (IBRO)- LARC PROLAB grant. Comisión Sectorial de Investigación Científica (CSIC), Uruguay; Programa de Desarrollo de las Ciencias Básicas (PEDECIBA), Uruguay; Fondo de Convergencia Estructural del MERCOSUR (COF 03/1111); Banco de Seguros del Estado, Uruguay; Agencia Nacional de Investigación e Innovación (ANII); International Center for Genetic Engineering and Biotechnology (ICGEB-CRP/URY19-01). FNK received International Society for Neurochemistry (ISN) and IBRO awards, and a CAPES fellowship to perform this project. KJ, LMS, RAS, GG, MPK are CNPq Research Fellows. We thank all members of the transgenic animal unit (UATE) of the Institut Pasteur de Montevideo for assistance.

Appendix A. Supplementary data

Supplementary data to this article can be found online at https://doi.org/10.1016/j.bbih.2020.100191.

References

American Psychiatric Association, 2013. Diagnostic and Statistical Manual of Mental Disorders: Diagnostic and Statistical Manual of Mental Disorders, fifth ed. American Psychiatric Association, Arlington, VA. https://doi.org/10.1176/appi.books.9780890425596.744053. 2013.

Bailey, K.R., Crawley, J.N., 2009. Anxiety-related behaviors in mice. In: Buccafusco, J.J. (Ed.), Methods of Behavior Analysis in Neuroscience, second ed. CRC Press/Taylor & Francis., Boca Raton (FL.

Biedermann, S.V., Biedermann, D.G., Wenzlaff, F., Kurjak, T., Nouri, S., Auer, M.K., Wiedemann, K., Briken, P., Haaker, J., Lonsdorf, T.B., Fuss, J., 2017. An elevated plus-maze in mixed reality for studying human anxiety-related behavior. BMC Biol. 15, 125. https://doi.org/10.1186/s12915-017-0463-6.

Bourin, M., 2020. Experimental anxiety model for anxiety disorders: relevance to drug discovery. Adv. Exp. Med. Biol. 1191, 169–184. https://doi.org/10.1007/978-981-32-9705-0_11.

Capuron, L., Miller, A.H., 2011. Immune system to brain signaling: neuropsychopharmacological implications. Pharmacol. Ther. 130, 226–238. https://doi.org/10.1016/j.pharmthera.2011.01.014.

Choi, S.C., Simhadri, V.R., Tian, L., Gil-Krzewska, A., Krzewski, K., Borrego, F., Coligan, J.E., 2011. Cutting edge: mouse CD300f (CMRF-35–Like Molecule-1) recognizes outer membrane-exposed phosphatidylserine and can promote phagocytosis. J. Immunol. 187, 3483–3487. https://doi.org/10.4049/jimmunol.1101549.

Clark, G.J., Ju, X., Tate, C., Hart, D.N., 2009. The CD300 family of molecules are evolutionarily significant regulators of leukocyte functions. Trends Immunol. 30, 209–217. https://doi.org/10.1016/j.it.2009.02.003.

Copeland, W.E., Shanahan, L., Worthman, C., Angold, A., Costello, E.J., 2012. Generalized anxiety and C-reactive protein levels: a prospective, longitudinal analysis. Psychol. Med. 42, 2641–2650. https://doi.org/10.1017/S0033291712000554.

Costello, H., Gould, R.L., Abrol, E., Howard, R., 2019. Systematic review and meta-analysis of the association between peripheral inflammatory cytokines and generalised anxiety disorder. BMJ Open 9, e027925. https://doi.org/10.1136/bmjopen-2018-027925.

Craske, M.G., Stein, M.B., Eley, T.C., Milad, M.R., Holmes, A., Rapee, R.M., Wittchen, H.U., 2017. Anxiety disorders. Nat. Rev. Dis. Prim. 3, 17024 https://doi.org/10.1038/nrdp.2017.24.

Décarie-Spain, L., Sharma, S., Hryhorczuk, C., Issa-Garcia, V., Barker, P.A., Arbour, N., Alquier, T., Fulton, S., 2018. Nucleus accumbens inflammation mediates anxiodepressive behavior and compulsive sucrose seeking elicited by saturated dietary fat. Mol. Metab. 10, 1–13. https://doi.org/10.1016/j.molmet.2018.01.018.

Donner, N.C., Lowry, C.A., 2013. Sex differences in anxiety and emotional behavior. Pflügers Archiv 465, 601–626. https://doi.org/10.1007/s00424-013-1271-7.

Haller, H., Cramer, H., Lauche, R., Gass, F., Dobos, G.J., 2014. The prevalence and burden of subthreshold generalized anxiety disorder: a systematic review. BMC Psychiatr. 14, 128. https://doi.org/10.1186/1471-244X-14-128.

Hodes, G.E., Epperson, C.N., 2019. Sex differences in vulnerability and resilience to stress across the life span. Biol. Psychiatr. 86, 421–432. https://doi.org/10.1016/j.biopsych.2019.04.028.

Inoue, E., Watanabe, Y., Egawa, J., Sugimoto, A., Nunokawa, A., Shibuya, M., Igeta, H., Someya, T., 2015. Rare heterozygous truncating variations and risk of autism spectrum disorder: whole-exome sequencing of a multiplex family and follow-up study in a Japanese population. Psychiatr. Clin. Neurosci. 69, 472–476. https://doi.org/10.1111/pcn.12274.

Kaczkurkin, A.N., Moore, T.M., Ruparel, K., Ciric, R., Calkins, M.E., Shinohara, R.T., Elliott, M.A., Hopson, R., Roalf, D.R., Vandekar, S.N., Gennatas, E.D., Wolf, D.H., Scott, J.C., Pine, D.S., Leibenluft, E., Detre, J.A., Foa, E.B., Gur, R.E., Gur, R.C., Satterthwaite, T.D., 2016. Elevated amygdala perfusion mediates developmental sex differences in trait anxiety. Biol. Psychiatr. 80, 775–785. https://doi.org/10.1016/j.biopsych.2016.04.021.

Keswani, T., Roland, J., Herbert, F., Delcroix-Genete, D., Bauderlique-Le, Roy, H., Gaayeb, L., Cazenave, P.A., Pied, S., 2020. Expression of CD300lf by microglia contributes to resistance to cerebral malaria by impeding the neuroinflammation. Gene Immun. 21, 45–62. https://doi.org/10.1038/s41435-019-0085-9.

Lago, N., Kaufmann, F.N., Negro-Demontel, M.L., Alí-Ruiz, D., Ghisleni, G., Rego, N., Arcas-García, A., Vitureira, N., Jansen, K., Souza, L.M., Silva, R.A., Lara, D.R., Pannunzio, B., Abin-Carriquiry, J.A., Amo-Aparicio, J., Martin-Otal, C., Naya, H., McGavern, D.B., Sayós, J., López-Vales, R., Kaster, M.P., Peluffo, H., 2020. CD300f immunoreceptor is associated with major depressive disorder and decreased microglial metabolic fitness. Proc. Natl. Acad. Sci. U.S.A. 117, 6651–6662. https://doi.org/10.1073/pnas.1911816117.

Lahiri, D.K., Nurnberger Jr., J., 1991. A rapid non-enzymatic method for the preparation of HMW DNA from blood for RFLP studies. Nucleic Acids Res. 19, 5444. https://doi.org/10.1093/nar/19.19.5444.

Lee, S.M., Kim, E.J., Suk, K., Lee, W.H., 2011. CD300F blocks both MyD88 and TRIF-mediated TLR signaling through activation of Src homology region 2 domain-containing phosphatase 1. J. Immunol. 186, 6296–6303. https://doi.org/10.4049/jimmunol.1002184.

Li, Z., Ma, L., Kulesskaya, N., Vôikar, V., Tian, L., 2014. Microglia are polarized to M1 type in high-anxiety inbred mice in response to lipopolysaccharide challenge. Brain Behav. Immun. 38, 237–248. https://doi.org/10.1016/j.bbi.2014.02.008.

Lister, R.G., 1987. The use of a plus-maze to measure anxiety in the mouse. Psychopharmacology (Berl) 92, 180–185. https://doi.org/10.1007/BF00177912.

Martínez-Barriocanal, Á., Arcas-García, A., Magallon-Lorenz, M., Ejarque-Ortíz, A., Negro-Demontel, M.L., ComasCasellas, E., Schwartz Jr., S., Malhotra, S., Montalban, X., Peluffo, H., Martín, M., Comabella, M., Sayós, J., 2017. Effect of specific mutations in Cd300 complexes formation; potential implication of Cd300f in multiple sclerosis. Sci. Rep. 7, 13544. https://doi.org/10.1038/s41598-017-12881-8.

Matsukawa, T., Izawa, K., Isobe, M., Takahashi, M., Maehara, A., Yamanishi, Y., Kaitani, A., Okumura, K., Teshima, T., Kitamura, T., Kitaura, J., 2015. Ceramide-CD300f binding suppresses experimental colitis by inhibiting ATP-mediated mast cell activation. Gut 65, 777–787. https://doi.org/10.1136/gutjnl-2014-308900.

McKim, D.B., Weber, M.D., Niraula, A., Sawicki, C.M., Liu, X., Jarrett, B.L., Ramirez-Chan, K., Wang, Y., Roeth, R.M., Sucaldito, A.D., Sobol, C.G., Quan, N., Sheridan, J.F., Godbout, J.P., 2018. Microglial recruitment of IL-1β-producing monocytes to brain endothelium causes stress-induced anxiety. Mol. Psychiatr. 23, 1421–1431. https://doi.org/10.1038/mp.2017.64.

Murray, C.J., Vos, T., Lozano, R., Naghavi, M., Flaxman, A.D., Michaud, C., et al., 2012. Disability-adjusted life years (DALYs) for 291 diseases and injuries in 21 regions, 1990-2010: a systematic analysis for the global burden of disease study 2010. Lancet 380, 2197–2223. https://doi.org/10.1016/S0140-6736(12)61689-4.

Peluffo, H., Solari-Saquieres, P., Negro-Demontel, M.L., Francos-Quijorna, I., Navarro, X., López-Vales, R., Sayós, J., Lago, N., 2015. CD300f immunoreceptor contributes to peripheral nerve regeneration by the modulation of macrophage inflammatory phenotype. J. Neuroinflammation 12, 145. https://doi.org/10.1186/s12974-015-0364-y.

Polderman, T.J.C., Benyamin, B., de Leeuw, C.A., Sullivan, P.F., van Bochoven, A., Visscher, P.M., Posthuma, D., 2015. Meta-analysis of the heritability of human traits based on fifty years of twin studies. Nat. Genet. 47, 702–709. https://doi.org/10.1038/ng.3285.

Ramirez, K., Fornaguera-Trías, J., Sheridan, J.F., 2017. Stress-Induced microglia activation and monocyte trafficking to the brain underlie the development of anxiety and depression. Curr. Top. Behav. Neurosci. 31, 155–172. https://doi.org/10.1007/7854_2016_25.

Rojas-Carvajal, M., Fornaguera, J., Mora-Gallegos, A., Brenes, J.C., 2018. Testing experience and environmental enrichment potentiated open-field habituation and grooming behaviour in rats. Anim. Behav. 137 https://doi.org/10.1016/j.anbehav.2018.01.018.

Rubio, G., López-Ibor, J.J., 2007. Generalized anxiety disorder: a 40-year follow-up study. Acta Psychiatr. Scand. 115, 372–379. https://doi.org/10.1111/j.1600-0447.2006.00896.x.

Samuels, B.A., Hen, R., 2011. Novelty-suppressed feeding in the mouse. In: Gould, T. (Ed.), Mood and Anxiety Related Phenotypes in Mice. Humana Press, pp. 107–121. https://doi.org/10.1007/978-1-61779-313-4_7.

Shiba, E., Izawa, K., Kaitani, A., Isobe, M., Maehara, A., Uchida, K., Maeda, K., Nakano, N., Ogawa, H., Okumura, K., Kitamura, T., Shimizu, T., Kitaura, J., 2017. Ceramide-CD300f binding inhibits lipopolysaccharide-induced skin inflammation. J. Biol. Chem. 292, 2924–2932. https://doi.org/10.1074/jbc.M116.768366.

Stein, D.J., Vasconcelos, M.F., Albrechet-Souza, L., Ceresér, K.M.M., de Almeida, R.M.M., 2017 Oct 24. Microglial Over-Activation by Social Defeat Stress Contributes to Anxiety- and Depressive-Like Behaviors. Front Behav. Neurosci. 11, 207. https://doi.org/10.3389/fnbeh.2017.00207.

Sturman, O., Germain, P.L., Bohacek, J., 2018. Exploratory rearing: a context- and stress-sensitive behavior recorded in the open-field test. Stress 21, 443–452. https://doi.org/10.1080/10253890.2018.1438405.

Vesga-López, O., Schneier, F.R., Wang, S., Heimberg, R.G., Liu, S.-M., Hasin, D.S., Blanco, C., 2008. Gender differences in generalized anxiety disorder: results from the national epidemiologic survey on alcohol and related conditions (NESARC). J. Clin. Psychiatr. 69, 1606–1616.

Vieira, M.M., Ferreira, T.B., Pacheco, P.A., Barros, P.O., Almeida, C.R., Araújo-Lima, C.F., Silva-Filho, R.G., Hygino, J., Andrade, R.M., Linhares, U.C., Andrade, A.F., Bento, C.A., 2010. Enhanced Th17 phenotype in individuals with generalized anxiety disorder. J. Neuroimmunol. 229, 212–218. https://doi.org/10.1016/j.jneuroim.2010.07.018.

Wang, Y.L., Han, Q.Q., Gong, W.Q., Pan, D.H., Wang, L.Z., Hu, W., Yang, M., Li, B., Yu, J., Liu, Q., 2018. Microglial activation mediates chronic mild stress-induced depressive- and anxiety-like behavior in adult rats. J. Neuroinflammation 15, 21. https://doi.org/10.1186/s12974-018-1054-3.

Wingo, A.P., Gibson, G., 2015. Blood gene expression profiles suggest altered immune function associated with symptoms of generalized anxiety disorder. Brain Behav. Immun. 43, 184–191. https://doi.org/10.1016/j.bbi.2014.09.016.

Wittchen, H.U., 2002. Generalized anxiety disorder: prevalence, burden, and cost to society. Depress. Anxiety 16, 162–171. https://doi.org/10.1002/da.10065.

Xi, H., Katschke Jr., K.J., Helmy, K.Y., Wark, P.A., Kljavin, N., Clark, H., Eastham-Anderson, J., Shek, T., Roose-Girma, M., Ghilardi, N., van Lookeren Campagne, M., 2010. Negative regulation of autoimmune demyelination by the inhibitory receptor CLM-1. J. Exp. Med. 207, 7–16. https://doi.org/10.1084/jem.20091508.

Zaqueu Lima, T., Roberto Sardinha, L., Sayos, J., Eugenio Mello, L., Peluffo, H., 2017. Astrocytic expression of the immunoreceptor CD300f protects hippocampal neurons from amyloid-β oligomer toxicity in vitro. Curr. Alzheimer Res. 14, 778–783. https://doi.org/10.2174/1567205014666170202121709.

Zimmerman, G., Shaltiel, G., Barbash, S., Cohen, J., Gasho, C.J., Shenhar-Tsarfaty, S., Shalev, H., Berliner, S.A., Shelef, I., Shoham, S., Friedman, A., Cohen, H., Soreq, H., 2012. Post-traumatic anxiety associates with failure of the innate immune receptor TLR9 to evade the pro-inflammatory NFκB pathway. Transl. Psychiatry 2, e78. https://doi.org/10.1038/tp.2012.4.

scientific reports

Check for updates

OPEN

Microglial CD300f immune receptor contributes to the maintenance of neuron viability in vitro and after a penetrating brain injury

Daniela Alí-Ruiz[1,2], Nathalia Vitureira[3] & Hugo Peluffo[1,2,4,5]✉

Emerging evidences suggest that immune receptors participate in diverse microglial and macrophage functions by regulating their immunometabolism, inflammatory phenotype and phagocytosis. CD300f, a TREM2-like lipid sensing immune receptor, that integrates activating and inhibitory cell-signalling pathways, modulates inflammation, efferocytosis and microglial metabolic fitness. In particular, CD300f overexpression was described to be neuroprotective after an acute brain injury, suggesting a role for this immune receptor in neurotrophic interactions. Thus, we hypothesised that CD300f modulates neuronal survival through neuron-microglial interactions. In order to study its biological function, we used in vitro and in vivo approaches, CD300f$^{-/-}$ animals and rCD300f-Fc, a fusion protein that interrupts the endogen interaction between CD300f receptor-ligands. In hippocampal cocultures containing neurons and mixed glia, we observed that rCD300f-Fc, but not control IgGs induced neuronal death. In accordance, in vivo studies performed by injecting rCD300f-Fc or control IgGs into rat or WT or CD300 KO mice neocortex, showed an increased lesioned area after a penetrating brain injury. Interestingly, this neuronal death was dependent on glia, and the neurotoxic mechanism did not involve the increase of proinflammatory cytokines, the participation of NMDA receptors or ATP release. However, exogenous addition of glial cell line-derived neurotrophic factor (GDNF) prevented this process. Taken together, our results suggest that CD300f modulates neuronal survival in vitro and after a penetrating brain injury in vivo and that CD300f inhibition alters microglial phenotype generating a neurotoxic microenvironment.

Immune receptors play a critical role in regulating immune and inflammatory processes in the central nervous system (CNS). They primarily function by adjusting the threshold and duration of myeloid cell responses[1,2]. The CD300 family of immune receptors consist of several activating and inhibitory members[2]. The existence of a CD300-like molecule in ancient vertebrates and the maintenance of its function predicts an essential role of this family in innate immunity[3,4]. On the other hand, CD300f has a particular interest given its ability to mediate activating and inhibitory signals in myeloid innate immune cells[5,6] and its modulatory role in microglial immunometabolic phenotype and synaptic pruning[7]. In line with its role in modulating inflammatory phenotypes, it has been shown that CD300f mediates anti-inflammatory signaling by decreasing mast cell degranulation and allergic responses[8] and counteracting macrophage activation by interfering with several TLR signaling cascades[9]. On the contrary, the antibody-dependent activation of CD300f in microglia cultures potentiates lipopolysaccharide (LPS)/TLR4 mediated responses[10]. Moreover, CD300f ligands are present in the CNS in vivo and in nervous system primary cultures[11], and CD300f overexpression after an acute brain injury is neuroprotective[11]. However, the role of CD300f signaling in cell–cell neurotrophic interactions is not well understood.

The CD300f immune receptor shares many characteristics with TREM2, a key immune receptor for determining the phenotype of microglia and macrophages, and one of the main risk factor genes for the development of Alzheimer's Disease (AD) and Nasu Hakola Disease[1]. In accordance, mounting evidence showed that CD300f

[1]Neuroinflammation and Gene Therapy Lab., Institut Pasteur de Montevideo, Montevideo, Uruguay. [2]Departamento de Histología y Embriología, Facultad de Medicina, UdelaR, Montevideo, Uruguay. [3]Departamento de Fisiología, Facultad de Medicina, Universidad de la República, Montevideo, Uruguay. [4]Unitat de Bioquímica i Biología Molecular, Departamento de Biomedicina, Facultat de Medicina i Ciències de la Salut, Universitat de Barcelona (UB), Barcelona, Spain. [5]Institut de Neurociències, Universitat de Barcelona (UB), Barcelona, Spain. ✉email: hugo.peluffo@pasteur.edu.uy

has been associated with a neuroprotective response against Tau pathology[12] further highlighting its pivotal role in nervous system function in both health and disease[7,13]. Interestingly, CD300f is among the most up-regulated genes in brain microglia/macrophages after several proinflammatory insults such as intraperitoneal LPS injection[7,14], spinal cord injury[15], or with age in a mouse tauopathy model[12]. Moreover, its upregulation has been associated to promyelinating microglia after a demyelinating stimuli[16]. The inhibition of CD300f using a soluble rCD300f-Fc fusion protein delayed peripheral nerve regeneration after a sciatic nerve injury[17]. Genetic variants of CD300f have also been associated to non-classical inflammatory functions of microglial and potentially CNS barrier-associated macrophages (BAM), leading to the modulation of neuropsychiatric conditions such as major depressive disorder and anxiety[7,18]. In spite of all these accumulated functional data indicating a role for CD300f and its ligands in neuronal survival, the underlying cellular mechanisms are not well understood.

To explore the role of CD300f in neuroprotection, we used CD300f deficient mice (CD300f$^{-/-}$) and the rCD300f-Fc fusion protein which interrupts the endogenous interaction between CD300f receptor and its ligands, both in vitro and in vivo[17]. By using hippocampal cocultures containing neurons and glia, we observed that CD300f inhibition promotes neuronal death compared to controls. This effect was dependent on glia, because no cell death was detected in enriched hippocampal neuronal cultures treated with rCD300f-Fc. Moreover, we found that conditioned media derived from rCD300f-Fc-treated cocultures induced neuronal death when applied to enriched neuronal cultures. However, conditioned media derived from enriched glial cultures treated with rCD300f-Fc did not affect neuronal survival. In accordance with these results, in vivo studies performed by injecting rCD300f-Fc or control IgGs into wild type (WT) rat or mouse neocortex showed an increased lesioned area. However, no effect on the lesion volume was observed after injecting rCD300f-Fc in CD300f$^{-/-}$ mice, suggesting that the effect of the rCD300f-Fc fusion protein is specific. Taken together, our data suggest that CD300f plays a key role in neuroprotection and that neuron-glia interactions are essential in this process, probably by promoting the release of gliotransmitters. Moreover, CD300f inhibition may alter microglial phenotype generating a neurotoxic microenvironment.

Methods

Cell cultures

Animal care and protocols were approved by the Committee of Ethics in Animal Research (CHEA-UDELAR), Uruguay. Dissociated hippocampal neuron-glia cocultures were prepared from P0–P1 rat pups as described previously with minor modifications[19]. Coverslips were coated by adding a 5 mM acetic acid solution containing 5 µg/ml poly-d-lysine (Sigma-Aldrich) and 0.4 mg/ml rat-tail collagen. Mixed glial cultures were plated with BME-based culture media (GibCo) containing 10% fetal calf serum (GibCo), Glutamax (GibCo), 20 mM D-glucose (GibCo), HEPES (1%), pyruvate (1%) and penicillin/streptomycin (GibCo). After 6–7 days in vitro (DIV), dissociated hippocampal cells were plated onto a glial monolayer and maintained in Neurobasal-based culture media (GibCO) containing B-27 (GibCo), Glutamax, 20 mM D-glucose and penicillin/streptomycin. After 24–48 h AraC (4 µm, Sigma-Aldrich) was added to minimize proliferation. Cultures were used for experiments at 14–15 DIV[20]. Conditioned media were generated by treating mixed glial cultures or cocultures at 12 DIV for 72 h with rat CD300f-Fc (1.0 µg/ml, Sinobiological custom bulk produced without preservatives) or control IgG (1.0 µg/ml). Enriched hippocampal neuronal cultures were prepared by seeding 150,000 neurons in 12 mm coverslips, which were manually counted by using a Neubauer counting chamber with trypan blue to exclude dead cells. After 12 DIV, they were treated for 72 h with rCD300f-Fc or control IgG, or with conditioned media diluted 1:2 alone or with GDNF; 1.0 ng/ml), CPP (3-(2-Carboxypiperazin-4-yl)propyl-1-phosphonic acid, a selective N-methyl-D-aspartate (NMDA)-type receptor antagonist; 100 µM), or CBX (carbenoxolone, the gap junction locker; 100 µM).

Immunocytochemistry

Cells were fixed in 4% paraformaldehyde (PFA 4%, Sigma-Aldrich), 15 min at room temperature (RT), permeabilized with PBS containing 0.1% TritonX-100 (PBS-T, Sigma-Aldrich), and blocked in PBS (Sigma-Aldrich) containing 0.2 M glycine, 10% FBS (Sigma-Aldrich), and 0.1% TritonX-100 (Sigma-Aldrich), for 1h at RT. For estimating cell numbers, the following primary antibodies were added in PBS containing 5% FBS and incubated for 2h at RT: mouse anti-βIII Tubulin (1:1000, Cat. No. G7121, Promega, USA), mouse anti-APC (1:300, Cat. No. OP80, Calbiochem, Germany), rabbit anti-IBA1 (1:1000, Cat. No. 019-19741, Wako, Japan), or rabbit anti-GFAP (1:1000, Cat. No. Z0334, DAKO, Denmark). After three washes with PBS-T cells were incubated with secondary fluorescently conjugated antibodies Alexa Fluor 488 or 594 (Invitrogen) and DyLight 649 (Jackson ImmuneResearch). Negative controls, without primary antibody incubation, were made to rule out non-specific staining. DAPI (1:300, Sigma, Milwaukee, Wisconsin, USA) was used for nuclei detection. As an assay for evaluating the specificity of rCD300f-Fc neurotoxicity, the following primary antibodies were used: mouse anti-mouse myeloid-associated immunoglobulin-like receptor five (MAIRV)/CMRF-35-like molecule1 (CLM1) (1:20, MAB27881 R&D Systems, Minneapolis, MN, USA) and goat anti-mouse CLM1/CD300f (1:50 Invitrogen, Catalog # PA5-47,399).

MTT assay

Cell viability was indirectly estimated by the MTT assay, which is based on the cellular reduction of tetrazolium salts. Cells were incubated with MTT (final concentration 0.5 mg/ml) for 2 h for allowing intracellular reduction of the soluble MTT to the insoluble formazan dye. Then, the media was carefully removed without disturbing the formazan crystals formed by viable cells and 100 µL of dimethyl sulfoxide (DMSO) was added to solubilize the formazan crystals. Absorbance was measured at 570 nm using a microplate reader (Thermo/Labsystem Multiskan MS, Thermo Fisher Scientific, Waltham, MA USA).

Image analysis

Images were acquired on an epifluorescence microscope (Olympus IX8) at 20X and analyzed using Fiji software. All pictures were obtained following the same pattern by generating a cross and placing its center at the center of the well. One picture was taken per field, and 15 fields in total were used per well. The number of βIII-Tubulin-positive neurons per well was determined by summing neurons from all photos acquired per well. In each experiment, the number of βIII-Tubulin-positive cells were counted and normalized to control conditions (untreated cells).

Animals and in vivo *injection*

All experimental work was approved by the UDELAR Ethical Commission (Exp. No. 070153-000528-14) and the Ethics Commission for the Use of Animals (CEUA) of the Institut Pasteur de Montevideo (No. 006-20) and conducted according to directives of the Federation of Laboratory Animal Science Associations (FELASA). Data are reported in accordance with ARRIVE guidelines. The animals used in this study were: adult (8–10 weeks) 6.Cg-Tg(Thy1-YFPH)2Jrs male mouse heterozygote for yellow fluorescent protein (YFP-H) (Jackson Laboratories), adult (4 to 5 months old) male C57BL/6 wild type (WT) mice and CD300f$^{-/-}$ mice (Genentech, Bar Harbor, ME, USA[13]), adult (4 to 5 months old) male Wistar rats. Animals were injected at neocortex (coordinates L: − 0.15; V: − 0.1 cm) using a stereotaxic frame under isoflurane (Abbott, Abbott Park, IL, USA) anesthesia and a nanoinjector (2 µl at 0.4 µl/min during 5 min; Quintessential Stereotaxic Nanoinjector, Stoelting CO. Wood Dale, IL, USA) with saline solution (0.9% NaCl), rCD300f-IgG (30 µg/ml) or control IgG (30 µg/ml). The needle was left in place for an additional 5 min to allow diffusion into the brain parenchyma. Treatments were randomly distributed among animals in each cage. Three days after the lesion was performed, animals were anesthetized and perfused intracardially with 4% PFA in 0.1 M phosphate buffer (pH 7.4). Brains were post-fixed with PFA 4% (2 h), cryoprotected in 30% sucrose, and frozen with CO_2. Parallel cryostat coronal Sects. (30 µm) of the entire brain were prepared, stained with Nissl and used for quantification of the lesioned and total area of the hemisphere. The brain tissue sections were immersed in toluidine blue solution (15 ml of solution A composed by 0.5% toluidine blue in water and 200 ml of solution B composed by three parts of acetic acid 0.2 M and two parts of sodium acetate 0.2 M) for 20 min, rinsed with distilled water, dehydrated in ethanol solutions with increasing concentrations and cleared in xylene. Then, the sections were mounted with DPX mounting medium (Sigma-Aldrich), covered with cover slips, and observed under a light microscope. Damaged neurons were identified by loss of Nissl staining, whereas healthy neurons exhibited Nissl substance within the cytoplasm, a more relaxed chromatin structure, and well-defined nucleoli.

Quantification of the lesioned Nissl pale area was performed using Fiji software with parallel microscope observation (using 10X and 20X magnification). The lesion area and the total lesioned hemisphere area were used to calculate the lesion volume and the total (ipsilateral) hemisphere volume; data were expressed as "% of lesioned hemisphere" to correct for the possible edema effect. Neurotoxicity in YFP mouse brains was determined by the number of YFP-positive neurons counted in the contralateral hemisphere minus those counted in the injured hemisphere. Values were expressed as "% of neuronal death".

Statistical analysis

One-way analysis of variance (ANOVA) followed by Holm-Sidak´s test or Tukey's post-hoc analysis were used for experimental data with normal distribution. Statistical analyses were performed with Prism 8 software and data was shown as mean ± SEM, considering $p < 0.05$ as statistically significant. The number of independent experiments performed are indicated in the figures. We did not perform any outlier test and did not eliminate any potential outlier.

Ethical approval

All experimental work was approved by the UDELAR University Ethical Commission (Exp. No. 070153-000528-14) and the CEUA if the Institut Pasteur de Montevideo (No. 006-20) conducted according to directives of the Federation of Laboratory Animal Science Associations (FELASA).

Results

CD300f inhibition in neuron-glial cocultures is neurotoxic

In order to explore the role of CD300f in modulating neuron-glia interactions underlying neuroprotection in vitro, we first analyzed the cellular composition of hippocampal dissociated cocultures by immunolabeling against several cell-type specific markers. We found 36% βIII-Tubulin positive neurons, 38% GFAP positive astrocytes, 11% IBA1 positive microglia and 15% APC positive oligodendrocytes (Suppl. Figure 1). Next, we analyzed neuronal survival 72h after treating cocultures (at 12 DIV) with the soluble fusion protein rCD300f-Fc (1.0 µg/ml) or with control IgGs (1.0 µg/ml) (Fig. 1A,B). The rCD300f-Fc protein is composed by the extracellular domain of rat CD300f fused to a mouse IgG2a Fc region (rCD300f-IgG2a). This fusion protein inhibits the activation of CD300f by its endogenous ligands being a widely used strategy for modulating immune receptors[1,17]. Interestingly, treating cocultures with rCD300f-IgG2a induced a 52 ± 17% and 43 ± 17% decrease in the number of βIII-Tubulin positive neurons when compared to the untreated or mIgG2a controls, respectively (Fig. 1B,C). Moreover, incubation with LPS (1.0 µg/ml, 72h) together with IL1β (10 ng/ml, 72h), a well-known neurotoxic proinflammatory insult, showed a similar decrease in the number of βIII-Tubulin-positive neurons (51 ± 17%) (Fig. 1B,C). These data suggest that rCD300f plays a pivotal role in neuronal survival.

The IgG2a isotype can activate complement and Antibody-Dependent Cellular Cytotoxicity (ADCC). Thus, to avoid the putative non-specific effects of the rCD300f-IgG2a fusion protein, we generated and additional fusion protein composed by the extracellular domain of rat CD300f fused to the IgG1 Fc region, which has lower

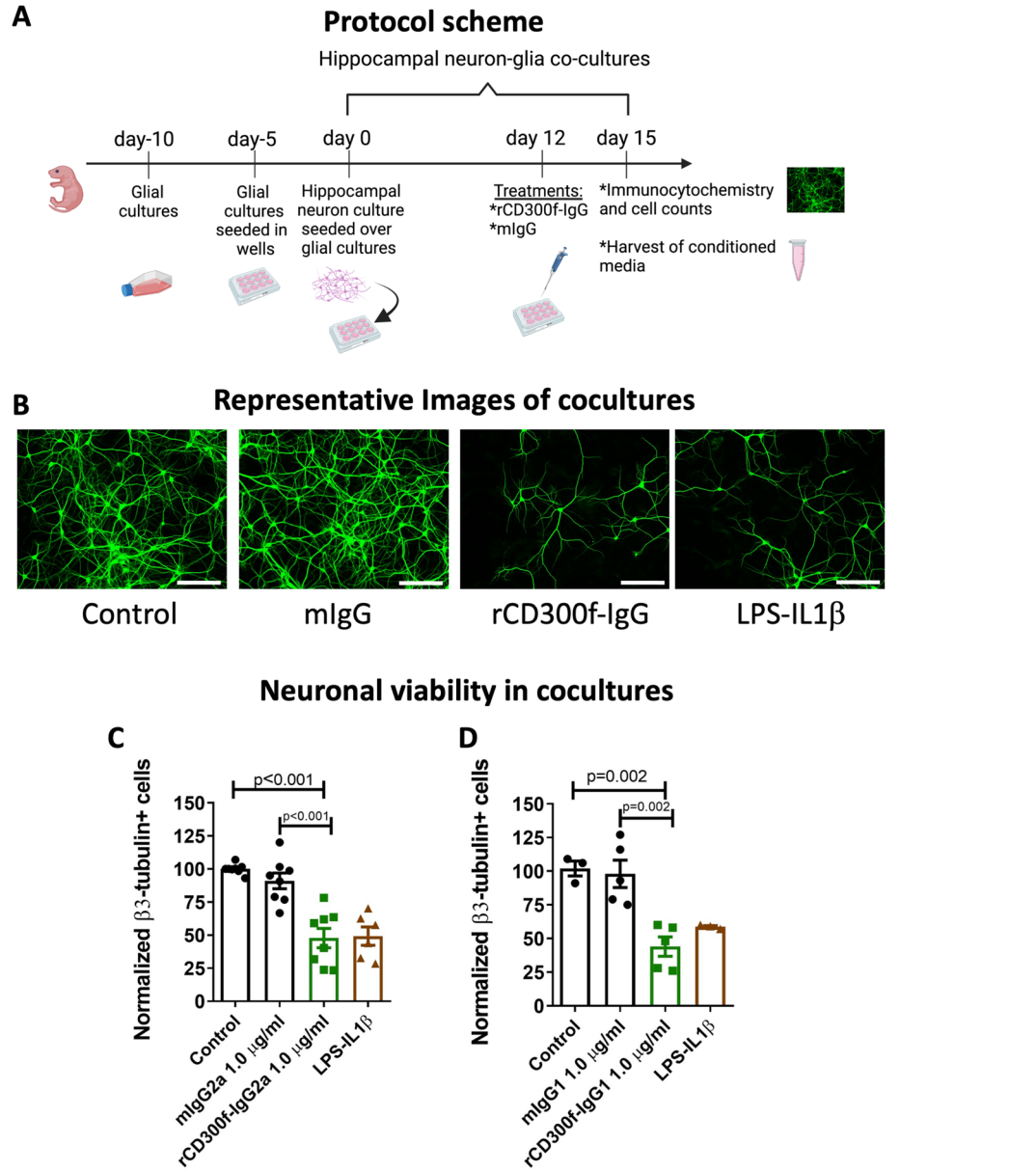

Figure 1. CD300f inhibition induced neurotoxicity in vitro. (**A**) Protocol scheme. (**B**) Representative images of neurons immunolabeled with β3–tubulin antibody in untreated cocultures, and treated with: mIgG2a, rCD300f-IgG, or LPS + IL1β. Scale bars 400 µM. (**C**,**D**) β3–tubulin-positive cells were counted 72 h post-incubation. Values are expressed as normalized to untreated controls. Four independent experiments were performed in (**C**) and (**D**) (two for each IgG isotype). Data show mean ± SEM; p corresponds to one way ANOVA followed by Tukey's test.

complement activation capacities and decreased ADCC triggering[21]. The incubation of hippocampal cocultures with rCD300f-IgG1 fusion protein (1.0 µg/ml for 72h) mimics the effect of CD300f inhibition by rCD300f-IgG2a, showing 60 ± 16% and 55 ± 16% of neuronal cell death when compared to untreated or mIgG2a controls, respectively (Fig. 1D). To further confirm the specificity of the neurotoxic effect, hippocampal cocultures were treated with rCD300f-IgG1 protein preincubated with two different blocking polyclonal anti-CD300f antibodies (rat anti-CD300f (R&D Systems) and goat anti-CD300f (Invitrogen). Notably, the neurotoxic effect was fully abolished in both cases when compared to their respective specific IgG controls or the anti-CD300f antibodies alone (Suppl. Figure 2).

CD300f inhibition in vivo is neurotoxic after a penetrating brain injury

To explore the role of CD300f in modulating neuronal survival in vivo, we injected saline, rCD300f-IgG2a (30 µg/ml) or control IgG2a (30 µg/ml) into rat neocortex and evaluated the lesion volume by Nissl staining (Fig. 2A). In accordance with our in vitro results, inhibiting CD300f after a penetrating cortical injury increase the % of

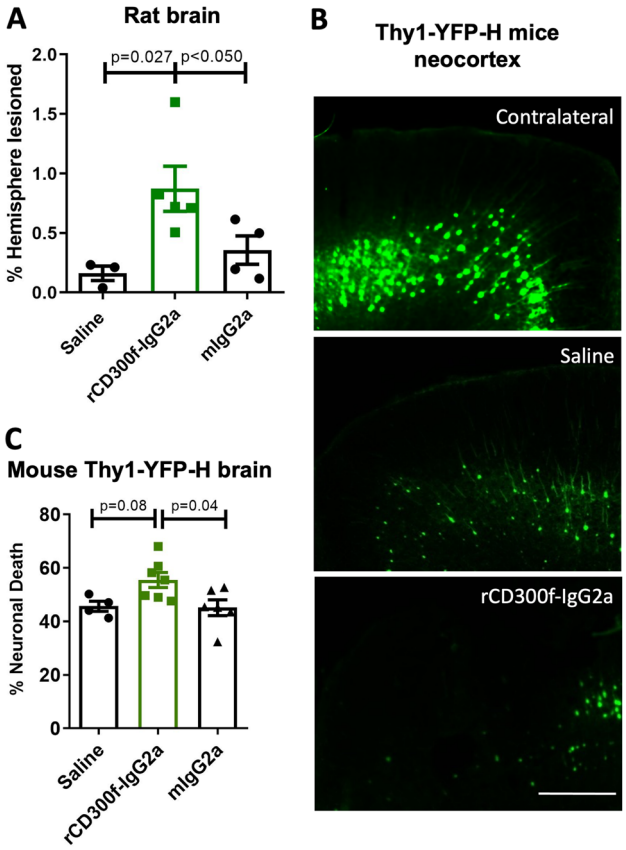

Figure 2. CD300f inhibition induced neurotoxicity in vivo. (**A**) Bar graphs showing the percentage of lesion volume in rat cortex 72 h after being injected with saline (n = 3), rCD300f-IgG2a (n = 5, 30 µg/ml), or control IgG2a (n = 4, 30 µg/ml) and measured by Nissl staining. (**B**) Representative images of mouse Thy1-YFP-H cortex injected with saline or rCD300f-IgG2a and contralateral non-injected cortex (Scale bars 100 µM). (**C**) Bar graph showing the number of YFP + cortical neurons in Thy1-YFP-H cortex after intracortical injection of saline (n = 4), rCD300f-IgG2a (n = 7, 30 µg/ml), or control IgG2a (n = 6, 30 µg/ml) Data show mean ± SEM; p corresponds to one way ANOVA followed by Holm-Sidak´s test.

lesioned hemisphere compared to controls injected with saline or mIgG2a (saline 0.16 ± 0.1%, rCD300f-IgG2a 0.87 ± 0.42% and mIgG2a 0.36 ± 0.24%) (Fig. 2A), suggesting that CD300f promotes neuronal survival both in vivo and in vitro. An increased neuronal death was also observed after neocortical injection of rCD300f-IgG2a (30 µg/ml) in Thy1-YFP-H mice, compared to saline or control IgG2a (30 µg/ml) (saline 46.2 ± 4.5%, rCD300f-IgG2a 58.2 ± 6.7% and mIgG2a 48.3 ± 4.6%)(Fig. 2B,C). Together these results suggest that blocking microglial CD300f signaling in vivo reduces trophic support for neurons and/or the production of neurotoxic mediators.

The neurotoxicity is glia-dependent and mediated by soluble mediators

To unravel if the mechanism by which rCD300f-Fc promotes neurotoxicity is cell-type specific, we incubated hippocampal enriched neuronal or mixed glial cultures with rCD300f-IgG2a or control IgG2a for 72 h and analyzed cell viability using the MTT reduction method. rCD300f-IgG2a did not affect neuronal survival in neuron-enriched cultures compared to controls, however, it induced a significative increase in MTT reduction. It is now known that in viability assays, MTT is mainly reduced by the coenzyme NAD(P)H and glycolytic enzymes of the endoplasmic reticulum and therefore, cellular MTT reduction represents a measure of the rate of glycolytic NAD(P)H production[22]. Thus, our data suggest an increased metabolic activity in neurons treated with rCD300f-IgG2a. Moreover, it opens up the possibility that soluble CD300f may be interacting with an endogenous ligand expressed in neuronal surface (Fig. 3A). Moreover, treating mixed glial cultures with rCD300f-IgG2a or control IgG2a show no decrease in cell viability (Fig. 3B). To further understand the CD300f-dependent neuronal death mechanism, we analyzed whether a soluble factor secreted by glial cells or neurons could be mediating this process. Thus, we treated hippocampal enriched neuronal cultures with conditioned media derived from rCD300f-IgG1 (1.0 µg/ml) or control IgG1 (1.0 µg/ml)-treated cocultures and counted the number of surviving neurons 72 h after. We observed a strong toxic effect of the conditioned medium harvested after CD300f inhibition, with a 64 ± 11% decrease of neuronal cell number when compared to control IgG1 (Fig. 3C). Moreover, the toxicity was not mediated by a combination of the rCD300f-IgG1 to other basal components of the conditioned media, as neuronal enriched cultures showed no toxicity when incubated with control cocultures conditioned media containing fresh rCD300f-IgG1 (1.0 µg/ml, Fig. 3C). Surprisingly, the conditioned media derived from

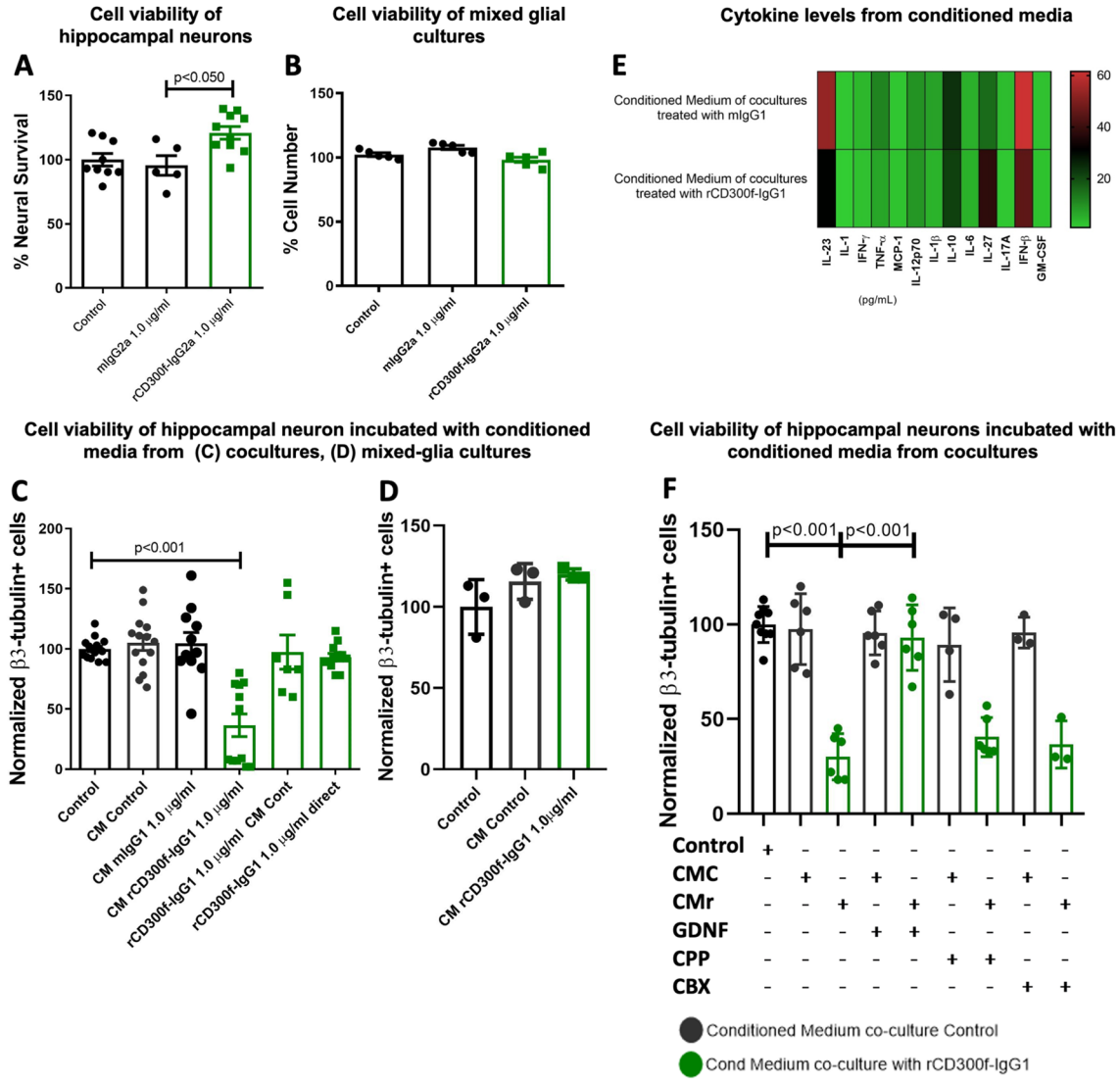

Figure 3. Conditioned media from high dose of CD300f-IgG-treated cocultures is neurotoxic. (**A**) Hippocampal enriched neuronal cultures were incubated with rCD300f-IgG2a or control IgG2a and neuronal viability was defined by MTT (two independent experiments were performed). (**B**) Mixed hippocampal glial cultures were incubated with rCD300f-IgG2a or control IgG2a and cellular viability was determinate by MTT (two independent experiments were performed). (**C**) Hippocampal enriched neuronal cultures were incubated with the conditioned media from cocultures treated with rCD300f-IgG1 (1.0 µg/ml) or control IgG1 (1.0 µg/ml), as additional controls we incubated neurons with control conditioned medium and fresh rCD300f-IgG1 (1.0 µg/ml), or fresh rCD300f-IgG1 (1.0 µg/ml) (three independent experiments were performed). (**D**) Hippocampal enriched neuronal cultures were incubated with mixed-glia conditioned media (one experiment is shown here where the conditioned media was neuron media, an additional experiment with glial media is shown in Suppl. Figure 3). (**E**) Cytokine levels were measured in conditioned media from glia cultures treated with rCD300f-IgG1 and from neuron-glia cocultures treated with IgG1 and rCD300f-IgG1. (**F**) Hippocampal enriched neuronal cultures were incubated with conditioned media from cocultures treated with rCD300f-IgG1 (1.0 µg/ml) or control IgG1 (1.0 µg/ml), and co-treated with glial-derived neurotrophic factor (GDNF, 1.0 ng/ml); NMDA glutamate receptor inhibitor 3-(2-Carboxypiperazin-4-yl)propyl-1-phosphonic acid (CPP, 100 µM), or GAP junction and connexin hemichannel inhibitor carbenoxolone (CBX, 100 µM) (two independent experiments were performed). Data show mean ± SEM; p corresponds to one way ANOVA followed by Tukey's test (**A**–**F**).

mixed glial cultures treated with rCD300f-IgG1 promotes no toxicity in neuronal enriched cultures related to the untreated control or IgG1 conditioned media (Fig. 3D and Suppl. Figure 3). Together, these results suggest that a more complex environment that includes neurons besides glial cells and soluble factors is important for the induction of the observed neurotoxicity, highlighting the role of neuron-glia interactions in this process.

CD300f immune receptor can negatively regulate proinflammatory activation of innate immune cells, including the activation of diverse Toll-like receptors[9]. We next analyzed whether inhibiting CD300f signaling would

induce a proinflammatory glial phenotype and thus neurotoxicity. Hence, cocultures were incubated with rCD300f-IgG1 (1.0 µg/ml) or control IgG1 (1.0 µg/ml) and the concentration of diverse cytokines was measured in culture media after 72 h by using the Biolegend LEGENDplexTM Mouse Inflammation Panel (13-plex). No significant alterations in IL23, IL1α, IL1β, IFNγ, IFNβ, TNFα, MCP1/CCL2, IL12p70, IL10, IL6, IL17A, IL27 and GM-CSF cytokine concentration was detected under these experimental conditions(Fig. 3E).

To further characterize the neurotoxic mechanism, we incubated enriched hippocampal neuronal cultures for 72 h with conditioned media from cocultures treated with rCD300f-IgG1 or control IgG1, and co-treated with: (i) glial-derived neurotrophic factor (GDNF, 1.0 ng/ml); (ii) NMDA glutamate receptor inhibitor 3-(2-Carboxypiperazin-4-yl) propyl-1-phosphonic acid (CPP, 100 µM), or (iii) GAP junction and connexin hemichannel inhibitor carbenoxolone (CBX, 100 µM). As expected, conditioned media derived from rCD300f-IgG1-treated cocultures promoted a 70 ± 12% or 69 ± 12% neuronal death when compared to controls (Fig. 3F). Interestingly, only GDNF was able to rescue neurotoxicity, showing no significant differences in neuronal survival compared with the one elicited by conditioned media from untreated or mIgG1-treated cocultures (Fig. 3F). These results suggest that soluble mediators such as glutamate or ATP are not involved in the neurotoxic mechanism, and thus other glial mediators such as toxic lipids or proteins could be modulating this process.

CD300f-IgG is not neurotoxic in CD300f$^{-/-}$ mice after a penetrating brain injury

Many CD300f ligands, such as phosphatidylserine, sphingomyelin or lipoproteins, are shared with other members of the CD300 family of immune receptors and with TREM2 immune receptor[23–25]. To address the question of whether the effects of rCD300f-Fc could be mediated by the inhibition of other immune receptors, CD300f$^{-/-}$ mice brains were injected intracortically with rCD300f-Fc (30 µg/ml) or control IgG (30 µg/ml) and the % of lesioned hemisphere was evaluated 72 h after by Nissl stain (Fig. 4A,B). As expected for a specific effect, while CD300f-IgG1 injection was neurotoxic for WT animals (70 ± 4% increased lesioned hemisphere when compared to control IgG1), no significant effect was observed by CD300f-IgG1 injection in CD300f$^{-/-}$ mice when compared to control IgG injection (Fig. 4C). Together, these data suggest that the neurotoxic effect induced by the fusion protein is indeed due to the inhibition of the endogenous CD300f receptor. Moreover, the intracortical injection of the control IgG1 or rCD300f-IgG1 into CD300f$^{-/-}$ mice showed a strong trend towards increasing the lesion volume when compared to WT mice injected with control IgGs (40 ± 4% increased lesioned hemisphere,

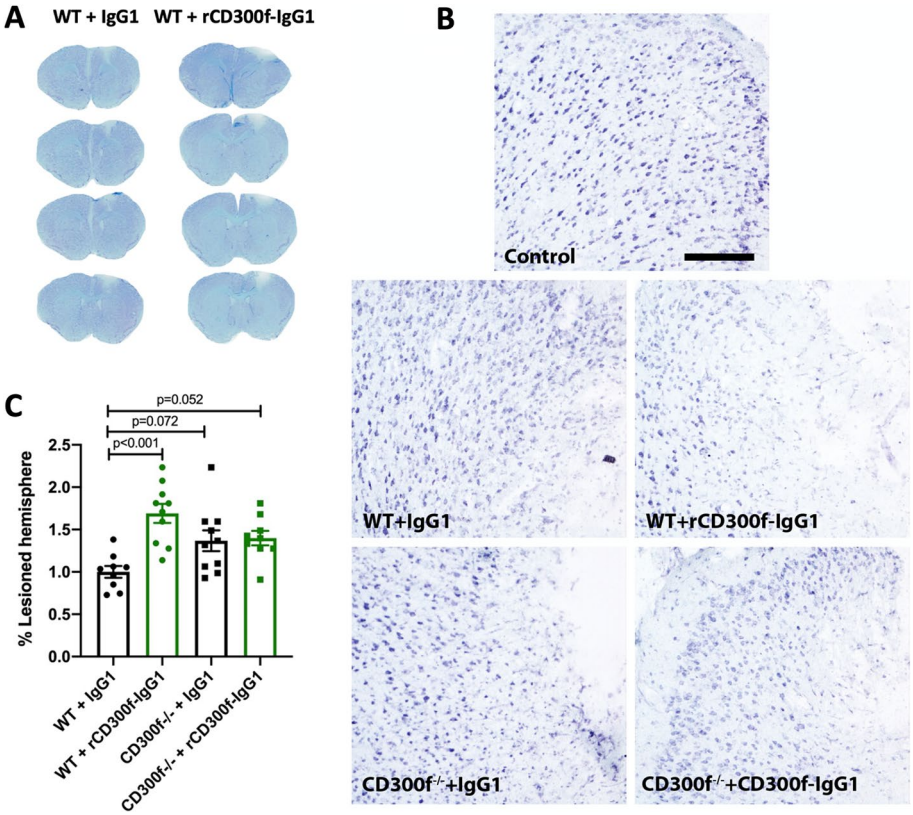

Figure 4. CD300f inhibition by rCD300f-Fc is specific. (**A**,**B**) Representative images of Nissl stained Sects. 72 h after WT or CD300f$^{-/-}$ animals were intracortically injected with IgG1 or rCD300f-IgG1 (Scale bar 200 µM). (**C**) Analysis of lesion volume was performed by Nissl staining 72 h after (WT injection of IgG1 n = 9, rCD300f-IgG1 n = 10, KO injection of IgG1 n = 10 and rCD300f-IgG1 n = 9). Two independent experiments were performed in different days including all treatments in each day. Data show mean ± SEM; p corresponds to one way ANOVA followed by Tukey's test.

$p = 0.072$ or 40 ± 3% increased lesioned hemisphere, $p = 0.052$ respectively) (Fig. 4C), suggesting that the absence of CD300f is neurotoxic after a penetrating brain injury.

Discussion

Here, we show that the CD300f immune receptor contributes to neuronal survival after a lesion by participating in glial-neuron interactions. Our data suggest that tonic microglial CD300f activation is necessary for maintaining healthy trophic interactions, and when disrupted, can trigger neurotoxic responses. In accordance, several lines of evidence suggest that tonic activation of TREM2 lipid-binding immune receptor also contributes to CNS homeostasis[1,26]. The tonic activation of CD300f and TREM2 lipid-binding immune receptors could be triggered by lipoprotein recognition, or myelin recycling structures. It still remains to be clarified which are the actual endogenous ligands under physiological conditions for these receptors.

Important lessons for understanding CD300f function may be learned from TREM2 biology, as both receptors share functions, part of their cell-type specific expression, they are putatively activated by similar ligands, and their signaling pathways are intermingled. In fact, CD300 immune receptors are the closest relatives to TREM receptors[1]. The spectrum of described ligands shared by TREM2 and CD300f include phospholipids and lipoproteins[8,27–30]. In particular, they recognize phospholipids such as phosphatidylserine and sphingomyelin that will contribute to sense and phagocytose apoptotic cells, and cellular debris such as myelin debris. TREM2 also recognizes Aβ, and though not clearly demonstrated, this could also be the case for CD300f and its closest relative CD300b, as they were found to interact with Aβ in an unbiased screening study using protein arrays[31]. In this way, these receptors may act as pathogen-associated molecular patterns (PAMP's) or damage-associated molecular patterns (DAMP's) receptors, enabling innate immune cells to rapidly recognize tissue damage or extracellular misfolded proteins that triggers interconnected signaling pathways contributing to microglial and barrier macrophage sensing of the surrounding events occurring in the CNS parenchyma (reviewed in[32]).

Though sharing similar phospholipid ligands, other molecules may act as co-ligands conferring specificity for different lipid-binding immune receptors. Staining cells with TREM2-Fc or CD300f-Fc fusion proteins show that many, but not all live cells, display ligands for these receptors despite abundant phospholipids ligands such as sphingomyelin exposed in the surface of all cells. Moreover, the staining of cells with CD300f-Fc show a patched profile highlighting specific cell surface domains where the ligands are exposed[11]. Taken together, these observations open the possibility that other molecules apart from the phospholipids, such as proteins, may act as co-receptors with phospholipids generating and additional level of complexity and specificity. We show here that, while the in vivo injection of rCD300f-Fc into WT brain induces an increase in lesion volume when compared to control IgGs, there is a similar lesion volume after the injection of rCD300f-Fc or control IgGs into CD300f$^{-/-}$ brains. This denotes that while the rCD300f-Fc protein inhibits the endogenous CD300f-ligand interactions in WT brains, it does not affect the CD300f$^{-/-}$ brain. More importantly, the lack of effects of rCD300f-Fc in CD300f$^{-/-}$ brains evidences that, though CD300f may share lipid ligands with other lipid-binding receptors, it possesses additional ligands that confer specific activation of this receptor. The lack of in vivo effect of the rCD300f-Fc fusion protein in CD300f$^{-/-}$ brain also ensures that the fusion protein is a specific tool for blocking CD300f-ligand interactions. Finally, the injection of control IgGs or rCD300f-Fc into CD300f$^{-/-}$ brains showed an increased lesion volume when compared to the injection of control IgGs into WT brains, confirming that indeed CD300f signaling deficiency induces enhanced neurotoxicity in vivo.

The inhibition of microglial CD300f-induced neurotoxicity, which was dependent on the presence of both neurons and glial cells, was mediated by soluble factors, and could be reversed by GDNF treatment. Thus, inhibiting microglial CD300f signaling could lead to a proinflammatory state toxic for cocultured neurons. In this sense, it has been shown that CD300f regulates microglial immunometabolic phenotype, being necessary for boosting its metabolism in response to inflammatory stimuli[7]. CD300f$^{-/-}$ mice showed increased depressive-like behaviors, that were potentiated by systemic and CNS inflammation induced by intraperitoneal LPS injection[7]. Depression has been shown to be induced under inflammatory conditions, and CD300f has been show to dampen inflammatory reactions in different systemic conditions[8,13,33]. Thus, CD300f$^{-/-}$ mice could display depressive-like behaviors due to low-grade CNS inflammation induced by the release of the negative signaling brake. However, only minor inflammatory profile of the brain or isolated microglial cells were altered in CD300f$^{-/-}$ mice[7]. Accordingly, the neurotoxicity observed after CD300f inhibition was not mediated by an increased proinflammatory cytokine release. We also showed that the underlying toxic mechanisms do not involve NMDA-dependent excitotoxicity, nor extracellular ATP-dependent toxicity. Regarding the cell-type responsible for neurotoxicity, as CD300f is only expressed in microglia and barrier macrophages in the CNS and mostly by myeloid cells in the periphery[5], it may be exerted directly by CD300f-expressing microglia and/or recruited macrophages or neutrophils after the penetrating brain injury. However, in cocultures, the CD300f-dependent neurotoxicity seems to be dependent on microglial cells, as they are the only CD300f-expressing cells in this experimental conditions[34,35]. Alternatively, CD300f inhibition may affect microglia-dependent protective mechanisms, as has been shown in vitro and after CNS lesions, where a TREM2-dependent microglial scavenging of toxic lipids such as oxidated phosphatidylcholine occurs[36]. Based on their ligand similarities, CD300f could putatively also scavenge oxidated phosphatidylcholine after the penetrating brain injury, while the inhibition of this process would potentiate neurotoxicity. Moreover, microglia can induce an astrocyte neurotoxic phenotype, a toxicity that is maintained in astrocyte conditioned media[37]. This effect was later found to be dependent on toxic long-chain saturated free fatty acids associated to APOE and APOJ lipoproteins[38]. Astrocytes have also been shown to be capable of inducing neurotoxic responses by producing reactive oxygen and nitrogen species[39], however these species are not stable in conditioned media and thus not responsible of the neurotoxic effect. Further studies will be needed for the identification of the toxic components involved in this process and the cell type that produce them.

Most immune receptors such as TREM1, CD200R, TREM2, and CD300f display soluble forms. A major source of soluble forms is the translation of an alternatively spliced transcript that lacks the transmembrane domain, and this is the case for both human and mouse CD300f[5,10]. However, proteolytic cleavage of surface-expressed immune receptors by matrix metalloproteases may also contribute to soluble forms production[1]. Evidence shows that the cleavage of cell surface immune receptors terminates their signaling, and reflects their activation level in vivo. Moreover, soluble forms may have their own functions, such as scavenging ligands and further restraining immune receptor activation, or even activating yet unknown receptors. For instance, soluble CD300b activates TLR4[40]. In addition, a beneficial effect has been reported after soluble TREM2 brain injection or overexpression in an Aβ pathology mice model[41]. Human longitudinal studies of Alzheimer's disease patients show that a higher CSF soluble TREM2 levels predicts slower cognitive decline and attenuated amyloid and tau signal in positron-emission tomography[42,43]. This is in contrast with the neurotoxic effects of soluble CD300f injection into normal mouse and rat brain reported here, suggesting that in spite of all the similarities between these two immune receptors they may also have their particularities.

Taken together, the results presented here and previous results related to CD300f[7,10,35], as well as the extensive work of other colleagues on CD200R1/CD200[44,45], TREM2[1], and Siglec[46,47] receptors support the notion that immune receptors contribute to restoring nervous system homeostasis after a lesion or under chronic neurodegenerative conditions, and constitute key regulators of microglial phenotype. Importantly, we also show evidences that, though lipid-binding immune receptors share many lipidic ligands, there are additional conditions or co-ligands that confer different specificities.

Data availability

All data will be available upon request to Hugo Peluffo.

Received: 30 July 2023; Accepted: 28 September 2023
Published online: 05 October 2023

References

1. Colonna, M. The biology of TREM receptors. *Nat. Rev. Immunol.* https://doi.org/10.1038/s41577-023-00837-1 (2023).
2. Borrego, F. The CD300 molecules: An emerging family of regulators of the immune system. *Blood* **121**, 1951–1960 (2013).
3. Clark, G. J. *et al.* The CD300 molecules regulate monocyte and dendritic cell functions. *Immunobiology* **214**, 730–736 (2009).
4. Nielsen, R. *et al.* A scan for positively selected genes in the genomes of humans and Chimpanzees. *PLoS Biol.* **3**, e170 (2005).
5. Alvarez-Errico, D. *et al.* IREM-1 is a novel inhibitory receptor expressed by myeloid cells. *Eur. J. Immunol.* **34**, 3690–3701 (2004).
6. Alvarez-Errico, D., Sayos, J. & Lopez-Botet, M. The IREM-1 (CD300f) inhibitory receptor associates with the p85alpha subunit of phosphoinositide 3-kinase. *J. Immunol.* **178**, 808–816 (2007).
7. Lago, N. *et al.* CD300f immunoreceptor is associated with major depressive disorder and decreased microglial metabolic fitness. *Proc. Natl. Acad. Sci. USA* **117**, 6651–6662 (2020).
8. Izawa, K. *et al.* The receptor LMIR3 negatively regulates mast cell activation and allergic responses by binding to extracellular ceramide. *Immunity* **37**, 827–839 (2012).
9. Lee, S. *et al.* CD300F Blocks Both MyD88 and TRIF-Mediated TLR Signaling through Activation of Src Homology Region 2 Domain-Containing Phosphatase 1. *J. Immunol.* https://doi.org/10.4049/jimmunol.1002184 (2011).
10. Ejarque-Ortiz, A. *et al.* The receptor CMRF35-like molecule-1 (CLM-1) enhances the production of LPS-induced pro-inflammatory mediators during microglial activation. *PLoS One* **10**, e0123928 (2015).
11. Peluffo, H. *et al.* Overexpression of the immunoreceptor CD300F has a neuroprotective role in a model of acute brain injury. *Brain Pathol.* **22**, 318–328 (2012).
12. Ising, C. *et al.* NLRP3 inflammasome activation drives tau pathology. *Nature* https://doi.org/10.1038/s41586-019-1769-z (2019).
13. Xi, H. *et al.* Negative regulation of autoimmune demyelination by the inhibitory receptor CLM-1. *J Exp Med* **207**, 7–16 (2010).
14. Bennett, M. L. *et al.* New tools for studying microglia in the mouse and human CNS. *Proc. Natl. Acad. Sci* https://doi.org/10.1073/pnas.1525528113 (2016).
15. Torres-Espin, A., Hernandez, J. & Navarro, X. Gene expression changes in the injured spinal cord following transplantation of mesenchymal stem cells or olfactory ensheathing cells. *PLoS One* **8**, e76141 (2013).
16. Lloyd, A. F. *et al.* Central nervous system regeneration is driven by microglia necroptosis and repopulation. *Nat. Neurosci.* https://doi.org/10.1038/s41593-019-0418-z (2019).
17. Peluffo, H. *et al.* CD300f immunoreceptor contributes to peripheral nerve regeneration by the modulation of macrophage inflammatory phenotype. *J. Neuroinflammation* **12**, 1–5 (2015).
18. Kaufmann, F. N. *et al.* Sex-dependent role of CD300f immune receptor in generalized anxiety disorder. *Brain Behav. Immun. Heal.* **11**, 100191 (2021).
19. Vitureira, N., Letellier, M., White, I. J. & Goda, Y. Differential control of presynaptic efficacy by postsynaptic N-cadherin and beta-catenin. *Nat. Neurosci.* **15**, 81–89 (2012).
20. Vitureira, N., Letellier, M., White, I. J. & Goda, Y. Differential control of presynaptic efficacy by postsynaptic N-cadherin and b -catenin. *Nat. Neurosci.* **15**, 81–89 (2011).
21. Clark, M. R. IgG effector mechanisms. in *Antibody Engineering* (ed. Capra, J.) 88–110 (Karger, 1997).
22. Stockert, J. C., Horobin, R. W., Colombo, L. L. & Blázquez-Castro, A. Tetrazolium salts and formazan products in cell biology: Viability assessment, fluorescence imaging, and labeling perspectives. *Acta Histochem.* **120**, 159–167 (2018).
23. Choi, S. *et al.* Cutting edge: Mouse CD300f (CMRF-35–Like Molecule-1) recognizes outer membrane-exposed phosphatidylserine and can promote phagocytosis. *J. Immunol.* **187**, 3483–3487 (2011).
24. Wang, Y. *et al.* TREM2 lipid sensing sustains the microglial response in an Alzheimer ' s disease model article TREM2 lipid sensing sustains the microglial response in an Alzheimer ' s Disease model. *Cell* **160**, 1061–1071 (2015).
25. Izawa, K. *et al.* Sphingomyelin and ceramide are physiological ligands for human LMIR3/CD300f, inhibiting FcepsilonRI-mediated mast cell activation. *J. Allergy Clin. Immunol.* **133**, 270–277 (2014).
26. Ulland, T. K. *et al.* TREM2 maintains microglial metabolic fitness in Alzheimer's disease. *Cell* **170**, 649-663.e13 (2017).
27. Atagi, Y. *et al.* Apolipoprotein E is a ligand for triggering receptor expressed on myeloid cells 2 (TREM2). *J. Biol. Chem.* **290**, 26043–26050 (2015).
28. Daws, M. R. *et al.* Pattern recognition by TREM-2: Binding of anionic ligands. *J. Immunol.* **171**, 594–599 (2003).
29. Wang, Y. *et al.* TREM2 lipid sensing sustains the microglial response in an Alzheimer's disease model. *Cell* **160**, 1061–1071 (2015).
30. Choi, S. C. *et al.* Cutting edge: Mouse CD300f (CMRF-35-like molecule-1) recognizes outer membrane-exposed phosphatidylserine and can promote phagocytosis. *J. Immunol.* **187**, 3483–3487 (2011).

31. Bozso, Z., Hlavanda, E. & Magyar, A. Interactions of pathological hallmark. *Proteins* **286**, 34088–34100 (2011).
32. Kober, D. L. & Brett, T. J. TREM2-ligand interactions in health and disease. *J. Mol. Biol.* **429**, 1607–1629 (2017).
33. Shiba, E. *et al.* Ceramide-CD300f binding inhibits lipopolysaccharide-induced skin inflammation. *J. Biol. Chem.* **292**, 2924–2932 (2017).
34. Zhang, Y. *et al.* An RNA-sequencing transcriptome and splicing database of glia, neurons, and vascular cells of the cerebral cortex. *J. Neurosci.* **34**, 11929–11947 (2014).
35. Peluffo, H. *et al.* Overexpression of the immunoreceptor CD300f has a neuroprotective role in a model of acute brain injury. *Brain Pathol.* **22**, 318–328 (2011).
36. Dong, Y. *et al.* Oxidized phosphatidylcholines found in multiple sclerosis lesions mediate neurodegeneration and are neutralized by microglia. *Nat. Neurosci.* **24**, 489–503 (2021).
37. Liddelow, S. A. *et al.* Neurotoxic reactive astrocytes are induced by activated microglia. *Nat. Publ. Gr.* https://doi.org/10.1038/nature21029 (2017).
38. Guttenplan, K. A. *et al.* Neurotoxic reactive astrocytes induce cell death via saturated lipids. *Nature* **599**, 102–107 (2021).
39. Cassina, P. *et al.* Peroxynitrite triggers a phenotypic transformation in spinal cord astrocytes that induces motor neuron apoptosis. *J. Neurosci. Res.* **67**, 21–29 (2002).
40. Phongsisay, V., Hara, H. & Yamasaki, S. LMIR5 extracellular domain activates myeloid cells through Toll-like receptor 4. *Mol. Immunol.* **62**, 169–177 (2014).
41. Zhong, L. *et al.* Soluble TREM2 ameliorates pathological phenotypes by modulating microglial functions in an Alzheimer's disease model. *Nat. Commun.* **10**, 1–16 (2019).
42. Morenas-Rodríguez, E. *et al.* Soluble TREM2 in CSF and its association with other biomarkers and cognition in autosomal-dominant Alzheimer's disease: A longitudinal observational study. *Lancet Neurol.* **21**, 329–341 (2022).
43. Ewers, M. *et al.* Increased soluble TREM2 in cerebrospinal fluid is associated with reduced cognitive and clinical decline in Alzheimer's disease. *Sci. Transl. Med.* **11**, eaav6221 (2019).
44. Hoek, R. M. *et al.* Down-regulation of the macrophage lineage through interaction with OX2 (CD200). *Science (80-)* **290**, 1768–1771 (2000).
45. Lago, N., Pannunzio, B., Amo-Aparicio, J., López-Vales, R. & Peluffo, H. CD200 modulates spinal cord injury neuroinflammation and outcome through CD200R1. *Brain. Behav. Immun.* **73**, 416–426 (2018).
46. Schwarz, F. *et al.* Siglec receptors impact mammalian lifespan by modulating oxidative stress. *Elife* **4**, e06184 (2015).
47. Wang, Y. & Neumann, H. Alleviation of neurotoxicity by microglial human Siglec-11. *J. Neurosci.* **30**, 3482–3488 (2010).

Acknowledgements

We thank Florencia Fontes and Mariela Santos (URBE) from the Facultad de Medicina UDELAR, and the personnel from the Unidad de Biotecnología Animal (UBAL) and from the Unidad de Bioimagenología Avanzada (UBA) from the Institut Pasteur de Montevideo.

Author contributions

DAR performed most of the experiments, analyzed data and contributed to drafting the manuscript. NV performed some experiments, analyzed data and contributed to drafting the manuscript. HP performed some experiments, analyzed data and drafted the original manuscript.

Funding

This work has been supported by grants from Comisión Sectorial de Investigación Científica (CSIC-UDELAR I + D 2020 ID 184), Uruguay; PEDECIBA, Uruguay; FOCEM (MERCOSUR Structural Convergence Fund), COF 03/1111; Banco de Seguros del Estado (BSE), Uruguay; PID2021-123272OB-I0/Financiado por MCIN/AEI/10.13039/501100011033/ y por FEDER Una manera de hacer Europa, and International Centre for Genetic Engineering and Biotechnology (ICGEB, CRP/URY19-01).

Competing interests

The authors declare no competing interests.

Additional information

Supplementary Information The online version contains supplementary material available at https://doi.org/10.1038/s41598-023-43840-1.

Correspondence and requests for materials should be addressed to H.P.

Reprints and permissions information is available at www.nature.com/reprints.

Publisher's note Springer Nature remains neutral with regard to jurisdictional claims in published maps and institutional affiliations.

Cell Reports

Article

CD300f immune receptor contributes to healthy aging by regulating inflammaging, metabolism, and cognitive decline

Graphical abstract

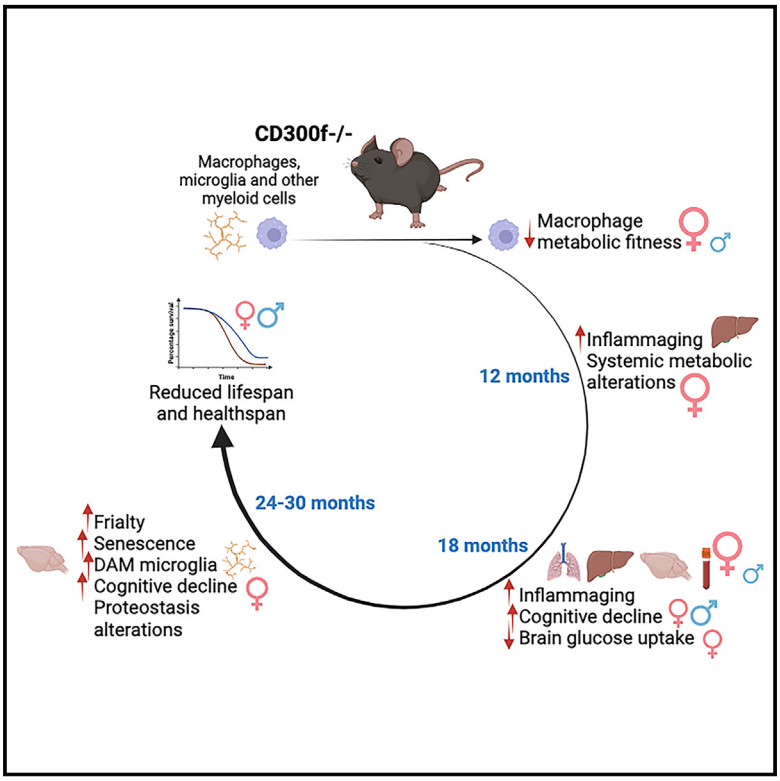

Highlights

- CD300f$^{-/-}$ mice show reduced lifespan, but no specific cause of death is identified
- This is associated with inflammaging, senescence, frailty, and cognitive decline
- CD300f$^{-/-}$ mice exhibit microglial aging states and sex-dependent metabolic changes
- Absence of CD300f reduces macrophage immunometabolic fitness in a sex-dependent way

Authors

Frances Evans, Daniela Alí-Ruiz, Natalia Rego, ..., Cristina Malagelada, Carlos Escande, Hugo Peluffo

Correspondence

hugo.peluffo@ub.edu

In brief

Evans et al. report that the absence of CD300f myeloid cell immune receptor in male and female mice induces a reduced lifespan. Animals display diverse aged-related conditions such as inflammaging, frailty, cognitive decline, brain senescence markers, microglial aging phenotypes, and reduced macrophage metabolic fitness, as well as sex-dependent metabolic alterations.

Evans et al., 2023, Cell Reports *42*, 113269
October 31, 2023
https://doi.org/10.1016/j.celrep.2023.113269

CellPress

Cell Reports

CellPress
OPEN ACCESS

Article

CD300f immune receptor contributes to healthy aging by regulating inflammaging, metabolism, and cognitive decline

Frances Evans,[1,2] Daniela Alí-Ruiz,[2] Natalia Rego,[3,4] María Luciana Negro-Demontel,[1,2] Natalia Lago,[2] Fabio Andrés Cawen,[2] Bruno Pannunzio,[1,2] Paula Sanchez-Molina,[5] Laura Reyes,[6] Andrea Paolino,[6] Jorge Rodríguez-Duarte,[7] Valentina Pérez-Torrado,[8] Almudena Chicote-González,[9,10] Celia Quijano,[11] Inés Marmisolle,[11] Ana Paula Mulet,[12] Geraldine Schlapp,[12] María Noel Meikle,[12] Mariana Bresque,[8] Martina Crispo,[12] Eduardo Savio,[6] Cristina Malagelada,[9,10] Carlos Escande,[8] and Hugo Peluffo[1,2,9,10,13,*]

[1]Department of Histology and Embryology, Faculty of Medicine, UDELAR, Montevideo, Uruguay
[2]Neuroinflammation and Gene Therapy Laboratory, Institut Pasteur de Montevideo, Montevideo, Uruguay
[3]Bioinformatics Unit, Institut Pasteur de Montevideo, Montevideo, Uruguay
[4]Faculty of Sciences, UDELAR, Montevideo, Uruguay
[5]Department of Cell Biology, Physiology and Immunology, and Institute of Neuroscience, Universitat Autònoma de Barcelona, Barcelona, Spain
[6]Uruguayan Center for Molecular Imaging (CUDIM), Montevideo, Uruguay
[7]Laboratory of Vascular Biology and Drug Development, INDICYO Program, Institut Pasteur Montevideo, Montevideo, Uruguay
[8]Metabolic Diseases and Aging Laboratory, INDICYO Program, Institut Pasteur de Montevideo, Montevideo, Uruguay
[9]Unitat de Bioquímica i Biologia Molecular, Departament de Biomedicina, Facultat de Medicina i Ciencies de la Salut, Universitat de Barcelona (UB), Barcelona, Spain
[10]Institut de Neurociències, Universitat de Barcelona (UB), Barcelona, Spain
[11]Departamento de Bioquímica y Centro de Investigaciones Biomédicas (CEINBIO), Facultad de Medicina, Universidad de la República, Montevideo, Uruguay
[12]Unidad de Biotecnología en Animales de Laboratorio, Institut Pasteur de Montevideo, Montevideo, Uruguay
[13]Lead contact
*Correspondence: hugo.peluffo@ub.edu
https://doi.org/10.1016/j.celrep.2023.113269

SUMMARY

Emerging evidence suggests that immune receptors may participate in many aging-related processes such as energy metabolism, inflammation, and cognitive decline. CD300f, a TREM2-like lipid-sensing immune receptor, is an exceptional receptor as it integrates activating and inhibitory cell-signaling pathways that modulate inflammation, efferocytosis, and microglial metabolic fitness. We hypothesize that CD300f can regulate systemic aging-related processes and ultimately healthy lifespan. We closely followed several cohorts of two strains of CD300f$^{-/-}$ and WT mice of both sexes for 30 months and observed an important reduction in lifespan and healthspan in knockout mice. This was associated with systemic inflammaging, increased cognitive decline, reduced brain glucose uptake observed by ^{18}FDG PET scans, enrichment in microglial aging/neurodegeneration phenotypes, proteostasis alterations, senescence, increased frailty, and sex-dependent systemic metabolic changes. Moreover, the absence of CD300f altered macrophage immunometabolic phenotype. Taken together, we provide strong evidence suggesting that myeloid cell CD300f immune receptor contributes to healthy aging.

INTRODUCTION

Aging is a multifactorial process that includes the lifelong accumulation of molecular damage, leading to age-related frailty, disability, and disease, and eventually death. Macrophages occupy multiple tissue niches and support tissue development, maintain homeostasis, and respond to invading pathogens. However, dysregulation of their functions can promote pathological processes including inflammatory diseases, cancer, fibrosis, and impaired tissue repair, all processes strongly associated with aging.[1,2] Emerging evidence suggests that microglia/macrophage immune receptors are involved in many aging-related processes such as energy metabolism, inflammation, and cognitive decline.[3,4] One canonical example is TREM2 lipid-sensing immune receptor, a key regulator of microglial phenotype strongly related to Alzheimer's disease (AD),[4,5] and also involved in adipose tissue and hepatic metabolism and control of inflammation.[1,6] CD300f is another lipid-sensing immune receptor that shares many properties with TREM2 including most of its ligands (i.e., phospholipids and

lipoproteins, among others), its expression pattern in microglia/macrophages (although CD300f is also present in other myeloid cells), its involvement in the regulation of microglia/macrophage phenotype and metabolic fitness,[7] and participation in phagocytic apoptotic cell clearance and synaptic pruning machinery.[7,8] In addition, due to their lipid-binding capacity, it has been proposed that TREM2, and putatively CD300f, may sense tissue damage by acting as damage-associated molecular pattern (DAMP) receptors.[9] CD300f is an exceptional immune receptor as it triggers activating and inhibitory intracellular cell-signaling pathways,[10,11] and indirectly modulates DAP12/TYROBP.[12] Most studies regarding the function of CD300f have shown that it has a protective and anti-inflammatory profile in mice models of multiple sclerosis,[13] lupus,[8,14] allergy,[15] or acute brain damage.[16] However, CD300f activation potentiated microglial proinflammatory profile when these cultures were stimulated with LPS.[17] Moreover, no changes in major proinflammatory signaling molecules were observed in CD300f$^{-/-}$ microglia *in vivo* after LPS intraperitoneal challenge,[7] suggesting complex roles of this immune receptor in the regulation of inflammation. CD300f is among the most upregulated genes in brain microglia/macrophages after several proinflammatory insults such as intraperitoneal LPS injection[7,18] or spinal cord injury,[19] and its upregulation has been associated to promyelinating microglia after demyelinating stimuli[20] and to the neuroprotective response against Tau pathology.[21] Genetic variants of CD300f have also been shown to be involved in human inflammatory and autoimmune disease susceptibility.[7,22,23] Interestingly, CD300f has also been associated to non-classical inflammatory functions of microglial and potentially CNS barrier-associated macrophages (BAMs), leading to modulation of neuropsychiatric conditions such as major depressive disorder and anxiety.[7,24]

Despite all this evidence implicating CD300f in different conditions associated with aging, no one has explored its role in age-dependent accumulation of tissue damage, age-related frailty, disability, and eventually reduced lifespan. Several additional lines of evidence implicate immune receptors in aging. One interesting report showed that the absence of the SiglecE inhibitory immune receptor shortened mice lifespan and was associated to several aging-related conditions.[3] Most of these immune receptors, including CD300f and TREM2 are upregulated with age.[25] Aging induces microglial and macrophage metabolic alterations that contribute to cognitive decline,[26] and both TREM2 and CD300f have been shown to be essential for maintaining microglial and macrophage metabolic fitness under different neuropathological conditions.[7,27] Moreover, most AD-associated genes are involved in phagocytosis/lysosomal pathways,[4] where these lipid binding immune receptors play a central role. Finally, analysis of genomic non-coding regions in AD also points toward microglia, BAMs, or other tissue-resident macrophages as central players,[28,29] again linking these cell types and their phenotype to age-related conditions. Taken together, the above reports put forward the question of whether immune receptors expressed on myeloid cells, and in particular CD300f, can regulate systemic aging-related processes such as metabolism, inflammation, neurodegeneration, and cognitive decline, and ultimately healthy lifespan.

RESULTS

CD300f regulates mice lifespan

Emerging evidence suggests that immune receptors could influence lifespan and aging-associated processes.[3] To explore this hypothesis, we aged CD300f$^{-/-}$ and wild-type (WT) mice and followed them closely for 30 months. Strikingly, CD300f$^{-/-}$ mice showed an important reduction in lifespan (Figure 1A). This effect was observed in three different cohorts, in two different animal facilities (Figures S1A and S1B), and was independent of sex (Figures S1C and S1D). To confirm this finding, we generated a new CD300f-deficient mouse line (CD300f$^{-/-IPMon}$), which also showed a similar reduction in lifespan (Figure 1B). It has been found that exposure of mice maintained under specific pathogen free (SPF) conditions to multiple mouse pathogens matures their immune system, which more closely resembles that seen in adult humans.[30] Interestingly, the reduced lifespan of CD300f$^{-/-}$ mice was observed both under SPF conditions (Figure S1B) and in a closer to real-life housing/immunologic environment (UDELAR animal facility, see materials and methods and Figure S1A).

Although a decreased lifespan was observed, no alterations were detected during aging between WT and CD300f$^{-/-}$ mice in body weight (Figures 1C and S1E) or in spontaneous locomotor activity (Figure 1D). The most common natural cause of age-related deaths in a wide range of mouse strains is cancer.[31] A similar frequency of neoplasms was observed macroscopically in WT and CD300f$^{-/-}$ mice (Figure 1E). However, we noted that CD300f$^{-/-}$ female mice tended to show increased incidence and size of tumors at the base of the skull reminiscent of pituitary tumors, a common aged-related pathology[31] (Figure S1F). To quantify this, we performed qPCR of several pituitary hormone genes from brain samples. Strongly increased mRNA levels for growth hormone (*hg*) and prolactin (*prl*) were observed in female CD300f$^{-/-}$ mice at age 30 months when compared with adult WT or CD300f$^{-/-}$ mice and aged-matched WT mice (Figure S1G). It has been shown that 18-month-old CD300f$^{-/-}$ mice are prone to develop autoimmune disease and splenomegaly only if stimulated with pristane and apoptotic cells.[8] Accordingly, we could not detect significant differences in spleen weight until age 30 months or in euthanized female (Figure 1F) or male (Figure S1H) mice, although CD300f$^{-/-}$ female mice displayed a strong tendency ($p = 0.077$) to show splenomegaly at 18 months, earlier than aged WT mice. Moreover, some WT and CD300f$^{-/-}$ mice that had to be euthanized due to ethical endpoint criteria showed splenomegaly (Figure 1F). We did not find alterations in most hepatic/renal clinical plasma markers (Table S1) or in many rutinary clinical blood parameters (Table S1). However, CD300f$^{-/-}$ aged females that had to be euthanized showed increased levels of gamma-glutamyl transferase (GGT) (Figure 1G), and elevated plasma levels of this enzyme have been significantly associated with all-cause mortality.[32] We found an important dispersion of the data with aging, a common finding in aging studies that reflect interindividual differences due to chronological age not matching biological age for each subject. For instance, some euthanized animals showed increased plasmatic alanine amino transferase (ALT), suggestive of hepatic damage (Figure 1H), and some showed reduced basal glycemia under *ad libitum* feeding (Figure 1I). In addition, some

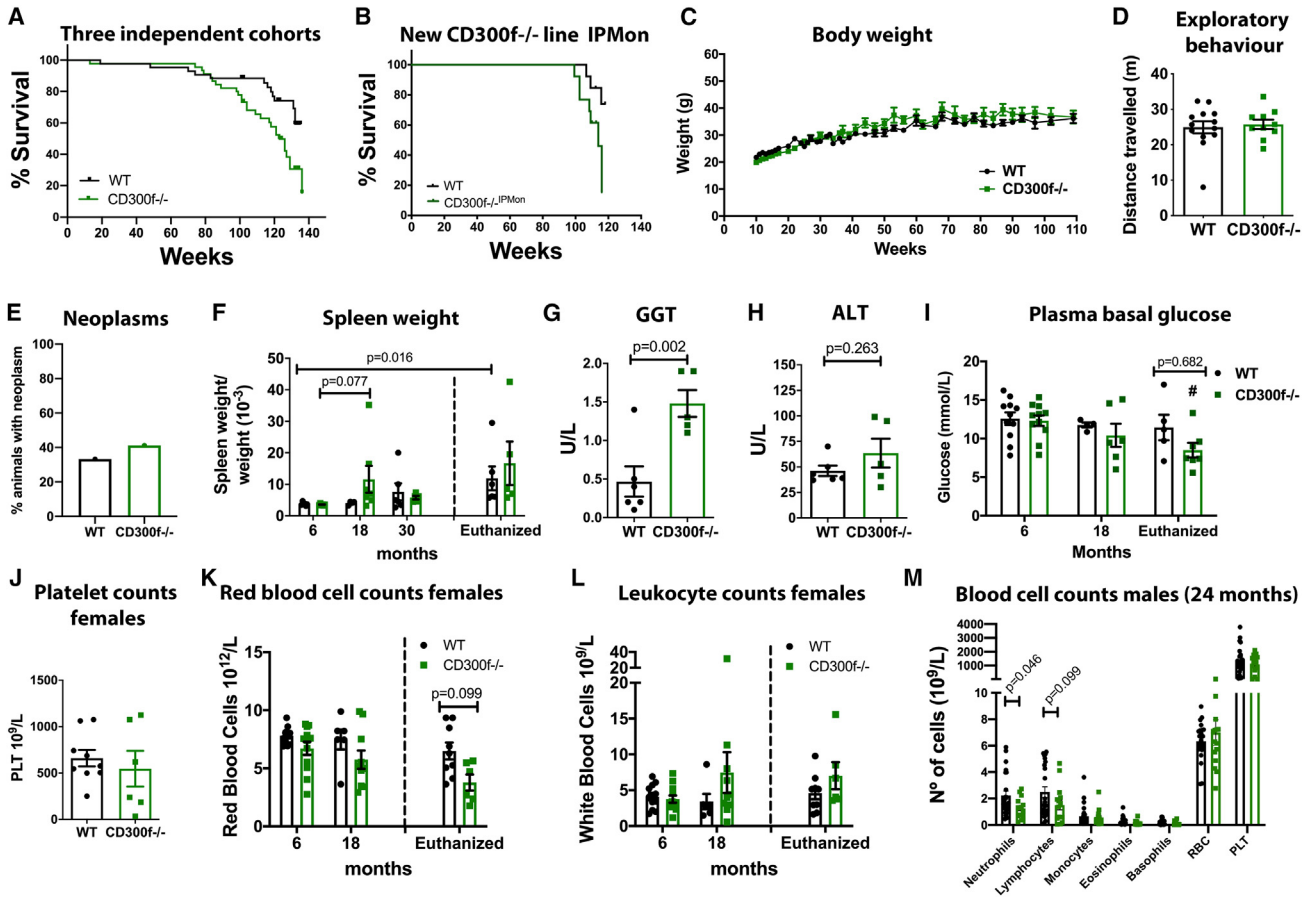

Figure 1. Absence of CD300f reduces lifespan

The lifespan of CD300f$^{-/-}$ and WT animals were followed for 30 months (A) (WT n = 57 and CD300f$^{-/-}$ n = 65, housed at IPMon and UDELAR, log rank Mantel-Cox test, p = 0.0008, median lifespan CD300f$^{-/-}$ 121 weeks) in three independent cohorts (A) and of a new CD300f$^{-/-IPMon}$ line generated (B) (WT n = 13 and CD300f$^{-/-IPMon}$ n = 13 all males, housed in UDELAR, log rank Mantel-Cox test, p = 0.047, median lifespan CD300f$^{-/-}$ 114 weeks). Body weight (males and females) (C). Twenty-five-month-old male and female exploratory behavior in the open field test (D). Percentage of animals with evident neoplasms when euthanized (E) (WT n = 18, CD300f$^{-/-}$ n = 17, lifespan until age 24 months). Relative spleen weight of female mice at the indicated ages (F). Plasma levels of GGT (G) and ALT (H) enzymes, and of platelets (J) in euthanized female mice. Female mice basal glycemia under *ad libitum* feeding at different ages or in female mice that were euthanized (I) (#p = 0.055 and p = 0.090 compared with 6-month-old adult WT or CD300f$^{-/-}$, two-way ANOVA p = 0.049 for age and p = 0.094 for genotype). Blood cell populations in females (K and L) and males (M) (30 months old).

18-month-old and euthanized females showed an important decrease in platelet counts (Figure 1J; Table S1). Also, some 18-month-old and euthanized CD300f$^{-/-}$ females showed anemia (Figure 1K; Table S1) and increased leukocyte counts (Figure 1L; Table S1), while 30-month-old males showed different alterations in white blood cell counts (Figure 1M; Table S1). Taken together, these data show that CD300f$^{-/-}$ mice have a decreased lifespan, and that the underlying cause of death is probably multifactorial and variable depending of the subject, as would be expected for aging.

Absence of CD300f induces inflammaging and systemic metabolic alterations

Chronic low-grade inflammation or inflammaging is a key aspect of aging that contributes to the pathogenesis of age-related diseases.[33] CD300f has been shown to be important to limit the severity of inflammatory conditions by negatively regulating the innate immune system.[10,13,15] To explore the hypothesis that CD300f may contribute to dampen the systemic low-grade inflammation that accumulates during aging, we aged CD300f$^{-/-}$ mice and explored the immune cell infiltration and expression of inflammatory markers in several tissues and plasma. Aging induced widespread inflammaging at 18 months as observed by increased plasma IL-1β, IL-1α, and IL-6 protein levels (Figure 2A) and increased mRNA for *il1β* in lungs (Figure 2B). Cytokines such as TNF-α, INF-β, and INF-γ, among other plasma cytokines measured, did not show significant changes (Figure S2A). Moreover, age-dependent liver accumulation of immune infiltrates in WT animals was observed as described previously (Figures 2C and 2D), a process that was increased in CD300f$^{-/-}$ mice (Figures 2C and 2D). These data are in accordance with the aging-associated accumulation of eosinophils in the adipose tissue at 5–8 months in CD300f$^{-/-}$ mice.[34] The hepatic infiltrates were more pronounced in

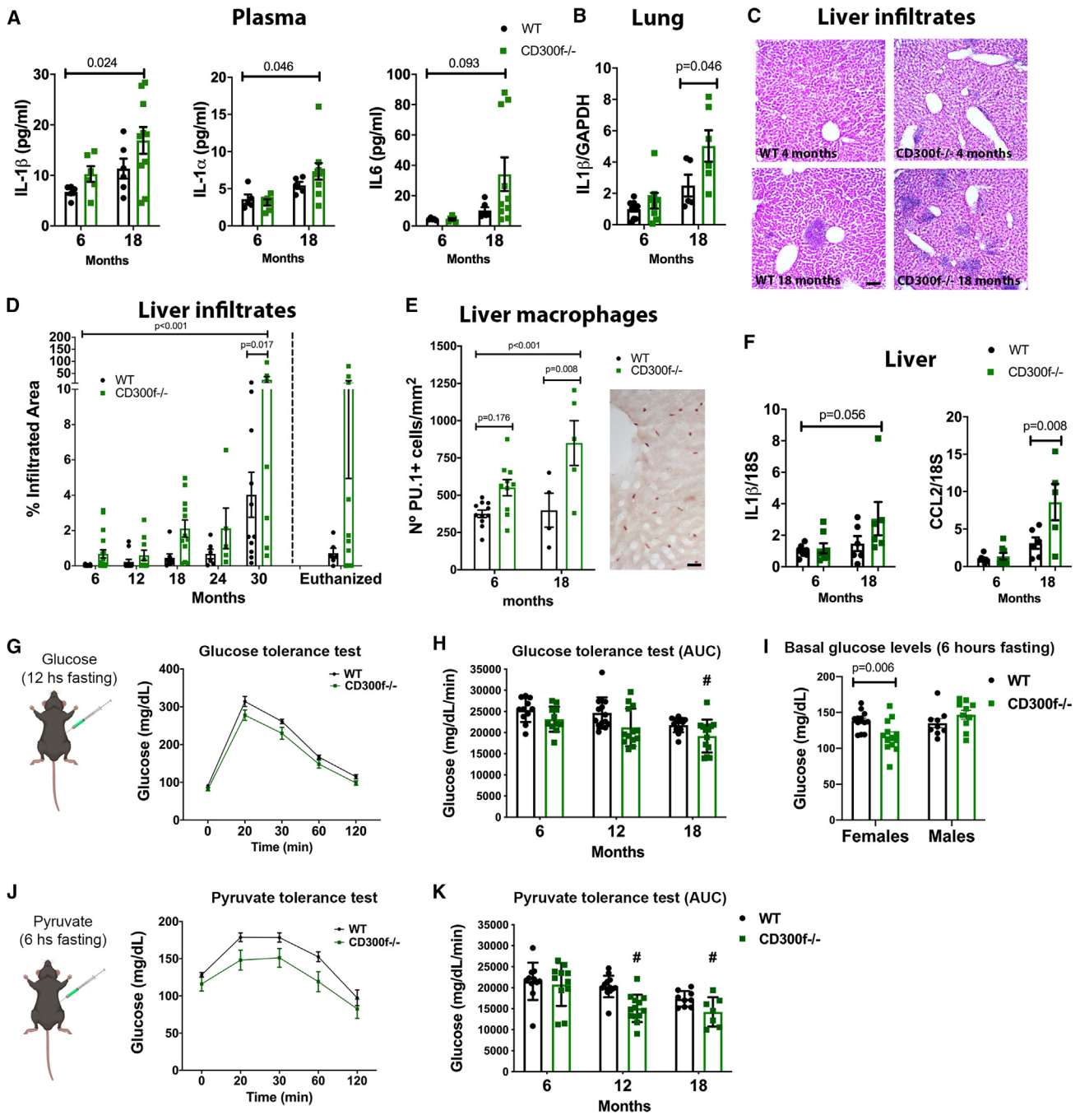

Figure 2. Absence of CD300f induces inflammaging and systemic glucose metabolism alterations

An age-dependent proinflammatory cytokine and chemokine increase in plasma (A) (ELISA), lung (B) (qPCR), and liver (F) (qPCR) was observed in 18-month-old CD300f$^{-/-}$ female mice. Age-dependent hepatic infiltrates were also increased in CD300f$^{-/-}$ mice (male and female pooled data) (C and D). Scale bar, 100 μm. Age-dependent increase in PU.1+ cells in the liver of CD300f$^{-/-}$ mice (females) (E). Scale bar, 50 μm. Glucose tolerance test in adult female mice (G) and at different ages (H) (#p < 0.01 compared with 6- and 12-month-old adult WT, two-way ANOVA p = 0.001 for age and p = 0.001 for genotype) after 12 h fasting. Basal glycemia after 6 h fasting in female and male 18-month-old mice (I). Pyruvate tolerance test in 18-month-old females (J) and at different ages (K) (#p < 0.02 compared with 6- and 12-month-old adult WT, two-way ANOVA p < 0.001 for age and p = 0.002 for genotype) after 6 h fasting. AUC, area under the curve.

CD300f$^{-/-}$ female than male mice, an effect also observed in WT female and male mice (Figures S2B and S2C). The increased liver inflammation in CD300f$^{-/-}$ female mice included increased numbers of PU.1 macrophages (Figure 2E). In accordance, the mRNA for *il1β*, *ccl2* (Figure 2F), and *ccl3* (Figure S2D) were elevated in 18-month-old CD300f$^{-/-}$ female liver. Despite liver

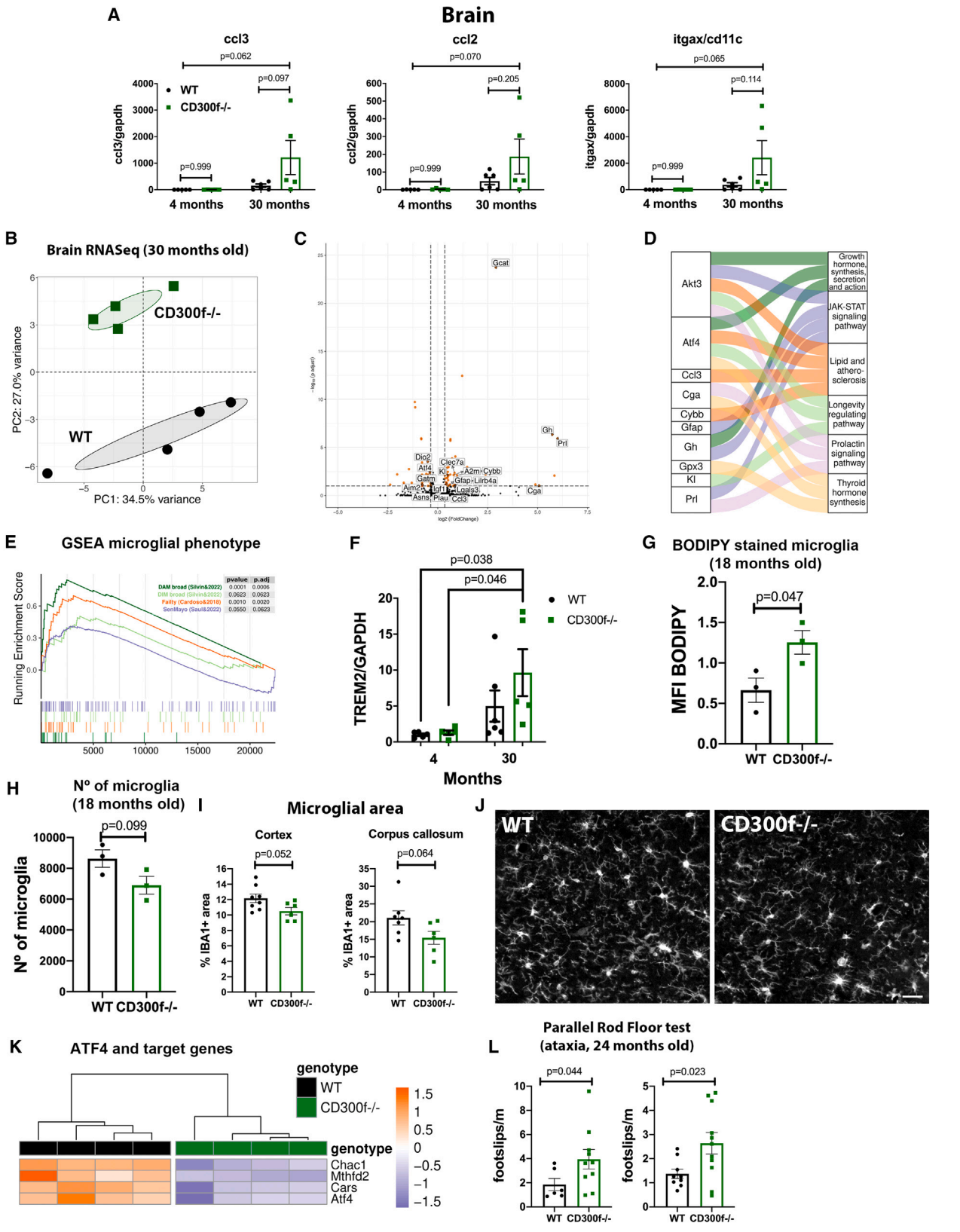

(legend on next page)

inflammation, no general hepatoxicity could be detected by measuring plasma AST and ALT enzymes at 18 and 30 months in most animals (Table S1). Moreover, bone marrow-derived macrophage (BMDM) cultures from adult WT and CD300f$^{-/-}$ female mice showed increased NLRP3 inflammasome expression after LPS stimulation in the latter (Figure S2E), also suggesting increased inflammatory profile of CD300f$^{-/-}$ myeloid cells.

Macrophages and immune receptors such as TREM2 have been shown to regulate both liver and fat tissue metabolism.[1,35] Thus, to explore whether CD300f immune receptor could alter macrophage phenotype and influence systemic metabolism during aging, we explored the age-related alterations in glucose handling and clearing capacity in adult and aged WT and CD300f$^{-/-}$ mice. Adult male and female WT and CD300f$^{-/-}$ mice were able to maintain similar basal plasmatic glucose levels under *ad libitum* feeding and after 6 or 12 h fasting (Figures 2H and 2I), and showed no alteration in glucose buffering capacity as observed after an intraperitoneal glucose challenge (glucose tolerance test [GTT]; and as reported previously[34]) (Figures 2G, 2H, S3A, and S3H). However, 12- and 18-month-old female but not male CD300f$^{-/-}$ mice showed a reduced under the curve area after the GTT, suggesting alterations in glucose-buffering capacity. This effect was not due to differences in insulin sensibility in CD300f$^{-/-}$ mice (mostly due to muscle glucose uptake), as no alterations were observed after an intraperitoneal insulin challenge (insulin tolerance test) in CD300f$^{-/-}$ male and female mice until 18 months, the last age tested (Figures S2F, S2G, and S3I). Interestingly, a short 6-h starvation demonstrated the reduced capacity of 18-month-old CD300f$^{-/-}$ females to sustain basal plasmatic glucose levels (Figure 2I). In this context, the alteration in glucose metabolism could be due to hepatic dysfunction. To test this hypothesis, an intraperitoneal pyruvate injection challenge was performed (pyruvate tolerance test), which mainly evaluates the hepatic gluconeogenesis potential. Interestingly, while WT female mice tend to show a reduced hepatic gluconeogenesis from age 18 months, female, but not male, CD300f$^{-/-}$ mice showed reduced hepatic gluconeogenesis earlier, from age 12 months (Figures 2J, 2K, and S3H).

Absence of CD300f induces age-related CNS alterations

The brain is a central organ affected by aging. Accordingly, signs of inflammaging were also observed in the brain of 30-month-old CD300f$^{-/-}$ mice by qPCR for chemokines *ccl2*, *ccl3*, and *itgax/cd11c* (Figure 3A). To further understand the biological role of CD300f in CNS aging, we analyzed the whole-brain transcriptome by RNA-seq of 30-month-old WT and CD300f$^{-/-}$ female mice (Table S2). The general RNA-seq gene expression profiles of both groups were different, as observed by principal-component analysis (Figure 3B). In fact, 67 genes were significantly differentially expressed (Figure 3C and S4A; Table S3). An over-representation analysis of these genes highlighted an enrichment in KEGG pathways associated to longevity regulation, JAK-STAT and PI3K signaling (Figure 3D; Table S4). These data are in accordance with gene set enrichment analysis (GSEA) of aged microglia that showed increased STAT3 activation.[36] Alteration in the expression of well-known genes related to longevity such as *gh*, *igf1*, *prl*, *kl*, and *gcat* was observed (Figure 3C). For instance, *gcat*, one of the most upregulated genes in CD300f$^{-/-}$ brain, has been shown to be downregulated during normal aging in different species, and knockdown of GCAT increases lifespan in *Caenorhabditis elegans*.[37] This association prompted us to analyze senescence markers in the brain of CD300f$^{-/-}$ mice. A recent report compiled a senescence gene set termed SenMayo, which is able to accurately quantify the degree of senescent cells in RNA-seq samples from several tissues including the brain and microglia of mice and humans.[38] When a GSEA was performed on our RNA-seq data using the SenMayo mouse gene set, a significant enrichment in senescence markers was observed in the CD300f$^{-/-}$ brain (Figure 3E; Table S5). Moreover, GSEA also showed that the brains of 30-month-old CD300f$^{-/-}$ female mice were significantly enriched for disease-associated microglia (DAM)-upregulated genes (including *clec7a*, *ccl3*, *lilrb4*, *cybb*, *lgals3*, and *igf1*) previously observed in aging, AD, and other neurodegenerative conditions[39,40] (Figures 3C and S4B; Table S5). Immunohistochemical analysis for one of the main DAM markers CLEC7A showed a significant increased immunoreactivity in all animals analyzed and increased CLEC7A+ cells only in some animals (Figures S4C–S4E). TREM2 has been shown to be essential for microglial DAM phenotype induction[39] and, in accordance, qPCR showed that TREM2 is upregulated in CD300f$^{-/-}$ 30-month-old aged brains (Figure 3F). A recent study[41] suggests that, among the classical DAM microglia,[39] there is a defined population derived from monocytes termed disease inflammatory macrophages (DIMs) that would accumulate in the brain mainly during aging and neuroinflammation. Interestingly, 30-month-old CD300f$^{-/-}$ mouse brains also showed a significant signature for DIM macrophages (Figures 3E and S4B; Table S5). An additional fact pointing toward an aged microglial phenotype in CD300f$^{-/-}$ 18-month-old brains is the increase in their lipid droplet content (Figure 3G).[42] Microglia have been shown to increase in their number and expression of proinflammatory markers with age.

Figure 3. Absence of CD300f induces age-related brain alterations

Brain inflammatory marker mRNA expression in adult and 30-month-old WT and CD300f$^{-/-}$ female mice was analyzed by qPCR (A). The transcriptome of 30-month-old female brains was analyzed by bulk RNA-seq (B, C, and K). Principal-component analysis (B), volcano plot highlighting differentially expressed genes (C), and KEGG pathway enrichment results (D) of the RNA-seq. The plot depicts the relationships among differentially expressed genes and over represented KEGG pathways ($p < 0.001$, FDR-adjusted p value < 0.2). Gene expression changes in the brain of 30-month-old CD300f$^{-/-}$ compared with WT mice exhibited both frailty and senescent signatures as well as enhanced microglial DAM state and a recruited macrophage DIM profile (E). GSEA plot shows, for the five gene lists, the running enrichment score as well as the position of the specific genes in the ranked gene sorting. qPCR for TREM2 expression in 30-month-old female brains (F). Quantification of microglial BODIPY+ lipid droplet content by flow cytometry in 18-month-old female brains (neocortex) (G). Quantification of microglial numbers by anti-CD11b/CD45 staining and flow cytometry of 18-month-old female brains (neocortex) (H). Quantification of IBA1 staining in 30-month-old female brains by immunohistochemistry (I and J). Scale bar, 20 μm. Normalized expression of ATF4 mRNA and some of its target genes (K) in 30 month-old-female brains. The parallel rod floor test (PRFT) was performed for analyzing ataxia in two independent cohorts of 24-month-old WT and CD300f$^{-/-}$ female mice at two different animal facilities (L). MFI, mean fluorescent intensity.

However, in the aged brains of CD300f$^{-/-}$ female mice, a trend toward displaying reduced numbers of microglia at 18 months (Figure 3H), or in the percentage of the IBA1-stained area at 30 months, was observed (Figures 3I and 3J).

Further exploration of brain RNA-seq results showed that KEGG enrichment analysis also highlighted growth hormone secretion and the action pathway. Indeed, the increase in mRNA for *gh*, *prl*, and *cga* (alpha polypeptide shared by several pituitary hormones) confirmed the previous qPCR data suggesting that CD300f$^{-/-}$ female mice develop pituitary neoplasms. Another differentially expressed gene in 30-month-old CD300f$^{-/-}$ female mice brain was *atf4*, which is a central effector of the integrated stress response. Proteostasis alteration is a hallmark of aging, and upregulation of pathways such as *atf4* have been associated to conditions that extend lifespan.[43] Interestingly, 30-month-old CD300f$^{-/-}$ mice showed decreased mRNA for *atf4* and some of its target genes (Figures 3C and 3K). Finally, the RNA-seq study also detected increased mRNA levels of inflammatory markers related to astrocytes (*gfap*), microglia (*clec7a*), and chemokines (*ccl3*) (Figure 3C). This confirmed whole-brain qPCR analysis of expression of chemokines (*ccl3*) (Figure 3A).

Frailty, another hallmark of aging, is considered an overall measure of unexplained heterogeneity in the accumulation of health-related problems of people of the same chronological age.[44] Interestingly, the frailty indexes have been shown to be similar in mice and people across the life course[45]; they are clinically relevant and predict rodent mortality in a similar manner as clinical frailty indices for humans.[45] The brain of CD300f$^{-/-}$ mice showed a significant enrichment for the frailty markers suggested by Cardoso et al.[46] such as *kl*, *csf1*, *gh*, and *plau* (Figure 3E). Other genes that, although non-significantly differentially expressed, contribute to the frailty running enrichment score in the GSEA were *gpnmb, tgfb1*, *c3*, *c1qa*, *c1qb*, and *c1qc* (Figure 3E; Table S5). Frailty includes decline in muscle strength and coordination[47]; also, in support of the increased frailty of aged CD300f$^{-/-}$ mice, two different cohorts of female mice displayed motor coordination deficits at age 24 months (Figure 3L).

Cognitive decline, and in particular learning and memory, is another defining feature of aging.[48] To uncover putative differences in cognitive decline, CD300f$^{-/-}$ mice were exposed to two different tests for evaluating learning and memory: the novel object recognition (NOR) test that provides an index of recognition memory, and the Barnes maze test that evaluates spatial learning and memory. No differences were observed in the performance of 18-month-old females in the NOR test (Figure 4A). However, 24-month-old CD300f$^{-/-}$ females, but not 22-month-old males, displayed a decreased capacity for the recognition of a new object (Figures 4B, 4C, and S5E). In a similar fashion, while 12-month-old mice of both sexes did not show learning and memory alterations in the Barnes maze (Figures 4D, 4G, S5A, and S5C), 18-month-old CD300f$^{-/-}$ female and male mice began to show alterations in memory for the escape position (Figures 4E, 4H, S5B, and 5D). This loss of memory was also observed in CD300f$^{-/-}$ females at age 24 months (Figures 4F and 4I–4J).

Taken together, and in accordance with the putative increased aging phenotype of the CD300f$^{-/-}$ mice, our results show an age-dependent brain inflammaging, senescence, enhanced age and neurodegeneration of microglial/macrophage (DAM/DIM) state, frailty/motor coordination deficits, and cognitive decline.

Absence of CD300f induces age-related decrease in CNS glucose uptake

Early brain hypometabolism observed by ^{18}F-fluorodeoxyglucose positron emission tomography (^{18}F-FDG PET) scans is a hallmark of aging and is associated to AD and cognitive decline.[49] Alterations in brain microglial immune receptors such as TREM2 or GRN induce profound changes in microglial phenotype and brain function. Independently of the inflammatory profile of these TREM2$^{-/-}$ and GRN$^{-/-}$ brains, they share decreased global glucose uptake,[50,51] which, at least in the case of TREM2, is age dependent.[52] We reproduced these experiments using ^{18}F-FDG PET/computed tomography scans imaging in adult and aged (18 months old) CD300f$^{-/-}$ and WT mice. Although no changes were observed in adult mice, 18-month-old CD300f$^{-/-}$ female mice showed a decreased global brain ^{18}F-FDG uptake (Figures 5A–5C), an effect that was evident in all of the brain areas analyzed (Figure 5D). Of note, we only observed this effect in aged female but not aged male mice (Figure 5C). Remarkably, the studies describing reduction of glucose uptake in TREM2$^{-/-}$, TREM2^{T66M} AD mutation, or Grn$^{-/-}$ mice were performed only in females aged 8–12 months, and no data are available for male mice.[50–52]

Elevated blood lactate can decrease brain ^{18}FDG uptake due to a switch in energy substrate usage[53]; however, no alterations in blood lactate levels were observed in CD300f$^{-/-}$ mice under basal conditions (Figure 5E). Moreover, the decrease in brain glucose uptake was not due to alterations in circulating glucose availability as glycemia did not change under physiological conditions (Figure 1I). Taken together, these results suggest that microglia/macrophage CD300f may be involved in age-dependent brain glucose uptake reduction that contributes to cognitive decline. Whether the reduced glucose uptake represents neuronal death, reduced brain metabolism, or alternative substrate utilization of, for instance, lactate or ketone bodies needs to be determined.

Absence of CD300f induces macrophage metabolic alterations

Aging induces a decrease of glycolysis and oxidative phosphorylation rates in aged human and mice macrophages.[26] This prostaglandin E2-dependent decrease of metabolic fitness of microglia/macrophages was shown to worsen age-dependent cognitive decline.[26] Moreover, CD300f deficiency decreased microglial glycolysis and oxidative phosphorylation under inflammatory conditions in female mice.[7] However, it is not known whether this is restricted to microglial cells or if it extends to other monocyte/macrophage populations of the organism. Thus, we isolated WT and CD300f$^{-/-}$ BMDM and analyzed their metabolic profile using a Seahorse Extracellular Flux Analyzer. BMDM were cultured in limiting M-CSF (5 ng/mL) concentrations as this was shown to better uncover metabolic fitness alterations.[27] Female CD300f$^{-/-}$ BMDM showed reduced basal extracellular acidification rates (ECAR) (Figure 6A) and basal mitochondrial oxygen

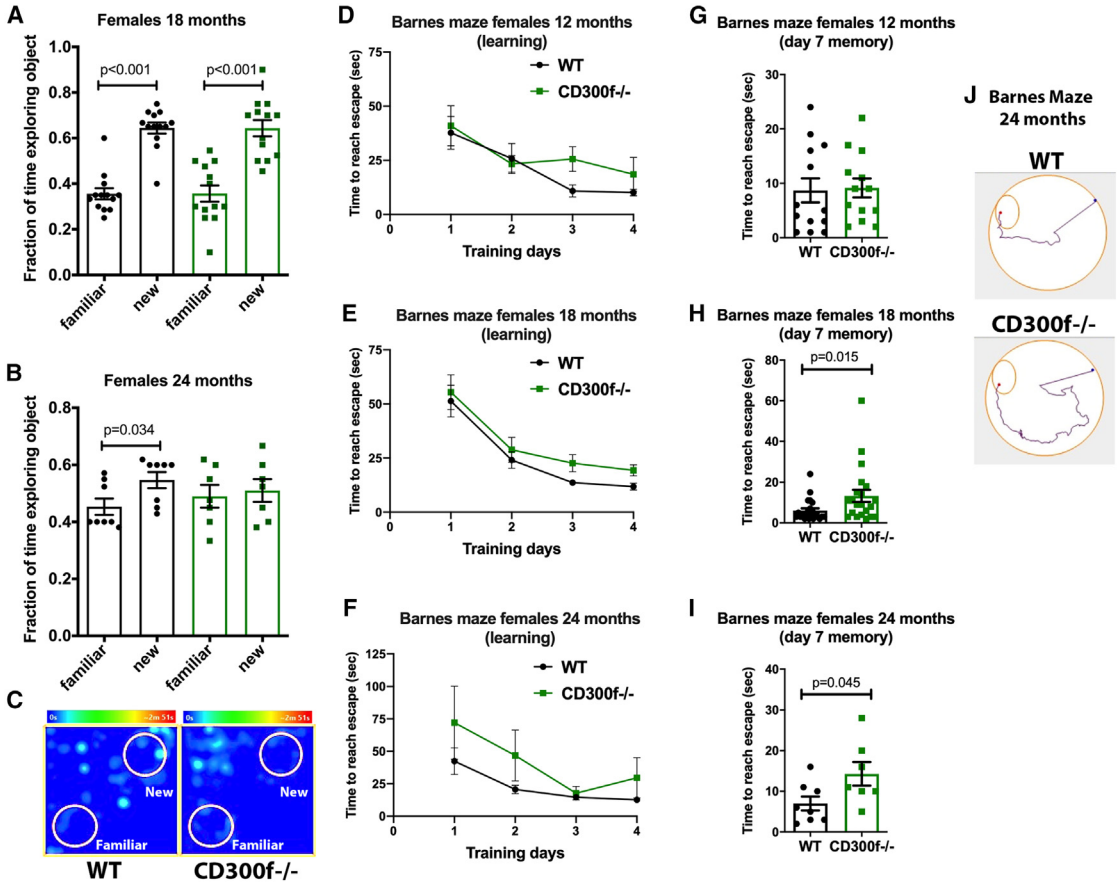

Figure 4. Absence of CD300f induces age-related cognitive decline

WT and CD300f$^{-/-}$ mice were followed for 24 months using the novel object recognition (NOR) and Barnes maze tests. CD300$^{-/-}$ females at 18 months showed no alterations in the NOR test (A), but lost the ability to recognize a new object at age 24 months (B and C). In the Barnes maze test experiments, CD300f$^{-/-}$ females did not show significant alterations in the time needed to learn which was the escape hole at age 12, 18, and 24 months (D, E, and F, respectively), or in memory 3 days after the last learning session at age 12 months (G) (day 7 from the beginning of the test). However, CD300f$^{-/-}$ females showed increased time for reaching the escape hole at age 18 and 24 months (H, I, and J).

consumption rates (OCR) (Figure 6B). Moreover, they also showed a decrease in maximum respiration rates and spare respiratory capacity, indicative of an impaired capacity for metabolic reprograming in response to a sudden increase in energy demands (Figures 6C and 6D). No significant differences were observed in the ATP-dependent and ATP-independent OCR of WT and CD300f$^{-/-}$ BMDM (Figure S6). However, male CD300f$^{-/-}$ macrophages did not show alterations in basal OCR (Figures 6E and 6G) nor in basal ECAR (Figures 6F and 6H), and only a tendency to decreased spared respiratory capacity. Moreover, inhibition of mitochondrial respiration induced the expected increase in ECAR in WT and CD300f$^{-/-}$ male BMDM (Figure 6F), while female CD300f$^{-/-}$ BMDM were not able to reprogram their metabolism under these conditions (Figure 6F). The absence of CD300f also demonstrated an alteration at the level of mechanistic target of rapamycin (mTOR) activation, a central coordinator of cellular metabolism in female BMDM. No changes were observed in the phosphorylation of the mTOR targets S6 or 4EBP1 under basal culture conditions with high MCSF concentrations (20 ng/mL), in MCSF limiting conditions (5 ng/mL), or after inhibition of mTOR by rapamycin (Figures 6I and 6J). However, after LPS treatment, WT BMDM increased mTOR activity, as observed by the increase in the phosphorylation of its target S6, while CD300f$^{-/-}$ BMDM did not (Figures 6I and 6J). Also, phosphorylated 4EBP1 showed a trend toward a decrease in CD300f$^{-/-}$ LPS-treated BMDM. Taken together, these data suggest that the absence of CD300f derails macrophage metabolic fitness with a more pronounced effect in females. In addition to this effect in microglial cells,[7] it could contribute to the diverse age-associated effects observed in CD300f$^{-/-}$ mice such as increased cognitive decline.

DISCUSSION

The main finding of this study is that CD300f$^{-/-}$ male and female mice have shortened lifespan and healthspan. The underlying causes of death are probably multifactorial and variable depending on the subject, as would be expected for aging. CD300f deficiency leads to widespread deficits in microglia/macrophage

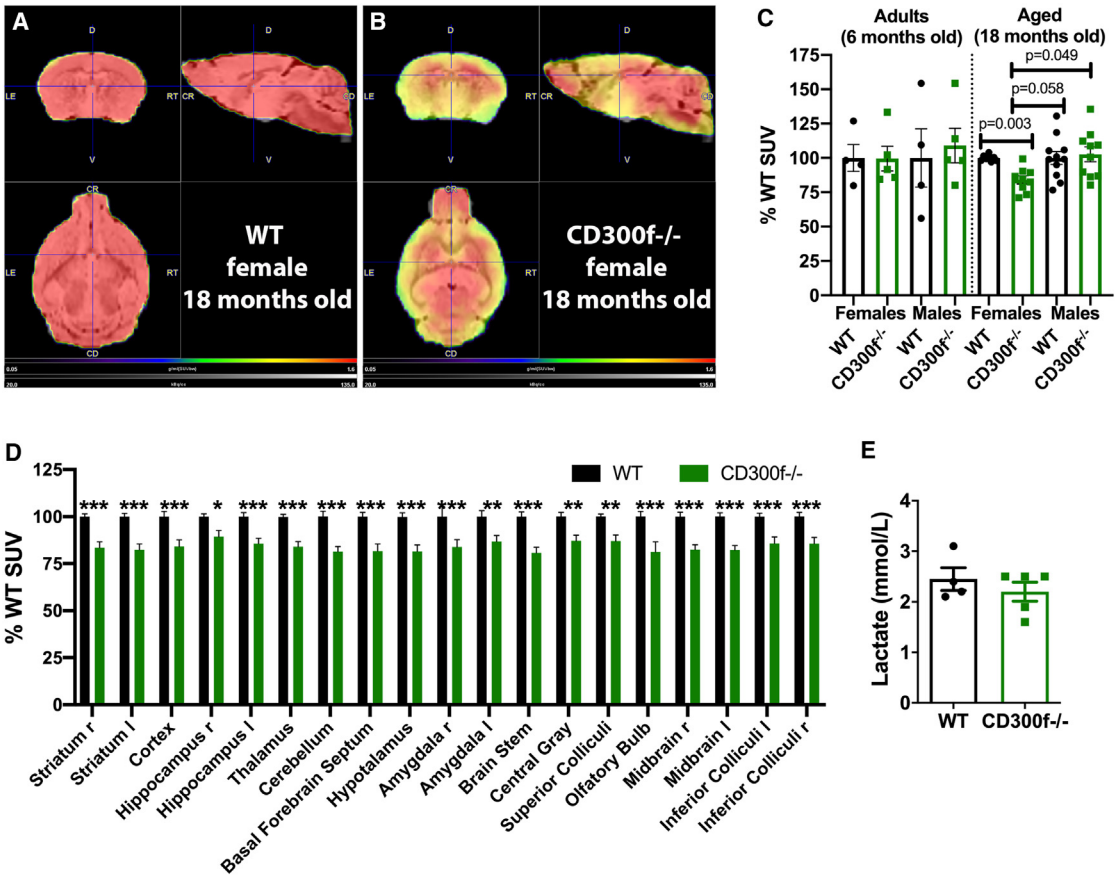

Figure 5. Absence of CD300f reduces brain glucose uptake in aged females

Adult (6 months) and aged (18 months) WT and CD300f$^{-/-}$ male and female mice were subjected to ^{18}F-FDG PET/computed tomography scans (A and B). Aged CD300f$^{-/-}$ female mice showed a reduced ^{18}F-FDG standard uptake value (SUV) when compared with the other groups (C) (n = 8 for WT and n = 9 for CD300f$^{-/-}$ 18-month-old female mice, Brown-Forsythe ANOVA test followed by Dunnett's T3 multiple comparisons test). This reduction was observed in all brain areas analyzed (D) (r, right; l, left; *p < 0.05, **p < 0.01, ***p < 0.001 by two-tailed Student's t test). The standardized uptake value (SUV) units are the average activity per volume unit (kBq/cc) subsequently corrected for injected radioactivity and mouse weight. No alterations were observed in basal blood lactate levels (E) (18-month-old female mice).

metabolic fitness, which, with aging, may alter the function of macrophages of different tissues, inducing inflammaging, senescence, cognitive decline, proteostasis alteration, systemic metabolic changes, and frailty.

Maximum lifespan has been the foremost criteria in aging research. However, while informative, longevity by itself is an incomplete estimation of health, assessment of physiologic, behavioral, and pathological states of the mice coupled to lifespan extension generates a more accurate characterization of the aging process and its associated diseases.[54] Defining what constitutes health and therefore healthy aging in mice or humans is not a simple task. Some evidence points toward the notion that CD300f$^{-/-}$ mice display several hallmarks of aging and aging-associated pathologies that are associated to decreased healthspan. They include earlier emergence of different neoplasms, chronic low-grade organismal inflammation or inflammaging, frailty, alterations in brain proteostasis pathways, increased brain senescence and cognitive decline, and, in the case of females, also systemic metabolic alterations.

An important process that makes it difficult to understand the possible cause of death during aging is the fact that biological age differs from chronological age and between subjects.[55] We were unable to determine one specific pathology associated to CD300f deficiency, as would be anticipated for the non-synchronous aging process in combination with the wide variety of pathologies associated with aging. In fact, an important dispersion of the data was observed with time, supporting differences in chronological and biological age and the gradual but unsynchronous emergence of aging-associated pathologies. Although we have not ruled out every possible cause of death, we have analyzed many relevant biological parameters. No general alterations were observed, neither in clinical blood markers of renal and hepatic pathologies nor in most blood cell counts until age 18 months. Scattered CD300f$^{-/-}$ mice showed pathological alterations in different systems as strongly reduced platelet counts (thrombocytopenia), increased spleen weight (putatively indicative of autoimmune diseases), hypoglycemia, or anemia. Thus, our data point to

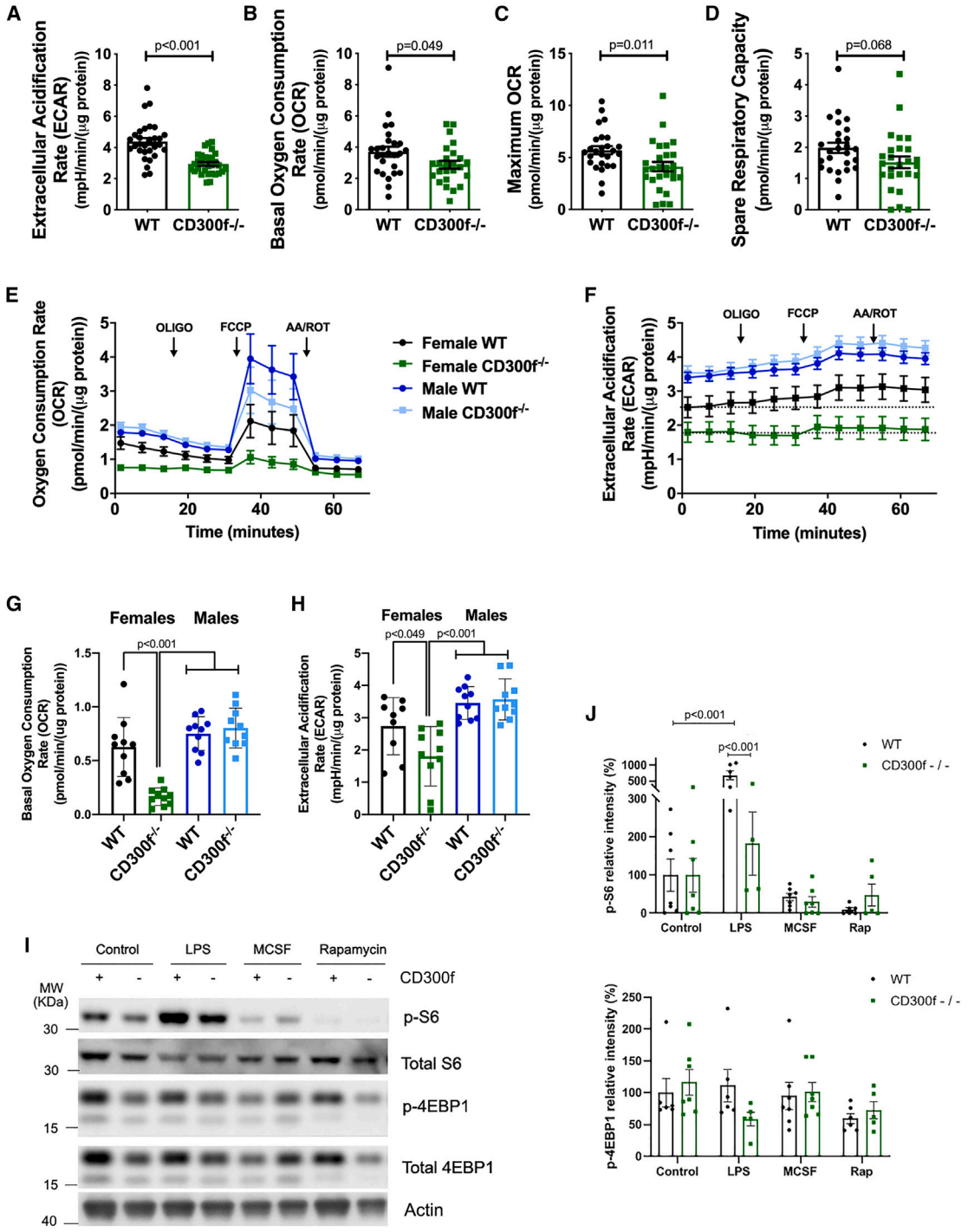

Figure 6. Absence of CD300f alters macrophage metabolism

Basal extracellular acidification rate (ECAR) (A) and oxygen consumption rate (OCR) (B) were decreased in CD300f$^{-/-}$ BMDM from adult female mice under limiting MCSF concentrations (5 ng/mL) when compared with WT. Moreover, they also showed impaired maximum respiration rates (C) and spare respiratory capacity (D). The OCR and ECAR under different conditions were compared between female and male BMDM cultures (E–H). Female BMDM cultures were incubated with 20 ng/mL MCSF, and treated with vehicle, 100 ng/mL LPS, or 100 µM rapamycin (Rap), or only incubated with 5 ng/mL MCSF, and the phosphorylation of several mTOR signaling pathway components was analyzed by western blot (I and J).

the absence of an important unique underlying pathology in CD300f$^{-/-}$ mice; however, they do point to the expected general causes of death related to aging. Accordingly, increased plasma GGT was observed in CD300f$^{-/-}$ female mice that had to be euthanized due to ethical endpoint considerations, and elevated circulating levels of this enzyme have been associated with all causes of mortality.[32]

We have found several sex-related alterations in aged CD300f$^{-/-}$ males and females, such as systemic metabolic alterations, macrophage metabolism, reduced brain glucose uptake, or earlier cognitive decline in females. For instance, hepatic gluconeogenesis capacity decreased with age in WT female mice, and this effect occurred earlier in CD300f$^{-/-}$ female mice than in WT mice, and was not observed in male mice. Also, CD300f$^{-/-}$ female mice showed reduced capacity for discriminating a new object in the NOR test at age 24 months, while CD300f$^{-/-}$ male mice did not. This correlates with the known epidemiology of AD dementia, which shows that females are more affected.[56] Accordingly, sex differences regarding the role of CD300f have also been described for psychiatric conditions such as depression and anxiety.[7,24] Better understanding of sex and gender differences is leading to improved care and treatment for both women and men, and identifying new mechanisms and molecular targets will provide better treatment and care for both. However, regarding lifespan, we observed that CD300f$^{-/-}$ mice of both sexes show a similar reduction. This could imply that the reduced lifespan in both females and males is related to the general aging processes not dependent on sex, or alternatively that both sexes display different causes of death due to different age-associated pathologies with similar reductions in lifespan. This should be analyzed in detail in further studies.

CD300f has been shown to regulate microglial phenotype, and here we extend these data to other macrophage populations. This could expand the effect of CD300f deficiency to the whole organism, affecting tissue-resident macrophages around the body and in different organs. As a putative DAMP receptor, CD300f may cooperate with other receptors such as TREM2 to sense DAMPs and other toxic lipids derived from chronic low-grade tissue damage during aging,[57] clearing them from the extracellular space and at the same time dampening the inflammatory reaction, contributing to the reestablishment of homeostasis. CD300f can in fact also inhibit the proinflammatory signaling of PAMP receptors such as Toll-like receptors.[58] This is particularly important for the CNS, as it tolerates inflammation badly; also, it contains an important amount of lipids and lipid debris generated by normal myelin turnover, after a lesion, or under chronic neurodegenerative conditions. According to a recent study,[41] DAM microglia are embryonically derived and would appear only in the context of neurodegeneration and not significantly during normal aging. Conversely, the same study suggested that monocyte-derived DIMs would accumulate mainly with age, neuroinflammation and, at least, AD-related neurodegeneration. Our analysis of microglial and macrophage phenotype by RNA-seq showed increased DAM and DIM stages in 30-month-old female CD300f$^{-/-}$ mice. Thus, these data would point toward increased aging but also neurodegenerative processes in the CD300f$^{-/-}$ brain. Moreover, in opposition to TREM2, CD300f would contribute to the maintenance of the microglial homeostatic phenotype during aging. If the maintenance of the microglial homeostatic phenotype is necessary for healthy brain aging or, on the contrary, if the DAM phenotype is an important reaction of microglial cells to cope with aging-associated brain changes needs to be established in future studies.

The aging-related longevity pathways of growth, metabolism, nutrient sensing, autophagy, and stress response are intertwined, as demonstrated by many connected effector proteins that interact either directly or through their network neighbors. Strategies such as dampening mTOR or activating AMP-activated protein kinase modulate aging and extend lifespan.[59] These connected signaling pathways indicate the interplay between metabolism and molecular and cellular defenses against aging and its associated pathologies such as AD. A robust example is that aged macrophages display metabolic alterations and induce cognitive decline, an effect that is reversed by the restitution of macrophage metabolism.[26] There is transcriptomic and biochemical experimental evidence for the *in vivo* importance of CD300f−/− in microglial metabolic fitness,[7] and CD300f has also been recently shown to be among the top 20 upregulated genes in microglia of naive mice after specific genetic microglial mTOR activation.[60] The same work reported that activation of microglial mTOR induced increased microglia homing to Aβ plaques, reduced accumulation of plaques, maintained spine density, and improved memory in 5xFAD mice. We show here that, as occurs with microglia,[7] the absence of CD300f in macrophages alters their metabolic fitness, affecting mitochondrial function and mTOR activation. In this context, our data suggest that, because of its role in metabolic activation and autophagy, CD300f may function as a costimulatory molecule that sustains microglia/macrophage transition to different relevant phenotypes that are triggered by various receptors engaged by tissue injury or dysfunction, such as apoptotic cells, debris, Aβ plaques, and myelin damage. In this way, CD300f malfunction would affect myelin debris phagocytosis/myelin recycling, lipoprotein interaction and lipid metabolism, neuroinflammation, and synaptic pruning, ultimately enhancing neurodegeneration and cognitive decline. Understanding CD300f function in the CNS, the role of single-nucleotide polymorphisms or their therapeutic CD300f activation could contribute to the design of new treatment paradigms for AD and other aged-related neuropathologies.

In wider terms, this work suggests that the study of the biology of immune receptors in the context of aging could contribute to the elucidation of novel predictors of both health and lifespan, and may identify therapeutic targets for attenuating aging and abrogating age-related diseases. More than 90% of individuals over 65 years of age have at least one chronic disease, such as cardiovascular disease, cancer, dementia, diabetes, osteoarthritis, or osteoporosis, and >70% have at least two such conditions.[61] Thus, on a wider perspective, therapeutic strategies to target fundamental aging mechanisms, as opposed to treating each age-associated disease separately, could have a tremendous effect on global health.

Limitations of the study

Although we have employed multiple approaches and thoroughly analyzed many parameters to discover a single specific cause of death of CD300f$^{-/-}$ mice, we could not determine a single alteration leading to the reduced lifespan. We could not follow some parameters such as cardiovascular alterations. However, aging also induces cardiovascular alterations and thus this could fit in the hypothesis of CD300f participating in maintaining health during aging. Another limitation was determined by the cost of these experiments and the necessity to obtain animals for analysis of the putative causes of death and mechanisms of injury or aging. We decided to stop the experiments before losing all CD300f$^{-/-}$ mice (despite close follow-up many times the animals were found dead and could not be collected) and thus did not obtain data regarding the median lifespan of the WT mice. Total male data show a 104-week median survival for CD300f$^{-/-}$ mice and at least 136 weeks for WT male mice (Figure S1D). Total female median survival was 121 weeks for CD300f$^{-/-}$ mice and at least 134 weeks for WT mice (Figure S1C), indicating a decrease of around 23% for males and 10% for females. However, although this estimation is probably similar to the real median survival for male mice (data from ≅55% mice alive), it is an underestimation for female mice (data from ≅65% mice alive) as the data used for median survival for WT mice are the latest data available at the end of the experiment. In this context, when analyzing the putative progression of survival curves, the estimated reduction in lifespan for female mice is probably similar to that of male mice. We are aware that the data presented here may not be true for human aging. Data relating CD300f with longevity, for instance, in centenarian human cohorts would strengthen the hypothesis proposed in this work. Another limitation of this study is that this manuscript analyzed bulk RNA-seq data obtained from whole brains of aged mice, and the data represent an average of genes expressed by different cell types and in different brain regions. GSEA analysis clearly showed interesting changes in microglia/macrophage phenotypes, although more specific experiments (e.g., RNA-seq of FACS-sorted microglia or single-cell RNA-seq) are required to discard effects of the change of cell proportions with aging or genotype, and further dissect their phenotypes. Finally, because CD300f is expressed on circulating monocytes, tissue-resident macrophages in the periphery and other myeloid cells, it will be important to unravel the relative role of CD300f expression in peripheral cells versus CD300f expressed by microglia and BAMs in the nervous system. Addressing these questions will contribute to a more comprehensive understanding of the significance of CD300f in the context of neurodegeneration and aging.

STAR★METHODS

Detailed methods are provided in the online version of this paper and include the following:

- KEY RESOURCES TABLE
- RESOURCE AVAILABILITY
  - Lead contact
  - Materials availability
  - Data and code availability
- EXPERIMENTAL MODEL AND STUDY PARTICIPANT DETAILS
- METHOD DETAILS
  - Complete blood count
  - Hepatic and renal function
  - Metabolic tests: Glucose tolerance test, pyruvate tolerance test, and insulin tolerance test
  - Histological and immunohistochemistry procedures
  - RNA extraction and qPCR
  - RNA sequencing and transcriptomic analysis
  - Flow cytometry
  - Novel object recognition (NOR)
  - Barnes Maze test
  - Parallel rod floor test (ataxia)
  - Bone marrow derived macrophages cultures
  - Measurement of oxygen consumption rates
  - Western blotting
  - PET/CT imaging
- QUANTIFICATION AND STATISTICAL ANALYSIS

SUPPLEMENTAL INFORMATION

Supplemental information can be found online at https://doi.org/10.1016/j.celrep.2023.113269.

ACKNOWLEDGMENTS

This work has been supported by grants from Comisión Sectorial de Investigación Científica (CSIC-UDELAR I+D 2020 ID 184 and ID 424, Espacio Interdisciplinario - UDELAR Centros 2015 and Espacio Interdisciplinario-UDELAR Grupos 2021), Uruguay; PEDECIBA, Uruguay; FOCEM (MERCOSUR Structural Convergence Fund), COF 03/1111; Banco de Seguros del Estado (BSE), Uruguay; Ministerio de Ciencia e Innovación, Gobierno de España (PID2021-123272OB-I0/Financiado por MCIN/AEI/10.13039/501100011033/ y por FEDER Una manera de hacer Europa), and International Centre for Genetic Engineering and Biotechnology (ICGEB, CRP/URY19-01). N.L. is a recipient of a Marie Skłodowska-Curie Individual Fellowship (H2020-MSCA-IF-2020 no. 101030280). We thank Mauro Costa-Mattioli for interesting discussions; and Florencia Fontes and Mariela Santos and the rest of the URBE Facultad de Medicina UDELAR personnel, and Sergio Ancheta and the rest of the UBAL-Institut Pasteur de Montevideo personnel.

AUTHOR CONTRIBUTIONS

H.P., M.L.N.-D., F.E., and N.L. conceived the study. F.E. performed most of the experiments. B.P., F.A.C., N.L., M.L.N.-D., P.S.-M., A.C.-G., A.P., L.R., J.R.-D., V.P.-T., and M.B. performed the experiments. N.R. performed all bioinformatics analysis. L.R., A.P., H.P., and E.S. performed and analyzed PET experiments. M.N.M., G.S., A.P.M., and M.C. generated the CD300f$^{-/-IPMon}$ mice. F.E., H.P., N.R., C.E., C.Q., C.M., and N.L. analyzed and discussed the results. H.P. drafted the original manuscript and F.E., N.R., C.E., M.C., N.L., E.S., C.M., P.S.-M., and C.Q. contributed to the edition of the final version. All authors have read and agreed to the published version of the manuscript.

DECLARATION OF INTERESTS

The authors declare no competing interests.

Received: March 10, 2023
Revised: August 25, 2023
Accepted: September 28, 2023

REFERENCES

1. Jaitin, D.A., Adlung, L., Thaiss, C.A., Weiner, A., Li, B., Descamps, H., Lundgren, P., Bleriot, C., Liu, Z., Deczkowska, A., et al. (2019). Lipid-Associated Macrophages Control Metabolic Homeostasis in a Trem2-Dependent Manner. Cell *178*, 686–698.e14. https://doi.org/10.1016/j.cell.2019.05.054.
2. Wynn, T.A., and Vannella, K.M. (2016). Macrophages in Tissue Repair, Regeneration, and Fibrosis. Immunity *44*, 450–462. https://doi.org/10.1016/j.immuni.2016.02.015.
3. Schwarz, F., Pearce, O.M.T., Wang, X., Samraj, A.N., Läubli, H., Garcia, J.O., Lin, H., Fu, X., Garcia-Bingman, A., Secrest, P., et al. (2015). Siglec receptors impact mammalian lifespan by modulating oxidative stress. Elife *4*, e06184. https://doi.org/10.7554/eLife.06184.
4. Podleśny-Drabiniok, A., Marcora, E., and Goate, A.M. (2020). Microglial Phagocytosis: A Disease-Associated Process Emerging from Alzheimer's Disease Genetics. Trends Neurosci. *43*, 965–979. https://doi.org/10.1016/j.tins.2020.10.002.
5. Lewcock, J.W., Schlepckow, K., Di Paolo, G., Tahirovic, S., Monroe, K.M., and Haass, C. (2020). Emerging Microglia Biology Defines Novel Therapeutic Approaches for Alzheimer's Disease. Neuron *108*, 801–821. https://doi.org/10.1016/j.neuron.2020.09.029.
6. Perugorria, M.J., Esparza-Baquer, A., Oakley, F., Labiano, I., Korosec, A., Jais, A., Mann, J., Tiniakos, D., Santos-Laso, A., Arbelaiz, A., et al. (2019). Non-parenchymal TREM-2 protects the liver from immune-mediated hepatocellular damage. Gut *68*, 533–546. https://doi.org/10.1136/gutjnl-2017-314107.
7. Lago, N., Kaufmann, F.N., Negro-Demontel, M.L., Alí-Ruiz, D., Ghisleni, G., Rego, N., Arcas-García, A., Vitureira, N., Jansen, K., Souza, L.M., et al. (2020). CD300f immunoreceptor is associated with major depressive disorder and decreased microglial metabolic fitness. Proc. Natl. Acad. Sci. USA *117*, 6651–6662. https://doi.org/10.1073/pnas.1911816117.
8. Tian, L., Choi, S.C., Lee, H.N., Murakami, Y., Qi, C.F., Sengottuvelu, M., Voss, O., Krzewski, K., and Coligan, J.E. (2016). Enhanced efferocytosis by dendritic cells underlies memory T-cell expansion and susceptibility to autoimmune disease in CD300f-deficient mice. Cell Death Differ. *23*, 1086–1096. https://doi.org/10.1038/cdd.2015.161.
9. Deczkowska, A., Keren-Shaul, H., Weiner, A., Colonna, M., Schwartz, M., and Amit, I. (2018). Disease-Associated Microglia: A Universal Immune Sensor of Neurodegeneration. Cell *173*, 1073–1081. https://doi.org/10.1016/j.cell.2018.05.003.
10. Alvarez-Errico, D., Aguilar, H., Kitzig, F., Brckalo, T., Sayós, J., and López-Botet, M. (2004). IREM-1 is a novel inhibitory receptor expressed by myeloid cells. Eur. J. Immunol. *34*, 3690–3701.
11. Alvarez-Errico, D., Sayós, J., and López-Botet, M. (2007). The IREM-1 (CD300f) inhibitory receptor associates with the p85alpha subunit of phosphoinositide 3-kinase. J. Immunol. *178*, 808–816.
12. Martínez-Barriocanal, A., Comas-Casellas, E., Schwartz, S., Jr., Martín, M., and Sayós, J. (2010). CD300 heterocomplexes, a new and family-restricted mechanism for myeloid cell signaling regulation. J. Biol. Chem. *285*, 41781–41794. https://doi.org/10.1074/jbc.M110.140889.
13. Xi, H., Katschke, K.J., Jr., Helmy, K.Y., Wark, P.A., Kljavin, N., Clark, H., Eastham-Anderson, J., Shek, T., Roose-Girma, M., Ghilardi, N., and van Lookeren Campagne, M. (2010). Negative regulation of autoimmune demyelination by the inhibitory receptor CLM-1. J. Exp. Med. *207*, 7–16, jem.20091508 [pii]. https://doi.org/10.1084/jem.20091508.
14. Tian, L., Choi, S.C., Murakami, Y., Allen, J., Morse, H.C., Qi, C.F., Krzewski, K., and Coligan, J.E. (2014). P85alpha recruitment by the CD300f phosphatidylserine receptor mediates apoptotic cell clearance required for autoimmunity suppression. Nat. Commun. *5*, 3146. https://doi.org/10.1038/ncomms4146.
15. Izawa, K., Yamanishi, Y., Maehara, A., Takahashi, M., Isobe, M., Ito, S., Kaitani, A., Matsukawa, T., Matsuoka, T., Nakahara, F., et al. (2012). The receptor LMIR3 negatively regulates mast cell activation and allergic responses by binding to extracellular ceramide. Immunity *37*, 827–839. https://doi.org/10.1016/j.immuni.2012.08.018.
16. Peluffo, H., Alí-Ruiz, D., Ejarque-Ortíz, A., Heras-Alvarez, V., Comas-Casellas, E., Martínez-Barriocanal, A., Kamaid, A., Alvarez-Errico, D., Negro, M.L., Lago, N., et al. (2012). Overexpression of the immunoreceptor CD300F has a neuroprotective role in a model of acute brain injury. Brain Pathol. *22*, 318–328. https://doi.org/10.1111/j.1750-3639.2011.00537.x.
17. Ejarque-Ortiz, A., Solà, C., Martínez-Barriocanal, Á., Schwartz, S., Martín, M., Peluffo, H., and Sayós, J. (2015). The receptor CMRF35-like molecule-1 (CLM-1) enhances the production of LPS-induced pro-inflammatory mediators during microglial activation. PLoS One *10*, e0123928. https://doi.org/10.1371/journal.pone.0123928.
18. Bennett, M.L., Bennett, F.C., Liddelow, S.A., Ajami, B., Zamanian, J.L., Fernhoff, N.B., Mulinyawe, S.B., Bohlen, C.J., Adil, A., Tucker, A., et al. (2016). New tools for studying microglia in the mouse and human CNS. Proc. Natl. Acad. Sci. USA *113*, E1738–E1746. https://doi.org/10.1073/pnas.1525528113.
19. Torres-Espín, A., Hernández, J., and Navarro, X. (2013). Gene expression changes in the injured spinal cord following transplantation of mesenchymal stem cells or olfactory ensheathing cells. PLoS One *8*, e76141. https://doi.org/10.1371/journal.pone.0076141.
20. Lloyd, A.F., Davies, C.L., Holloway, R.K., Labrak, Y., Ireland, G., Carradori, D., Dillenburg, A., Borger, E., Soong, D., Richardson, J.C., et al. (2019). Central nervous system regeneration is driven by microglia necroptosis and repopulation. Nat. Neurosci. *22*, 1046–1052.
21. Ising, C., Venegas, C., Zhang, S., Scheiblich, H., Schmidt, S.V., Vieira-Saecker, A., Schwartz, S., Albasset, S., McManus, R.M., Tejera, D., et al. (2019). NLRP3 inflammasome activation drives tau pathology. Nature *575*, 669–673. https://doi.org/10.1038/s41586-019-1769-z.
22. Danik, J.S., Paré, G., Chasman, D.I., Zee, R.Y.L., Kwiatkowski, D.J., Parker, A., Miletich, J.P., and Ridker, P.M. (2009). Novel loci, including those related to Crohn disease, psoriasis, and inflammation, identified in a genome-wide association study of fibrinogen in 17 686 women: the Women's Genome Health Study. Circ. Cardiovasc. Genet. *2*, 134–141. https://doi.org/10.1161/CIRCGENETICS.108.825273.
23. Ban, M., McCauley, J.L., Zuvich, R., Baker, A., Bergamaschi, L., Cox, M., Kemppinen, A., D'Alfonso, S., Guerini, F.R., Lechner-Scott, J., et al. (2010). A non-synonymous SNP within membrane metalloendopeptidase-like 1 (MMEL1) is associated with multiple sclerosis. Gene Immun. *11*, 660–664. https://doi.org/10.1038/gene.2010.36.
24. Kaufmann, F.N., Lago, N., Alí-Ruiz, D., Jansen, K., Souza, L.D.M., Silva, R.A., Lara, D.R., Ghisleni, G., Peluffo, H., and Kaster, M.P. (2021). Sex-dependent role of CD300f immune receptor in generalized anxiety disorder. Brain Behav. Immun. Health *11*, 100191. https://doi.org/10.1016/j.bbih.2020.100191.
25. Grabert, K., Michoel, T., Karavolos, M.H., Clohisey, S., Baillie, J.K., Stevens, M.P., Freeman, T.C., Summers, K.M., and McColl, B.W. (2016). Microglial brain region-dependent diversity and selective regional sensitivities to aging. Nat. Neurosci. *19*, 504–516. https://doi.org/10.1038/nn.4222.
26. Minhas, P.S., Latif-Hernandez, A., McReynolds, M.R., Durairaj, A.S., Wang, Q., Rubin, A., Joshi, A.U., He, J.Q., Gauba, E., Liu, L., et al. (2021). Restoring metabolism of myeloid cells reverses cognitive decline in ageing. Nature *590*, 122–128. https://doi.org/10.1038/s41586-020-03160-0.
27. Beatty, W.L., Loboda, A.A., Huang, S.C.C., Ulrich, J.D., Sergushichev, A., Ulland, T.K., Song, W.M., Zhou, Y., Cairns, N.J., Kambal, A., et al. (2017). TREM2 Maintains Microglial Metabolic Fitness in Alzheimer ' s Disease Article TREM2 Maintains Microglial Metabolic Fitness in Alzheimer ' s Disease. Cell *170*, 649–663.e13. https://doi.org/10.1016/j.cell.2017.07.023.
28. Alexi, N., Inge, R.H., Nicole, G.C., Johannes, C.M.S., Miao, Y., Rong, H., Claudia, Z.H., Monique, P., Jiayang, X., Yin, W., et al. (2019). Brain cell

type – specific enhancer – promoter interactome maps and disease-risk association. Science *1139*, 1134–1139.

29. Novikova, G., Kapoor, M., Tcw, J., Abud, E.M., Efthymiou, A.G., Chen, S.X., Cheng, H., Fullard, J.F., Bendl, J., Liu, Y., et al. (2021). Integration of Alzheimer's disease genetics and myeloid genomics identifies disease risk regulatory elements and genes. Nat. Commun. *12*, 1610. https://doi.org/10.1038/s41467-021-21823-y.
30. Hamilton, S.E., Badovinac, V.P., Beura, L.K., Pierson, M., Jameson, S.C., Masopust, D., and Griffith, T.S. (2020). New Insights into the Immune System Using Dirty Mice. J. Immunol. *205*, 3–11. https://doi.org/10.4049/jimmunol.2000171.
31. Pettan-Brewer, C., and M Treuting, P. (2011). Practical pathology of aging mice. Pathobiol. Aging & Age-related Dis. *1*, 7202. https://doi.org/10.3402/pba.v1i0.7202.
32. Ndrepepa, G., Colleran, R., and Kastrati, A. (2018). Gamma-glutamyl transferase and the risk of atherosclerosis and coronary heart disease. Clin. Chim. Acta *476*, 130–138. https://doi.org/10.1016/j.cca.2017.11.026.
33. Franceschi, C., Garagnani, P., Parini, P., Giuliani, C., and Santoro, A. (2018). Inflammaging: a new immune–metabolic viewpoint for age-related diseases. Nat. Rev. Endocrinol. *14*, 576–590. https://doi.org/10.1038/s41574-018-0059-4.
34. Rozenberg, P., Reichman, H., Zab-Bar, I., Itan, M., Pasmanik-Chor, M., Bouffi, C., Qimron, U., Bachelet, I., Fulkerson, P.C., Rothenberg, M.E., and Munitz, A. (2017). CD300f: IL-5 cross-talk inhibits adipose tissue eosinophil homing and subsequent IL-4 production. Sci. Rep. *7*, 5922. https://doi.org/10.1038/s41598-017-06397-4.
35. Morgantini, C., Jager, J., Li, X., Levi, L., Azzimato, V., Sulen, A., Barreby, E., Xu, C., Tencerova, M., Näslund, E., et al. (2019). Liver macrophages regulate systemic metabolism through non-inflammatory factors. Nat. Metab. *1*, 445–459. https://doi.org/10.1038/s42255-019-0044-9.
36. Hickman, S.E., Kingery, N.D., Ohsumi, T.K., Borowsky, M.L., Wang, L.c., Means, T.K., and El Khoury, J. (2013). The microglial sensome revealed by direct RNA sequencing. Nat. Neurosci. *16*, 1896–1905. https://doi.org/10.1038/nn.3554.
37. Ravichandran, M., Priebe, S., Grigolon, G., Rozanov, L., Groth, M., Laube, B., Guthke, R., Platzer, M., Zarse, K., and Ristow, M. (2018). Impairing L-Threonine Catabolism Promotes Healthspan through Methylglyoxal-Mediated Proteohormesis. Cell Metabol. *27*, 914–925.e5. https://doi.org/10.1016/j.cmet.2018.02.004.
38. Saul, D., Kosinsky, R.L., Atkinson, E.J., Doolittle, M.L., Zhang, X., LeBrasseur, N.K., Pignolo, R.J., Robbins, P.D., Niedernhofer, L.J., Ikeno, Y., et al. (2022). A new gene set identifies senescent cells and predicts senescence-associated pathways across tissues. Nat. Commun. *13*, 4827. https://doi.org/10.1038/s41467-022-32552-1.
39. David, E., Baruch, K., Lara-Astaiso, D., Matcovitch-Natan, O., Dvir-Sztern-feld, R., Ulland, T.K., Keren-shaul, H., Spinrad, A., Weiner, A., Toth, B., et al. (2017). Article A Unique Microglia Type Associated with Restricting Development of Alzheimer ' s Disease Article A Unique Microglia Type Associated with Restricting Development of Alzheimer ' s Disease. Cell *169*, 1276–1290.e17. https://doi.org/10.1016/j.cell.2017.05.018.
40. El Fatimy, R., Beckers, L., O'Loughlin, E., Baufeld, C., Calcagno, N., Krasemann, S., Madore, C., Cialic, R., Xu, Y., Fanek, Z., et al. (2017). The TREM2-APOE Pathway Drives the Transcriptional Phenotype of Dysfunctional Microglia in Neurodegenerative Diseases Article The TREM2-APOE Pathway Drives the Transcriptional Phenotype of Dysfunctional Microglia in Neurodegenerative Diseases. Immunity *47*, 566–581.e9. https://doi.org/10.1016/j.immuni.2017.08.008.
41. Silvin, A., Uderhardt, S., Piot, C., Da Mesquita, S., Yang, K., Geirsdottir, L., Mulder, K., Eyal, D., Liu, Z., Bridlance, C., et al. (2022). Dual ontogeny of disease-associated microglia and disease inflammatory macrophages in aging and neurodegeneration. Immunity *55*, 1448–1465.e6. https://doi.org/10.1016/j.immuni.2022.07.004.
42. Marschallinger, J., Iram, T., Zardeneta, M., Lee, S.E., Lehallier, B., Haney, M.S., Pluvinage, J.V., Mathur, V., Hahn, O., Morgens, D.W., et al. (2020). Lipid-droplet-accumulating microglia represent a dysfunctional and proinflammatory state in the aging brain. Nat. Neurosci. *23*, 194–208. https://doi.org/10.1038/s41593-019-0566-1.
43. Li, W., Li, X., and Miller, R.A. (2014). ATF4 activity: A common feature shared by many kinds of slow-aging mice. Aging Cell *13*, 1012–1018. https://doi.org/10.1111/acel.12264.
44. Mitnitski, A.B., Mogilner, A.J., and Rockwood, K. (2001). Accumulation of deficits as a proxy measure of aging. Sci. World J. *1*, 323–336. https://doi.org/10.1100/tsw.2001.58.
45. Rockwood, K., Blodgett, J.M., Theou, O., Sun, M.H., Feridooni, H.A., Mitnitski, A., Rose, R.A., Godin, J., Gregson, E., and Howlett, S.E. (2017). A Frailty Index Based on Deficit Accumulation Quantifies Mortality Risk in Humans and in Mice. Sci. Rep. *7*, 43068. https://doi.org/10.1038/srep43068.
46. Cardoso, A.L., Fernandes, A., Aguilar-Pimentel, J.A., de Angelis, M.H., Guedes, J.R., Brito, M.A., Ortolano, S., Pani, G., Athanasopoulou, S., Gonos, E.S., et al. (2018). Towards frailty biomarkers: Candidates from genes and pathways regulated in aging and age-related diseases. Ageing Res. Rev. *47*, 214–277. https://doi.org/10.1016/j.arr.2018.07.004.
47. Ingram, D.K., London, E.D., Reynolds, M.A., Waller, S.B., and Goodrick, C.L. (1981). Differential effects of age on motor performance in two mouse strains. Neurobiol. Aging *2*, 221–227.
48. Flood, J.F., and Morley, J.E. (1990). Pharmacological enhancement of long-term memory retention in old mice. J. Gerontol. *45*, 101–104. https://doi.org/10.1093/geronj/45.3.B101.
49. Kyrtata, N., Emsley, H.C.A., Sparasci, O., Parkes, L.M., and Dickie, B.R. (2021). A Systematic Review of Glucose Transport Alterations in Alzheimer's Disease. Front. Neurosci. *15*, 626636. https://doi.org/10.3389/fnins.2021.626636.
50. Götzl, J.K., Brendel, M., Werner, G., Parhizkar, S., Monasor, L.S., Kleinberger, G., Colombo, A., Deussing, M., Wagner, M., Winkelmann, J., et al. (2019). Opposite microglial activation stages upon loss of PGRN or TREM 2 result in reduced cerebral glucose metabolism. EMBO Mol. Med. *11*, e9711. https://doi.org/10.15252/emmm.201809711.
51. Kleinberger, G., Brendel, M., Mracsko, E., Wefers, B., Groeneweg, L., Xiang, X., Focke, C., Deußing, M., Suárez-Calvet, M., Mazaheri, F., et al. (2017). The FTD -like syndrome causing TREM 2 T66M mutation impairs microglia function, brain perfusion, and glucose metabolism. EMBO J. *36*, 1837–1853. https://doi.org/10.15252/embj.201796516.
52. Xiang, X., Wind, K., Wiedemann, T., Blume, T., Shi, Y., Briel, N., Beyer, L., Biechele, G., Eckenweber, F., Zatcepin, A., et al. (2021). Microglial activation states drive glucose uptake and FDG-PET alterations in neurodegenerative diseases. Sci. Transl. Med. *13*, eabe5640. https://doi.org/10.1126/scitranslmed.abe5640.
53. Smith, D., Pernet, A., Hallett, W.A., Bingham, E., Marsden, P.K., and Amiel, S.A. (2003). Lactate: A preferred fuel for human brain metabolism in vivo. J. Cerebr. Blood Flow Metabol. *23*, 658–664. https://doi.org/10.1097/01.WCB.0000063991.19746.11.
54. Campisi, J., Kapahi, P., Lithgow, G.J., Melov, S., Newman, J.C., and Verdin, E. (2019). From discoveries in ageing research to therapeutics for healthy ageing. Nature *571*, 183–192. https://doi.org/10.1038/s41586-019-1365-2.
55. Horvath, S., and Raj, K. (2018). DNA methylation-based biomarkers and the epigenetic clock theory of ageing. Nat. Rev. Genet. *19*, 371–384. https://doi.org/10.1038/s41576-018-0004-3.
56. Lenz, S., and Peterson, J. (2020). It's Time to Act – the Challenges of Alzheimer's and Dementia for Women.
57. Dong, Y., D'Mello, C., Pinsky, W., Lozinski, B.M., Kaushik, D.K., Ghorbani, S., Moezzi, D., Brown, D., Melo, F.C., Zandee, S., et al. (2021). Oxidized phosphatidylcholines found in multiple sclerosis lesions mediate

neurodegeneration and are neutralized by microglia. Nat. Neurosci. *24*, 489–503. https://doi.org/10.1038/s41593-021-00801-z.

58. Lee, S.M., Kim, E.J., Suk, K., and Lee, W.H. (2011). CD300F blocks both MyD88 and TRIF-mediated TLR signaling through activation of Src homology region 2 domain-containing phosphatase 1. J. Immunol. *186*, 6296–6303. https://doi.org/10.4049/jimmunol.1002184.
59. Zhang, Z.D., Milman, S., Lin, J.R., Wierbowski, S., Yu, H., Barzilai, N., Gorbunova, V., Ladiges, W.C., Niedernhofer, L.J., Suh, Y., et al. (2020). Genetics of extreme human longevity to guide drug discovery for healthy ageing. Nat. Metab. *2*, 663–672. https://doi.org/10.1038/s42255-020-0247-0.
60. Shi, Q., Chang, C., Saliba, A., and Bhat, M.A. (2022). Microglial mTOR Activation Upregulates Trem2 and Enhances b-Amyloid Plaque Clearance in the 5XFAD Alzheimer's Disease Model. J. Neurosci. *42*, 5294–5313. https://doi.org/10.1523/JNEUROSCI.2427-21.2022.
61. Marengoni, A., Angleman, S., Melis, R., Mangialasche, F., Karp, A., Garmen, A., Meinow, B., and Fratiglioni, L. (2011). Aging with multimorbidity: A systematic review of the literature. Ageing Res. Rev. *10*, 430–439. https://doi.org/10.1016/j.arr.2011.03.003.
62. Bushnell B. (2014). BBMap: A fast, accurate, splice-aware aligner. https://www.osti.gov/biblio/1241166.
63. Ewels, P., Magnusson, M., Lundin, S., and Käller, M. (2016). MultiQC: Summarize analysis results for multiple tools and samples in a single report. Bioinformatics *32*, 3047–3048.
64. Dobin, A., Davis, C.A., Schlesinger, F., Drenkow, J., Zaleski, C., Jha, S., Batut, P., Chaisson, M., and Gingeras, T.R. (2013). STAR: Ultrafast universal RNA-seq aligner. Bioinformatics *29*, 15–21.
65. Liao, Y., Smyth, G.K., and Shi, W. (2014). featureCounts: An efficient general purpose program for assigning sequence reads to genomic features. Bioinformatics *30*, 923–930.
66. Anders, S., and Huber, W. (2010). Differential expression analysis for sequence count data. Genome Biol *11*, R106.
67. Love, M.I., Huber, W., and Anders, S. (2014). Moderated estimation of fold change and dispersion for RNA-seq data with DESeq2. Genome Biol. *15*, 550.
68. Lê, S., Josse, J., and Husson, F. (2008). FactoMineR: An R package for multivariate analysis. J. Stat. Softw. *25*, 1–18.
69. Kassambara, A. and Mundt, F. (2020) Factoextra: Extract and Visualize the Results of Multivariate Data Analyses. R Package Version 1.0.7. https://cran.r-project.org/web/packages/factoextra/index.html.
70. Wu, T., Hu, E., Xu, S., Chen, M., Guo, P., Dai, Z., Feng, T., Zhou, L., Tang, W., Zhan, L., et al. (2021). clusterProfiler 4.0: A universal enrichment tool for interpreting omics data. Innovation *2*, 100141. https://doi.org/10.1016/j.xinn.2021.100141.
71. Yu, G., Wang, L.G., Han, Y., and He, Q.Y. (2012). ClusterProfiler: An R package for comparing biological themes among gene clusters. OMICS A J. Integr. Biol. *16*, 284–287. https://doi.org/10.1089/omi.2011.0118.
72. Yu, G.. enrichplot: Visualization of Functional Enrichment Result. R package version 1.20.3. https://yulab-smu.top/biomedical-knowledge-mining-book/.
73. Carlson, M. (2019). org.Mm.eg.db: Genome wide annotation for Mouse. R package version 3.8.2.
74. Schlapp, G., Goyeneche, L., Fernández, G., Menchaca, A., and Crispo, M. (2015). Administration of the nonsteroidal anti-inflammatory drug tolfenamic acid at embryo transfer improves maintenance of pregnancy and embryo survival in recipient mice. J. Assist. Reprod. Genet. *32*, 271–275.
75. Dobin, A., Davis, C.A., Schlesinger, F., Drenkow, J., Zaleski, C., Jha, S., Batut, P., Chaisson, M., and Gingeras, T.R. (2013). STAR: Ultrafast universal RNA-seq aligner. Bioinformatics *29*, 15–21.
76. Dobin, A., and Gingeras, T.R. (2016). Optimizing RNA-Seq Mapping with STAR, in Data Mining Techniques for the Life Sciences (New York: Springer), pp. 245–262. https://link.springer.com/protocol/10.1007/978-1-4939-3572-7_13.
77. Zhu, A., Ibrahim, J.G., and Love, M.I. (2019). Heavy-tailed prior distributions for sequence count data: Removing the noise and preserving large differences. Bioinformatics *35*, 2084–2092.
78. Keren-shaul, H., Spinrad, A., Weiner, A., Colonna, M., Schwartz, M., Amit, I., Keren-shaul, H., Spinrad, A., Weiner, A., Matcovitch-natan, O., et al. (2017). A Unique Microglia Type Associated with Restricting Development of Alzheimer's Disease. Cell *169*, 1276–1290.e17.

STAR★METHODS

KEY RESOURCES TABLE

REAGENT or RESOURCE	SOURCE	IDENTIFIER
Antibodies		
Rabbit polyclonal anti-IBA1	Wako	Cat # 019-19741 RRID:AB_839504
Rabbit polyclonal anti-PU1	Cell Signaling Technology	Cat # 2258 RRID:AB_2186909
Brilliant Violet 785™ anti-mouse CD45.2 antibody	BioLegend	Cat# 109839, RRID:AB_2562604
Brilliant Violet 605(TM) anti-mouse/human CD11b	BioLegend	Cat# 101237, RRID:AB_11126744
APC anti-P2RY12	BioLegend	Cat# 848006, RRID:AB_2721469
InVivoPlus anti-mouse CD16/CD32	Bio X Cell	Cat# BE0307, RRID:AB_2736987
Rabbit monoclonal anti-phospho S6 (Ser235/236)	Cell Signaling Technology	Cat # 4858 RRID:AB_916156
Mouse monoclonal anti-S6	Cell Signaling Technology	Cat # 2317 RRID:AB_2238583
Rabbit monoclonal antiphospho- 4E-BP1 (Thr37/46)	Cell Signaling Technology	Cat # 2855 RRID:AB_560835
Rabbit monoclonal anti-4E-BP1	Cell Signaling Technology	Cat # 9644 RRID:AB_2097841
Goat Anti-Rabbit IgG Antibody, Peroxidase Conjugated	Milipore	Cat# AP132P RRID:AB_90264
Anti-actin antibody conjugated to horseradish peroxidase	Merck	Cat # A3854 RRID:AB_262011
Goat anti-mouse conjugated to horseradish peroxidase	Thermo Fisher Scientific	Cat # 31430 RRID:AB_228307
Goat anti-rabbit conjugated to horseradish peroxidase	Thermo Fisher Scientific	Cat # 31460 RRID:AB_228341
Rat anti-mouse CLEC7a/DECTIN1	Novus	Cat # MAB17561 RRID:AB_2081654
Rabbit monoclonal anti-mouse/human NLRP3	Cell Signaling Technology	Cat # 15101T RRID:AB_2722591
Chemicals, peptides, and recombinant proteins		
M16 medium	Sigma Aldrich	Cat #M7292
Embryo tested mineral oil	Sigma Aldrich	Cat # 76235
GeneArt™ CRISPR Nuclease mRNA	Invitrogen	Cat # A29378
Paraformaldehyde	Sigma Aldrich	Cat #P6148
Ethylene glycol	Sigma Aldrich	Cat # 324558
Polyvinylpyrrolidone	Sigma Aldrich	Cat # PVP40
Hematoxylin Solution, Mayer's	Sigma Aldrich	Cat # MHS16
Eosin B	Sigma Aldrich	Cat # 861006
Triton X-100	Sigma Aldrich	Cat #T8787
Fetal Bovine Serum	Invitrogen	Cat # A99835
3,3′-Diaminobenzidine (DAB)	Sigma Aldrich	Cat #D8001
DPX Mountant for histology	Sigma Aldrich	Cat # 06522
TRIzol Reagent	Invitrogen	Cat # A93003
M-MLV reverse transcriptase	Invitrogen	Cat # 28025013
TaqMan Fast Advanced Master Mix	Applied Biosystems	Cat # 4444557
Percoll® PLUS	Sigma Aldrich	Cat # GE17-5445-02
BODIPY™ 493/503 (4,4-Difluoro-1,3,5,7,8-Pentamethyl-4-Bora-3a,4a-Diaza-*s*-Indacene)	Invitrogen	Cat #D3922
DMEM/F-12, GlutaMAX™ supplement	Gibco	Cat # 10565018
Recombinant Mouse M-CSF (carrier-free)	Biolegend	Cat # 576406
Lipopolysaccharides from Escherichia coli O55:B5	Sigma Aldrich	Cat #L2880
L-Glutamine	Sigma Aldrich	Cat #G8540

(*Continued on next page*)

Continued

REAGENT or RESOURCE	SOURCE	IDENTIFIER
Sodium pyruvate	Sigma Aldrich	Cat #P5280
Dextrose	Sigma Aldrich	Cat #D9434
HEPES	Sigma Aldrich	Cat # PHR1428
Oligomycin from Streptomyces diastatochromogenes	Sigma Aldrich	Cat #O4876
Carbonyl cyanide 4-(trifluoromethoxy) phenylhydrazone	Sigma Aldrich	Cat #C2920
Antimycin A from Streptomyces sp.	Sigma Aldrich	Cat # A8674
Rotenone	Sigma Aldrich	Cat #R8875
Bicinchoninic Acid solution	Sigma Aldrich	Cat #B9643
18F-2-fluor-2-desoxi-*d*-glucosa (18F-FDG)	Synthetized in house at CUDIM	N/A
Heparin sodium salt	Sigma Aldrich	Cat #H3149
Rapamycin from Streptomyces hygroscopicus	Sigma Aldrich	Cat #R0395
Bio-Rad Protein Assay Dye Reagent Concentrate	Bio-Rad	Cat #5000006
NuPAGE™ 4 to 12%, Bis-Tris	Invitrogen	Cat # NP0321BOX
NuPAGE ™ MOPS SDS Running buffer	Invitrogen	Cat # NP0001
iBlot2® Transfer Stack	Invitrogen	Cat # IB23002
Restore™ PLUS Western Blot Stripping Buffer	Thermo Fisher Scientific	Cat # 46430
Insulin 2.5cc - 40UI CANINSULIN	MSD Animal Health	N/A
Critical commercial assays		
Direct-zol RNA Miniprep Plus Kits	Zymo Research	Cat #R2070
TruSeq Stranded mRNA LT Sample Prep Kit	Illumina	15031047 Rev. E
LEGENDplex Mouse Inflammation Panel (13-plex)	Biolegend	Cat # 740446
Seahorse XFp FluxPak	Agilent Technologies	Cat # 103022-100
Deposited data		
Raw data RNAseq	This article	Deposited in NCBI (SRA) under accession number SRR21771247-SRR21771254 (PRJNA885873).
Experimental models: Organisms/strains		
C57BL/6J	The Jackson Laboratory	RRID:IMSR_JAX:000664
CD300f knockout mice (CD300f$^{-/-}$)	Xi et al., 2010[13] -Genentech	N/A
CD300f knockout mice (CD300f$^{-/-IPMon}$)	This article	MGI:7525705
B6D2F1	UBAL Facility	N/A
Oligonucleotides		
See Table S6		N/A
Software and algorithms		
ImageJ (Rasband, NIH)	NIH	https://ImageJ.nih.gov/ij/download.html
BBMap	Bushnell, 2014[62]	https://www.osti.gov/biblio/1241166
FastQC v0.11.9	Andrews 2010	http://www.bioinformatics.babraham.ac.uk/projects/fastqc/
MultiQC v1.11	Ewels et al., 2016[63]	https://multiqc.info
STAR 2.7.10a	Dobin et al., 2013[64]	https://github.com/alexdobin/STAR
FeatureCounts v2.0.1	Liao et al., 2014[65]	https://subread.sourceforge.net
DESeq2 v1.36.0	Anders and Huber, 2010[66]; Love et al. 2014[67]	https://bioconductor.org/packages/release/bioc/html/DESeq2.html
FactoMineR v2.4	Lê et al., 2008[68]	https://CRAN.R-project.org/package = FactoMineR

(*Continued on next page*)

Continued

REAGENT or RESOURCE	SOURCE	IDENTIFIER
Factoextra v1.0.7	Kassambara & Mundt, 2020[69]	https://CRAN.R-project.org/package = factoextra
Pheatmap v1.0.12	Kolde 2019	https://CRAN.R-project.org/package = pheatmap
EnhancedVolcano v1.14.0	Blighe et al. 2014	https://github.com/kevinblighe/EnhancedVolcano
ClusterProfiler 3.17	Wu et al. 2021[70] Yu et al. 2012[71]	https://bioconductor.org/packages/clusterProfiler
Enrichplot v1.16.2	Yu 2022[72]	https://bioconductor.org/packages/enrichplot
Org.Mm.e.g.,.db 3.8.2	Carlson 2019[73]	https://bioconductor.org/packages/org.Mm.eg.db
AnyMaze software	Stoelting Co.	https://www.any-maze.com/
PMOD software, v. 3.8	PMOD Technologies, Ltd., Zurich, Switzerland	N/A
Prism 8 software version 8.2.1	GraphPad	https://www.graphpad.com/
Biorender		https://www.biorender.com/
Other		
Accu-Check active glucose strips	Roche	Cat # 06656757

RESOURCE AVAILABILITY

Lead contact

Further information and requests for resources and reagents should be directed to and will be fulfilled by the lead contact, Hugo Peluffo (Hugo.Peluffo@ub.edu).

Materials availability

All unique/stable reagents generated in this study are available from the lead contact with a completed materials transfer agreement.

Data and code availability

- RNA-seq data have been deposited at NCBI and are publicly available as of the date of publication. Accession numbers are listed in the key resources table. Microscopy data reported in this paper will be shared by the lead contact upon request.
- This paper does not report original code.
- Any additional information required to reanalyze the data reported in this paper is available from the lead contact upon request.

EXPERIMENTAL MODEL AND STUDY PARTICIPANT DETAILS

All experimental protocols were approved by the Institutional Animal Ethics Committee (protocol number 014–16, 014-14, 007–18, 021–22), in accordance with national law 18.611 and international animal care guidelines (Guide for the Care and Use of Laboratory Animal). Both male and female mice were used with ages from 6 to 30 month old. The sex and the age of the mice is indicated in the text and figure legends. Mice were housed under SPF conditions on individually ventilated cages (5–6 mice per cage, Tecniplast, Milan, Italy) containing chip bedding (Toplit 6, SAFE, Augy, France), in a controlled environment at 20 ± 1°C with a relative humidity of 40–60%, in a 14/10 h light-dark cycle. Autoclaved food (Labdiet 5K67, PMI Nutrition, IN, US) and autoclaved filtered water were administered *ad libitum*.

Homozygous CD300f knockout mice (CD300f−/− from Genentech, termed CD300f$^{-/-}$ herein) on a C57BL6J (The Jackson Lab, RRID:IMSR_JAX:000664) background were backcrossed to homozygosis two times with the C57BL/6J WT colony of the Institut Pasteur de Montevideo to ensure that WT animals represent proper controls. Mice were housed separated by genotype, except for one cohort. The criteria for animal sacrifice of the aging cohorts were decided by the Laboratory Animal Biotechnology Unit (UBAL) animal facility personnel that were unaware of the genotype and in accordance with their welfare protocols. Intensive monitoring of aged mice was performed to avoid unnecessary suffering and loss of valuable data when mice are found dead. However, excessive censoring of mice can impact aging studies and longevity estimation due to easily observable external non-lethal lesions. To take these two concepts into account, animals were considered to be at the endpoint and euthanized when they showed one or more

clinical signs suggestive of imminent death such as reluctance to move, low body temperature, anorexia, slow or laborious respiration, 20% loss of body weight relative to baseline, ascites, or persistent rectal or uterine prolapses.

A new CD300f knockout mice line was generated (C57BL/6J-Cd300lf<em1Ipmon>/Ipmon, MGI:7525705, termed CD300f$^{-/-IPMon}$ herein). All animal procedures to generate the knock-out line were performed at the SPF animal facility of the UBAL of Institut Pasteur de Montevideo. The CD300f$^{-/-IPMon}$ knockout line was produced using CRISPR/Cas9 system. Cytoplasmic microinjection was performed in C57BL/6J (The Jackson laboratory, RRID:IMSR_JAX:000664) zygotes using a mix of 100 ng/μL GeneArt CRISPR Nuclease mRNA (Invitrogen, Cat # A29378) and 25 ng/μL of each sgRNA (2 guides were used, Figure S7) (Synthego), diluted in standard microinjection buffer. Viable embryos were cultured overnight in M16 medium (Sigma Aldrich, Cat #M7292) microdrops under embryo tested mineral oil (Sigma Aldrich, Cat # 76235), in 5% CO2 in air at 37°C. The next day, 2-cell embryos were transferred into the oviduct of B6D2F1 0.5 days postcoitum pseudopregnant females (20 embryos/female in average), following surgical procedures established in our animal facility. For surgery, recipient females were anesthetized with a mixture of ketamine (110 mg/kg, Pharmaservice, Ripoll Vet, Montevideo, Uruguay) and xylazine (13 mg/kg, Seton 2%; Calier, Montevideo, Uruguay). Tolfenamic acid was administered subcutaneously (1 mg/kg, Tolfedine, Vetoquinol, Madrid, Spain) in order 18 to provide analgesia and anti-inflammatory effects.[74] Pregnancy diagnosis was determined by visual inspection by an experienced animal caretaker two weeks after embryo transfer, and litter size was recorded on day 7 after birth. Pups were tail-biopsied and genotyped 21 days after birth, and mutant animals were maintained as founders. Genetic modification (Figure S7) was confirmed by Sanger sequencing. The CD300f$^{-/-IPMon}$ line was established after producing F4 homozygous animals that were used for experiments.

To obtain data relevant for aging under closer to physiological conditions in non-laboratory animals, one cohort of CD300f−/− (Genentech) mice and one of CD300f$^{-/-IPMon}$ mice were maintained at a specific location of the URBE animal facility of the Faculty of Medicine (UDELAR) which is not specific pathogen free (SPF). Mice were housed on individually non-ventilated cages (5–6 mice per cage, Tecniplast, Milan, Italy), in a controlled environment at 20 ± 1°C with a relative humidity of 40–60%, in a 14/10 h light dark cycle. Autoclaved food (Labdiet 5K67, PMI Nutrition, IN, US) and autoclaved filtered water were administered *ad libitum*. Under these conditions, animals may be infected with *Corynebacterium kutscheri*, *Mycoplasma pulmonis*, Murine hepatitis virus (MHV), Sendai virus (HVJ), Minute virus of mice (MVM), Theiler's murine encephalomyelitis virus (TMEV-GDVII), but are free from endo and ectoparasites and zoonosis.

METHOD DETAILS

Complete blood count

For complete blood counts, blood was drawn from mice (by cardiac puncture using deep anesthesia or from the submandibular vein) and immediately transferred to tubes containing EDTA potassium salts as an anticoagulant and evaluated on an automated analyzer BC-5000Vet (Mindray Medical International Ltd., Shenzhen, China). Among the hematological parameters examined were total white blood cells (WBC) count, lymphocyte count, neutrophils count, monocyte count, basophils count, eosinophil count, red blood cells (RBC) count, hemoglobin (HGB) concentration, hematocrit (HCT) level, mean corpuscular volume (MCV), mean corpuscular hemoglobin (MCH), mean corpuscular hemoglobin concentration (MCHC), platelet (PLT) count and the mean platelet volume (MPV).

Hepatic and renal function

To assess liver and kidney function whole blood from cardiac puncture was analyzed using the Pointcare V2 Chemistry Analyzer (Tianjin MNCHIP Technologies Co., China). The parameters determined were total proteins (TP), albumin (ALB) level, globulin (GLO) level, ALB/GLO ratio, total bilirubin (TBIL) level, alanine aminotransferase (ALT) level, aspartate aminotransferase (AST) level, gamma glutamyl transpeptidase (GGT) level, blood urea nitrogen (BUN) level, creatinine (CRE) level, BUN/CRE ratio and glucose (GLU) level.

Metabolic tests: Glucose tolerance test, pyruvate tolerance test, and insulin tolerance test

Mice subjected to the glucose tolerance test (GTT) were fasted for 12–14 h and injected via i.p. with a dextrose solution (1.5 g/kg, Sigma Aldrich, Cat #D9434). For the pyruvate tolerance test (PTT) and insulin tolerance test (ITT) mice were fasted for 6 h and were injected via i.p. with sodium pyruvate (1.5 g/kg, Sigma Aldrich, Cat #P5280) or insulin (0.5 U/kg, MSD Animal Health, 2.5cc - 40UI CANINSULIN). Blood samples were obtained from the tail at 0, 10, 20, 60 and 120 min after i.p injection and glucose concentration were determined using Accu-Check active glucose strips and a glucometer (Roche, Cat # 06656757).

Histological and immunohistochemistry procedures

Deeply anesthetized mice with ketamine/xylazine were intracardially perfused with ice-cold 4% solution of paraformaldehyde (PFA) (Sigma Aldrich, Cat #P6148) in phosphate buffer and the different tissues and organs were collected. The tissues were postfixed at 4°C in the same fixative for 3–4 h, cryoprotected with a 30% sucrose solution in phosphate buffer for 72 h at 4°C and rapidly frozen in liquid nitrogen and stored at −80°C. Parallel sections of brain (coronal) and liver were obtained using a cryostat (Leica CM1850 UV). Thirty μm-thick sections were either mounted in gelatinized slides or stored as free-floating sections in an antifreeze solution containing 30% sucrose, 30% ethylene glycol and 1% polyvinylpyrrolidone (Sigma Aldrich, Cat # PVP40) in PBS at −20°C. Liver sections

were stained with Mayer's Hematoxylin (Sigma Aldrich, Cat # MHS16) and Eosin (Sigma Aldrich, Cat # 861006). The percentage of infiltrated area in the liver sections was assessed in at least 5 different x4 fields by an observer blinded for the genotype group.

For immunohistochemical staining anti-Iba1 (1:1600, Wako, Cat # 019–19741, RRID:AB_839504), anti-CLEC7a/DECTIN1 (Novus, Cat # MAB17561) and anti-PU1 (1:400, Cell Signaling, Cat # 2258 RRID:AB_2186909) antibodies were used to label microglia and macrophages/monocytes in brain and liver. In all cases, frozen free-floating sections were washed with PBS-1% Triton X-100 (PBS-T) and incubated for 10 min with 2% H2O2 and 70% methanol in PBS solution to block endogenous peroxidase. An antigen retrieval treatment was applied to unmask the PU.1 nuclear antigen by incubating the liver sections in sodium citrate buffer (pH 8.5) for 40 min at 80°C and 20 min at room temperature (RT), previous to the endogenous peroxidase inhibition. Non-specific binding was avoided by incubating the sections for 1 h at RT with blocking buffer (BB) containing 10% fetal bovine serum (FBS) (Invitrogen, Cat # A99835) in PBS-T. The sections were then incubated with the corresponding primary antibody overnight at 4°C. After washing, the sections were incubated for 1 h at room temperature with an anti-mouse antibody conjugated to horseradish peroxidase (Thermo Fisher Scientific, Cat # 31430, RRID:AB_228307) for the CLEC7a antigen and with an anti-rabbit IgG Antibody, Peroxidase Conjugated (Millipore, Cat# AP132P, RRID:AB_90264) for IBA1 and PU1. Following a washing step, the sections were further incubated for 3–5 min with 3,3-diaminobenzidine (Sigma Aldrich, Cat #D8001), washed and mounted in DPX (Sigma Aldrich, Cat # 06522).

RNA extraction and qPCR

Total RNA was isolated from frozen brain, liver, or lung using TRIzol Reagent (Invitrogen, Cat # A93003), and further purified employing the Direct-zol RNA MiniPrep Plus kit (Zymo Research, Cat #R2070) following the manufacturer's protocol. All samples were treated with DNase I. RNA concentrations were quantified using Nanodrop and reversed transcribed using M-MLV reverse transcriptase (Invitrogen, Cat # 28025013) and random primers (Invitrogen, Cat #48190011). Quantitative PCR (qPCR) was performed using Applied Biosystems TaqMan reagents including Fast Advanced Master Mix (Cat # 4444557) and the following probes: *il1β* (Cat # Mm01336189_m1), *il6* (Cat # Mm00446190_m1), *ccl2* (Cat # Mm00441242_m1), *ccl3* (Cat # Mm00441259_g1), *trem2* (Cat # Mm04209424_g1), *cd11c/itgax* (Cat # Mm00498698_m1), *gh* (Cat # Mm00433590_g1), *prl* (Cat # Mm00599950_m1) and *gapdh* (Cat # Mm99999915_g1). The relative gene expression of each sample was determined with the 2-ΔΔCT (Livak) method of analysis. Target genes were normalized to the reference gene *gapdh*. qPCR was performed using the QuantStudio 3 apparatus with the following cycling conditions: 50°C for 2 min, 95°C for 2 min, 40 cycles at 95°C for 1 s and 60°C for 20 s.

RNA sequencing and transcriptomic analysis

For the RNAseq experiment, one brain hemisphere of four CD300f−/− and four WT 30 months old female mice were processed to extract total RNA, as described above. RNA quality was determined in a Bioanalyzer 2100 (Agilent). An RNA Integrity Number (RIN) higher than 8 was considered acceptable to continue to library construction and sequencing, which was carried out at Macrogen (Korea). TruSeq Stranded mRNA LT Sample Prep Kit (Illumina, 15031047 Rev. E) was used for library construction and paired-end reads (150x2 base pairs) were obtained by Illumina sequencing. Raw data were deposited in NCBI (SRA) under accession number SRR21771247-SRR21771254 (PRJNA885873). BBduk[62] was used to trim the reads. Sequence quality of raw and processed reads was assessed with FastQC v0.11.9 (Andrews 2010, http://www.bioinformatics.babraham.ac.uk/projects/fastqc/) and MultiQC v1.11.[63] STAR[75] was used to map the reads to the mouse genome using GRCm39.primary_assembly and Gencode release M25 gene annotations; alignment was performed using standard ENCODE options.[76] Expression counts were obtained at the gene level using FeatureCounts v2.0.1[65] with options -p -s 2 *-M*–fraction. Summary results of read numbers, mapping and gene counts are indicated in Table S2.

Given the obtained read count matrix, the R package DESeq2 v1.36.0 was used to normalize the data, correct for the different sequencing depth of the libraries and to test for differential expression. A minimum pre-filtering of the count matrix was done to keep only those rows that have at least 10 reads. Principal component analyses were performed with the R packages FactoMineR v2.4[68] and factoextra v1.0.7[69] and was based in variance stabilized transformation of data (vst, blind = TRUE) after selection of the 500 top leading genes. To test for differential expression and estimate the log2 fold changes (log2FC) between CD300f−/− and WT genotypes, Wald tests were performed for both the hypothesis |log2FC|>0 and |log2FC|>1. Shrinkage of effect size estimates (log2FC) was done by the apeglm method[77] implemented in DESeq2. For multiple testing correction, we used a stratified false discovery approach, with Benjamini and Hochberg FDR corrected p values. We defined as differentially expressed genes those presenting FDR-corrected p value <0.1 and abs(log2FC corrected by apeglm) > 0.35, a threshold that implies a minimum effect size of about 25%. Expression heatmaps were based on vst data (blind = FALSE) and produced with the R pheatmap v1.0.12 package (Kolde 2019 _pheatmap: Pretty Heatmaps_. R package version 1.0.12, https://CRAN.Rproject.org/package=pheatmap>); for each gene set of interest, only those genes with average expression value above 10 and |apeglm log2FC|>0.35 were included in the heatmap. Volcano plots were produced with the R/Bioconductor package EnhancedVolcano v1.14.0 (Blighe K., Rana S., Lewis M. EnhancedVolcano 2019: publication-ready volcano plots with enhanced coloring and labeling, https://github.com/kevinblighe/EnhancedVolcano). Functional analysis was performed through over-representation analysis (ORA) of KEGG pathways and Gene Ontology (Biological Process domain) terms. Gene set enrichment analysis (GSEA) of particular gene sets was also conducted. The R/Bioconductor packages ClusterProfiler[70,71], enrichplot (Yu G. 2022. enrichplot: Visualization of Functional Enrichment Result. R package version 1.16.2, https://yulab-smu.top/) and org.Mm.e.g.,.db (Carlson M. 2019 Genome wide annotation for Mouse. R package version 3.8.2.) were used for these functional analyses. Gene sets of interest were obtained from the following

sources: ATF4 gene set was kindly provided by Mauro Costa-Matioli; disease associated microglia (DAM) and disease inflammatory macrophages (DIM) gene sets were obtained from[41,78] (broad DAM, conserved DAM, "Keren-Shaul" DAM, broad DIM and conserved DIM); the frailty gene list was obtained from (46); the SenMayo senescence gene signature was obtained from[38]. We also evaluated the lipid-droplet accumulation microglia phenotype using gene lists specified in[42], though no enrichment was found by the GSEA analysis.

Flow cytometry

Mice brains were placed into a Dounce homogenizer with RPMI and thoroughly homogenized. After adding 30% of Percoll PLUS (Sigma Aldrich, Cat # GE17-5445-02), the homogenized samples were centrifuged at 800 g for 15 min. The supernatant was discarded and the pellet was resuspended in FACS buffer (2% FBS in DPBS) and further centrifuged at 800 g for 5 min. Samples were then stained with BODIPY 493/503 (Invitrogen, Cat #D3922) 2M together with an antibody mixture containing brilliant Violet 785 anti-mouse CD45.2 antibody (BioLegend, Cat# 109839, RRID:AB_2562604), brilliant Violet 605(TM) anti-mouse/human CD11b (BioLegend, Cat# 101237, RRID:AB_11126744), APC anti-P2RY12 (BioLegend, Cat# 848006, RRID:AB_2721469) and InVivoPlus anti-mouse CD16/CD32 (Bio X Cell, Cat# BE0307, RRID:AB_2736987) in FACS buffer. All the antibodies were diluted 1/250. Samples were incubated in dark for 15 min at 37°C followed by a wash with FACS buffer. The samples were immediately analyzed using a BD FACSymphony A5 cytometer.

Novel object recognition (NOR)

Mice were placed in a white acrylic chamber (25 × 25 cm base and 35 cm height) over the course of three days during the habituation, familiarization and testing sessions. Before each session, mice were transferred and adapted, for at least 1 h, to the room where behavioral procedures were conducted. On day 1, mice were habituated to the chamber for 5 min. The next day, in the familiarization session, mice were placed in the chamber, for 10 min, with two identical objects laid on the diagonal. On the third day, during the testing session, one of the familiar objects was replaced by a new object. Mice were allowed to explore the objects for 10 min. No preference for the familiar or the novel object was previously verified on a pilot test. The objects and chamber were cleaned before and between sessions with 70% ethanol to remove odor cues. Testing sessions

were recorded using AnyMaze software (Stoelting Co.) and later analyzed by a trained observer blinded to the experimental group. The time exploring each object over a 20 s period of exploration of both objects was analyzed.

Barnes Maze test

The Barnes Maze apparatus and protocol have been previously described[26], and consisted on a white circular acrylic slab (75 cm in diameter and elevated 58 cm above the floor), with twenty holes at regular distances (5 cm in diameter and located 5 cm from the perimeter). A black acrylic escape box (19 × 8 × 7 cm) was placed under one of the holes. Four different spatial cues were located around the maze and remained unaltered throughout the entire test. Before each phase, mice were transferred and adapted, for at least 1 h, to the room where behavioral procedures were conducted. On day one, mice were subjected to a habituation phase in which they were first placed in the escape box for 1 min and later allowed to freely explore the maze for 5 min or until they entered the escape box. There was an interval of at least 1 h before initiating the training phase. The training phase consisted of two sessions in which the mice was placed in one of the quadrants of the maze and allowed to freely explore the apparatus until they entered the escape box or after 3 min had elapsed. The training sessions (2 per day) were conducted for four consecutive days. The maze was cleaned between the sessions with 70% ethanol. Three days after the final training day (Day 7), mice underwent a 1 min probe trial in which the escape box was removed from the apparatus. During the trial sessions and probe trial the time latency to encounter the escape box was recorded.

Parallel rod floor test (ataxia)

Mice in their home cages were placed for 30 min in the behavior testing room for

habituation to the new environment. After habituation, mice were placed in the parallel rod floor apparatus (Stoelting Co.) coupled to the ANY-maze Software for animal tracking. This apparatus consists of a clear acrylic chamber enclosure (20 cm × 20 cm x 30 cm height) with a floor consisting of 1.6-mm diameter rods that are spaced 6.5 mm apart and elevated 1.2 cm above a metal plate. The computer records a foot fault when the mouse's paw slips through the parallel rods and contacts the metal plate closing the circuit. The mice are placed in the apparatus and are allowed to freely explore for 10 min in the absence of the researcher. The apparatus was cleaned with 70% ethanol before continuing with the next mouse.

Bone marrow derived macrophages cultures

Bone marrow derived macrophages (BMDM) were isolated from adult female and male WT and CD300f$^{-/-}$ mice as previously described elsewhere. Briefly, bone marrow was flushed from the femur and tibia with DMEM/F12 (Gibco, Cat # 10565018) supplemented with Penicillin/Streptomycin and 10% FBS (complete DMEM/F12). Cells were plated on to 100 mm bacteriological Petri dish with complete DMEM/F12 and 20 ng/mL recombinant mouse macrophage colony stimulating factor protein (M-CSF) (Biolegend, Cat #576406). On day 4, cells were subcultured in XFe24 plates at 100,000 cells per well or at 200.000 cells per well in XFe96 plates.

Measurement of oxygen consumption rates

Oxygen consumption rates (OCR) and extracellular acidification rates (ECAR) were determined using Seahorse XFe24 extracellular flux analyzer (Agilent Technologies) for initial female cell cultures, or Seahorse XFe Pro 96 for experiments comparing male and female cells. BMDM seeded on XFe24 plates were pretreated for 18 h with 100 ng/mL Lipopolysaccharide (LPS) (Sigma Aldrich, Cat #L2880) in complete DMEM/F12 and 5 ng/mL M-CSF. Prior to the metabolic measurements, cells were incubated for 1 h with Seahorse media (DMEM supplemented with 1 mM sodium pyruvate, 5 mM glucose, 2 mM glutamine, 5 mM HEPES, pH 7.4), in a stove at 37°C without CO2. Following the initial basal measurements, successive measurements were then made after the sequential addition of 2.5 μM oligomycin (Sigma Aldrich, Cat #O4876), 2 μM carbonyl cyanide- 4-(trifluoromethoxy) phenylhydrazine (FCCP) (Sigma Aldrich, Cat #C2920) (two 1 μM additions), and a mixture of 2.5μM antimycin (AA) (Sigma Aldrich, Cat # A8674) and 2.5 μM rotenone (Rot) (Sigma Aldrich, Cat #R8875). After each assay, the protein content of each well was determined with the bicinchoninic acid (BCA) assay and the OCR and ECAR were normalized to the protein content. The non-mitochondrial respiration (AA/Rot-resistant respiration) was subtracted from all the OCR. Maximum oxygen consumption rate (or maximum respiration rate) was determined after the addition of FCCP, and spare respiratory capacity was calculated as the difference between the maximum and basal OCR. ATP-independent respiration was determined after the addition of oligomycin. ATP-dependent respiration was calculated subtracting the ATP-independent respiration from the basal oxygen consumption rate.

Western blotting

BMDM cultures were incubated with 20 ng/mL MCSF alone or in addition with LPS (Sigma Aldrich, Cat #L2880) 100 ng/mL for 12 h or with Rapamycin 100 μM (Sigma Aldrich, Cat #R0395) for 1.5 h in DMEM/F12 media. An additional group was generated by incubation in low MSCF (5 ng/mL) for 12 h. Whole-cell extracts were lysed and centrifuged at 14,000 × g to remove cell debris and protein concentration was measured using Bradford reagent (Bio-Rad, Cat #5000006), following the manufacturer's instructions. Samples (15–20 μg) were mixed with loading buffer and resolved in 4–12% polyacrylamide gels (NuPAGETM NovexTM 4–12% Bis-Tris) (Invitrogen, Cat # NP0321BOX) using the NuPAGE TM MOPS SDS Running buffer (Invitrogen, Cat # NP0001). The transference to a nitrocellulose membrane was performed using iBlot2 Transfer Stack supports (Invitrogen, Cat # IB23002).

The following primary antibodies were used (1:1,000 if not stated otherwise): rabbit monoclonal anti-phospho S6 (Ser235/236) (Cell Signaling Technology, Cat # 4858, RRID:AB_916156), mouse monoclonal anti-S6 (Cell Signaling Technology, Cat # 2317, RRID:AB_2238583), rabbit monoclonal antiphospho-4E-BP1 (Thr37/46) (Cell Signaling Technology, Cat # 2855, RRID:AB_560835), rabbit monoclonal anti-NLRP3 (Cell Signaling Technology, Cat # 15101T) and rabbit monoclonal anti-4E-BP1 (Cell Signaling Technology, Cat # 9644, RRID:AB_2097841). Membranes were incubated with the antibodies for 16 h at 4°C in agitation. Anti-actin antibody conjugated to horseradish peroxidase (1:100,000), (Merck, Cat # A3854, RRID:AB_262011) was incubated for 30 min at RT and used as loading control. Anti-mouse and anti-rabbit secondary antibodies produced in goat and conjugated to horseradish peroxidase (1:10,000) (Thermo Fisher Scientific, Cat # 31430, RRID:AB_228307 and Cat # 31460, RRID:AB_228341 respectively) were incubated for 1h at RT. Chemiluminescent images were acquired using a Chemidoc imager (BioRad) and quantified by computer-assisted densitometric analysis (ImageJ). To remove the signals and allow the incubation with other antibodies the Restore PLUS Western Blot Stripping Buffer (Thermo Fisher Scientific, Cat # 46430) was used.

PET/CT imaging

Brain glucose uptake was evaluated by *in vivo* imaging using positron emission tomography/computed tomography (PET/CT) scans with 18F-2-fluor-2-desoxi-*d*-glucosa (18F-FDG) as radiotracer. The study was performed in the Centro Uruguayo de Imagenología Molecular (CUDIM). A nanoScan PET/CT Mediso Preclinical Imaging system based on LYSO scintillators for small animal PET imaging was used. This scanner has a spatial resolution of 0.9 mm and a transaxial field of view (FOV) of 8.0 cm. The data were acquired in list mode in a 212 × 212 × 235 matrix with a pixel size of 0.4 × 0.4 × 0.4 mm and a coincidence window width of 1.0 nsec. The animals were anesthetized with 2% isoflurane in an oxygen flow of 2 L/min, placed in prone position on the scanner bed, and injected i.v. via the caudal vein tail with 100–200 μL of 18F-FDG (25.67 ± 6.09 MBq). PET images (static studies) acquisition started 20 min after radiotracer administration and performed over 30 min. Sinograms were reconstructed using 3D maximum likelihood expectation maximization (MLEM) with 4 iterations and 6 subsets. Semiquantitative analysis was done using PMOD software, v. 3.8 (PMOD Technologies, Ltd., Zurich, Switzerland). PET studies were co-registered with the corresponding CT scan studies for anatomical localization. The images were displayed as coronal, sagittal and axial slices. Using the PFUS module, the brain images were spatially normalized to the mouse brain magnetic resonance imaging (MRI) template included in the PMOD software, to scale the images to the Paxinos and Watson coordinate system (Paxinos and Watson, 1998). The images were previously masked to exclude extracerebral activity and enhance the normalization data. The inverse mathematical transformation was estimated and applied to the volumes-of-interest (VOIs) included in the PMOD mouse brain atlas to fit the VOIs for each animal. The average activity per volume unit (kBq/cc) was subsequently corrected for injected radioactivity and mouse weight and expressed in standardized uptake value (SUV) units. Different VOIs representing brain areas were selected for further evaluation.

QUANTIFICATION AND STATISTICAL ANALYSIS

Continuous variables were evaluated using Student's two-tailed t test, one-way analysis of variance (ANOVA), or two-way ANOVA for repeated measures followed by Sidak's post hoc test, as appropriate. ANOVA followed by Tukey's post-hoc analysis was used for experimental data with more than two experimental groups and normal distribution. For qPCR analysis, non-parametrical Mann-Whitney test was used. Statistical analyses were performed with the Prism 8 software (version 8.2.1) and data were presented as mean ± SEM, considering $p < 0.05$ as statistically significant. Figures were created with BioRender.